

A Thesis Submitted for the Degree of PhD at the University of Warwick

Permanent WRAP URL:

<http://wrap.warwick.ac.uk/163963>

Copyright and reuse:

This thesis is made available online and is protected by original copyright.

Please scroll down to view the document itself.

Please refer to the repository record for this item for information to help you to cite it.

Our policy information is available from the repository home page.

For more information, please contact the WRAP Team at: wrap@warwick.ac.uk

**Free radical polymerisation of vinyl acetate
in the presence of sulfur-based chain transfer agents**

By

Matthew K Donald

A Thesis Submitted in Fulfilment of the Requirements for the
Degree of Doctor of Philosophy

Department of Chemistry, University of Warwick

March 2021

Table of Contents

I - List of Figures	iv
II - List of Tables	xii
III - List of Schemes	xv
IV - Acknowledgements	xvii
V - Declaration.....	xviii
VI - Table of Abbreviations	xix
VII - General Introduction.....	xxi
1 Chain transfer in vinyl acetate free radical polymerisation	1
1.1 Introduction	2
1.1.1 Industrial significance of vinyl acetate/vinyl alcohol.	2
1.1.2 Free radical polymerisation of vinyl acetate.	2
1.1.2.1 Initiation	3
1.1.2.2 Propagation.....	4
1.1.2.3 Termination.....	6
1.1.2.4 Chain transfer	6
1.1.3 Determining chain transfer constants.	10
1.1.3.1 The Mayo approach	10
1.1.3.2 The Smith approach	11
1.1.3.3 Gilbert's approach.....	13
1.2 Results and discussion	14
1.2.1 A new interpretation of cumulative MW data.....	14
1.2.2 Hypothesis validation: Monte Carlo simulations.	15
1.2.3 Free radical solution polymerisation of vinyl acetate.....	20
1.2.4 Applying the newly proposed CLD-method.	27
1.3 Conclusion	30
1.4 Experimental.....	30
1.5 References	33
2 Vinyl acetate chain transfer agent studies.....	37
2.1 Introduction	38
2.1.1 Vinyl acetate chain transfer.	38
2.1.2 The use of disulfides as chain transfer agents.....	47
2.1.3 Chapter aims.....	51
2.2 Results and discussion	52

2.2.1	5-methyl furfural.....	52
2.2.2	Linear disulfides.....	60
2.2.3	Disulfide oxidation.	72
2.2.4	Cyclic disulfide.....	75
2.2.5	Looking at end groups: Linear disulfides.....	77
2.2.6	Conclusions and future work.....	81
2.3	Experimental.....	83
2.4	References	87
3	Inducing branching in vinyl acetate free radical polymerisation	92
3.1	Introduction.....	93
3.1.1	Influencing polymer architecture.	93
3.1.2	Inducing branching in vinyl acetate polymerisation.	102
3.1.3	Branched polymer characterisation.....	107
3.1.4	Experimental aims.	111
3.2	Results and discussion	113
3.2.1	1,3,5-triallyl-1,3,5-triazine- 2,4,6(1H,3H,5H)-trione (TTT).....	113
3.2.2	Alternate comonomer proposal.	118
3.2.3	Divinyl adipate (DVA).	121
3.2.4	1,4-Butanediol divinyl ether (BDDVE).....	129
3.2.5	Saponification and reacetylation of branched PVAc.....	134
3.2.6	Conclusions and future work.....	150
3.3	Experimental.....	151
3.4	References	154
4	Disulfide chain transfer agents in the soap free emulsion polymerisation of vinyl acetate.....	162
4.1	Introduction.....	163
4.1.1	Application of VAc/VOH polymers: Influencing the S-PVC morphological control.....	163
4.1.2	Emulsion polymerisation of vinyl acetate.....	165
4.1.2.1	Emulsion polymerisation introduction.....	165
4.1.2.2	Emulsion polymerisation of vinyl acetate	170

4.1.2.3	Chain transfer in vinyl acetate emulsion polymerisation	173
4.1.2.4	Soap-free emulsion polymerisation of vinyl acetate	177
4.1.2.5	A note on (P)VAc hydrolysis.....	181
4.1.3	Colloidal stability.	181
4.1.3.1	General challenge.....	181
4.1.3.2	DLVO theory	181
4.1.3.3	Steric stabilisation	183
4.1.3.4	Other causes of instability - depletion/bridging flocculation.....	184
4.1.4	Key aims of chapter.	184
4.2	Results and discussion	184
4.2.1	Soap free emulsion polymerisation of vinyl acetate.	184
4.2.2	Disulfide chain transfer agents in VAc emulsion polymerisation.	194
4.2.3	S-PVC synthesis.....	213
4.2.3.1	Synthesis and analysis.....	213
4.2.3.2	Future work	217
4.2.4	Conclusions.....	218
4.3	Experimental.....	218
4.4	References	222
VIII - Conclusions and Outlook.....		229
IX - Supporting Information		236

I List of Figures

General Introduction

Figure VII.1	Schematic representation of the suspension polymerisation of VCM.	xxii
Figure VII.2	Chemical structures of poly(vinyl acetate) (PVAc) and poly(vinyl alcohol) (PVOH).	xxiv

Chapter 1

Figure 1.1.3.2.1	Evolution of the normalised ratio of chain transfer agent to monomer (s/m) vs monomer conversion, p , where $C_{tr,S} = 1, 2, 5, 10, 100, 200, 500$.	12
Figure 1.2.2.1	$dW/d(\log M)$ distributions produced from the simulations of the free radical polymerisation of vinyl acetate in the presence of a chain transfer agent where $C_{tr,S} = 180$ and $[S]_{p=0}/[M]_{p=0} = 1 \times 10^{-4}$ as a function of monomer conversion, p .	16
Figure 1.2.2.2	$\ln N(i)$ distributions produced from the simulations of the free radical polymerisation of vinyl acetate in the presence of a chain transfer agent where $C_{tr,S} = 180$. $C_{tr,S}[S]_{p=0}/[M]_{p=0}$ was fixed at 0.018.	17
Figure 1.2.2.3	$d \ln N(i)/di$ vs conversion, p , produced from the simulations of the free radical polymerisation of vinyl acetate in the presence of a chain transfer agent where $C_{tr,S} = 180$, $[S]_{p=0}/[M]_{p=0} = 5 \times 10^{-5}$ and $i = 400$.	19
Figure 1.2.2.4	Instantaneous, $\ln n(i)$, and cumulative, $\ln N(i)$, distributions at $p = 0.005, 0.010, 0.020$ and 0.050 , produced from the simulations of the free radical polymerisation of vinyl acetate in the presence of a chain transfer agent where $C_{tr,S} = 180$, $[S]_{p=0}/[M]_{p=0} = 1 \times 10^{-4}$.	20
Figure 1.2.3.1	Monomer conversion, p , as a function of time (mins) for the solution polymerisation of VAc. $[S]_{p=0}/[M]_{p=0} = 1 \times 10^{-2}, 1 \times 10^{-3}, 1 \times 10^{-4}, 5 \times 10^{-5}$ and 1×10^{-5} .	22
Figure 1.2.3.2	$dw/d \log M$ vs molecular weight, MW (g mol^{-1}), and the corresponding Mark-Houwink-Sakurada plot of intrinsic viscosity, $[\eta]$ (dL g^{-1}) vs molecular weight, MW (g mol^{-1}), for a sample of PVAc. The reported K and α values are the result of fitting the data to Equation 1.2.2.1 (fit region 55,000 – 1,500,000 g mol^{-1}).	23
Figure 1.2.3.3	$dw/d \log M$ vs molecular weight, MW (g mol^{-1}), plots as a function of time for $[S]_{p=0}/[M]_{p=0} = 1 \times 10^{-2}, 1 \times 10^{-3}, 1 \times 10^{-4}, 5 \times 10^{-5}$ and 1×10^{-5} .	24

Figure 1.2.3.4	In $N(i)$ vs degree of polymerisation, i , as a function of time for $[S]_{p=0}/[M]_{p=0} = 1 \times 10^{-3}, 1 \times 10^{-4}, 5 \times 10^{-5}$ and 1×10^{-5} .	25
Figure 1.2.3.5	Example GC chromatogram of a sample taken from the polymerisation reactions.	26
Figure 1.2.3.6	Calibration curve for the ratio of the GC peak areas of DDT and n-dodecane vs the analytical concentration ratio.	26
Figure 1.2.3.7	Normalised ratio of chain transfer agent to monomer, s/m , vs monomer conversion, p , for the free radical polymerisation of VAc in the presence of DDT.	27

Chapter 2

Figure 2.1.2.3	Structures of less reactive aliphatic type disulfides. Being 2-hydroxyethyl disulfide, 3,3'-Dithiodipropionic acid, Bis-(2-ethyl hexyl) disulfide, propyl ester of bis-(β -carboxyethyl) disulfide, and bis- (β -chloroacetoxyethyl) disulfide.	49
Figure 2.1.2.4	Structures of more reactive disulfides. Being diphenyl disulfide, di(2-methyl phenyl) disulfide, di(2,3,5,6-tetramethyl phenyl)disulfide(8), di(2-chloromethyl phenyl) disulfide, di(2-bromomethyl phenyl) disulfide and di(isopropyl-xanthogen) disulfide.	50
Figure 2.2.1.1	^1H NMR (300 MHz, CDCl_3) between 1.5 and 2.5 ppm of the crude samples withdrawn from the free radical polymerisation of vinyl acetate in ethyl acetate in the presence of 1 wt% MFF wrt VAc.	53
Figure 2.2.1.2	$dW/d\log$ vs molecular weight (MW, gmol^{-1}), molecular weight distributions for the free radical polymerisation of vinyl acetate in ethyl acetate in the presence of 1 wt% MFF wrt VAc after 180 and 1440 mins.	54
Figure 2.2.1.3	$\ln N(i)$ vs i for the samples withdrawn after 180 mins and 1440 mins during the free radical polymerisation of vinyl acetate in the presence of 1 wt% MFF.	54
Figure 2.2.1.4	^1H NMR shift assignments for the protons a, b, c and d from the structure in Scheme 2.2.1.2 of MFF.	56
Figure 2.2.1.5	^1H NMR shift assignments for the protons e and f, and the structure to which they correlate.	56
Figure 2.2.1.6	Partial monomer conversion for the copolymerisation of VAc and DBM, and the copolymerisation of VAc and MA, both in the presence of MFF. The weight ratios of VA/comonomer/MFF employed were 100/10/1.	58
Figure 2.2.1.7	Molecular weight distributions, $dW/d\log M$ vs MW (gmol^{-1}), as a function of time for the copolymerisation of vinyl acetate and dibutyl maleate (top), and the copolymerisation of vinyl acetate and methyl acrylate (bottom), both in the presence of MFF. The weight ratios of VAc/comonomer/MFF employed were 100/10/1.	59

Figure 2.2.2.1	Monomer conversion, p , as a function of time (mins) for the solution polymerizations of vinyl acetate at varying concentrations of dibutyl disulfide, 1 , and 2-hydroxyethyl disulfide, 2 .	62
Figure 2.2.2.2	Molecular weight distributions, $dW/d\log M$ vs MW (gmol^{-1}), for the solution polymerisation of vinyl acetate in the presence of varying quantities of 1 and 2 .	63
Figure 2.2.2.3	Molecular weight distributions, $dW/d\log M$ vs MW (gmol^{-1}), as a function of conversion, for the solution polymerisation of VAc in the presence of 1 and 2 , both at $[S]/[M] = 1 \times 10^{-4}$. The legend details the time (mins) of the sample and the corresponding monomer conversion, p , in the form Time (mins) / p .	65
Figure 2.2.2.4	Mayo plots, showing \bar{X}_n^{-1} and $2\bar{X}_w^{-1}$ vs $[S]/[M]$ at a variety of concentrations.	67
Figure 2.2.2.5	Gilbert plots of $\ln N(i)$ vs i for 1 and 2 employed at a variety of concentrations. The overlaid black lines are the linear portions from which the slope was extracted to calculate $C_{tr,S}$.	70
Figure 2.2.3.1	300 MHz ^1H NMR spectra, recorded in CDCl_3 , for Dibutyl disulfide (bottom, red) and the oxidation product (top, black).	73
Figure 2.2.3.2	Monomer conversion, p , as a function of time (mins) for the solution polymerizations of vinyl acetate in the presence of dibutyl disulfide and the oxidised thiosulfinate, both employed at $[S]/[M] = 5 \times 10^{-3}$.	74
Figure 2.2.4.1	Monomer conversion, p , as a function of time (mins) for the solution copolymerisation of vinyl acetate and 3 at varying concentrations of 3 .	76
Figure 2.2.4.2	Molecular weight distributions, $dW/d\log M$ vs MW (gmol^{-1}), as a function of time, for the solution polymerisation of VAc in the presence of 3 , where $[3]/[M] = 5 \times 10^{-4}$. The legend details the time (mins) of the sample.	77
Figure 2.2.5.1	Monomer conversion, p , as a function of time (mins) for the solution polymerisation of VAc in the presence of 1 . $[1]/[M] = 7.59 \times 10^{-2}$.	78
Figure 2.2.5.2	$dW/d\log M$ MWD for PVAc formed at $[1]/[M] = 7.59 \times 10^{-2}$, $p = 0.25$.	79
Figure 2.2.5.3	400 MHz ^1H NMR spectra of PVAc formed at $[1]/[M] = 7.59 \times 10^{-2}$, $p = 0.25$. recorded in $d_6\text{-DMSO}$.	80
Figure 2.2.5.4	ESI mass spectrum for PVAc formed in the presence of $[1]/[M] = 7.59 \times 10^{-2}$, with the highlighted red region between $1100 < m/z < 1450$ from the full spectrum then expanded.	81

Chapter 3

Figure 3.1.1.1	Some commonly targeted polymeric architectures.	94
----------------	---	----

Figure 3.1.1.2	Copolymerisation of A type MM with A-A and B-B monomers according to Flory's theory.	94
Figure 3.1.1.3	Copolymerisation of A type MM with a B-B monomer in accordance with FS theory.	96
Figure 3.1.2.1	Structure of allyl isopropyl carbonate. Note the proton on the tertiary carbon of the isopropyl group is particularly susceptible to chain transfer.	103
Figure 3.1.3.1	Depiction of the hydrodynamic volume of a linear and star polymer of the same MW.	108
Figure 3.1.4.1	Plot of the normalised ratio, s/m , defined in Equation 3.1.5.3, demonstrating how s/m changes as a function of monomer conversion when $C_{tr,s} = 223$ and 0.221 .	112
Figure 3.1.4.2	Predicted structure of branched PVAc, formed through copolymerisation with a difunctional MVM in the presence of a CTA, DBDS.	113
Figure 3.2.1.1	Chemical structure of 1,3,5-triallyl-1,3,5-triazine-2,4,6(1H,3H,5H)-trione (TTT).	113
Figure 3.2.1.2	Monomer conversion, p , vs time (mins) for the free radical solution copolymerisation of vinyl acetate and TTT in the presence of DBDS. The ratios of VA/DBDS/TTT are detailed in the figure legend.	114
Figure 3.2.1.3	$dW/d\log M$ vs MW (g mol^{-1}) MW distributions and the Mark-Houwink plots of intrinsic viscosity, $[\eta]$ (dL g^{-1}), vs MW (g mol^{-1}) for the 120 mins samples taken during the free radical solution copolymerisation of vinyl acetate and TTT in the presence of DBDS. Mol ratios VA/DBDS/TTT = $100/1/X$ where $X = 0.0, 0.1, 0.5, 1.0$ and 2.0 .	116
Figure 3.2.2.1	Copolymer composition plot, constructed from Equation 3.2.2.1, where F_{VAc} (fraction of VAc in the polymer) is plotted against f_{VAc} (fraction of VAc in the monomer mixture), where $r_{VAc} = 0.99$ and $r_{DVA} = 0.79$, and where $r_{VAc} = 3.0$ and $r_{EVE} = 0$.	120
Figure 3.2.3.1	Monomer conversion, p , vs time (mins) for the free radical solution copolymerisation of vinyl acetate and DVA in the presence of DBDS. The ratios of VAc/DBDS/DVA are detailed in the figure legend.	121
Figure 3.2.3.2	$dW/d\log M$ vs MW (g mol^{-1}) MW distributions (top) and the Mark-Houwink plots of intrinsic viscosity, $[\eta]$ (dL g^{-1}), vs MW (g mol^{-1}) (bottom) for the 120 mins samples taken during the free radical solution copolymerisation of vinyl acetate and in the presence of DBDS. Mole ratio VAc/DBDS/DVA = $100/1/0, 100/1/0.5, 100/1/1.0, 100/1/3.0$ and $100/3/3.0$.	123
Figure 3.2.3.3	$dW/d\log M$ vs MW (g mol^{-1}) MW distributions and the Mark-Houwink plots of intrinsic viscosity, $[\eta]$ (dL g^{-1}), vs MW (g mol^{-1}) for samples taken during the free radical solution copolymerisation of vinyl acetate and DVA in the presence of	125

	DBDS. Mol ratio VAc/DBDS/TTT = 100/1/1. Data is shown for monomer conversions of 0.02, 0.06, 0.12, 0.18 and 0.57.	
Figure 3.2.3.4	dW/dlog M vs MW (g mol ⁻¹) MW distributions and the Mark-Houwink plots of intrinsic viscosity, $[\eta]$ (dL g ⁻¹), vs MW (g mol ⁻¹) for samples taken during the free radical solution polymerisation of vinyl acetate in the presence of 1 mol% DBDS. Data is shown for monomer conversions of 0.08, 0.14, 0.22 and 0.66.	128
Figure 3.2.4.1	Monomer conversion, p , vs time (mins) for the free radical solution copolymerisation of vinyl acetate and BDDVE in the presence of DBDS. The ratios of VAc/DBDS/BDDVE are detailed in the figure legend.	129
Figure 3.2.4.2	dW/dlog M vs MW (g mol ⁻¹) MW distributions (top) and the Mark-Houwink plots of intrinsic viscosity, $[\eta]$ (dL g ⁻¹), vs MW (g mol ⁻¹) (bottom) for the 120 mins samples taken during the free radical solution copolymerisation of vinyl acetate with BDDVE in the presence of DBDS.	132
Figure 3.2.4.3	dW/dlog M vs MW (gmol ⁻¹) MW distributions and the Mark-Houwink plots of intrinsic viscosity, $[\eta]$ (dLg ⁻¹), vs MW (g mol ⁻¹) for samples taken during the free radical solution copolymerisation of vinyl acetate and BDDVE in the presence of DBDS. Mol ratio VAc/DBDS/BDDVE = 100/1/1. Data is shown for monomer conversions of 0.04, 0.08, 0.12, 0.16 and 0.55.	133
Figure 3.2.5.1	400 MHz ¹ H NMR spectra, recorded in d ₆ -DMSO, for the polymers isolated from the reactions in the presence of 1 mol% DBDS wrt VAc, with no comonomer, 1 mol% DVA and 1 mol% BDDVE.	136
Figure 3.2.5.2	Isolated and dried PVOH. DVA (100/1/1), No comonomer (100/1/0), BDDVE (100/1/1), No CTA or comonomer (100/0/0) and commercial PVOH (Mowiol 6-98, M _w = 47,000).	138
Figure 3.2.5.3	400 MHz ¹ H NMR spectra, recorded in d ₆ -DMSO, for the polymers isolated from the reactions in the presence of 1 mol% DBDS wrt VA, with no comonomer, 1 mol% DVA and 1 mol% BDDVE.	139
Figure 3.2.5.4	400 MHz ¹ H NMR spectra, recorded in d ₆ -DMSO, for the polymers isolated from the hydrolysis of the PVAc formed in the presence of 1 mol% DBDS wrt VAc, with no comonomer, and in the absence of both DBDS and comonomer.	140
Figure 3.2.5.5	400 MHz ¹ H NMR spectra, recorded in d ₆ -DMSO, for the PVOH formed through saponification of low MW PVAc (solution polymerisation with $[\text{DBDS}]/[\text{VAc}] = 7.65 \times 10^{-2}$) between 6-0 ppm, with the spectra between 7.5 ppm and 5 ppm highlighted.	142
Figure 3.2.5.6	400 MHz ¹ H NMR spectra between 5.0 and 4.0 ppm, recorded in d ₆ -DMSO, for the PVOH formed through saponification of low MW PVAc (solution polymerisation with $[\text{DBDS}]/[\text{VAc}] = 7.65 \times 10^{-2}$).	143

Figure 3.2.5.7	400 MHz ^1H NMR spectra between 7.5 and 11.0 ppm, recorded in d_6 -DMSO, for the PVOH (bottom, red) formed through saponification of low MW PVAc (top, grey) (solution polymerisation with $[\text{DBDS}]/[\text{VAc}] = 7.65 \times 10^{-2}$).	144
Figure 3.2.5.8	General structure of Psittacofulvin.	145
Figure 3.2.5.9	Isolated and dried PVAc, formed after acetylation of PVOH. DVA (100/1/1), No comonomer (100/1/0), and BDDVE (100/1/1).	146
Figure 3.2.5.10	400 MHz ^1H NMR spectra, recorded in d_6 -DMSO, for the PVAc samples reacetylated from the PVOH samples, from the polymers isolated from the reactions in the presence of 1 mol% DBDS wrt VAc, with no comonomer, 1 mol% DVA and 1 mol% BDDVE.	146
Figure 3.2.5.11	$dW/d\log M$ vs MW (g mol^{-1}) MW distributions for the reactions before hydrolysis (Reaction state A) and after reacetylation (Reaction state B). The reactions shown are that without comonomer, with 1 mol% DVA and with 1 mol% BDDVE.	148
Figure 3.2.5.12	Mark Houwink plots of $[\eta]$ (dL g^{-1}) vs MW (g mol^{-1}) for the reactions before hydrolysis (Reaction state A) and after reacetylation (Reaction state B). The reactions shown are that without comonomer, with 1 mol% DVA and with 1 mol% BDDVE.	149

Chapter 4

Figure 4.1.1.1	Schematic representation of the suspension polymerisation of VCM.	164
Figure 4.1.2.1.1	General mechanistic steps involved in particle formation/entry in emulsion polymerisation.	166
Figure 4.1.2.3.1	Examples of some of the RAFT agents used in the study by Nomura to control the emulsion polymerisation of VAc.	176
Figure 4.1.2.4.1	Structure of the surfmer and surfactant used in the in studies by El-Aasser and coworkers.	179
Figure 4.1.2.4.2	Structures of the sodium salts of 2-acrylamido-2-methyl-1-propanesulfonic acid (Na-AMPS) and 3-allyloxy-2-hydroxypropane sulfonate (Na-AHPSA).	179
Figure 4.1.2.4.3	Structure of the maleate derived monomer synthesised in the work by Sun <i>et al.</i>	180
Figure 4.1.3.2.1	The potential energy of two lyophobic colloids at short distances, as a function of the interparticle separation.	183
Figure 4.2.1.1	Cumulative (top) and instantaneous (bottom) VAc conversion (top) for the semi-batch soap free emulsion copolymerisation of VAc and Na-AMPS (0.5 mol% wrt VAc) in the presence of varying concentrations of buffer.	188

Figure 4.2.1.2	Z-average particle size ($d \cdot \text{nm}$) (top) and PDI (bottom) vs time for the semi-batch soap free emulsion copolymerisation of VAc and Na-AMPS (0.5 mol% wrt VAc) in the presence of varying concentrations of buffer.	189
Figure 4.2.1.3	Z-average particle size ($d \cdot \text{nm}$) vs $p^{1/3}$ for the semi-batch soap free emulsion copolymerisation of VAc and Na-AMPS (0.5 mol% wrt VAc) in the presence of varying concentrations of buffer.	190
Figure 4.2.1.4	Cumulative and instantaneous VAc conversion vs time for the semi-batch soap free emulsion copolymerisation of VAc and Na-AMPS (0.5 mol% wrt VAc), with and without DDT.	192
Figure 4.2.1.5	Z-Average particle size and PDI vs time for the semi-batch soap free emulsion copolymerisation of VAc and Na-AMPS (0.5 mol% wrt VAc), with and without DDT.	192
Figure 4.2.1.6	SEM image of the final latex produced during the soap free emulsion copolymerisation of VAc and Na-AMPS (0.5 mol% wrt VAc) in the presence 8.5×10^{-3} M sodium bicarbonate, without (left) and with (right) 1 wt% DDT in the feed. (Scale bars = 500 nm).	193
Figure 4.2.2.1	Cumulative and instantaneous VAc conversion for the semi-batch soap free emulsion copolymerisation of VAc and Na-AMPS (0.5 mol% wrt VAc), in the presence of DBDS.	195
Figure 4.2.2.2	Z-average particle size and PDI for the semi-batch soap free emulsion copolymerisation of VAc and Na-AMPS (0.5 mol% wrt VAc), in the presence of DBDS. $[\text{DBDS}]/[\text{VAc}]$ in feed = 0, 1.22×10^{-3} , 2.38×10^{-3} , 4.76×10^{-3} and 9.40×10^{-3} .	196
Figure 4.2.2.3	Particle size distributions by scattering intensity and number for the semi-batch soap free emulsion copolymerisation of VAc and Na-AMPS (0.5 mol% wrt VAc), in the presence of $[\text{DBDS}]/[\text{VAc}] = 4.76 \times 10^{-3}$. The distributions correlate to the samples withdrawn after 60 mins, 100, 120 and 240 mins.	197
Figure 4.2.2.4	Particle size distributions by scattering intensity and number for the semi-batch soap free emulsion copolymerisation of VAc and Na-AMPS (0.5 mol% wrt VAc), in the presence of $[\text{DBDS}]/[\text{VAc}] = 9.4 \times 10^{-3}$. The distributions correlate to the samples withdrawn after 60 mins, 100, 120 and 240 mins.	198
Figure 4.2.2.5	SEM images taken of the final latexes, formed at $[\text{DBDS}]/[\text{VAc}]$ in the feed of 1.22×10^{-3} , 2.38×10^{-3} , 4.76×10^{-3} and 9.40×10^{-3} .	199
Figure 4.2.2.6	$dw/d\log M$ vs MW distribution for the semi-batch soap free emulsion copolymerisation of VAc and Na-AMPS (0.5 mol% wrt VAc), in the presence of varying $[\text{DBDS}]/[\text{VAc}]$.	200
Figure 4.2.2.7	$dw/d\log M$ vs MW distributions as a function of time for the semi-batch soap free emulsion copolymerisation of VAc and Na-AMPS (0.5 mol% wrt VAc), in the presence of $[\text{DBDS}]/[\text{VAc}] = 2.38 \times 10^{-3}$.	202

Figure 4.2.2.8	Plots of [DBDS]/[VAc] in the feed vs \bar{X}_n^{-1} and vs $2\bar{X}_w^{-1}$ for the final latexes obtained in the semi-batch soap free emulsion copolymerisation of VAc and Na-AMPS (0.5 mol% wrt VAc), in the presence of varying [DBDS]/[VAc].	203
Figure 4.2.2.9	Plots of [DBDS]/[VAc] in the feed vs \bar{X}_n^{-1} and vs $2\bar{X}_w^{-1}$ for the final latexes obtained in the semi-batch soap free emulsion copolymerisation of VAc and Na-AMPS (0.5 mol% wrt VAc), in the presence of varying [DBDS]/[VAc].	205
Figure 4.2.2.10	Plots of Z-Average particle size and PDI vs time for the semi-batch soap free emulsion copolymerisation of VAc and Na-AMPS. Na-AMPS = 0.5 mol% and 0.25 mol% wrt VAc respectively.	207
Figure 4.2.2.11	Cumulative VAc conversion vs time where Na-AMPS = 0.50 mol% and 0.25 mol% wrt VAc, as well as instantaneous VAc conversion vs time where Na-AMPS = 0.50 mol% and 0.25 mol% wrt VAc.	208
Figure 4.2.2.12	SEM image of the final latex formed in the presence of Na-AMPS fed at 0.25 mol% wrt VAc.	208
Figure 4.2.2.13	Structure of the sodium salt of 3-allyloxy-2-hydroxy-1-propanesulfonic acid (Na-AHPSA).	209
Figure 4.2.2.14	Cumulative VAc conversion and instantaneous VAc conversion for the soap free emulsion copolymerisation of VAc and Na-AHPSA/Na-AMPS, in the presence of DBDS ([DBDS]/[VAc] = 4.76×10^{-3}).	210
Figure 4.2.2.15	Plots of Z-Average particle size and PDI vs time for the semi-batch soap free emulsion copolymerisation of VAc and Na-AHPSA. Na-AHPSA = 0.5 mol% and 0.25 mol% wrt VAc respectively. Also included is the data wherein Na-AHPSA was added batchwise.	211
Figure 4.2.2.16	SEM images taken of the final latexes, formed in the presence of 0.5 mol% and 0.25 mol% Na-AHPSA fed alongside VAc, as well as 0.5 mol% Na-AHPSA added batchwise.	212
Figure 4.2.3.1.1	Proposed involvement of surfactant free latex particles in the suspension polymerisation of VCM.	214
Figure 4.2.3.2.1	Example SEM images of freeze fractured PVC particles.	217

II List of Tables

Chapter 1		
Table 1.1.2.2.1	Preexponential factor, A , activation energy, E_a , and the corresponding value for k_p at 60 °C for some common vinyl monomers.	5
Table 1.2.3.1	Reagent quantities employed for the solution polymerisation of VAc in the presence of DDT.	21
Table 1.2.4.1	Chain transfer constants ($C_{tr,S}$) for the free radical polymerisations of VAc in the presence of DDT at 60 °C using CLD approach 1.	28
Table 1.2.4.2	Chain transfer constants ($C_{tr,S}$) for the free radical polymerisations of VAc in the presence of DDT at 60 °C using CLD approach 2.	29

Chapter 2		
Table 2.1.1.1	Values for $k_{tr,S}$ to some common solvents for MMA, Sty and VAc free radical polymerisation at 60 °C.	39
Table 2.1.1.2	Collection of chain transfer agents, and their corresponding $C_{tr,S}$ values in the free radical polymerisation of vinyl acetate.	41
Table 2.2.1.1	Integral values from the ^1H NMR spectra for the protons a, b, c and d defined in Scheme 2.2.1.2, with the values normalised to the integral of proton c at 7.18 ppm.	55
Table 2.2.2.1	Collated rate data for the free radical polymerisation of vinyl acetate in the presence of varying quantities of 1 and 2 . Rate % is reported relative to the experiment in the absence of S.	61
Table 2.2.2.2	Collated MW data from the solution polymerisations in the presence of varying quantities of 1 and 2 , where p is monomer conversion (determined gravimetrically) and M_n , M_w and Đ_M are the number and weight average MWs and the dispersity respectively determined through SEC analysis of the produced polymers after 1 h.	64
Table 2.2.2.3	$C_{tr,S}$ values for both 1 and 2 , determined via the Mayo method using both \overline{X}_n^{-1} and $2\overline{X}_w^{-1}$.	68
Table 2.2.2.4	$C_{tr,S}$ values determined through the Gilbert CLD approach for the low conversion samples of polymerisations of vinyl acetate performed at varying concentrations of 1 and 2 .	71
Table 2.2.2.5	Proposed kinetic scheme for the addition of VAc radicals to disulfides.	72

Chapter 3

Table 3.2.1.1	Rate of polymerisation, R_p for the free radical copolymerisation of VAc and TTT in the presence of DBDS. R_p is determined by fitting a linear relation to the conversion time data points and extracting the slope. The Rate % is calculated relative to the experiment performed at VAc/DBDS/TTT = 100/1/0.	115
Table 3.2.1.2	Monomer conversion, p , number average and weight average MWs (M_n and M_w respectively) and the Mark-Houwink parameters K and α for the 120 mins samples in the series of copolymerisation's of VAc with TTT in the presence of DBDS.	117
Table 3.2.3.1	Rate of polymerisation, R_p for the free radical copolymerisation of VAc and DVA in the presence of DBDS. The Rate % is calculated relative to the experiment performed at VAc/DBDS/DVA = 100/1/0.	122
Table 3.2.3.2	Monomer conversion, p , number average and weight average MWs (M_n and M_w respectively) and the Mark-Houwink parameters K and α for the 120 mins samples in the series of copolymerisations of VAc with DVA in the presence of DBDS.	122
Table 3.2.3.3	Monomer conversion, p , and the corresponding MW distribution parameters M_n and M_w being the number average MW and the weight average MW, and the Mark-Houwink parameters K and α for samples withdrawn from the copolymerisation where VAc/DBDS/DVA = 100/1/1.0.	126
Table 3.2.3.4	Monomer conversion, p , and the corresponding MW distribution parameters M_n and M_w being the number average MW and the weight average MW, as well as the Mark-Houwink parameters K and α for the samples from the homopolymerisation of VAc with 1 mol% DBDS.	127
Table 3.2.4.1	Rate of polymerisation, R_p for the free radical copolymerisation of VAc and BDDVE in the presence of DBDS. The Rate % is calculated relative to the experiment performed at VAc/DBDS/DVA = 100/1/0.	130
Table 3.2.4.2	Monomer conversion, p , number average and weight average MWs (M_n and M_w respectively) and the Mark-Houwink parameters K and α for the 120 mins samples in the series of copolymerisation's of VAc with BDDVE in the presence of DBDS.	130
Table 3.2.4.3	Monomer conversion, p , and the corresponding MW distribution parameters M_n and M_w being the number average MW and the weight average MW, and the Mark-Houwink parameters K and α for samples withdrawn from the copolymerisation where VAc/DBDS/BDDVE = 100/1/1.0.	134
Table 3.2.5.1	MW distribution parameters M_n and M_w being the number average MW, the weight average MW, and the Mark-Houwink parameters K and α for the polymers before hydrolysis (reaction	147

state A) and after hydrolysis and subsequent acetylation (reaction state B).

Chapter 4

Table 4.1.2.1.1	Aqueous free radical reactions possible before radical entry, and their corresponding rates.	167
Table 4.1.2.1.2	Influence of particle size on R_t where 2 radicals are isolated within the particle.	168
Table 4.1.2.2.1	$[M]_{\text{aq,sat}}$, being the saturated monomer concentration in water at 50 °C for some monomers commonly polymerised through emulsion polymerisation.	172
Table 4.2.1.1	Reagent quantities for the modified soap free emulsion copolymerisation of VAc and Na-AMPS.	185
Table 4.2.1.2	pH recorded directly after polymerisation and after 4 months, as well as observations of the latex stability after 4 months for a series of buffer compositions and concentrations.	186
Table 4.2.2.1	Rate of VAc conversion (mol s^{-1}) vs feed rate of VAc (mol s^{-1}) in the semi-batch soap free emulsion copolymerisation of VAc and Na-AMPS (0.5 mol% wrt VAc), with varying concentrations of DBDS in the feed.	194
Table 4.2.2.2	Number average (M_n) and weight average (M_w) molecular weights for the final latexes produced during the semi-batch soap free emulsion copolymerisation of VAc and Na-AMPS (0.5 mol% wrt VAc), in the presence of varying $[\text{DBDS}]/[\text{VAc}]$.	201
Table 4.2.2.3	Molecular weight range of each distribution seen in Figure 4.2.2.8 from which $C_{tr,S}^{app}$ was determined using Gilberts CLD method.	205
Table 4.2.3.1.1	Description of the samples test in S-PVC synthesis.	215
Table 4.2.3.1.2	Summary of the properties of the PVC granules produced in the presence of SYN 2 and the PVAc latexes described in Table 4.2.3.1.1.	216

III List of Schemes

General Introduction

Scheme VII.1	Synthetic scheme describing the production of vinyl acetate through the oxidative addition of acetic acid to ethylene, catalyzed by palladium.	xxv
Scheme VII.2	Depiction of the process of transfer to polymer occurring through the acetoxy protons in vinyl acetate free radical polymerisation, followed by subsequent propagation of the formed radical to form branches.	xxvii

Chapter 1

Scheme 1.1.2.1	Processes involved in free radical polymerisation.	3
Scheme 1.1.2.2.1	Demonstration of the different addition modes for PVAc during propagation.	5
Scheme 1.1.2.4.1	Depiction of the available transfer to polymer modes for PVAc, through extraction of protons from the backbone or through the acetoxy side groups.	8
Scheme 1.1.2.4.2	Mechanism for the chain transfer reaction from a propagating vinyl acetate radical to a thiol.	9

Chapter 2

Scheme 2.1.1.1	Events evolved during chain transfer in free radical polymerisation, specifically chain transfer to species Y-X, and subsequent reinitiation of M by X \cdot .	38
Scheme 2.1.2.1	Proposed mechanism for the chain transfer reaction of VAc to a disulfide.	47
Scheme 2.1.2.2	Proposed mechanism for the chain transfer reaction of VAc to a cyclic disulfide.	48
Scheme 2.1.2.3	Mechanism for the “two component iniferter” reaction in the study by Cho <i>et al.</i> wherein VAc is polymerised in the presence of ACPROL and allyl alcohol, to yield PVAc with hydroxyl groups at each terminus.	51
Scheme 2.2.1.1	Structure of 5-methyl furfural (MFF).	52
Scheme 2.2.1.2	Proposed mechanism for addition to furfuryl rings, suggested by Davidenko and supported through the difference in chain transfer activity between this study and that of Stockmayer.	55

Scheme 2.2.2.1	Structures of the linear disulfides used in this work, dibutyl disulfide and 2-hydroxyethyl disulfide.	60
Scheme 2.2.2.2	Proposed mechanism of addition of a propagating radical to a disulfide.	71
Scheme 2.2.3.1	Reaction mechanism for the conversion of dibutyl disulfide to the corresponding thiosulfinate, through oxidation by m-CPBA.	73
Scheme 2.2.4.1	Reaction mechanism for “copolymerisation” of vinyl acetate with a cyclic disulfide, DL- α -lipoic acid.	75
Scheme 2.2.6.1	Proposed oxidation of the terminal thioether functionality to the corresponding sulfoxide and sulfone.	82

Chapter 3

Scheme 3.1.1.1	Potential copolymerisation processes between propagating radicals and pendant vinyl groups, both intermolecularly and intramolecularly.	97
Scheme 3.2.2.1	Chemical structures for divinyl adipate (DVA) and 1,4-butanediol divinyl ether (BDDVE).	118
Scheme 3.2.2.2	Branched structure of the copolymer of VAc and DVA.	119
Scheme 3.2.2.3	Branched structure of the copolymer of VAc and BDDVE.	119
Scheme 3.2.5.1	Mechanism for the alkaline saponification of PVAc in methanol.	134
Scheme 3.2.5.2	Proposed mechanism for the saponification of the linkages of DVA. This reaction is likely to occur in both polymer and monomer.	135
Scheme 3.2.5.3	Mechanism for the acetylation of poly(vinyl alcohol) to poly(vinyl acetate) utilising acetic anhydride.	145

Chapter 4

Scheme 4.1.2.2.1	Demonstration of the radical formed after transfer to monomer, and the proposed cyclisation to form a butyrolactonyl radical.	171
------------------	---	-----

IV Acknowledgements

During the course of my PhD, I have had the joy of meeting some amazing people, who have all supported me along the way. Be that academic, financial, or personal support, I could not have completed this journey without you all, friends, family, and colleagues, thank you!

I would like to thank Sam Wilson-Whitford, for taking me under his wing back when I was a master's student, and assisting throughout my PhD with knowledge, banter, and lack of ability on a pool table. For learning to let it slide when I use the wrong word for something... eventually! And of course, not making me feel guilty when asking for a lunchtime pint. Thanks for everything! Andrea, for introducing me to Italian culture, and never saying no to a night on the sofa or a night out alike, it means a lot! Pat, for providing the means for me to get semi decent at Mario cart, as well as all of the other adventures we have had over the years, they will not be forgotten. Josh, for being the best hipster housemate anyone could ever ask for, who introduced me to good coffee, inspired my love for craft beer, and gave me an appreciation for the more refined things in life... Although I'm still not convinced by the grapefruit/sausage combination... And Callum, for the fact that no conversation we have ever had has been normal! A special thanks goes to Maria, who not only taught me Italian cookery, but also did her best to convert me into a functioning adult, hopefully I have done you proud. Sarah for making the best chocolate chip cookies in the land (there just isn't a close second), although I won't miss all the Taylor Swift!

And of course, to the boss Stefan, who went above and beyond his role as academic supervisor, and supported me extensively throughout this roller coaster of a journey, from undergraduate through to PhD thesis submission. You were always up for a laugh when it was appropriate, and never shyed away from socialising with us all. More than this, I have learnt so much from your approach to research, both through your unique ideas and your scientific methodology, and I believe this has made me a better scientist, and given me the confidence to believe in my abilities. And to the rest of the BonLab past and present: Brooke, Ross, Jamie, Wai, Yuan-Zhi, Josh R, Naemah, Chris, Niko, Corinna, Melody, and all of the master's students, a big thank you to you all!


A huge thank you goes to my parents. All of this would not have been possible without your continued support, and I am eternally grateful for all you have done to allow this to happen.

And finally, to Niki, you have been a constant through the last 10 years of my life, and I could not be happier than I am now with you. You have kept me motivated to finish my studies, and I am very much looking forwards to writing Chapter 5 with you! For this I am eternally grateful.

V Declaration

I hereby declare that the work presented in this thesis, submitted for the degree of Doctor of Philosophy at the University of Warwick, consists of my own work. The contents have been produced by myself, and has not been used as part of a previous submission for any degree, excluding the following:

- (i) Chapter 1: The loop extension script used during the Monte-Carlo simulations was written by Nikita L Slade.
- (ii) Chapter 2: The mass spectrometry data obtained for low molecular weight poly(vinyl acetate) was collected by Bryan Marzullo, PhD student in the group of Professor Peter O'Connor at the University of Warwick.
- (iii) Chapter 4: The suspension polymerisations of vinyl chloride, and the analysis of the resultant granules, were performed by Julija Ivanova, Matthew Coulshed and Lauren Payne at Synthomer plc, Harlow, Essex.

Signed.....  Date..... 30/03/21

Print name Mr MATTHEW K DONALD

VI Table of Abbreviations

1,2-PB	1,2-polybutadiene	DVA	Divinyl adipate
AEE	Allyl ethyl ether	DVB	Divinylbenzene
AIBN	Azobisisobutyronitrile	DVE	Divinyl ether
ATRP	Atom transfer radical polymerisation	EDGMA	Ethylene glycol dimethacrylate
BDA	But-2-ene-1,4-diacrylate	EIA	Ethyl iodoacetate
BDDVE	1,4-Butanediol divinyl ether	Et-OAc	Ethyl acetate
BEHM	Bis(2-ethylhexyl) maleate	Et-Sty	Ethyl styrene
BHT	Butylated hydroxytoluene	EVE	Ethyl vinyl ether
CCTP	Catalytic chain transfer polymerisation	FBD	Final bulk density
CLD	Chain length distribution	FID	Flame ionisation detector
CMC	Critical micelle concentration	FS	Flory-Stockmayer
CPA	Cold plasticiser absorption	GC	Gas chromatography
CTA	Chain transfer agent	GSD	Grain size distribution
CTAB	Hexadecyl(trimethyl)ammonium bromide	HEDS	Hydroxyethyl disulfide
DBDS	Di- <i>n</i> -butyl disulfide	IPr	Inlet pressure
DBM	Dibutyl maleate	LPO	Lauryl peroxide
DDT	<i>n</i> -dodecanethiol	LS	Light scatter
DH	Degree of hydrolysis	MA	Methyl acrylate
DLS	Dynamic light scattering	MAIB	Dimethyl 2,2'-azobisisobutyrate
DMAEM	2-(dimethylamino)ethyl methacrylate	MC	Monte Carlo
A		MeOH	Methanol
DMF	N,N-dimethylformamide	MFF	5-methyl furfural
DMSO	Dimethylsulfoxide	MHS	Mark-Houwink-Sakurada
DP	Degree of polymerisation	MM	Multifunctional monomer
DPr	Differential pressure	MMA	Methyl methacrylate
DRI	Differential refractive index	MVM	Multi vinyl monomers
		MW	Molecular weight

MWD	Molecular weight distribution	RDRP	Reversible deactivation radical polymerisation
Na-AHPSA	2-acrylamido-2-methyl-1propanesulfonic acid	SEC	Size exclusion chromatography
Na-AMPS	3-allyloxy-2-hydroxypropane sulfonate	SEM	Scanning electron microscopy
NIPAm	N-isopropylacrylamide	S-PVC	Suspension PVC
NMR	Nuclear magnetic resonance	Sty	Styrene
ODTCH	1-oxa-4,5-dithia-cycloheptane	THF	Tetrahydrofuran
PTFE	poly(tetrafluoroethylene)	TSC	Total solids content
PVAc	Poly(vinyl acetate)	TTT	1,3,5-triallyl-1,3,5-triazine-2,4,6(1H,3H,5H)-trione
PVC	Poly(vinyl chloride)	UV	Ultraviolet
PVOH	Poly(vinyl alcohol)	VAc	Vinyl acetate
RAFT	Reversible addition-fragmentation chain transfer	VCM	Vinyl chloride
RBF	Round bottomed flask	VDW	Van Der Waals
		VS	Viscometry

VII General Introduction

Polyvinyl chloride (PVC) is a widely used material across a range of applications, such as piping, window frames, blood bags and food packaging. PVC is the third most widely produced synthetic polymer worldwide,¹ and around 80 % of all PVC production is via suspension polymerisation.² The production of PVC through suspension polymerisation yields polymeric granules, which are typically then processed via extrusion into the desired product, which in its pure form is a rigid and brittle material.

The glass transition temperature (T_g) is a good measure for the physical properties of an amorphous polymeric material, such as PVC, where the chains are heavily intertwined in random orientations. As per the definition set out by the International union of pure and applied chemistry (IUPAC), conformational changes of segments of the polymer chain become infinitely slow below T_g , resulting in a glassy, brittle material.³ Above T_g , the constituent segments possess enough thermal energy to rotate and vibrate, leading to a rubbery, viscous material. The rigidity of PVC is reflected in its high glass transition temperature ($T_g = 80\text{ }^\circ\text{C}$).⁴ Introduction of plasticisers, such as phthalates,^{5,6} increases the free volume available to each chain, and consequently reduce the energy required to undergo conformational changes, reducing T_g and ultimately allowing the mechanical properties to be tuned. As a direct example, Beirnes and Burns found that when blending di-octyl phthalate (DOP) with PVC, at a weight fraction of 17 %, T_g dropped to $\approx 19\text{ }^\circ\text{C}$, and at a weight fraction of 29 % T_g dropped even further to $\approx -23\text{ }^\circ\text{C}$.⁷

Plasticizer incorporation is thought to occur in two stages.⁸ Firstly, the plasticizer enters the granule structure, governed by capillary forces, and promoted by the porosity of the granule. Secondly, the plasticizer diffuses from the voids into the polymer matrix. These additives are typically introduced during polymer processing at elevated temperatures to aid with incorporation, but mainly to speed up the diffusion, with the processing typically occurring at temperatures $\gg T_g$. Other additives such as: heat stabilizers, fillers and lubricants can also influence the properties of the resultant resin, and therefore broaden the range of applications in which PVC may be used. One key consideration in the synthesis of PVC is the toxicity and difficulty in handling the monomer, vinyl chloride monomer (VCM), which is highly carcinogenic

and is gaseous under atmospheric condition. This leads to the requirement that unreacted monomer is removed after polymerisation. The polymerisation is performed under pressure, typically at 8-10 bar, in order to have the monomer in liquid form. This adds further safety concerns and potentially hazardous implications to the synthesis. Infact, such is the potential severity of any accidents which may occur under these pressures, the vessels in which polymerisation is performed must conform to strict regulations, notably the pressure equipment safety regulations (PESR, 2016). The necessary conformance with these regulations, and the associated hazards in handling the materials, often restrict study of VCM suspension polymerisation to industrial laboratories.

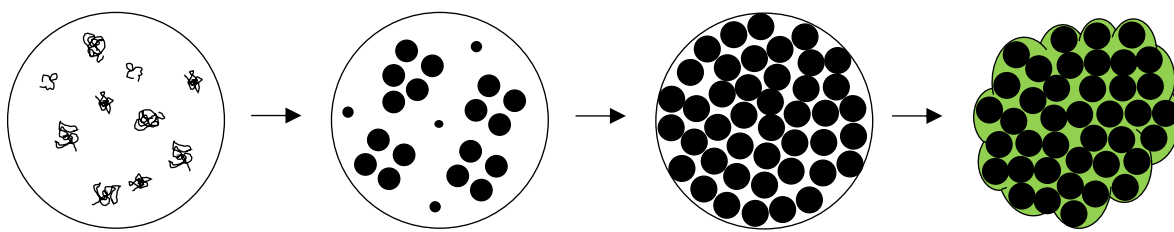


Figure VII.1: Schematic representation of the suspension polymerisation of VCM.

During the suspension polymerisation of VCM, precipitation of polymer chains occurs inside the monomer droplets due to the polymer, PVC, being insoluble in the monomer. As polymerisation proceeds these precipitated chains aggregate and grow, forming a continuous network of particles throughout the VCM droplet. As is depicted in Figure VII.1, the result of this mechanism is a PVC granule which is highly porous, with the porosity influenced by the stability of the precipitating chains and subsequent aggregates. A stabiliser can be used to impart stability to the aggregates, and therefore influence the final porosity of the granule.⁹ This porosity is a desirable quality, as not only does it aid with the removal of residual monomer, but it also facilitates the incorporation of the aforementioned additives, therefore a good stabiliser is a necessary component in the formulation. Poly(vinyl acetate) (PVAc)/poly(vinyl alcohol) (PVOH) copolymers are commonly used as stabilizers for this purpose.¹⁰⁻¹² Copolymers with high hydroxyl contents (typically > 70 %) are used as primary stabilizers, residing at the interface of the VCM droplet, influencing the overall size and resistance to coalescence. Additionally, during polymerisation, a skin is formed around the droplet, which is a graft copolymer between PVC and the PVAc/PVOH copolymer. This skin contributes to the overall colloidal stability of the polymerizing droplet, but also acts as a scaffold for the droplet, which commonly infills pores as

the droplet contracts, and can give the granules a popcorn like appearance. Copolymers with low hydroxyl contents (typically < 55 mol% acetate)¹³ are used as secondary stabilizers, partitioning more into the droplet, and influencing the stability of the precipitating aggregates, and consequently the porosity of the final granule. These PVAc/PVOH copolymers are typically formed through multi step processes, first through synthesis of PVAc in solution polymerisation, and then a subsequent saponification to the desired hydroxyl content (otherwise referred to as the degree of hydrolysis, DH). This brings us to the initial purpose of this body of work: is it possible to produce PVAc stabilizers using a more efficient process?

The main idea was to see if emulsion polymerisation could be used in place of solution polymerisation to prepare PVAc polymers suitable to be used as stabilizers. Emulsion polymerisation has a number of advantages over solution polymerisation in that it does not use an organic solvent, water as polymerisation medium has a high heat capacity lowering the risk of a thermal runaway, the product is a polymer latex with a low viscosity, and compartmentalization of radicals can lead to fast polymerisation and access to high molecular weight. It is proposed that the use of a polymerisable surfactant (to be discussed in Chapter 4) during the emulsion polymerisation will impart stability to the latex and enable control of the particle size. Introduction of these latex particles into the suspension polymerisation of VCM may impart a stabilizing effect. Importantly, the aforementioned stabilizing moieties, introduced through copolymerisation with a polymerizable surfactant, could offer some interesting interfacial activity during the suspension polymerisation of VCM, beyond that observed with PVAc/PVOH copolymers produced through solution polymerisation. It may then be possible to produce a stabiliser which contributes both to the stability of the VCM droplet, as well as the precipitating aggregates, in one step, without the need to selectively hydrolyse the PVAc and combine products of differing compositions, making this a very attractive solution.

Collision of a latex particle of this nature with a droplet of VCM would likely result in wetting of the latex particle with VCM, and subsequent swelling due to the compatibility with PVAc. Suppose that this particle then swells with VCM to such an extent that it disintegrates into its constituent chains. Depending on the functionality, molecular weight, and architecture of the polymer chain, it could then migrate to the droplet interface, or be withdrawn into the droplet and influence the internal morphology during polymerisation by stabilizing the precipitating PVC aggregates. By introducing a hydrophilic comonomer into the formulation, the initial latex

will achieve colloidal stability, however, once introduced to an emulsion of VCM droplets in water, the charged residues could facilitate the polymer chain's ability to stabilize monomer droplets, or indeed PVC aggregates during polymerisation. With one step, both the stability and grain size, as well as the porosity of PVC granules, may be influenced, removing the need for subsequent hydrolysis and purification.

It is important to carefully consider the architectural design of the PVAc (Figure VII.1) based macromolecules. Not only are the average molecular weights and the molecular weight distribution important, the chemical composition of each polymer chain, more specifically the sequence of repeat units (being acetate, alcohol, or when comonomers are used other moieties), and the chemistry of the chain ends, together with the chain topology (here linear or branched) will collectively determine the physical properties and behavior. PVAc itself is a relatively soft ($T_g = 31.4\text{ }^\circ\text{C}$)¹⁴ and polar polymer, which leads to its widespread application in coatings and adhesives, however, the free radical polymerisation (FRP) of vinyl acetate (VAc) is not a trivial process, with the polymer radical exhibiting extreme reactivity which results in some unusual behaviours.¹⁵⁻¹⁷ Also, its alcohol counterpart (PVOH) (Figure VII.1) is in high demand, and is particularly useful for applications such as textile sizing¹⁸⁻²⁰ and the production of fibers.²¹⁻²³ PVOH is the most widely produced synthetic water-soluble polymer worldwide (the structures of both polymers are given in Figure VII.1).²⁴ The necessity to saponify PVAc to form PVOH^{25,26} (due to vinyl alcohol tautomerizing to acetaldehyde)^{27,28} has led to a large demand for PVAc, and the demand has led to interest both commercially and academically. The interest is also fueled by the reactivity of the PVAc radical, which leads to fast reactions times, but also to some abnormal behaviors during FRP.

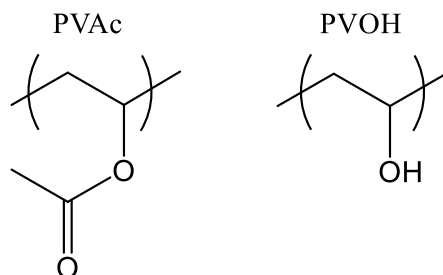
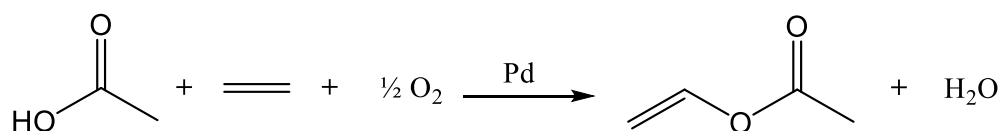


Figure VII.2: Chemical structures of poly(vinyl acetate) (PVAc) and poly(vinyl alcohol) (PVOH).

A process to synthesize VAc was described in a 1914 patent by Klatte,²⁹ wherein the reaction of acetylene with acetic acid was detailed, catalyzed by a mercury salt. This synthesis route was improved upon in the 1960s, through the oxidative addition of acetic acid to ethylene (as per Scheme VII.1) with the aid of catalysts such as palladium complexes, which was found to be a much more cost efficient approach and is the main process used today.^{30,31}

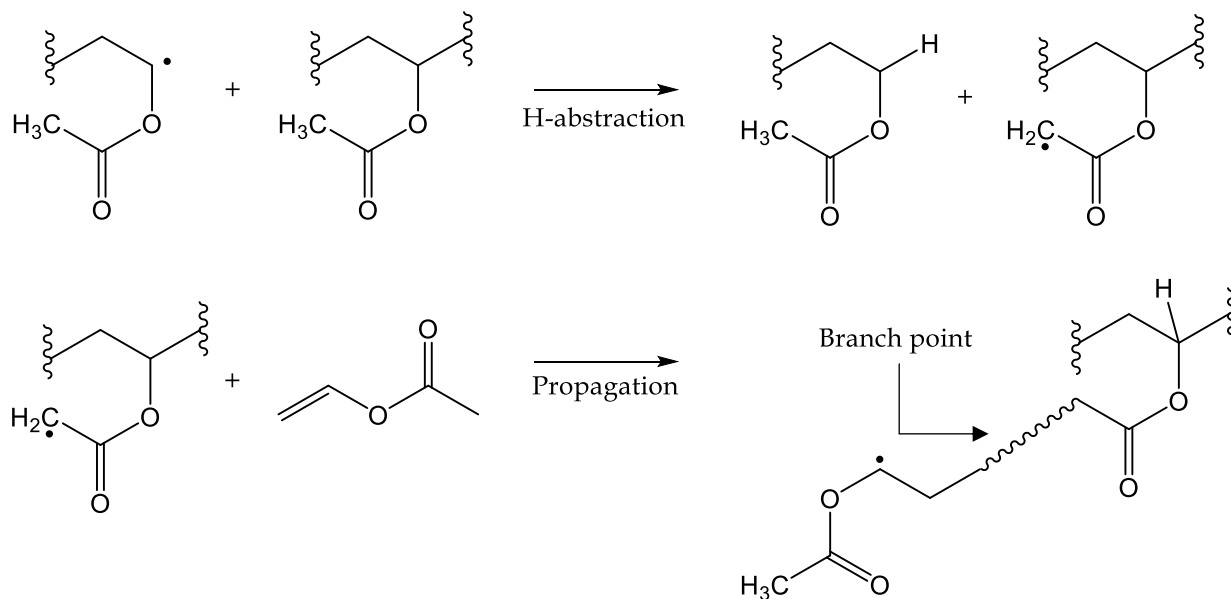


Scheme VII.1: Synthetic scheme describing the production of vinyl acetate through the oxidative addition of acetic acid to ethylene, catalyzed by palladium.

As previously mentioned, polymerisation most commonly occurs through free radical solution or emulsion polymerisation. Unlike other monomers polymerized through FRP, such as styrene, or the methacrylic monomers, the radical formed during polymerisation lacks stability through delocalization/resonance, and as a result is particularly reactive. This leads to high rates of propagation and susceptibility to chain transfer. The propagation rate constant, k_p , for VAc is particularly high at 8548 L mol⁻¹ s⁻¹ at 60 °C,³² particularly when compared to other monomers polymerized through FRP such as styrene (341 L mol⁻¹ s⁻¹)³³ and methyl methacrylate (822 L mol⁻¹ s⁻¹)³⁴. The high rate of propagation, and consequently the high rate of polymerisation, can lead to issues with thermal run away, although this makes it attractive as a commercial polymer, and as such the benefits of emulsion polymerisation mean it is a commonly applied technique to produce PVAc. The high reactivity of the polymeric radical also results in some abnormal behaviors, such as the prevalence of head addition, which will be covered extensively in Chapter 1.

The instability of the polymeric radical deems it particularly susceptible to chain transfer, including transfer to polymer ($C_{polymer} = 7 \times 10^{-4}$ at 60 °C)³⁵. Transfer to polymer has been shown to occur primarily through the acetoxy protons of the side groups instead of the backbone,³⁶⁻³⁸ which is due to the radical formed at the acetoxy position achieving stability through resonance with the C=O group.³⁸ The consequence of this transfer reaction is the formation of a macroradical capable of undergoing further polymerisation, which can lead to a non-linear topology (as per Scheme VII.2). Crucially, the rate of chain transfer to polymer is proportional to the polymer

concentration. During emulsion polymerisation the polymer concentration is particularly high, especially at high overall monomer conversion, or during a starved fed reaction, as polymerisation primarily occurs in a polymer rich particle phase. This can lead to highly branched, or even cross-linked particles of PVAc if no efforts are taken to reduce the molecular weight. Similarly, transfer to monomer is also a prevalent reaction pathway ($C_M = 2.5 \times 10^{-4}$ at 60 °C)³⁹, again proceeding through abstraction of acetoxy protons. Again, this value is significant compared to that for other monomers such as styrene ($C_M = 6.0 \times 10^{-5}$ at 60 °C)⁴⁰ or methyl methacrylate ($C_M = 7.0 \times 10^{-6}$ at 60 °C).⁴¹ Transfer to monomer is most prevalent at low monomer conversion, where the concentration of monomer remains high. In the case of transfer to monomer in emulsion polymerisation, the monomeric radical can undergo exit from the particle and terminate in the water phase, which can have a bearing on the kinetics of the polymerisation (to be covered in chapter 4). The potential for cross-linking due to transfer to polymer may be catastrophic to the proposed action of these latexes as stabilizers, as disintegration of the latex particle into its constituent chains is desired when swollen in VCM. Therefore, reducing the molecular weight, and thereby reducing the number of cross links/branch points per polymer chain was deemed essential. To achieve this, it is important to consider that the formation of a polymer chain is a statistical process, and is highly influenced by the constituent steps, being initiation, propagation, chain transfer, and termination. The interplay between the kinetics of each of these processes dictate the number of monomer units per polymer chain (and therefore the molecular weight), and with an intimate knowledge of each, it is possible to conceive of methods to influence the individual processes, and therefore influence the molecular weight and properties of the polymer.



Scheme VII.2: Depiction of the process of transfer to polymer occurring through the acetoxy protons in vinyl acetate free radical polymerisation, followed by subsequent propagation of the formed radical to form branches.

Mayo was the first to consider the kinetic chain length, δ , of a polymer chain as the ratio of the rate of chain growth and the rate of chain death, as per Equation VII. 1.⁴² Here, the rate of chain growth is simply the rate of propagation (R_p), and the rate of chain death is the summation of the rates of termination (R_t) and chain transfer (R_{ct}), all of which can be described by the corresponding rate laws:

$$\delta = \bar{X}_n = \frac{R_p}{R_t + R_{ct}} = \frac{k_p [M][R]}{2 k_t [R]^2 + k_{tr,S} [S][R]} \quad (\text{VII. 1})$$

where \bar{X}_n is the number average degree of polymerisation, k_p , k_t and $k_{tr,S}$ are the rate coefficients of propagation, termination, and chain transfer respectively, and $[M]$, $[S]$ and $[R]$ are the concentrations of monomer, chain transfer agent (CTA) and radical species, respectively. It is now logical to suggest that a reduction in δ can be achieved via an increase in the rate of chain death or a decrease in the rate of chain growth. For example, if we consider a system in the absence of chain transfer, a decrease in $[M]$ or an increase in $[R]$ would result in a decrease in δ . Alternatively, δ can be reduced through introduction of a CTA, where the concentration and the value of $k_{tr,S}$ governs the extent of the reduction.

Mayo proceeded to invert Equation VII. 1,⁴² allowing a linear relation to emerge, and to isolate the contributions of CTAs to δ :

$$\frac{1}{\delta} = \frac{1}{\bar{X}_n} = \frac{2 k_t [R]^2 + k_{tr,S} [S][R]}{k_p [M][R]} = \frac{1}{\bar{X}_{n,t}} + C_{tr,S} \frac{[S]}{[M]} \quad (\text{VII. 2})$$

Mayo defined the slope of this linear plot as the chain transfer constant ($C_{tr,S}$) being the ratio $k_{tr,S}/k_p$, and $\bar{X}_{n,t}$ being the number average degree of polymerisation in the absence of chain transfer, i.e. chains formed through bimolecular termination.

The process of chain transfer does not influence the overall radical concentration, and assuming reinitiation is fast, does not influence the rate of polymerisation. The value of $C_{tr,S}$ for most systems can be measured trivially by performing a series of polymerisations at different $[S]/[M]$, and measuring \bar{X}_n (most commonly through size exclusion chromatography). These results can then be plotted in the form of Equation VII. 2, and the value of $C_{tr,S}$ extracted from the slope. However, as will be covered at length in Chapter 1, this is not the case for systems where $k_{tr,S} \gg k_p$, i.e. where $C_{tr,S} \gg 1$. For this work, the use of conventional thiol CTAs was first explored, as they are the most widely used in the FRP of VAc. It was noted that the values for $C_{tr,S} \gg 1$, with values of 48 and 260 previously measured for *n*-butanethiol⁴³ and 2-mercaptoethanol⁴⁴ respectively (using alternate cumulative methods).

The issue with Mayo's equation is the assumption that the measured value of \bar{X}_n is its instantaneous value, i.e. the distribution is that formed at the exact value of $[S]/[M]$ defined. This is a reasonable assumption when $C_{tr,S} \approx 1$ and when the polymerisation is halted at low monomer conversion, i.e. the ratio $[S]/[M]$ remains essentially unchanged. The relationship between $[S]/[M]$, monomer conversion and $C_{tr,S}$ was described by Smith in 1946⁴⁵:

$$\frac{[S]}{[M]} = \frac{[S]_{p=0}}{[M]_{p=0}} (1 - p)^{C_{tr,S}-1} \quad (\text{VII. 3})$$

where p is monomer conversion, and the subscript $p = 0$ denotes the starting concentration of the corresponding reagent. When $C_{tr,S} \gg 1$, substantial drift in $[S]/[M]$ will occur. It should be clear that when sampling a polymerisation reaction, the sample contains polymer chains formed from the start of the reaction to the sample time. If $[S]/[M]$ does change significantly, the obtained cumulative molecular weight distribution, and the corresponding value of \bar{X}_n , can no longer be

assumed to be equal to the instantaneous values, and as a result a dramatic error is introduced into the calculation. For example, running an experiment at $[S]_{p=0}/[M]_{p=0} = 1 \times 10^{-2}$, where $C_{tr,S} = 200$, if a sample were to be taken at $p = 0.01$, the value of $[S]/[M]$ would have dropped to 1.35×10^{-3} , which correlates to 13.53 % of the starting ratio. This would result in huge errors in the application of Equation VII.2, despite the low conversion value which is often deemed good experimental protocol. The chain length distribution method developed by Gilbert and coworkers (the specifics of which will be covered in Chapter 1) suffers from a similar issue,⁴⁶⁻⁴⁸ in that the molecular weight distribution must be assumed to be its instantaneous value.

The kinetics of the chain transfer process, specifically for transfer from PVAc to a thiol, are explored in Chapter 1, to understand the influence of a thiol on the polymerisation and assess the suitability for use in the final formulation. An overview of the methods commonly used to measure $C_{tr,S}$ will be given, and their shortcomings put into context. Through necessity, this will then lead to the development of a new method to determine $C_{tr,S}$ from cumulative molecular weight data, which can be applied to systems where $C_{tr,S} \gg 1$ by accounting for the variation of $[S]/[M]$ with p . This new method is then validated *in silico*, and subsequently applied to experimental data to determine $C_{tr,S}$ for *n*-dodecanethiol in VAc FRP at 333.15 K.

The measurement of $C_{tr,S}$ will highlight the potential difficulties in the use of thiols as CTAs in VAc FRP. A CTA with a value of $C_{tr,S}$ closer to unity would reduce these issues and finding such a species is the main goal of Chapter 2. One class of compounds which had great potential were disulfides. Disulfides were found to possess chain transfer constants close to unity in previous works,^{39,49} but also, as they are “bis-type” CTAs, the resultant polymers were thought to be telechelic.⁴⁹⁻⁵¹ This was a very attractive additional behavior and may provide interesting applications in future studies. Chapter 2 demonstrates the measurement of the chain transfer constants of these species, using the instantaneous approaches outlined by Mayo and Gilbert with low conversion samples, due to $C_{tr,S}$ being so much closer to unity. Also included is the previously unexplored kinetics of the polymerisations, demonstrating some unexpected behavior, drawing into question the mechanism through which the chain transfer step occurs. Further to this, direct analysis of the end groups is provided by mass spectrometry, proving the telechelic structure. The measured values of $C_{tr,S}$ are close to unity, and as such the molecular weight distribution is less subject to drift with increasing monomer conversion, opening the doors to applications where control of the molecular weight distribution is important.

Molecular architecture can also influence the properties of a polymer. For example, measurable differences in solubility, solution viscosity, rheological properties and significant end group functionality have all been demonstrated when changing polymer topology.⁵²⁻⁵⁷ One common method to obtain non-linear architectures in FRP is to introduce branch points via a multi-functional comonomer, or so called multi vinyl monomer (MVM). Copolymerisation with MVMs was explored extensively in the 1930s-1950s, with systems such as styrene/divinyl benzene.⁵⁸⁻⁶³ The production of polymers with unreacted vinyl groups leads to the potential for intermolecular addition, and if allowed to proceed to high enough conversion, results in gelation. To delay macro-gel formation, and therefore produce highly branched polymer chains, the number of cross links per polymer chain must be reduced. One approach may be to reduce the rate of polymerisation through introduction of a retarder.⁶⁴ Similarly, increasing the initiator concentration will result in an increase in the rate of termination, and consequently reduce the molecular weight, whilst also introducing chain end functionality.⁶⁵⁻⁶⁷ Alternatively, and more commonly, the use of a CTA can reduce the molecular weight and consequently delay/prevent macro gel formation.⁶⁸⁻⁷⁶ Again, this process will produce polymers with a more defined degree of polymerisation and topology when a CTA with a value for $C_{tr,S}$ close to unity is used, therefore this was an interesting avenue to explore once the potential of disulfide CTAs was realized.

The potential applications of branched PVAc/PVOH are discussed in Chapter 3, and a comprehensive literature survey is provided to demonstrate the difficulties in controlling architecture in such a reactive system. Although other methods are discussed, copolymerisation with an MVM was deemed the most trivial approach, which leads to a discussion of the kinetics of the copolymerisation of VAc with a range of MVMs. di-*n*-butyl disulfide (DBDS) is used as CTA to reduce molecular weight and prevent macrogelation, with the additional caveat of introducing thioether groups at the end of each branch that is terminated via chain transfer. Vially, proof that the approach produced branched polymers is provided through dual detection size exclusion chromatography. To the best of the authors knowledge, this is the first data presented on the production of branched PVAc, using a combination of an MVM and a CTA, wherein significant drift in the ratio $[S]/[M]$ is avoided due to the CTA selection, and as such, is a particularly attractive approach to produce said polymers, and the corresponding PVOHs on a commercial basis.

After consideration of molecular weight and architectural control in solution, Chapter 4 moves onto the optimization of the colloidal formulation. Firstly, a simple formulation is conceived, which includes buffers to regulate pH (to minimize the hydrolysis of PVAc), and a charged comonomer to offer colloidal stability. One key observation in the process is the emulsion polymerisation of VAc is not trivial, again due in part to the high reactivity of the polymeric radical, but also due to the high-water solubility of the monomer. This water solubility results in significant aqueous polymerisation and can lead to radical exit after transfer to monomer. It is demonstrated that without the use of a CTA, molecular weight distributions cannot be measured due to gelation of the polymer particles.

Given the demonstrated benefits of using DBDS as CTA, this was then applied to the emulsion copolymerisation. The influence of DBDS on the kinetics, particle size and molecular weight distributions are all discussed as part of this study. The implementation of a CTA is not a trivial addition, as the CTA derived radical can itself be relatively hydrophilic which can promote further radical exit, and therefore may have a significant bearing on the course of the polymerisation. Importantly however, it will be demonstrated that application of these CTAs leads to prevention of particle gelation and allows the molecular weight distribution to be shifted dependent on the CTA concentration applied. Latexes formed with different charged comonomers, and different molecular weights are then tested as stabilizers in the suspension polymerisation of PVC, and the properties of the resultant PVC granules are compared to those formed using conventional stabilizers.

It is hoped that the content of this thesis will advance the understanding of the FRP of VAc, particularly in mediating the molecular weight utilizing sulfur containing CTAs. It will be demonstrated that applications which require a molecular weight reduction will benefit greatly from a CTA which will limit drift in the molecular weight distribution as a function of monomer conversion. The two applications demonstrated, being production of highly branched PVAc and production of soap free PVAc latexes for use as stabilizers, are just a few examples of where this chemistry can be applied to great effect. The use of bis-type CTAs is demonstrated, although not exploited fully herein, and opportunities to introduce a great deal more functionality into the polymers is a certain possibility, with this work hopefully inspiring further studies in this area.

References

- 1 Y. Saeki and T. Emura, *Prog. Polym. Sci.*, 2002, **27**, 2055–2131.
- 2 M. V. Titow, *PVC Technology*, Springer Science & Business Media, London, 1984.
- 3 M. Hess, G. Allegra, J. He, K. Horie, J. S. Kim, S. V. Meille, V. Metanovski, G. Moad, R. F. T. Stepto, M. Vert and J. Vohlídal, *Pure Appl. Chem*, 2013, **85**, 1017–1046.
- 4 F. P. Reding, E. R. Walter and F. J. Welch, *J. Polym. Sci.*, 1962, **56**, 225–231.
- 5 M. Rahman and C. S. Brazel, *Prog. Polym.*, 2004, **29**, 1223–1248.
- 6 D. L. Buszard, in *PVC Technology*, 1984, pp. 181–213.
- 7 K. J. Beirnes and C. M. Burns, *J. Appl. Polym. Sci.*, 1986, **31**, 2561–2567.
- 8 J. A. Wingrave, *J. Vinyl Addit. Technol.*, 1980, **2**, 204–208.
- 9 R. Darvishi, M. N. Esfahany and R. Bagheri, *Ind. Eng. Chem. Res.*, 2015, **54**, 10953–10963.
- 10 M. Zerfa, *PhD Thesis, Univ. Loughbrgh.*, 1994, 292.
- 11 H. Nilsson, T. Norviit, C. Silvegren and B. Tornell, *J. Vinyl Technol.*, 1985, **7**, 119–122.
- 12 D. E. Witenhafer and J. A. Davidson, *J. Polym. Sci. Phys. Ed.*, 1980, **18**, 51–69.
- 13 S. Ormondroyd, *Br. Polym. J.*, 1988, **20**, 353–359.
- 14 T. Sato and T. Okaya, *Polym. J.*, 1992, **24**, 849–856.
- 15 K. Kolter, A. Dashevsky, M. Irfan and R. Bodmeier, *Int. J. Pharm.*, 2013, **457**, 470–479.
- 16 S. Ebnesajjad, *Adhesives Technology Handbook, 2nd ed*, 2008.
- 17 A. Kaboorani and B. Riedl, *Compos. Part A Appl. Sci. Manuf.*, 2011, **42**, 1031–1039.
- 18 F. L. Marten, *US Patent 4844709*, 1989.
- 19 H. K. Inskip and R. L. Adelman, *US Patent 3689469*, 1972.
- 20 R. Rees, *US Patent 4222922*, 1980.
- 21 F. Sharifi, Z. Bai, R. Montazami and N. Hashemi, *RSC Adv.*, 2016, **6**, 55343–55353.

- 22 A. Paknahad, D. G. Petre, S. C. G. Leeuwenburgh and L. J. Sluys, *Acta Biomater.*, 2019, **96**, 582–593.
- 23 B. Ding, H. Y. Kim, S. C. Lee, D. R. Lee and K. J. Choi, *Fibers Polym.*, 2002, **3**, 73–79.
- 24 F. L. Marten, in *Kirk-Othmer Encyclopedia of Chemical Technology*, (Ed.), 2002.
- 25 W. O. Herrmann and W. Haehnel, *Patent 450286*, 1924.
- 26 W. O. Herrmann and W. Haehnel, *Ber. Dtsch. Chem. Ges.*, 1927, **60**, 1658–1663.
- 27 J. M. Hay and D. Lyon, *Nature*, 1967, **216**, 790–791.
- 28 B. Capon, D. S. Rycroft, T. W. Watson and C. Zueco, *J. Am. Chem. Soc.*, 1981, **103**, 1761–1765.
- 29 F. Klatter, *US1084581*, 1914.
- 30 H. Holzrichter, W. Krönig and B. Frenz, *US Patent 3275680*, 1966.
- 31 R. E. Robinson, *US Patent 3190912*, 1965.
- 32 C. Barner-Kowollik, S. Beuermann, M. Buback, R. A. Hutchinson, T. Junkers, H. Kattner, B. Manders, A. N. Nikitin, G. T. Russell and A. M. van Herk, *Macromol. Chem. Phys.*, 2017, **218**, 1600357.
- 33 M. Buback, R. G. Gilbert, R. A. Hutchinson, B. Klumperman, F. -D Kuchta, B. G. Manders, K. F. O’Driscoll, G. T. Russell and J. Schweer, *Macromol. Chem. Phys.*, 1995, **196**, 3267–3280.
- 34 S. Beuermann, M. Buback, T. P. Davis, R. G. Gilbert, R. A. Hutchinson, O. F. Olaj, G. T. Russell, J. Schweer and A. M. Van Herk, *Macromol. Chem. Phys.*, 1997, **198**, 1545–1560.
- 35 G. C. Berry and R. G. Craig, *Polymer.*, 1964, **5**, 19–30.
- 36 W. H. McDowell and W. O. Kenyon, *J. Am. Chem. Soc.*, 1940, **62**, 415–417.
- 37 S. Imoto, J. Ukida and T. Kominami, *Kobunshi Kagaku*, 1957, **14**, 101.
- 38 D. Britton, F. Heatley and P. A. Lovell, *Macromolecules*, 1998, **75**, 2828–2837.
- 39 J. T. Clarke, R. O. Howard and W. H. Stockmayer, *Makromol. Chemie*, 1960, **44**, 427–447.

- 40 A. V Tobolsky and J. Offenbach, *J. Polym. Sci*, 1955, **XVI**, 311–314.
- 41 J. L. O'Brien and F. Gornick, *J. Am. Chem. Soc*, 1955, **77**, 4757–4763.
- 42 F. R. Mayo, *J. Am. Chem. Soc.*, 1943, **65**, 2324–2329.
- 43 C. Walling, *J. Am. Chem. Soc.*, 1948, **70**, 2561–2564.
- 44 T. Sato and T. Okaya, *Makromol. Chem.*, 1993, **173**, 163–173.
- 45 W. V. Smith, *J. Am. Chem. Soc.*, 1946, **68**, 2059–2064.
- 46 R. G. Gilbert, *Emulsion polymerisation: a mechanistic approach*, 1995.
- 47 P. A. Clay and R. G. Gilbert, *Macromolecules*, 1995, **28**, 552–569.
- 48 D. Kukulj, T. P. Davis and R. G. Gilbert, *Macromolecules*, 1998, **31**, 994–999.
- 49 W. H. Stockmayer, R. O. Howard and J. T. Clarke, *J. Am. Chem. Soc.*, 1953, **75**, 1756–1757.
- 50 H. M. Pierson and A. H. Weinstein, *J. Polym. Sci*, 1955, **216**, 221–246.
- 51 A. V Tobolsky and B. Baysal, *J. Am. Chem. Soc.*, 1953, **75**, 1757.
- 52 C. Schubert, C. Osterwinter, C. Tonhauser, M. Schömer, D. Wilms, H. Frey and C. Friedrich, *Macromolecules*, 2016, **49**, 8722–8737.
- 53 C. J. G. Plummer, A. Luciani, T. Q. Nguyen, L. Garamszegi, M. Rodlert and J. A. E. Manson, *Polym. Bull.*, 2002, **49**, 77–84.
- 54 J. R. Dorgan, D. M. Knauss, H. A. Al-Muallem, T. Huang and D. Vlassopoulos, *Macromolecules*, 2003, **36**, 380–388.
- 55 T. H. Mourey, S. R. Turner, M. Rubinstein, J. M. J. Fréchet, C. J. Hawker and K. L. Wooley, *Macromolecules*, 1992, **25**, 2401–2406.
- 56 C. J. Hawker and J. M. J. Fréchet, *J. Chem. Soc. Perkin Trans. 1*, 1992, 2459–2469.
- 57 M. G. McKee, G. L. Wilkes, R. H. Colby and T. E. Long, *Macromolecules*, 2004, **37**, 1760–1767.
- 58 H. Staudinger and W. Heuer, *Ber. Dtsch. Chem. Ges.*, 1934, **67**, 1164–1172.

- 59 H. Staudinger and E. Husemann, *ibid*, 1935, **68**, 1618–1634.
- 60 H. Staudinger and E. Husemann, *Ber. Dtsch. Chem. Ges*, 1935, **68**, 1618–1634.
- 61 K. G. Blaikie and R. N. Crozier, *Ind. Eng. Chem.*, 1936, **28**, 1155–1159.
- 62 R. G. W. Norrish and E. F. Brookman, *Proc. R. Soc. Lond.*, 1937, **A163**, 205–220.
- 63 W. H. Stockmayer, *J. Chem. Phys.*, 1944, **12**, 125.
- 64 T. Sato, N. Sato, M. Seno and T. Hirano, *J. Polym. Sci. Part A Polym. Chem.*, 2003, **41**, 3038–3047.
- 65 T. Sato, K. Nomura, T. Hirano and M. Seno, *Polym. J.*, 2006, **38**, 240–249.
- 66 T. Sato, N. Higashida, T. Hirano and M. Seno, *J. Polym. Sci. A-1 Polym. Chem.*, 2004, **42**, 1609–1617.
- 67 T. Sato, M. Hashimoto, M. Seno and T. Hirano, *Eur. Polym. J.*, 2004, **40**, 273–282.
- 68 H. Chen, K. Ishizu, T. Fukutomi and T. Kakurai, *J. Polym. Sci. A-1 Polym. Chem.*, 1984, **22**, 2123–2130.
- 69 H. Chen, Y. M. Won, K. Ishizu and T. Fukutomi, *Polym. J.*, 1985, **17**, 687–692.
- 70 N. O. Brien, A. Mckee, D. C. Sherrington, A. T. Slark and A. Titterton, *Polymer.*, 2000, **41**, 6027–6031.
- 71 O. Eckardt, B. Wenn, P. Biehl, T. Junkers and F. H. Schacher, *React. Chem. Eng.*, 2017, **2**, 479–486.
- 72 D. L. Popescu and N. V. Tsarevsky, *Macromol. Rapid Commun.*, 2012, **33**, 869–875.
- 73 T. Zhao, H. Zhang, D. Zhou, Y. Gao, Y. Dong, U. Greiser, H. Tai and W. Wang, *RSC Adv.*, 2015, **5**, 33823–33830.
- 74 F. Isaure, P. A. G. Cormack and D. C. Sherrington, *Macromolecules*, 2004, **37**, 2096–2105.
- 75 F. Isaure, P. A. G. Cormack and D. C. Sherrington, *J. Mater. Chem.*, 2003, **13**, 2701–2710.
- 76 P. A. Costello, I. K. Martin, A. T. Slark, D. C. Sherrington and A. Titterton, *Polymer.*, 2002, **43**, 245–254.

1

Chain transfer in vinyl acetate free radical polymerisation

Abstract

Herein vinyl acetate free radical polymerisation is discussed, detailing the key features and nuances. A focus on chain transfer highlights the difficulties of measuring transfer constants in such reactive systems. A new method of determining the chain transfer constant using molecular weight distribution data is proposed. It is specifically designed for systems where its value is substantially greater than 1. In these cases, the classical Mayo equation and Gilbert's chain length distribution method fall short, in that the concentration ratio of chain transfer agent to monomer can no longer be assumed to be constant. Significant composition drift invalidates the use of both. In our new proposed method, the analytical concentration ratio of chain transfer agent to monomer ($t = 0$ s) and monomer conversion data are used in combination with data for the cumulative molecular weight distributions as input. An analytical solution for the cumulative weight distribution was determined, which is used to calculate the cumulative number and chain length distributions. Chain transfer constants are found either by fitting the natural logarithmic chain length distribution data at a given monomer conversion, or by plotting the fitted values for the slopes obtained from the natural logarithmic chain length distribution data at a set degree of polymerization, as a function of monomer conversion. The method is validated by analyses of molecular weight data obtained from Monte Carlo simulations. This methodology was used to determine an experimental value of *ca.* 223 as a chain transfer constant of *n*-dodecanethiol in vinyl acetate free radical polymerization at 333.15 K, which is in excellent agreement with the Smith method.

Publication(s):

Parts of this chapter were reproduced from: M. K. Donald and S. A. F. Bon, *Polym. Chem.*, 2020, **11**, 4281–4289 by permission of The Royal Society of Chemistry.

1.1 Introduction

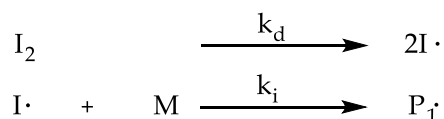
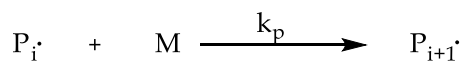
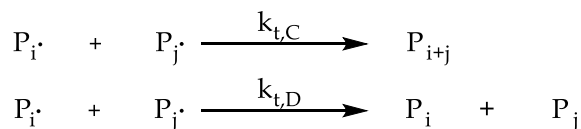
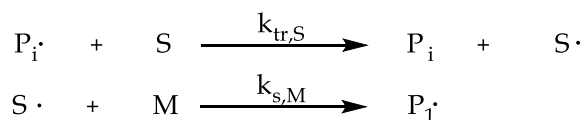
1.1.1 Industrial significance of vinyl acetate/vinyl alcohol.

Vinyl acetate (VAc) is a particularly important vinyl ester monomer, which finds widespread use in industry. The first patent regarding the production of VAc appeared in 1914, wherein the inventors exploited the reaction of acetylene and various acids to produce a variety of vinyl esters.¹ It is commonly polymerised as a precursor to poly(vinyl alcohol) (PVOH), typically via solution polymerisation in methanol. It is required as an intermediate in the production of PVOH due to vinyl alcohol existing in equilibrium with acetaldehyde, with the latter being the favoured tautomer.^{2,3} Typically, the conversion from poly(vinyl acetate) (PVAc) to PVOH occurs through alkaline saponification, a process which was first optimised in a 1924 patent⁴, and later published in 1927 by Herrmann and Haehnel,⁵ and has been adopted with widespread effect in the literature and in industry.

PVOH is an important polymer due to its high modulus and strength,⁶ as well as its alkaline resistance. By volume, it is the most widely produced synthetic water-soluble polymer in the world,⁷ and finds use in textile sizing⁸⁻¹⁰ and production of fibers,¹¹⁻¹³ as well as acting as a stabiliser in heterogenous systems,¹⁴ amongst other applications. PVAc itself is also very useful industrially, and is found in a multitude of products serving many purposes, with the most common being a film forming polymer in coatings¹⁵ and in adhesive formulations.^{16,17}

1.1.2 Free radical polymerisation of vinyl acetate.

The instability of the PVAc radical leads to some unusual behaviours during free radical polymerisation. Scheme 1.1.2.1 shows the processes involved in a free radical polymerisation: initiation, propagation, termination, and chain transfer.

Initiation:**Propagation:****Termination:****Chain Transfer:****Scheme 1.1.2.1:** Processes involved in free radical polymerisation.**1.1.2.1 Initiation**

As seen in Scheme 1.1.2.1, the first step in a free radical polymerisation is the production of an active radical species which can initiate polymerisation. This radical species is generated through decomposition of the initiator, either through thermal decomposition, UV light or chemical reaction. Once this radical species has been generated, it can then undergo addition to the first monomer unit, which in turn signifies the start of a propagating polymer chain. It is important to note that, by their very nature, radical species are particularly unstable, and as such, are prone to an array of side reactions. One important consideration during thermal decomposition is that the primary radicals produced can recombine before escaping the solvent cage.¹⁸ This can result in only a proportion of initiator derived radicals going on to initiate polymer chains. This proportion is described by the initiator efficiency, f , and can be defined as the ratio of the rate of initiation of propagating chains to the rate of initiator disappearance, as expressed in Equation 1.1.2.1.1. Assuming that the decomposition is rate limiting, the rate of initiation, R_i , is shown in Equation 1.1.2.1.2. In these equations, k_i and k_d are the rate coefficients for addition of an initiator derived radical to monomer and the decomposition of initiator respectively (see Scheme 1.1.2.1), and $[I\cdot]$, $[M]$ and $[I_2]$ are the concentrations of initiator derived radicals, monomer, and initiator, respectively.

$$f = \frac{k_i[I\cdot][M]}{2k_d[I_2]} \quad (1.1.2.1.1)$$

$$R_i = 2k_{df}[I_2] \quad (1.1.2.1.2)$$

Two common classes of initiators used in free radical polymerisation are azo-initiators and peroxides, with both commonly used in the free radical polymerisation of VAc. Both classes of initiators exhibit similar behaviours with VAc, which are not commonplace with other vinyl monomers, namely the presence of head addition. Some authors have found up to 20 % of chains initiated by a 2-cyano-2-propyl radical, that derived from decomposition of azobisisobutyronitrile (AIBN), bore end groups resulting from head addition. This was demonstrated by Bevington *et al.* (1987)¹⁹ through nuclear magnetic resonance (NMR) analysis of end groups of PVAc synthesised through solution polymerisation at 60 and 100 °C, in the presence of isotopically labelled AIBN (¹³CN-AIBN). The authors suggested that the tendency for this initiation pathway increased at elevated temperatures.

Similar behaviour has been observed for benzoyl peroxide. Utilising electron paramagnetic resonance, and with the use of a “spin trap” (a molecule which stabilises radicals allowing an increase in lifetime), Solomon *et al.* (1982)²⁰ and Tabner *et al.* (1984)²¹ both independently concluded that addition occurred at a head: tail ratio of 3: 10 at 60 °C. The presence and origin of this head addition phenomena will be discussed further during Section 1.1.1.2 (propagation).

1.1.2.2 Propagation

Subsequent addition of a propagating radical species to more monomer is classified as propagation, as seen in Scheme 1.1.2.1. After addition to monomer, the stability of the newly formed radical plays a large role in determining how quickly this will react further. Typically, propagating radicals which are unstable undergo rapid addition to further monomer, and as such have a large rate coefficient for propagation, k_p .

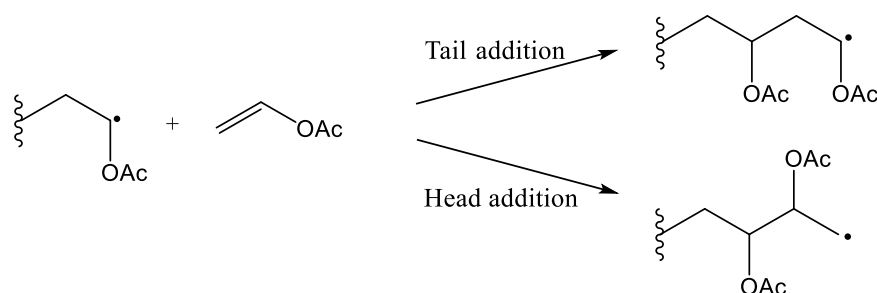
During pulsed-laser polymerisation experiments, Van Herk *et al.* (2017) found a pre-exponential factor, A , and an activation energy, E_a of $1.35 \times 10^7 \text{ L mol}^{-1} \text{ s}^{-1}$ and 20.4 kJ mol^{-1} respectively for k_p in VAc free radical polymerisation.²² This leads to a value for k_p of $8548 \text{ L mol}^{-1} \text{ s}^{-1}$ at 333.15 K, which is in line with that reported by others.²³ Comparing this to literature values for other common vinyl monomers, as seen in Table 1.1.2.2.1, clearly demonstrates this

high reactivity, exceeding the value for styrene and methyl methacrylate by an order of magnitude.

Table 1.1.2.2.1: Preexponential factor, A , activation energy, E_a , and the corresponding value for k_p at 60 °C for some common vinyl monomers.

Monomer	k_p (60 °C) L mol ⁻¹ s ⁻¹	A L mol ⁻¹ s ⁻¹	E_a kJ mol ⁻¹	Ref
Vinyl acetate	8 548	1.35 × 10 ⁷	20.4	22
Methyl acrylate	27 340	1.41 × 10 ⁷	17.3	68
Styrene	341	4.27 × 10 ⁷	32.5	69
Methyl methacrylate	822	2.67 × 10 ⁶	22.4	70
Acrylonitrile	6892	1.79 × 10 ⁶	15.4	71

One consequence of this high reactivity is 1-2 % of VAc monomer additions proceed through head addition, whereas most other monomers proceed almost exclusively through tail addition.²⁴ The products of both head and tail addition can be seen in Scheme 1.1.2.2.1. This behaviour was originally revealed when Flory and Leutner (1948)²⁵ hydrolysed PVAc to PVOH. The authors then subjected the resultant polymer to periodate cleavage to reveal the number of 1,2-glycol units. Upon analysis of the polymer, these 1,2-glycol units are most commonly found at the end of chains, suggesting that the corresponding radical is unlikely to propagate further, and instead undergoes transfer/termination. The radical derived from tail addition to VAc experiences less stabilisation through resonance/inductive effects than is seen for other vinyl monomers, hence is at more risk of head addition.^{26,27}



Scheme 1.1.2.2.1: Demonstration of the different addition modes for PVAc during propagation.

The microstructure of high molecular weight (MW) PVAc, produced through emulsion polymerisation, has been probed through NMR studies. Analysis of ¹³C NMR spectra led

authors to deduce that in fact an equal number of head-to-head and tail-to-tail additions are observed,^{28,29} further complicating the characterisation of the polymer.

1.1.2.3 Termination

Bimolecular termination occurs when two radicals are removed from the system through either combination or disproportionation. Termination is often overlooked in VAc free radical polymerisation, due to the presence of such high rates of chain transfer, which typically dominate chain killing events (Section 1.1.2.4). Palit *et al.* (1968)³⁰ suggested that during VAc free radical polymerisation, disproportionation was the primary termination pathway, through end group analysis when using an acidic functionalised azo initiator (4,4'-azobis(4-cyanopentanoic acid)). The authors found 0.90 acidic end groups per chain on average, which increased to 0.96 when doubling the initiator concentration. A similar conclusion has been reached by others,³¹ however, these results did not take into account the occurrence of transfer to monomer and/or polymer, and therefore the observations cannot be attributed to disproportionation.

In fact, later work by Bamford *et al.* (1969) was able to correct for this, through use of the gelation technique.³² Here a graft polymer is produced through initiation from a system including a polymeric halogenated compound, being poly(vinyl tichloroacetate), which in the presence of manganese carbonyl complexes (and light) decomposes to yield radical sites on the polymer. These can then initiate monomer, as with a conventional graft polymerisation. Termination through coupling results in crosslinks between chains, however, termination through disproportionation results in branch formation. The times of gelation are compared to those of styrene under conditions where the rate of initiation is well understood. Clearly, the cross-linked systems will gel rapidly, with the time for gelation used to calculate the ratio k_{tD}/k_{tC} , which was calibrated with reference to styrene for which the ratio was assumed to be zero, i.e. termination occurred exclusively through combination. After correcting the gel time for the occurrence of transfer to polymer/monomer, Bamford was able to deduce that in VAc free radical polymerisation, termination occurred entirely through combination.

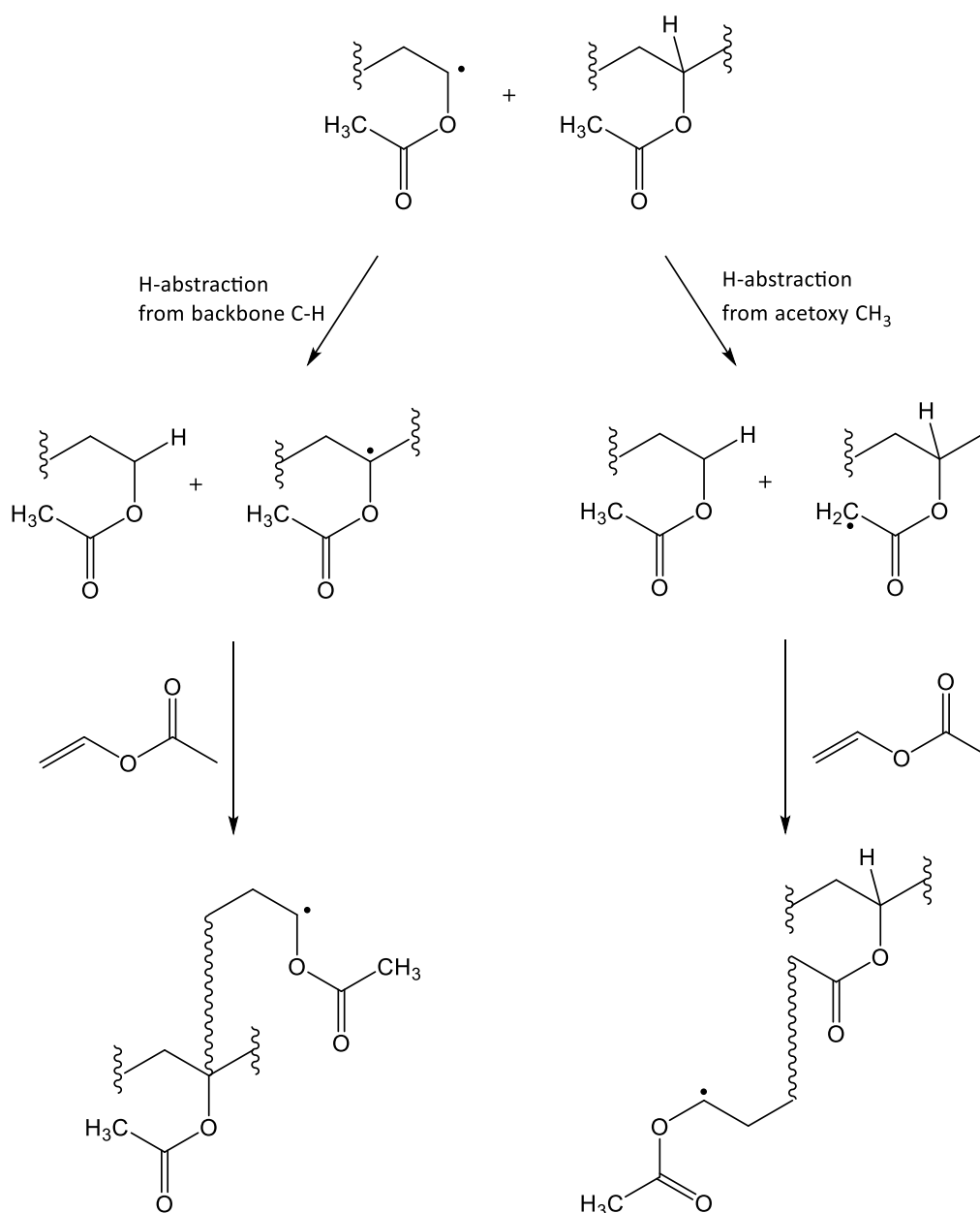
1.1.2.4 Chain transfer

If the radical activity of a propagating chain is transferred to another species, S , the result is a dead chain and a new radical which may then reinitiate through reaction with further monomer. This process, termed chain transfer, has no effect on the radical concentration, and assuming the reinitiation rate coefficient ($k_{s,M}$) is greater than or equal to the propagation rate

coefficient (k_p), no effect on the polymerisation rate. The early death of the chain results in a reduction of the degree of polymerisation (DP), and reinitiation results in the introduction of chain end functionality (chain transfer agent derived moiety). The concept of transfer of a radical species from one molecule to another was first discussed by Taylor and Jones in 1930,³³ before being cemented as a chain-transfer event in free radical polymerization by Flory in 1937.³⁴

As discussed by Stockmayer *et al.* (1960)³⁵ and others,^{36,37} due to the high reactivity of the PVAc derived radical, the presence of many organic species can dramatically reduce the MW of the produced polymer. In cases where the chain transfer agent (CTA) derived radical is more stable than that of PVAc, reinitiation can become unfavourable, and as a result a drop-in polymerisation rate may be observed. In the absence of reinitiation, termination is likely the fate of this radical, decreasing the radical concentration and therefore the polymerisation rate.

VAc radicals can also undergo transfer to monomer and polymer. These processes have been shown to occur through proton abstraction from the acetoxy side groups, producing branch points in the polymer through ester linkages. This was demonstrated in the work by McDowell and Kenyon (1940)³⁸, where the authors noticed a reduction in MW after PVAc was hydrolysed and subsequently reacetylated. Imoto *et al.* (1957) reported the frequency of proton abstraction from the acetoxy protons was greater than 40 times that from the backbone protons.³⁹ Lovell *et al.* (1998)⁴⁰ provided proof for this conjecture through a comprehensive NMR study. Studying the bulk and emulsion homopolymerisation of VAc, the authors were able to deduce that this was the predominant pathway in transfer to polymer reactions, although some evidence of backbone proton extraction was presented. These two transfer pathways can be seen in Scheme 1.1.2.4.1.

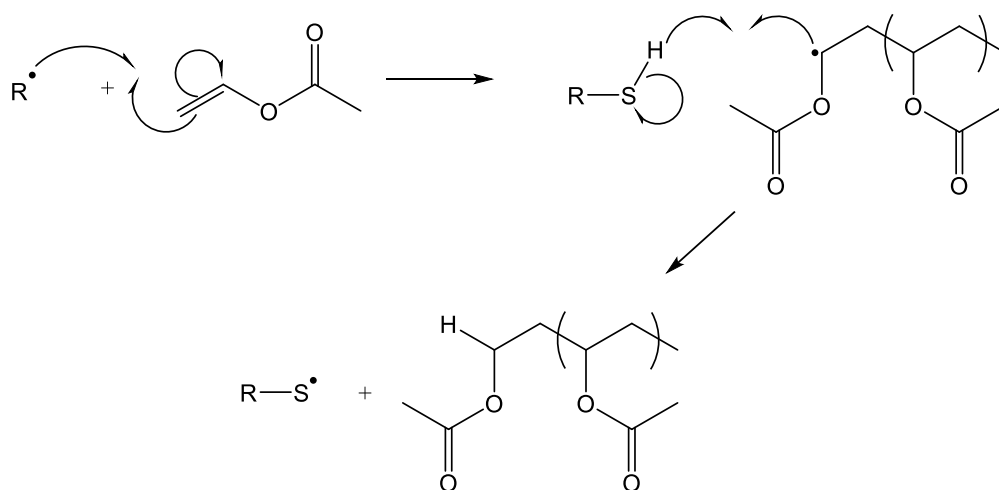


Scheme 1.1.2.4.1: Depiction of the available transfer to polymer modes for PVAc, through extraction of protons from the backbone or through the acetoxy side groups.

Backbone H-abstraction could occur as depicted or could occur intramolecularly (so called backbiting). Unlike the intermolecular transfer processes, backbiting does not transfer the radical activity to another chain, but instead relocates the radical, typically back to a few units from the omega end, resulting in short chain branches, and has been reported in VAc free radical polymerisation.^{41,42} The process of backbiting appears to be favoured by low monomer concentrations, commonly observed either at high monomer conversions or through utilisation of starved monomer feeds.⁴³ The consequence of intermolecular transfer (to monomer or polymer) is the production of long chain branches, and a resultant increase in

MW. If the extent of branching is to be reduced, then a transfer agent can be employed, which reduces the MW and consequently the number of branches per chain. This is particularly vital in heterogeneous polymerisations such as emulsion polymerisation, where the polymer concentration is particularly high.

VAc is commonly polymerised in methanol, which itself can act as a CTA, with a chain transfer constant of 6×10^{-4} at $60\text{ }^{\circ}\text{C}$.³⁵ This is the case with many of the common solvents in which vinyl acetate is polymerised,^{44,45} however, unlike methanol, many common solvents promote significant retardation, reducing the rate of polymerisation.^{35,46} When considering CTAs added specifically to reduce MW, these include aldehydes,³⁶ alcohols,³⁵ chloroform,^{35,45} or most commonly thiols,⁴⁷⁻⁴⁹ amongst others.³⁵ A detailed overview of chain transfer agents and their chain transfer constants will be given in Chapter 2. As seen in Scheme 1.1.2.4.2, chain transfer to thiols occurs through abstraction of the thiol hydrogen atom, producing a dead chain and a thiyl radical.



Scheme 1.1.2.4.2: Mechanism for the chain transfer reaction from a propagating vinyl acetate radical to a thiol.

Despite their widespread use industrially, there is little literature discussing the influence of thiols in vinyl acetate free radical polymerisation. Walling (1948) reported a chain transfer constant for transfer to *n*-butanethiol of 48 ± 14 through use of a radioactive S^{35} tracer for end group analysis.⁵⁰ Sato and Okaya (1993) utilized cumulative intrinsic viscosity data, originally suggested by Smith,⁵¹ to determine a value of 260 for chain transfer to 2-mercaptoethanol.⁵² Given that the chain transfer activity of these two thiols is expected to be comparable, there is clearly some ambiguity in the accuracy of determination. In any case, even if the value for *n*-butanethiol determined by Walling is an underestimation of its true value, a chain transfer

constant of this size is particularly difficult to determine using conventional approaches. These approaches will be discussed, and the issues arising from high chain transfer constants put into context.

1.1.3 Determining chain transfer constants.

1.1.3.1 The Mayo approach

To understand the significance of introducing a CTA into a polymerisation, knowledge of the magnitude of the rate coefficient for transfer to the chain transfer agent, $k_{tr,S}$, is essential. As discussed previously, Mayo undertook a mechanistic study in 1943, and proposed that for transfer dominated systems, the value of the number average degree of polymerisation, \overline{X}_n , that is the number average MW divided by the mass of the repeat unit (ignoring the mass contributions of the end groups), is equal to the rate of chain growth divided by the total rate of chain termination, as seen in Equation 1.1.3.1.1,⁵³ the reciprocal of which is the now famous Mayo equation (Equation 1.1.3.1.2).

$$\delta = \overline{X}_n = \frac{k_p [M] [R]}{2 k_t [R]^2 + k_{tr,S} [S] [R]} \quad (1.1.3.1.1)$$

$$\frac{1}{\delta} = \frac{1}{\overline{X}_n} = \frac{2 k_t [R]^2 + k_{tr,S} [S] [R]}{k_p [M] [R]} = \frac{1}{\overline{X}_{n,t}} + C_{tr,S} \frac{[S]}{[M]} \quad (1.1.3.1.2)$$

In this equation, δ is the kinetic chain length, k_t is the rate coefficient of bimolecular termination, k_p is the rate coefficient of propagation, $k_{tr,S}$ is the rate coefficient of chain transfer to compound S , $[R]$ is the overall radical concentration, $[M]$ is the monomer concentration, and $[S]$ is the concentration of the CTA. It is worth noting that the function of CTA can also be fulfilled by monomer, solvent, or initiator, however chain transfer to another polymer chain invalidates Mayo's expression. Mayo defined a chain transfer constant, $C_{tr,S}$, as the ratio of the rate coefficient of chain transfer to compound S and the rate coefficient of propagation, $k_{tr,S}/k_p$. $\overline{X}_{n,t}$ is the number average degree of polymerization in absence of chain transfer, i.e. polymer chains formed via bimolecular termination.

Mayo demonstrated that it was not necessary to measure any rates, only the number average molecular weight, M_n , at low conversion for a series of experiments at different $[S]/[M]$ ratios. However, the problem with this approach is the definition of "low conversion". How low do the conversions of S and M need to be for this equation to remain valid? This issue was later clarified, stating that $[S]/[M]$ must remain virtually unchanged, so that the degree of

polymerisation measured is essentially its instantaneous value.⁵⁴ Note that the other condition was for δ to be large. Keeping monomer conversion low, for example $< 5\%$, is generally considered to be a valid experimental condition for this approach, and accurate results will be obtained for values of $C_{tr,S} \approx 1$ under these circumstances. However, in cases where the value for the chain transfer constant significantly exceeds 1, a non-avoidable composition drift, expressed as a substantial and continuous drop in $[S]/[M]$, introduces considerable error during analysis.

It is important to consider that the molecular weight distribution (MWD) of a polymer made by free radical polymerization is a cumulative fingerprint for the mechanistic events that occurred throughout the polymerization process. In conventional free radical polymerization an understanding of initiation, propagation, termination, and chain-transfer kinetic events allows not only for an accurate interpretation of the polymerization reaction, but also for constructing a picture on how the polymer chains and thus the cumulative MWD is formed.

Rimmer and Collins (2005) expanded on this when attempting to determine transfer constants for transfer to solvent in VAc free radical polymerisation.⁵⁵ In their work, they differentiated Equation 1.1.3.1.2 with respect to $[S]$ leading to Equation 1.1.3.1.3.

$$\frac{\partial \frac{1}{\bar{X}_n}}{\partial [S]} = C_{tr,S} \frac{[1]}{[M]} \quad (1.1.3.1.3)$$

The value of $\partial(1/\bar{X}_n)/\partial[S]$ can be determined from plots of $1/\bar{X}_n$ vs $[S]$, which are then used to extract values for $C_{tr,S}$. The authors used then used this approach to determine transfer constants to 2-propanol (0.014 ± 0.002) and 2-isopropoxy-1-ethanol (0.016 ± 0.002) at 60°C .

1.1.3.2 The Smith approach

The experimental restriction in the use of Mayo's method was described by Smith in 1946.⁵¹ A beautiful alternative to determine chain transfer constants was described. Smith explained that in a homogenous system, such as a bulk or solution free radical polymerisation, the rate laws governing the disappearance of monomer and chain transfer agent were related to each other as follows:

$$\frac{d[M]}{dt} = -k_p[M][R] \quad (1.1.3.2.1)$$

$$\frac{d[S]}{dt} = -k_{tr,S}[S][R] \quad (1.1.3.2.2)$$

$$\frac{d[S]}{d[M]} = C_{tr,s} \frac{[S]}{[M]} \quad (1.1.3.2.3)$$

$$\frac{d \ln[S]}{d \ln[M]} = C_{tr,s} \quad (1.1.3.2.4)$$

By monitoring the concentrations of monomer and CTA, and plotting them on a log scale, a linear relationship emerges, the slope being the chain transfer constant. Integration leads to Equation 1.1.3.2.5, in which p is the monomer conversion.

$$\frac{[S]}{[M]} = \frac{[S]_{p=0}}{[M]_{p=0}} (1-p)^{C_{tr,s}-1} \quad (1.1.3.2.5)$$

$$\frac{s}{m} = \left(\frac{[S]}{[S]_{p=0}} \right) \left(\frac{[M]}{[M]_{p=0}} \right)^{-1} \quad (1.1.3.2.6)$$

$$\frac{s}{m} = (1-p)^{C_{tr,s}-1} \quad (1.1.3.2.7)$$

To illustrate the issue of composition drift, Figure 1.1.3.2.1 shows a plot of $(1-p)$ to the power $(C_{tr,s} - 1)$, as per Equation 1.1.3.2.7, being the normalised dimensionless form of the ratio of CTA to monomer, s/m , vs. p , for $C_{tr,s} = 1, 2, 5, 10, 100, 200$ and 500 up to 5 % monomer conversion ($p = 0.05$).

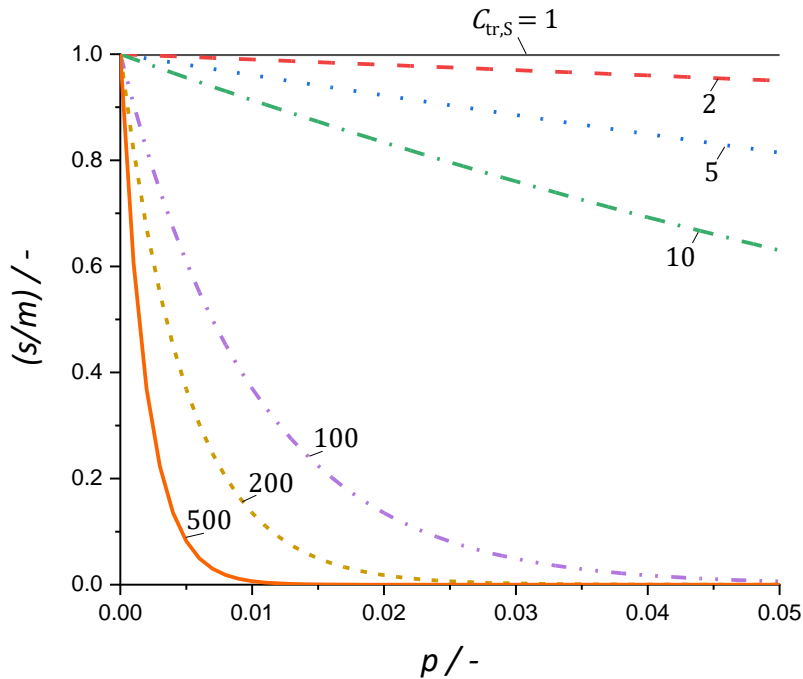


Figure 1.1.3.2.1: Evolution of the normalised ratio of chain transfer agent to monomer (s/m) vs monomer conversion, p , where $C_{tr,s} = 1$ (—), 2 (---), 5 (····), 10 (-·-·), 100 (- - -), 200 (- · - ·), 500 (—). The values of $C_{tr,s}$ are also overlaid on the plot for clarity.

It is evident from the plot that the ratio s/m drifts dramatically for high values of the chain transfer constant, as S is consumed more rapidly than M . Assuming that transfer is the exclusive mode of chain termination (ignoring bimolecular termination), the following holds for the instantaneous number average degree of polymerisation, when combining Equations 1.1.3.1.2 and 1.1.3.2.5:

$$\overline{X}_n = \frac{1}{C_{tr,S}} \frac{[M]_{p=0}}{[S]_{p=0}} (1-p)^{1-C_{tr,S}} = \frac{\overline{X}_{n,p=0}}{(1-p)^{C_{tr,S}-1}} \quad (1.1.3.2.8)$$

It should now be apparent that if the Mayo equation were used to determine the chain transfer constant in systems where its value exceeds 1, the experimental cumulative number degree of polymerization would have a considerably higher value than the instantaneous number degree of polymerization, as a result of composition drift, underestimating the true value of $C_{tr,S}$. Here, Mayo literally falls short.⁵³ The method discussed by Smith,⁵¹ and interestingly also adopted later by Mayo,⁵⁴ clearly addresses the issue. However, it does not directly link to MW data which may be unsettling for some. Smith tried to address this by using calculated values for the chain transfer constant to predict and validate measured intrinsic viscosities, and hence viscosity average MWs, as a function of monomer conversion.⁵¹ However, substantial broadening of the MWD, as a result of fast consumption of CTA, will complicate this approach.

1.1.3.3 Gilbert's approach

Gilbert and co-workers developed a new method which allowed extraction of chain transfer constants from size exclusion chromatography (SEC) data.⁵⁶⁻⁵⁸ The authors converted the SEC data into the number MWD, $n(M)$, expressing it as a function of the degree of polymerization i , $n(i)$. For the number distribution of propagating radicals in a free radical polymerization, the following holds:

$$n(i) = \left(\frac{1}{1+\alpha}\right)^{i-1} \left(\frac{\alpha}{1+\alpha}\right) \quad (1.1.3.3.1)$$

$$\alpha = \frac{2k_t[R]^2 + k_{tr,S}[S][R] + k_{tr,M}[M][R]}{k_p[M][R]} \quad (1.1.3.3.2)$$

In the limiting case where α approaches a value of zero, and thus at high values for kinetic chain length, the discrete number distribution can be approximated as:

$$\lim_{\alpha \rightarrow 0} n(i) = \alpha \exp(-\alpha i) \quad (1.1.3.3.3)$$

By looking at the limiting slope towards high MWs of the natural logarithmic version of this chain length distribution (CLD), the following holds for experiments carried out at a low rate of radical production by initiator decomposition (ignoring chains formed by bimolecular termination):

$$\lim_{\alpha \rightarrow 0} \frac{d \ln n(i)}{di} = -\tilde{\alpha} \quad (1.1.3.3.4)$$

$$\tilde{\alpha} = C_{tr,S} \frac{[S]}{[M]} + C_{tr,M} \quad (1.1.3.3.5)$$

Gilbert's method is powerful and has benefits in accuracy and precision and has been used and critically validated by others.⁵⁹ However, the data is interpreted similarly to Mayo's method, in that no composition drift is accounted for, and thus $[S]/[M]$ is considered to be a constant assuming an instantaneous interpretation of the MWD is valid. The following discussion and experimental work aims to correct for this, yielding more accurate values for $C_{tr,S}$.

1.2 Results and discussion

1.2.1 A new interpretation of cumulative MW data.

The previous discussions lead to the main hypothesis of this chapter. In experiments where the chain transfer constant is substantially higher than 1, composition drift in the form of a decreasing $[S]/[M]$ must be accounted for. Under the assumption of a low rate of radical generation, for any given moment in time, the corresponding instantaneous weight chain length distribution can be expressed as:

$$w(i) = \tilde{\alpha}^2 i \exp(-\tilde{\alpha} i) \quad (1.2.1.1)$$

Knowing that $[S]/[M]$ can be written as a function of monomer conversion, p , as shown in Equation 1.1.3.2.5, $\tilde{\alpha}$ can be written as:

$$\tilde{\alpha} = C_{tr,S} \frac{[S]_{p=0}}{[M]_{p=0}} (1-p)^{C_{tr,S}-1} + C_{tr,M} \quad (1.2.1.2)$$

For the cumulative weight chain length distribution, $W(i)$, the following holds:

$$W(i) = \frac{1}{p} \int_0^p \tilde{\alpha}^2 i \exp(-\tilde{\alpha} i) dp \quad (1.2.1.3)$$

It was found that an analytical solution for this defined integral exists:

$$W(i)|_{p=0}^{p=p} = \frac{1}{(1 - C_{tr,S})^3 i} (-ABCD - (C_{tr,S} - 1) \exp(-i\tilde{\alpha}) F)|_{p=0}^{p=p} \quad (1.2.1.4)$$

$$A = (1 - p) \exp(-C_{tr,M}i) \quad (1.2.1.5)$$

$$B = C_{tr,M}^2 C_{tr,S}^2 i^2 + C_{tr,S}(-2C_{tr,M}^2 i^2 + 2C_{tr,M}i + 1) + C_{tr,M}i(C_{tr,M}i - 2) \quad (1.2.1.6)$$

$$C = \left(C_{tr,S} \frac{[S]_{p=0}}{[M]_{p=0}} i(1 - p)^{C_{tr,S}-1} \right)^{\frac{1}{1-C_{tr,S}}} \quad (1.2.1.7)$$

$$D = \Gamma \left(\frac{1}{C_{tr,S} - 1}, C_{tr,S} \frac{[S]_{p=0}}{[M]_{p=0}} i(1 - p)^{C_{tr,S}-1} \right) \quad (1.2.1.8)$$

$$E = \left(2C_{tr,M}pi - 2C_{tr,M}i + \frac{[S]_{p=0}}{[M]_{p=0}} i(1 - p)^{C_{tr,S}} + p - 1 \right) \quad (1.2.1.9)$$

$$F = \left(C_{tr,S}E + 2C_{tr,M}(p - 1)i + C_{tr,S}^2 \frac{[S]_{p=0}}{[M]_{p=0}} i(1 - p)^{C_{tr,S}} \right) \quad (1.2.1.10)$$

The cumulative number chain length distribution can now easily be obtained knowing the following holds:

$$N(i) \propto \frac{W(i)}{i} \quad (1.2.1.11)$$

In analogy to Gilbert's method, the cumulative number distribution can now be used to extract and determine values for $C_{tr,S}$. All that is needed is accurate SEC data, the analytical ($t = 0$ s; $p = 0$) ratio of $[S]/[M]$, and monomer conversion data as input values.

1.2.2 Hypothesis validation: Monte Carlo simulations.

To validate this new approach, and to illustrate how data analysis was performed, a series of Monte Carlo (MC) simulations were performed using the free radical polymerisation of VAc in the presence of a chain transfer agent as a model system. For this, the mcPolymer v3.1 simulation package was used,⁶⁰ with the input model (see Experimental section and supporting information S1) and an in-house written loop-extension (see supporting information S2), to allow for a greater overall simulation system output. The loop-extension simply repeated the simulation a number of times (defined by the user, see Experimental section) and stored the number of chains of each length in a master distribution for each point

in time. The result was a much larger population in each distribution to increase the statistical certainty of the data, whilst still being able to execute the program (simply increasing the size of an individual simulation by too much led to the requirement for too much computation power). MC simulations were performed with the values for $C_{tr,S}$ being 180, 18, 1.8 and 0.18. $C_{tr,S} [S]_{p=0}/[M]_{p=0}$ was fixed at 0.018. The transfer constants to monomer and solvent were each fixed at 2.7×10^{-4} , which is in agreement with values found in literature.³⁵ Figure 1.2.2.1 shows the simulated $dW/d(\log M)$ distributions for $C_{tr,S} = 180$ and $[S]_{p=0}/[M]_{p=0} = 1 \times 10^{-4}$ as a function of monomer conversion.

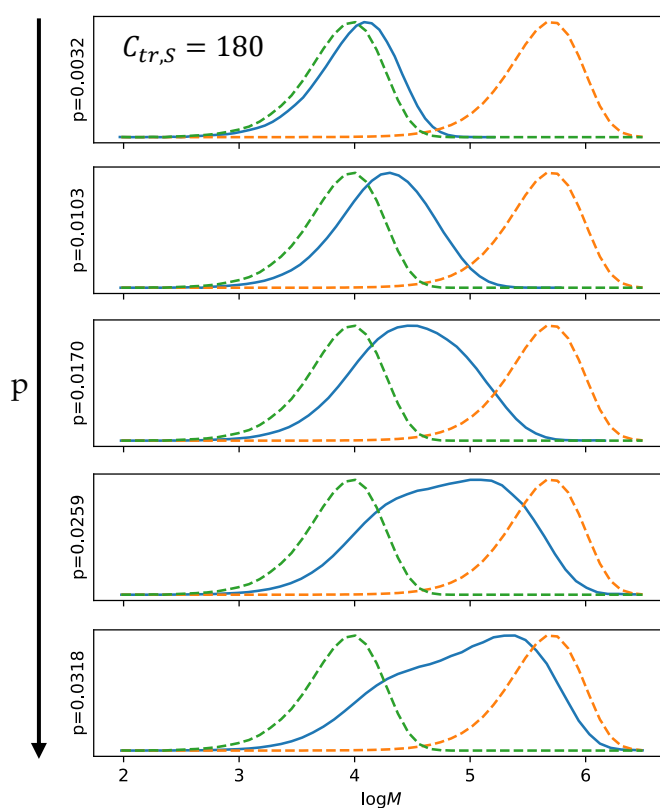


Figure 1.2.2.1: $dW/d(\log M)$ distributions produced from the simulations of the free radical polymerisation of vinyl acetate in the presence of a chain transfer agent where $C_{tr,S} = 180$ and $[S]_{p=0}/[M]_{p=0} = 1 \times 10^{-4}$ as a function of monomer conversion, p . At each value for p the dotted green distribution is the instantaneous distribution; the dashed orange distribution is the case where only transfer to monomer is present and the solid blue distribution is the cumulative distribution at the given value for p .

The green dashed distribution is the instantaneous $dW/d(\log M)$ distribution for $\tilde{\alpha} = C_{tr,S} [S]_{p=0}/[M]_{p=0}$, the orange dashed distribution is the case where $\tilde{\alpha} = C_{tr,M}$, the latter being the case where the chain transfer agent, S , has fully depleted. There is a pronounced shift from the instantaneous to the eventual transfer to monomer/solvent dominated scenario in the

simulated reaction (blue trace). This transition results in a drift to higher MW, and a significant broadening of the MWD. The reason is the pronounced composition drift in $[S]/[M]$, because of the high value for $C_{tr,S}$. This work features two approaches developed to determine $C_{tr,S}$ from this data. To relate to the Gilbert method,⁵⁶⁻⁵⁸ the natural logarithm of the number CLD is used, for different scenarios (see Figure 1.2.2.2). Displayed are the Monte Carlo simulation results for $\ln N(i)$ as function of chain length, i . The series of four simulations, where $C_{tr,S}$ $[S]_{p=0}/[M]_{p=0}$ was set at 0.018, with $C_{tr,S}$ varied at 180, 18, 1.8 and 0.18 respectively, were evaluated at different stages of monomer conversion. It is evident from the data that the cumulative CLDs cannot be considered as a constant, particularly with $C_{tr,S} = 180$ and 18 (top

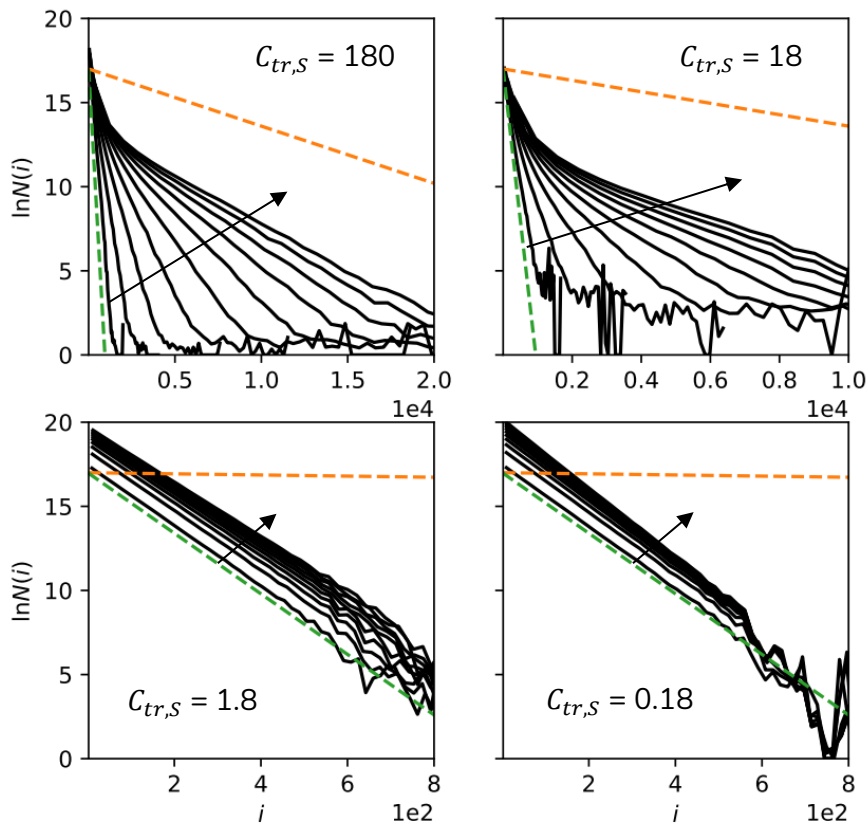


Figure 1.2.2.2: $\ln N(i)$ distributions produced from the simulations of the free radical polymerisation of vinyl acetate in the presence of a chain transfer agent where $C_{tr,S} = 180$ (top left, $p = 0.0032, 0.0066, 0.0103, 0.0139, 0.0170, 0.0202, 0.0235, 0.0259, 0.0288, 0.0318$), 18 (top right, $p = 0.0320, 0.0632, 0.0933, 0.1419, 0.1838, 0.2275, 0.2452, 0.27908, 0.3123, 0.3491$), 1.8 (bottom left, $p = 0.0241, 0.0531, 0.0947, 0.1396, 0.1696, 0.2406, 0.2600, 0.2999, 0.3377$) and 0.18 (bottom right, $p = 0.0305, 0.0864, 0.1396, 0.1887, 0.2125, 0.2356, 0.2689, 0.3008, 0.3313, 0.3425$). $C_{tr,S} [S]_{p=0}/[M]_{p=0}$ was fixed at 0.018. The dotted green distribution is the instantaneous distribution, $\ln n(i)$, for $\tilde{\alpha} = C_{tr,S}[S]_{p=0}/[M]_{p=0}$, the dashed orange distribution is the case where $\tilde{\alpha} = C_{tr,M}$.

left and right). Here, the limiting slope at high i decreases rapidly with increasing conversion, due to a drop in $[S]/[M]$. When $C_{tr,S} = 1.8$ a minor change in slope towards lower values is still observed, because of composition drift. For $C_{tr,S} = 0.18$, a gradual drift to steeper slopes is apparent, as the $[S]/[M]$ ratio drifts the opposite way. However, at low monomer conversion, this change is negligible. Here, the more straightforward Gilbert method can be used. To emphasise the key point: in cases where $C_{tr,S}$ is significantly larger than 1, the slope can no longer be considered to have a constant value and is a clear function of both chain length, i , and monomer conversion. Our new method is specifically designed to tackle this.

The first approach extracts a value for $C_{tr,S}$ by fitting the natural logarithmic CLD to the mathematical analytical solution (see Equations 1.2.1.4 to 1.2.1.11; remembering the assumptions made in Equations 1.1.3.3.1 to 1.1.3.3.3), at a fixed value for monomer conversion. For this code was generated in Python v3 (see supporting information S3), using the LMFIT package.^{61,62} Using the CLD and conversion data from Figure 1.2.2.2 as input, values for $C_{tr,S}$ could be extracted. For the series of input $C_{tr,S} = 180$, a mean value of 181.3 ± 7.0 was extracted for $i > 150$. For $C_{tr,S} = 18$ with i in the range 100–500 and for the 4 samples up to $p = 0.142$ at which $> 90\%$ of S had reacted, $C_{tr,S} = 18.24 \pm 0.45$. The results were in excellent agreement with our input value of the MC simulation. For the data for $C_{tr,S} = 1.8$ and 0.18 the use of the Gilbert method suffices as is observed from the green dotted line in the lower 2 panels of Figure 1.2.2.2.

The second approach is to fix the chain length at a value i and determine the slope of the natural logarithmic form of the number CLD at this value. For this, a localized 3rd order polynomial fitting procedure was used (see supporting information S4). This second method takes away the sensitivity in the accuracy of the conversion time data from experiments. The values for the slopes at different stages of monomer conversion are subsequently fitted to the analytical solution of $\partial \ln N(i)/\partial i$, as seen in Figure 1.2.2.3. For this, code in Python v3 (using the LMFIT package) was again implemented (see supporting information S5).^{61,62} Using the data for the slope values and conversion as input, $C_{tr,S}$ could again be extracted. An initially surprising and concerning observation was found when fitting the $C_{tr,S} = 180$ data. The more i was increased, the worse the output values became. For example, for $i = 500$ a value of 154 was extracted, for $i = 250$ a value of 163, and for $i = 200$, 170.

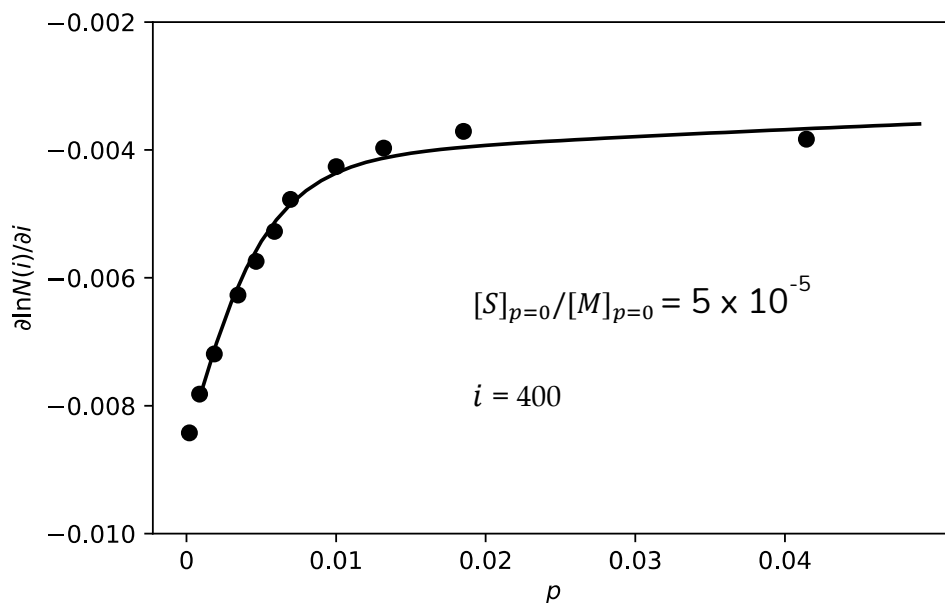


Figure 1.2.2.3: $d \ln N(i)/di$ vs conversion, p , produced from the simulations of the free radical polymerisation of vinyl acetate in the presence of a chain transfer agent where $C_{tr,S} = 180$, $[S]_{p=0}/[M]_{p=0} = 5 \times 10^{-5}$ and $i = 400$.

It was then determined that for accurate evaluation of $C_{tr,S}$, the ratio between the cumulative first derivative $\partial \ln N(i)/\partial i$ and the instantaneous first derivative $\partial \ln n(i)/\partial i$ had to be substantial, and ideally maximized. For the MC case of $C_{tr,S} = 180$ and $[S]_{p=0}/[M]_{p=0}$ of 10^{-4} , it became evident that this transition to steeper slopes was the case for approximate values of $i < 200$. This explains the observed behaviour (see Figure 1.2.2.4).

Lowering the concentration of chain transfer agent widens that window, as will be seen with the experimental data discussed later. In conclusion, the two procedures developed show that this method to determine the chain transfer constant using the cumulative CLD data is valid.

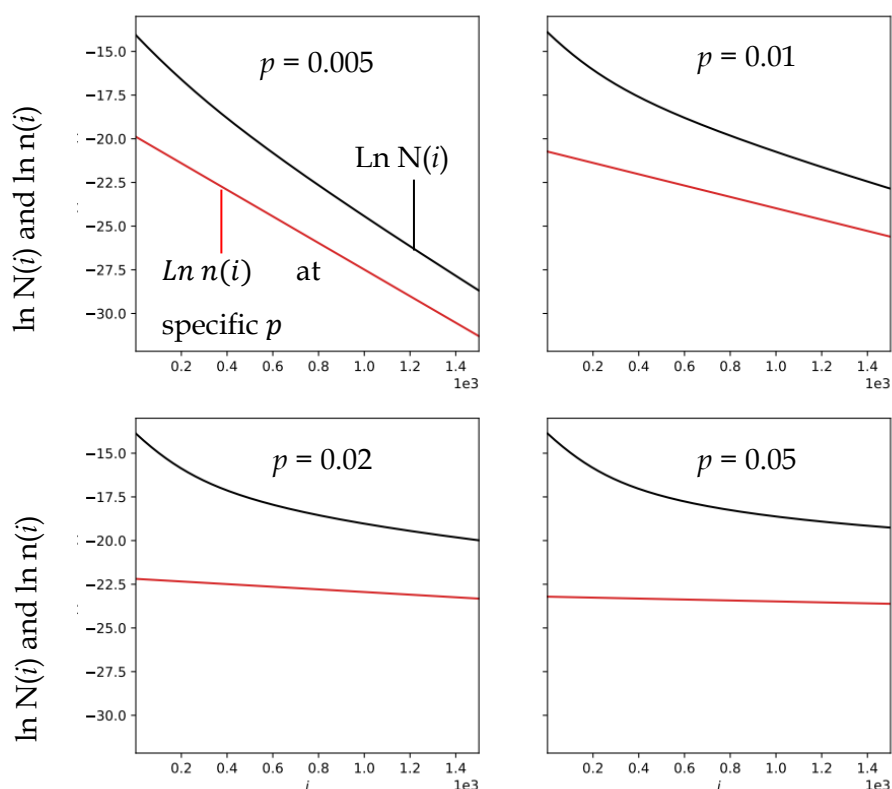


Figure 1.2.2.4: Instantaneous, $\ln n(i)$ (—), and cumulative, $\ln N(i)$ (—), distributions at $p = 0.005$ (top left), 0.010 (top right), 0.020 (bottom left) and 0.050 (bottom right), produced from the simulations of the free radical polymerisation of vinyl acetate in the presence of a chain transfer agent where $C_{tr,S} = 180$, $[S]_{p=0}/[M]_{p=0} = 1 \times 10^{-4}$.

1.2.3 Free radical solution polymerisation of vinyl acetate.

To apply the new hypothesis to experimental data, a series of free radical polymerizations of VAc were carried out in presence of *n*-dodecanethiol (DDT) as CTA (see Table 1.2.3.1 for reagent quantities). The formulations are modified from those used in the work of Okaya and Sato.⁵² The molar ratio of DDT to VAc was varied, that is 1.0×10^{-2} , 1.0×10^{-3} , 1.0×10^{-4} , 5.0×10^{-5} and 1.0×10^{-5} . *n*-Dodecane is added to a concentration of $\approx 6.5 \times 10^{-3}$ mol dm⁻³ as a concentration standard to follow [DDT] as a function of monomer conversion by gas chromatography (GC). The AIBN in ethyl acetate solution, detailed separately in the table, was injected once the system was at reaction temperature (60 °C) to confirm accurate, temperature dependant kinetics from $t = 0$ s. Values for the chain transfer constant were determined using three different methods, the method as described by Smith, and the two approaches of the newly proposed method.

Table 1.2.3.1: Reagent quantities employed for the solution polymerisation of VAc in the presence of DDT.

Reagent	Reagent amounts for varying $[\text{DDT}]_{p=0}/[\text{VAc}]_{p=0}$ (g)				
	1×10^{-2}	1×10^{-3}	1×10^{-4}	5×10^{-5}	1×10^{-5}
VAc	137.15	137.14	137.15	137.15	137.14
Ethyl acetate	28.34	28.30	28.30	28.29	28.29
Dodecane	0.1989	0.1995	0.2031	0.2003	0.2011
DDT	3.2279	0.3264	0.0321	0.0156	0.0032
AIBN	0.0234	0.0234	0.0236	0.0234	0.0237
Ethyl acetate	5.412	5.412	5.412	5.412	5.412

For all methods it is important to have accurate values for monomer conversion. A strong composition drift and thus rapid consumption of the chain transfer agent, indicated by the high literature values for $C_{tr,S}$, is expected.^{50,52} It was decided that gravimetric analysis was the most straightforward way to monitor the rate of polymerization. The results are plotted in Figure 1.2.3.1.

The overall rates of polymerization did not seem to vary considerably between runs, hereby indicating the absence of retardation. Under steady state conditions, the overall rate of polymerization can be calculated using standard free radical polymerization kinetics. Here, these values were $3.0\text{--}3.6 \times 10^{-4} \text{ M s}^{-1}$. A value for the rate coefficient of propagation for vinyl acetate of $8548 \text{ M}^{-1} \text{ s}^{-1}$ at 333.15 K was calculated, using a Arrhenius-type frequency factor of $1.35 \times 10^7 \text{ M}^{-1} \text{ s}^{-1}$ and an activation energy of 20.4 kJ mol^{-1} .²² Potnis and Deshpande reported a value of 0.3162 for $k_p/\sqrt{k_t}$ for the bulk polymerization of vinyl acetate at 333.15 K (hence, $k_t = 7.31 \times 10^8 \text{ M}^{-1} \text{ s}^{-1}$).⁶³ Taking a value for k_d of AIBN of $9.67 \times 10^{-6} \text{ s}^{-1}$,⁶⁴ and an estimated radical efficiency of 0.7 , gives us a rough value for k_t of $2.4 \times 10^8 \text{ M}^{-1} \text{ s}^{-1}$, which seems realistic.⁶⁵ The absence of retardation means that radical addition of the dodecyl sulfanyl radical to VAc

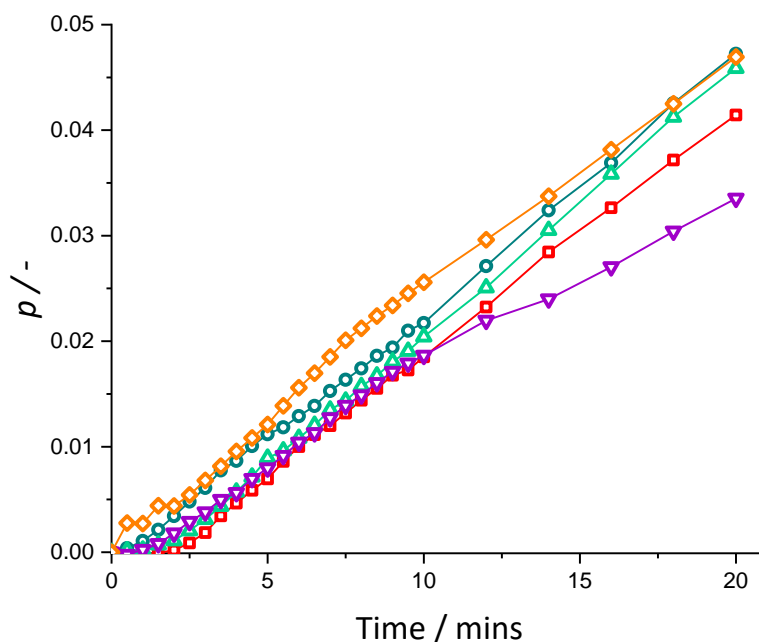


Figure 1.2.3.1: Monomer conversion, p , as a function of time (mins) for the solution polymerisation of VAc. $[S]_{p=0}/[M]_{p=0} = 1 \times 10^{-2}$ (◇), 1×10^{-3} (▽), 1×10^{-4} (△), 5×10^{-5} (□) and 1×10^{-5} (○).

is relatively fast and that chain transfer of the dodecyl sulfanyl radical to DDT can be neglected at our experimental conditions.

In order to obtain accurate MW information, a sample of PVAc was analysed through triple detection SEC, using light scattering, viscometry and a differential refractive index detector. The sample was of polymer formed during a solution polymerisation of VAc in ethyl acetate, in the presence of DDT ($[DDT]_{p=0}/[VAc]_{p=0} = 1 \times 10^{-5}$, $p = 7.2\%$, see Experimental section for more information). This allowed the determination of the Mark-Houwink-Sakurada parameters which could be used to apply the theory of universal calibration to subsequent samples, and allow accurate MW data to be obtained without the need for the additional light scattering data.⁶⁶

Given that the narrow standards used in this case to calibrate the SEC are of poly(styrene), it is necessary to consider that a chain of PVAc of identical MW to the standard may possess a different hydrodynamic volume due to different solvent interactions. Importantly however, polymers which elute at the same elution time possess the same hydrodynamic volume. As discussed by Benoit *et al.*,⁶⁶ according to the Einstein viscosity law, the product of the intrinsic viscosity, $[\eta]$, of a chain, and its MW is a measure of its hydrodynamic volume. As such, at a

given elution volume, Equation 1.2.3.1 can be used to relate the hydrodynamic volume of the standard, S, to the analyte, A.

Equation 1.2.3.2 shows the Mark-Houwink-Sakurada relation between $[\eta]$ and MW, with reference to the parameters, K and α . Using this knowledge, Equation 1.2.3.1 can be rewritten as Equation 1.2.3.3. The beauty of this equation is that if the values for K and α of both the analyte and the standard are known, an accurate MW of the analyte can be determined relative to the calibration curve determined from the standards, accounting for a difference in the solvent/polymer interaction. This will be built on further in Chapter 3 to discuss how branched polymers may be characterised.

$$[\eta]_S MW_S = [\eta]_A MW_A \quad (1.2.3.1)$$

$$[\eta] = K MW^\alpha \quad (1.2.3.2)$$

$$K_S MW_S^{1+\alpha_S} = K_A MW_A^{1+\alpha_A} \quad (1.2.3.3)$$

The MWD, and corresponding Mark-Houwink-Sakurada plot of the PVAc sample can be seen in Figure 1.2.3.2. K and α were determined in tetrahydrofuran (THF) (with 0.01 % BHT) at 30 °C as 5.01×10^{-5} dL/g and 0.78 respectively. These values are used for the remainder of this chapter to calculate the MW of PVAc relative to poly(styrene) standards ($K = 14.1 \times 10^{-5}$ dL mol⁻¹ and $\alpha = 0.70$ for poly(styrene),⁶⁷ without the need for additional detectors such as light scattering to give accurate MW data.

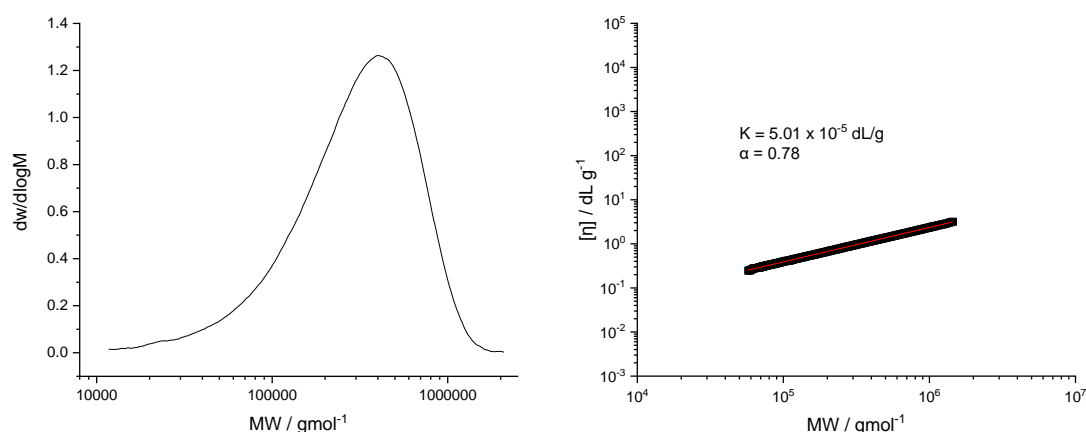


Figure 1.2.3.2: $dw/d\log M$ vs molecular weight, MW (g mol^{-1}), (left) and the corresponding Mark-Houwink-Sakurada plot (right) of intrinsic viscosity, $[\eta]$ (dL g^{-1}) vs molecular weight, MW (g mol^{-1}), for a sample of PVAc. The reported K and α values are the result of fitting the data to Equation 1.2.3.2 (fit region 55,000 – 1,500,000 g mol^{-1}).

Using this calibration, $dW/d(\log M)$ distributions were constructed for each $[S]_{p=0}/[M]_{p=0}$ ratio as a function of monomer conversion, p , and can be seen in Figure 1.2.3.3. These MWDs show rapid drift towards higher MW and associated broadening of the dispersity of the distributions. It is easy to see why this may complicate the accurate determination of the chain transfer constant, if using the cumulative number average MW. These experimental distributions appear to have a striking similarity to the *in silico* distributions seen previously in Figure 1.2.2.1.

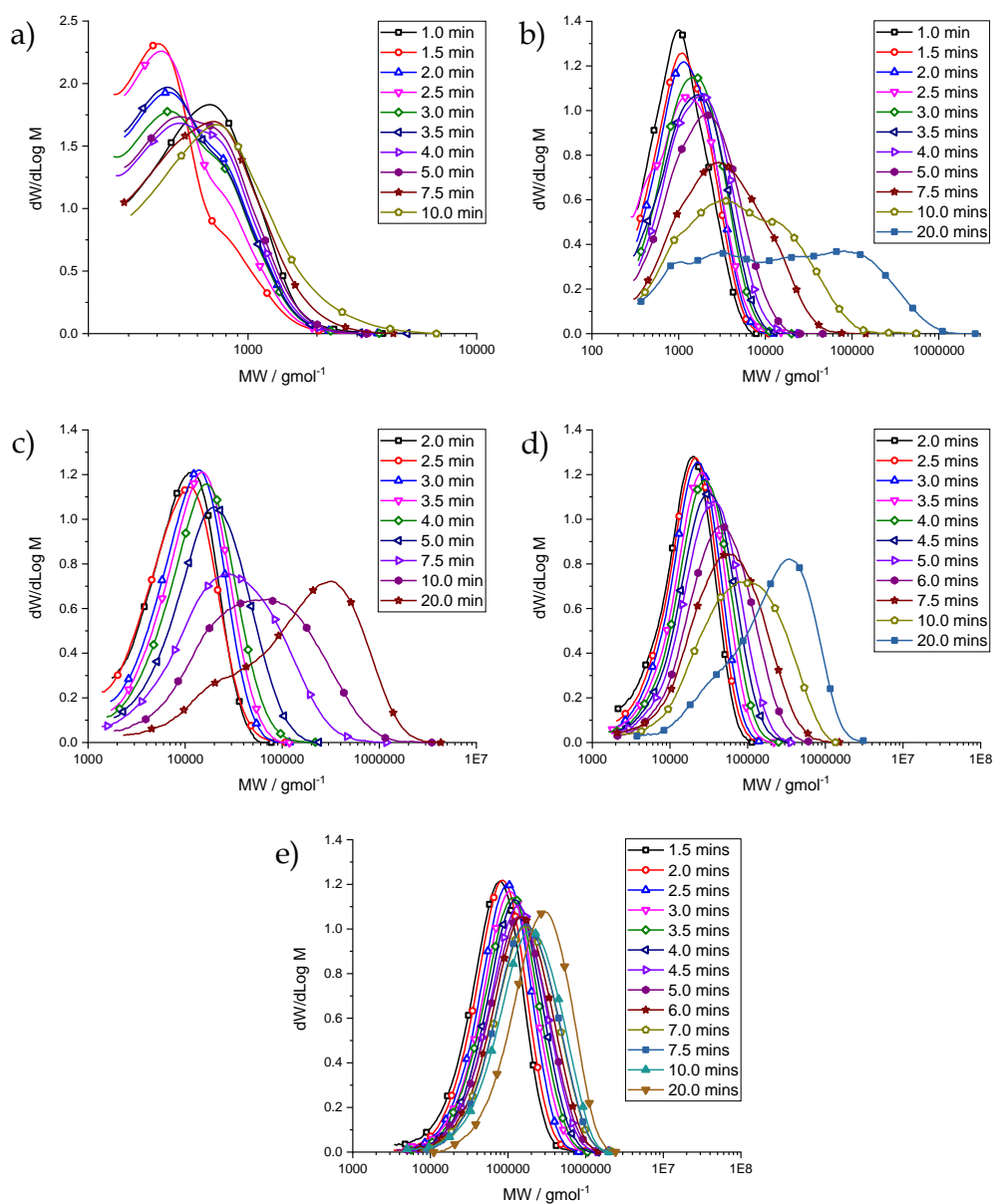


Figure 1.2.3.3: $dW/d\log M$ vs molecular weight, MW (g mol^{-1}), plots as a function of time for $[S]_{p=0}/[M]_{p=0} = 1 \times 10^{-2}$ (a), 1×10^{-3} (b), 1×10^{-4} (c), 5×10^{-5} (d) and 1×10^{-5} (e).

The $\ln N(i)$ plots for each $[S]_{p=0}/[M]_{p=0}$ ratio as a function of monomer conversion, p , can be seen in Figure 1.2.3.4. In this case, the gradient of the high MW end of the distribution is seen to decrease with increasing p , which can again be attributed to a decrease in $[S]/[M]$. This decrease in gradient at lower $[S]/[M]$ is consistent with Gilbert's theory. Going forwards, it is important to remember that the exponential form (Equation 1.1.3.3.3) for the number distribution is only valid for high values of the kinetic chain length (low α and $\tilde{\alpha}$).

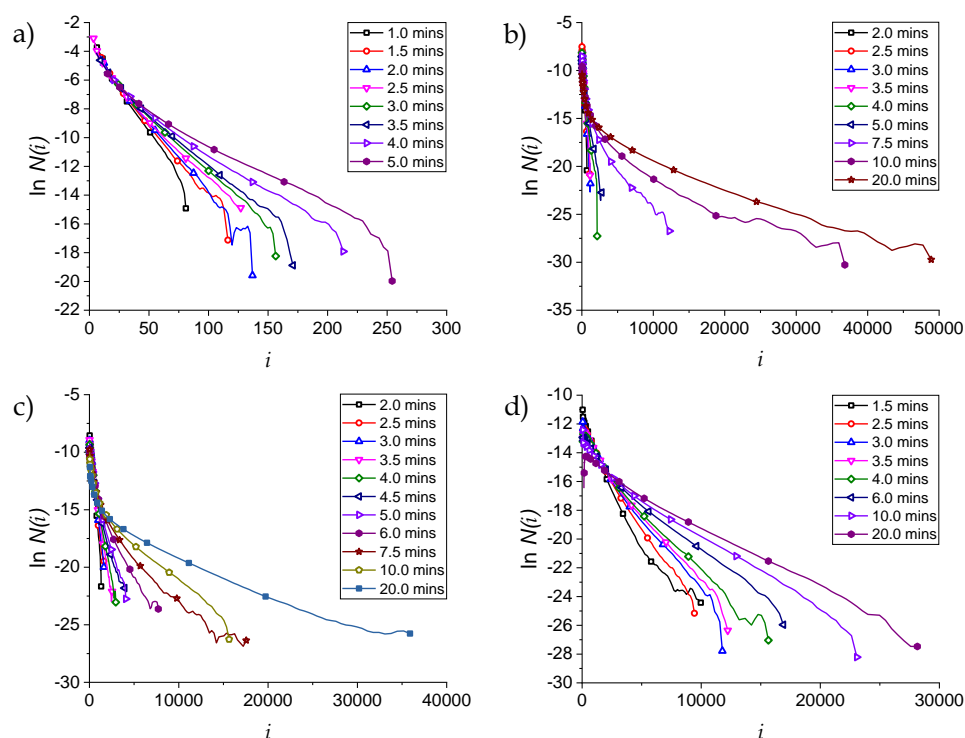


Figure 1.2.3.4: $\ln N(i)$ vs degree of polymerisation, i , as a function of time for $[S]_{p=0}/[M]_{p=0} = 1 \times 10^{-3}$ (a), 1×10^{-4} (b), 5×10^{-5} (c) and 1×10^{-5} (d).

Smith's method was first applied to determine a value for the chain transfer constant of DDT in the radical polymerization of VAc. For this (see Equations 1.1.3.2.5-1.1.3.2.7), knowledge of how the $[S]/[M]$ ratio changes as a function of monomer conversion is needed. GC was used to follow the concentration of CTA at different stages of monomer conversion, utilising n -dodecane as an internal standard. As can be seen in Figure 1.2.3.5, good separation could be achieved between n -dodecane and DDT using the chosen method (see experimental section). Ethyl acetate, VAc and chloroform (the chosen carrier solvent) all eluted at the same time under these conditions, due to comparable volatility, although as accurate conversion values were obtained through gravimetry, it was not deemed necessary to attempt to achieve separation between these species.

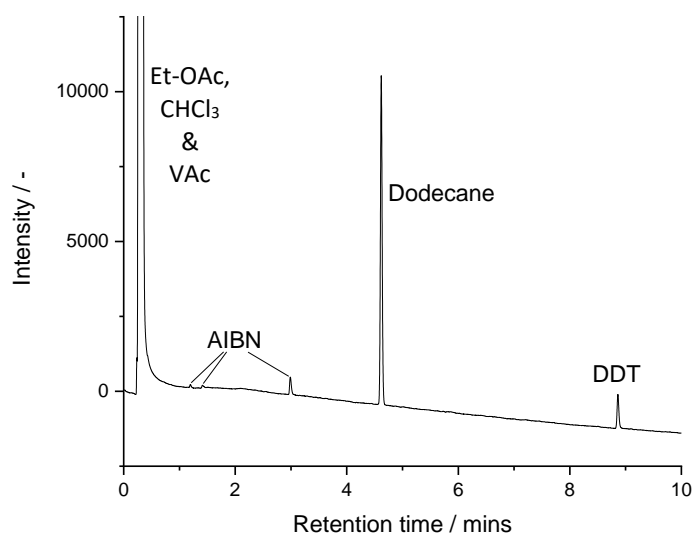


Figure 1.2.3.5: Example GC chromatogram of a sample taken from the polymerisation reactions.

The concentrations of DDT at any given conversion were calculated from the signal area ratios of DDT and *n*-dodecane determined from the GC data. For these purposes, it was assumed that the concentration of *n*-dodecane remained constant throughout reaction. A linear calibration function was created from a set of calibration standards, as seen in Figure 1.2.3.6, with a slope of 1.003 and an intercept of 2.066×10^{-3} . This was then used to back-calculate the experimental [DDT]/[Dodecane] ratio. From this the [DDT] could be determined from the analytical [Dodecane].

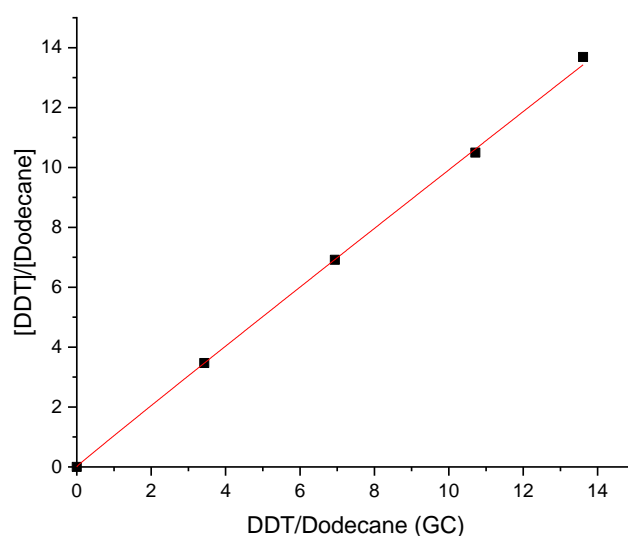


Figure 1.2.3.6: Calibration curve for the ratio of the GC peak areas of DDT and *n*-dodecane vs the analytical concentration ratio.

The obtained data sets were fitted with Equation 1.1.3.2.7, as discussed in Section 1, in Python v3 using the LMFIT package,^{61,62} to calculate values for $C_{tr,S}$. At a target $[S]_{p=0}/[M]_{p=0}$ of 1.0×10^{-3} , and at fixed experimental GC $[S]_{p=0}/[M]_{p=0}$ value of 9.74×10^{-4} , an approximate value of 196 was determined. Fitting with $[S]_{p=0}/[M]_{p=0}$ as an unknown parameter resulted in $C_{tr,S} = 190.3 \pm 6.3$, with $[S]_{p=0}/[M]_{p=0} = 9.46 \times 10^{-4} \pm 1.32 \times 10^{-5}$. For $[S]_{p=0}/[M]_{p=0}$ of 1.0×10^{-4} , and at fixed experimental GC $[S]_{p=0}/[M]_{p=0}$ value of 8.00×10^{-5} , resulted in a value for $C_{tr,S}$ of ca. 217. Fitting with $[S]_{p=0}/[M]_{p=0}$ as an unknown parameter resulted in $C_{tr,S} = 226.8 \pm 12.91$, with $[S]_{p=0}/[M]_{p=0} = 8.23 \times 10^{-5} \pm 1.68 \times 10^{-6}$. All GC data and monomer conversion data was then combined by transforming it to normalized s/m format, and fitting it without fixing $(s/m)_{p=0}$ to unity, as seen in Figure 1.2.3.7. The two data points in red were omitted from the fit due to doubtful accuracy in their monomer conversion data. This led to a combined value for $C_{tr,S}$ of 223.0 ± 7.33 , using the Smith method.

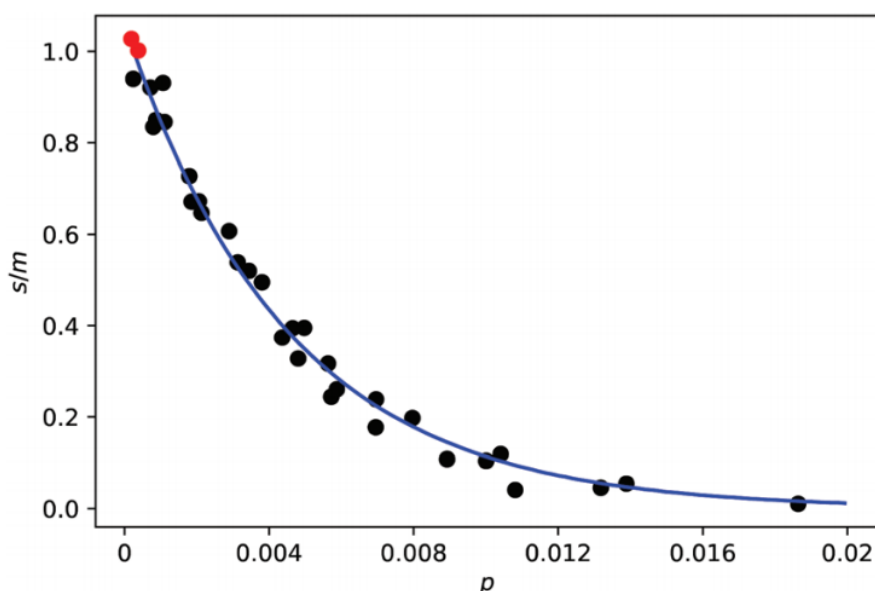


Figure 1.2.3.7: Normalised ratio of chain transfer agent to monomer, s/m , vs monomer conversion, p , for the free radical polymerisation of VAc in the presence of DDT.

When looking at the data, it becomes abundantly clear how quickly the concentration of CTA decreases relative to monomer and supports the changes in the MWD discussed previously.

1.2.4 Applying the newly proposed CLD-method.

Now, the new model is put to the test. For this the experimental SEC data from our series of free radical polymerizations of VAc in presence of DDT, at 60 °C were analysed as described in Section 1.2.1. It is important that the dominant factor which determines the kinetic chain length is transfer to DDT (Equation 1.1.3.3.2 and 1.2.1.2). Additionally, operating at too high

DDT concentrations would lead to extremely low MWs, resulting in the assumption made in Equation 1.1.3.3 becoming invalid. It also must be emphasised that correct interpretation of the SEC data is necessary. The Mark–Houwink–Sakurada relationship used to calculate values of the MWs cannot be applied to low MWs. This is due to the Flory characteristic ratio being a function of chain length. In addition to this, the intensity of the differential refractive index signal is influenced by the end groups for polymer chains of low MW. Moreover, from the discussion above, high DDT concentration would be detrimental to analysis with approach 2.

To be safe, the lower MW limit was set at a chain length of 150 (ca. 13 kg mol⁻¹). The upper limit for analysis was set at 1 % of the maximum height of intensity of the $\partial W/\partial \log M$ signal. The polymerization experiments carried out at 1×10^{-2} and 1×10^{-3} produced too low MWs (see Figure 1.2.3.3). At the lowest DDT loading, where $[S]_{p=0}/[M]_{p=0} = 1 \times 10^{-5}$, transfer to DDT is no longer the dominant pathway and competition between other modes of chain termination, such as transfer to monomer/solvent and bimolecular termination, become significant. This sets the limit at the other end for this method. For the 10^{-4} and 5×10^{-5} series, note that the actual analytical $[S]_{p=0}/[M]_{p=0}$ determined through GC were 8.00×10^{-5} and 3.56×10^{-5} respectively. Now fitting the cumulative CLD in logarithmic format, $\ln N(i)$, following the first method, resulted in the values provided in Table 1.2.4.1.

Table 1.2.4.1: Chain transfer constants ($C_{tr,s}$) for the free radical polymerisations of VAc in the presence of DDT at 60 °C using CLD approach 1.

$[DDT]_{p=0}/[VAc]_{p=0}$		$[DDT]_{p=0}/[VAc]_{p=0}$	
8.00×10^{-5}		3.56×10^{-5}	
p	$C_{tr,s}$	p	$C_{tr,s}$
0.00111	204.52 ± 0.94	0.00087	231.69 ± 0.31
0.00206	187.60 ± 1.78	0.00186	217.09 ± 0.77
0.00313	207.23 ± 0.55	0.00344	224.33 ± 0.79
0.00436	245.36 ± 4.36	0.00465	256.46 ± 0.90
0.00572	255.40 ± 2.42		

Data is presented up to the points where the DDT concentration drops below an acceptable measurable value. For $C_{tr,M}$ an estimated value of 3.4×10^{-4} was used, which accounts for transfer to solvent in addition to transfer to monomer ($C_{tr,M} + C_{tr,Solv}[Solv]/[M]$). The data is in good agreement with the value obtained with the Smith method, that is $C_{tr,S} = 223.0 \pm 7.33$, although, the values start to differ at increasing monomer conversion. This is because DDT depletes rapidly. In other words, other chain stopping events become increasingly dominant, leading to a lower accuracy of the fit. Beside this, there is an uncertainty in using a single conversion data point.

For these reasons, the second approach was then applied to the data sets. The local first derivative of $\partial \ln N(i)/\partial i$ is less sensitive, therefore a fit of the data of $\partial \ln N(i)/\partial i$ versus monomer conversion to the analytical solution of $\partial \ln N(i)/\partial i$ should improve the results. The results of fitting approach 2 are presented in Table 1.2.4.2.

Table 1.2.4.2: Chain transfer constants ($C_{tr,S}$) for the free radical polymerisations of VAc in the presence of DDT at 60 °C using CLD approach 2.

$[DDT]_{p=0}/[VAc]_{p=0}$		$[DDT]_{p=0}/[VAc]_{p=0}$	
8.00×10^{-5}		3.56×10^{-5}	
i	$C_{tr,S}$	i	$C_{tr,S}$
150	226 ± 23.31	200	246.4 ± 8.63
200	219 ± 10.82	300	229.7 ± 6.64
250	204.14 ± 7.35	400	224.5 ± 4.83
350	201.4 ± 4.11	600	216.2 ± 4.17
450	195.2 ± 8.70	800	223.1 ± 6.69
550	188.2 ± 7.56	1000	225.9 ± 11.23

The conclusions discussed in the MC results are now confirmed. For the 8×10^{-5} dataset the values of $C_{tr,S}$ become increasingly inaccurate for chain lengths above ca. 200. For the data set of 3.56×10^{-5} , however, consistent accurate values are obtained across the 200–1000 range for i . This reduction in the amount of CTA used broadens the range over which the ratio of the

cumulative first derivative, $\partial \ln N(i)/\partial i$, and the instantaneous first derivative, $\partial \ln n(i)/\partial i$, is significant enough to provide accurate variable extraction.

1.3 Conclusion

In summary, the newly developed CLD method for systems where the chain transfer constant is greater than 1 is valid. Both approaches are suitable to obtain values for $C_{tr,S}$, with the 2nd approach, which makes use of conversion data, being the most sensitive. It can be said with confidence that a combined value of $C_{tr,S} = 223.9 \pm 3.0$ accurately describes chain transfer to DDT in the free radical polymerisation of VAc at 333.15 K, which is in remarkable agreement with the value found using the Smith method.

1.4 Experimental

Materials

Vinyl acetate (Aldrich, $\geq 99\%$) was purified by passing through a column of basic alumina, followed by vacuum assisted distillation wherein the first and final 20 vol% of the distillate was discarded. Azobisisobutyronitrile (AIBN, from VWR) was purified by recrystallisation from methanol. *n*-Dodecanethiol (Aldrich, $\geq 98\%$), *n*-dodecane (Merck, $\geq 99\%$), ethyl acetate (Merck, $\geq 99.5\%$) and chloroform (Fisher scientific, $\geq 99.8\%$) were used without further purification.

Characterization methods

Gas chromatography (GC).

All GC analysis was performed on a Shimadzu GC2014 equipped with a Shimadzu A020i autosampler. The injection temperature was 200 °C. The carrier gas was hydrogen, supplied by an external hydrogen generator at a flow rate of 5.32 mL min⁻¹. The GC was fitted with a Restek Rxi1ms column (15 m length, 0.25 mm ID and 0.25 μm film thickness). The injection volume was 1 μL with splitless injection. The detector was a flame ionisation detector (FID) with a flame temperature of 300 °C, and a sampling rate of 40 ms. The heating profile was 60 °C for 2 minutes and then heated to 200 °C at 10 °C min⁻¹ where it remained for a further 2 minutes. Samples diluted in chloroform (6–8 drops of sample in 1.5 mL chloroform) were analysed through comparison of the peak area ratio, DDT/Dodecane. This ratio was compared to a calibration curve of known [DDT]/[Dodecane]. [Dodecane] was assumed constant throughout reaction and as such [DDT]_p could be determined. Caution: during GC

analysis the $t = 0$ s samples for the analytical concentration of *n*-dodecanethiol deviated with increasing amounts at low concentrations. It is believed that this is due to the oxidation of thiols by dissolved molecular oxygen. The $t = 0$ s target molar ratio of DDT to VAc of 1.0×10^{-3} , 1.0×10^{-4} , 5.0×10^{-5} , and 1.0×10^{-5} , came out as 9.74×10^{-4} , 8.00×10^{-5} , 3.56×10^{-5} , and 6.16×10^{-6} . Therefore, it is advised that extra care be taken in reactions that contain low concentrations of thiol.

Size exclusion chromatography (SEC).

Molecular weight distributions were determined on an Agilent Infinity II MDS instrument equipped with differential refractive index (DRI), viscometry (VS), dual angle light scatter (LS) and multiple wavelength UV detectors. The system was equipped with 2× PLgel Mixed C columns (300×7.5 mm) and a PLgel 5 μ m guard column. The eluent was THF with 0.01 % BHT (butylated hydroxytoluene). Samples were run at 1 mL min^{-1} at $30 \text{ }^\circ\text{C}$. Polystyrene standards (Agilent EasyVials) were used for calibration. Analyte samples were filtered through a PTFE filter with a $0.2 \mu\text{m}$ pore size before injection. The K and α values for PVAc were determined by a triple detection SEC set-up, with light scattering and viscometry used alongside DRI. Polymer MW information of each sample was then estimated using universal calibration, utilizing the calculated Mark–Houwink– Sakurada parameters, $K = 5.01 \times 10^{-5} \text{ dL mol}^{-1}$ and $\alpha = 0.78$ for poly(vinyl acetate), and literature values of $K = 14.1 \times 10^{-5} \text{ dL mol}^{-1}$ and $\alpha = 0.70$ for polystyrene.⁶⁷

Synthesis

Solution polymerization of vinyl acetate in the presence of *n*-dodecanethiol (example quantities for $[\text{DDT}]/[\text{VA}] = 5 \times 10^{-5}$).

In a typical reaction, vinyl acetate (137.15 g, 1.59 mol), ethyl acetate (28.3 g, 0.32 mol), *n*-dodecanethiol (0.0156 g, 7.71×10^{-5} mol) and *n*-dodecane (0.20 g, 1.18×10^{-3} mol) were added to a 3 necked RBF, fitted with a PTFE temperature probe, and an air condenser with aluminium fins, sealed with a rubber septum. A magnetic stirrer bar was added and the final neck was sealed with a rubber septum. Separately, AIBN (0.062 g, 3.78×10^{-4} mol) and ethyl acetate (14.2855 g, 0.16 mol) were added to a 20 mL crimp vial with a magnetic stirrer. The vial was crimp sealed with a PTFE crimp lid. The two vessels were then purged with N_2 for 1 h. After this time the RBF was submersed in a $60 \text{ }^\circ\text{C}$ oil bath under nitrogen, with a stir speed of 750 rpm. After the reaction temperature was confirmed to be $60 \text{ }^\circ\text{C}$, 6 mL of the AIBN solution was injected into the RBF under nitrogen. Samples of ≈ 5 mL were then withdrawn

under nitrogen at frequent intervals for analysis. The samples were immediately sealed to minimize evaporation and plunged into liquid nitrogen. A small amount of sample was retained for GC analysis, and the remainder was evaporated to determine conversion gravimetrically. SEC analysis was performed on the evaporated gravimetry samples. For $t = 5$ mins, $p = 7.0 \times 10^{-3}$, $M_n = 20,200 \text{ g mol}^{-1}$, $M_w = 43,900 \text{ g mol}^{-1}$, $[\text{DDT}]/[\text{VAc}] (\text{GC}) = 5.3 \times 10^{-6}$.

Modelling

Monte Carlo simulations.

The universal Monte Carlo simulator mcPolymer v3.1, which uses a Gillespie algorithm.⁶⁰ Propagation and termination were assumed to be independent of chain length. Our fixed input parameters were an initiator efficiency of 0.70, mass of vinyl acetate monomer 86.09 g mol^{-1} , concentration of vinyl acetate 8.634 mol L^{-1} , concentration of solvent 2.080 mol L^{-1} , concentration of initiator (AIBN) $7.80 \times 10^{-4} \text{ mol L}^{-1}$. For the rate coefficients: $k_d = 9.67 \times 10^{-6} \text{ s}^{-1}$, $k_p = 8548 \text{ L mol}^{-1} \text{ s}^{-1}$, $k_{tr,M} = k_{tr,solvent} = 2.317 \text{ L mol}^{-1} \text{ s}^{-1}$, $k_t = 2.4 \times 10^8 \text{ L mol}^{-1} \text{ s}^{-1}$. The values for the chain transfer constant were set at 0.18, 1.8, 18, and 180 respectively. $C_{tr,S}[S]_{p=0}/[M]_{p=0}$ was fixed at 0.018. Total number of molecules for an individual simulation was set between 1×10^8 and 1×10^9 . Each simulation was rerun in the form of loops to increase the overall end size and accuracy of the system (see supporting information S2 for the loop script). For $C_{tr,S} = 0.18$ each run had 1×10^8 molecules with 150,000 loops, for $C_{tr,S} = 1.8, 18$ and 180 these were 1×10^8 and 75,000, 1×10^9 and 75,000, and 1×10^9 and 186,500. The MC simulations were run on desktop computers with a windows operation system. The data obtained for $N(i)$ was analyzed using code written in Python v3, using the LMIFT nonlinear least-square minimization and curve-fitting package,^{61,62} run in JupyterLab 1.2.6 via Anaconda on a MacBook Pro with the MacOS Catalina operating system. All of the python code used to compute the described numbers is given in the supporting information section.

1.5 References

- 1 F. Klatte, *US1084581*, 1914.
- 2 J. M. Hay and D. Lyon, *Nature*, 1967, **216**, 790–791.
- 3 B. Capon, D. S. Rycroft, T. W. Watson and C. Zueco, *J. Am. Chem. Soc.*, 1981, **103**, 1761–1765.
- 4 W. O. Herrmann and W. Haehnel, *Patent 450286*, 1924.
- 5 W. O. Herrmann and W. Haehnel, *Ber. Dtsch. Chem. Ges.*, 1927, **60**, 1658–1663.
- 6 I. Sakurada, T. Ito and K. Nakamae, *J. polym. sci., C Polym. symp.*, 15, 1967, **15**, 75–91.
- 7 F. L. Marten, in *Kirk-Othmer Encyclopedia of Chemical Technology*, (Ed.), 2002.
- 8 F. L. Marten, *US Patent 4844709*, 1989.
- 9 H. K. Inskip and R. L. Adelman, *US Patent 3689469*, 1972.
- 10 R. Rees, *US Patent 4222922*, 1980.
- 11 F. Sharifi, Z. Bai, R. Montazami and N. Hashemi, *RSC Adv.*, 2016, **6**, 55343–55353.
- 12 A. Paknahad, D. G. Petre, S. C. G. Leeuwenburgh and L. J. Sluys, *Acta Biomater.*, 2019, **96**, 582–593.
- 13 B. Ding, H. Y. Kim, S. C. Lee, D. R. Lee and K. J. Choi, *Fibers Polym.*, 2002, **3**, 73–79.
- 14 M. Nakamae, K. Yuki, T. Sato and H. Maruyama, *Colloids Surfaces A Physicochem. Eng. Asp.*, 1999, **153**, 367–372.
- 15 K. Kolter, A. Dashevsky, M. Irfan and R. Bodmeier, *Int. J. Pharm.*, 2013, **457**, 470–479.
- 16 S. Ebnesajjad, *Adhesives Technology Handbook*, 2nd ed, 2008.
- 17 A. Kaboorani and B. Riedl, *Compos. Part A Appl. Sci. Manuf.*, 2011, **42**, 1031–1039.
- 18 G. Moad and D. H. Solomon, *The Chemistry of Radical Polymerization second fully revised edition*, 2006.
- 19 J. C. Bevington, S. W. Breuer, E. N. J. Heseltine, T. N. Huckerby and S. C. Varma, *J.*

- Polym. Sci. A-1 Polym. Chem.*, 1987, **25**, 1085–1092.
- 20 G. Moad, E. Rizzardo and D. Solomon, *Makromol. Chem., Rapid Commun.*, 1982, **3**, 533–536.
- 21 J. Lane and B. J. Tabner, *J. Chem. Soc. Perkin Trans. 2*, 1984, 1823–1826.
- 22 C. Barner-Kowollik, S. Beuermann, M. Buback, R. A. Hutchinson, T. Junkers, H. Kattner, B. Manders, A. N. Nikitin, G. T. Russell and A. M. van Herk, *Macromol. Chem. Phys.*, 2017, **218**, 1600357.
- 23 R. A. Hutchinson, J. R. Richards and M. T. Aronson, *Macromolecules*, 1994, **27**, 4530–4537.
- 24 C. S. Marvel, J. H. Sample and M. F. Roy, *J. Am. Chem. Soc.*, 1939, **61**, 3241–3244.
- 25 P. J. Flory and F. S. Leutner, *J. Polym. Sci.*, 1948, **3**, 880–890.
- 26 O. Vogl, M. F. Qin and A. Zilkha, *Prog. Polym. Sci.*, 1999, **24**, 1481–1525.
- 27 J. M. Tedder and J. C. Walton, *Tetrahedron*, 1980, **36**, 701–707.
- 28 D. W. Ovenall, *Macromolecules*, 1984, **17**, 1458–1464.
- 29 F. F. Vercauteren and W. A. B. Donners, *Polymer.*, 1986, **27**, 933–998.
- 30 A. K. Chaudhuri and S. R. Palit, *J. Polym. Sci. A-1 Polym. Chem.*, 1968, **6**, 2187–2196.
- 31 B. L. Funt and W. Pasika, *Can. J. Chem.*, 1960, **38**, 1865–1870.
- 32 C. H. Bamford, R. W. Dyson and G. C. Eastmond, *Polymer (Guildf.)*, 1969, **10**, 885–899.
- 33 H. S. Taylor and W. H. Jones, *J. Am. Chem. Soc.*, 1930, **52**, 1111–1121.
- 34 P. J. Flory, *J. Am. Chem. Soc.*, 1937, **59**, 241–253.
- 35 J. T. Clarke, R. O. Howard and W. H. Stockmayer, *Makromol. Chemie*, 1960, **44**, 427–447.
- 36 M. Matsumoto, J. Ukida, G. Takayama, T. Eguchi, K. Mukumoto, K. Imai, Y. Kazusa and M. Maeda, *Makromol. Chem.*, 1959, **32**, 13–36.
- 37 M. S. Matheson, E. E. Auer, E. B. Bevilacqua and E. J. Hart, *J. Am. Chem. Soc.*, 1949, **71**, 2610–2617.

- 38 W. H. McDowell and W. O. Kenyon, *J. Am. Chem. Soc.*, 1940, **62**, 415–417.
- 39 S. Imoto, J. Ukida and T. Kominami, *Kobunshi Kagaku*, 1957, **14**, 101.
- 40 D. Britton, F. Heatley and P. A. Lovell, *Macromolecules*, 1998, **75**, 2828–2837.
- 41 S. Amiya and M. Uetsuki, *Macromolecules*, 1982, **15**, 166–170.
- 42 Y. Morishima and S. Nozakura, *J. Polym. Sci. A-1 Polym. Chem.*, 1976, **14**, 1277–1282.
- 43 D. Britton, F. Heatley and P. A. Lovell, *Macromolecules*, 2000, **33**, 5048–5052.
- 44 S. L. Kapur and R. M. Joshi, *J. Polym. Sci.*, 1954, **14**, 489–496.
- 45 S. R. Palit and S. K. Das, *Proc. R. Soc. Lond. A. Math. Phys. Sci.*, 1954, **226**, 82–95.
- 46 M. Kamachi, D. J. Liaw and S. Nozakura, *Polym. J.*, 1979, **11**, 921–928.
- 47 Z. Sharaby, *US Patent 4931518*, 1990.
- 48 V. Chabrol, J. Batty, P. Shaw, C. Davis and M. Farrell, *WO2015145174A1*, 2015.
- 49 T. Origuchi, Y. Ikemura and H. Maki, *EP1757624B1*, 2007.
- 50 C. Walling, *J. Am. Chem. Soc.*, 1948, **70**, 2561–2564.
- 51 W. V. Smith, *J. Am. Chem. Soc.*, 1946, **68**, 2059–2064.
- 52 T. Sato and T. Okaya, *Makromol. Chem.*, 1993, **173**, 163–173.
- 53 F. R. Mayo, *J. Am. Chem. Soc.*, 1943, **65**, 2324–2329.
- 54 R. A. Gregg, D. M. Alderman and F. R. Mayo, *J. Am. Chem. Soc.*, 1948, **70**, 3740–3743.
- 55 S. Rimmer and S. Collins, *React. Funct. Polym.*, 2006, **66**, 177–186.
- 56 R. G. Gilbert, *Emulsion polymerisation: a mechanistic approach*, 1995.
- 57 P. A. Clay and R. G. Gilbert, *Macromolecules*, 1995, **28**, 552–569.
- 58 D. Kukulj, T. P. Davis and R. G. Gilbert, *Macromolecules*, 1998, **31**, 994–999.
- 59 G. Moad and C. L. Moad, *Macromolecules*, 1996, **29**, 7727–7733.
- 60 M. Drache and G. Drache, *Polymers (Basel)*, 2012, **4**, 1416–1442.

- 61 M. Newville, T. Stensitzki, D. Allen and A. Ingargiola, 2014, 10.5281/ZENODO.11813.
- 62 M. Newville, R. Otten, A. Nelson, A. Ingargiola, T. Stensitzki, D. Allan, A. Fox, F. Carter, Michal, D. Pustakhod, Y. Ram, Glenn, C. Deil, Stuermer, A. Beelen, O. Frost, N. Zobrist, G. Pasquevich, A. Hansen, T. Spillane, S. Caldwell, A. Polloreno, Andrewhannum, J. Zimmermann, J. Borreguero, J. Fraine, B. Maier, B. Gamari and A. Almarza, 2019, 10.5281/ZENODO.3588521.
- 63 S. P. Potnis and A. M. Deshpande, *Die Makromol. Chemie*, 1969, **125**, 48–58.
- 64 J. P. Van Hook and A. V. Tobolsky, *J. Am. Chem. Soc.*, 1958, **80**, 779–782.
- 65 H. Kattner and M. Buback, *Macromol. Chem. Phys.*, 2014, **215**, 1180–1191.
- 66 Z. Grubisic, P. Rempp and H. Benoit, *Polym. Lett.*, 1967, **5**, 753–759.
- 67 H. L. Wagner, *J. Phys. Chem. Ref. Data*, 1985, **14**, 1101–1106.
- 68 C. Barner-Kowollik, S. Beuermann, M. Buback, P. Castignolles, B. Charleux, M. L. Coote, R. A. Hutchinson, T. Junkers, I. Lacík, G. T. Russell, M. Stach and A. M. Van Herk, *Polym. Chem.*, 2014, **5**, 204–212.
- 69 M. Buback, R. G. Gilbert, R. A. Hutchinson, B. Klumperman, F. -D Kuchta, B. G. Manders, K. F. O'Driscoll, G. T. Russell and J. Schweer, *Macromol. Chem. Phys.*, 1995, **196**, 3267–3280.
- 70 S. Beuermann, M. Buback, T. P. Davis, R. G. Gilbert, R. A. Hutchinson, O. F. Olaj, G. T. Russell, J. Schweer and A. M. Van Herk, *Macromol. Chem. Phys.*, 1997, **198**, 1545–1560.
- 71 T. Junkers, S. P. S. Koo and C. Barner-Kowollik, *Polym. Chem.*, 2010, **1**, 438–441.

2

Vinyl acetate chain transfer agent studies

Abstract

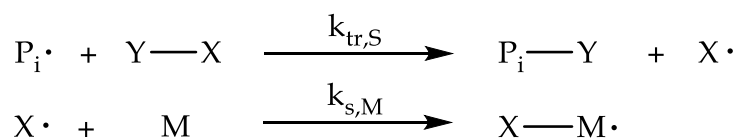
In this chapter, chain transfer agents for employment in the free radical polymerisation of vinyl acetate are discussed. Firstly, 5-Methyl furfural is tested for its chain transfer activity and is shown to impart significant retardation to the polymerisation rate. A chain transfer constant of 0.36 was determined at 333.15 K utilising the chain length distribution method. Given the extent of the retardation, the search was expanded to linear disulfides, and the molecular weight distributions of the polymers is shown to depend greatly on the concentration of disulfide employed. Specifically, dibutyl disulfide and 2-hydroxyethyl disulfide are discussed, and their chain transfer constants are measured at 333.15 K using the Mayo method and Gilbert's chain length distribution method. For dibutyl disulfide, chain transfer constants of 0.221 and 0.215 were obtained by the Mayo and Gilbert method, respectively. For 2-hydroxyethyl disulfide these numbers were 2.043 and 1.991, respectively. The origin of the retardation behaviour is then discussed. A low molecular weight poly(vinyl acetate) formed with dibutyl disulfide is then analysed through nuclear magnetic resonance and electrospray ionisation mass spectrometry, suggesting the polymer is telechelic. Additionally, kinetic data for reaction with a cyclic disulfide, DL- α -lipoic acid, is discussed, and the potential applications of the resultant copolymerisation are explored.

2.1 Introduction

2.1.1 Vinyl acetate chain transfer.

The molecular weight distribution (MWD) of poly(vinyl acetate) (PVAc), produced through free radical polymerisation of vinyl acetate (VAc), is dictated by an interplay between the mechanistic events of initiation, propagation, termination, and chain transfer. The kinetics of these processes were discussed at length in Chapter 1. The high tendency for a propagating radical to undergo transfer to monomer or polymer can result in nonlinear, branched polymers with high molecular weights (MWs). This is due to the nature of the transfer reactions, producing reactive sites capable of undergoing further propagation, transfer, or bimolecular termination through combination (again discussed in Chapter 1). In applications which require lower molecular weight (MW) polymer, with a defined linear chain architecture, these transfer reactions must be limited, at least from a relative point-of-view. One method to achieve this is to introduce a chain transfer agent (CTA).

As seen in Scheme 2.1.1.1, the process of chain transfer to a species (Y-X) is governed by the overall rate coefficient, $k_{tr,S}$, and results in the death of a propagating polymer chain, denoted $P_i\bullet$, and the transfer of the radical activity to the new species, denoted $X\bullet$. The radical species $X\bullet$ can then reinitiate polymerisation through reaction with monomer, M, with rate coefficient $k_{s,M}$. Initiator, monomer, polymer, and solvent can all act as a CTA, and can therefore all influence the MWD. The reactivity of the PVAc derived radical leads to a high susceptibility to chain transfer reactions. For example, for chain transfer to *n*-dodecanethiol, $C_{tr,S} = 223.9$ for VAc at 60 °C (Chapter 1), which gives a corresponding value of $k_{tr,S} = 1.9 \times 10^6 \text{ M}^{-1} \text{ s}^{-1}$ (assuming $k_p = 8548 \text{ M}^{-1} \text{ s}^{-1}$ at 60 °C as discussed previously)¹. However, $k_{tr,S}$ is only $5.5 \times 10^3 \text{ M}^{-1} \text{ s}^{-1}$ for styrene (Sty) ($C_{tr,S} = 16$, $k_p = 341 \text{ M}^{-1} \text{ s}^{-1}$)^{2,3} and $5.8 \times 10^2 \text{ M}^{-1} \text{ s}^{-1}$ for methyl methacrylate ($C_{tr,S} = 0.7$, $k_p = 822 \text{ M}^{-1} \text{ s}^{-1}$)^{4,5} at 60 °C. Although the PVAc radical is particularly reactive, transfer constants to initiator, monomer, polymer, and solvent are all typically much lower than 1 at 60 °C, which means that propagation is significantly faster, therefore, significant amounts of these species are needed to effectively reduce the MW. Having said



Scheme 2.1.1.1: Events evolved during chain transfer in free radical polymerisation, specifically chain transfer to species Y-X, and subsequent reinitiation of M by $X\bullet$.

that, compared to the transfer constants to other monomers, these values are still significantly higher. For illustration, using the previously given values for k_p , $k_{tr,S}$ for some common solvents in methyl methacrylate (MMA), Sty and VAc polymerisation are given in Table 2.1.1.1.

Table 2.1.1.1: Values for $k_{tr,S}$ to some common solvents for MMA, Sty and VAc free radical polymerisation at 60 °C. These are determined using literature values of $C_{tr,S}$ (MMA and Sty from ref ⁸⁴ and VAc from ref ¹⁴) and k_p (values previously defined).

Solvent	$k_{tr,S}$ (60 °C) / M ⁻¹ s ⁻¹		
	MMA	Sty	VAc
Benzene	3.3×10^{-3}	6.8×10^{-4}	1.0
Toluene	1.6×10^{-2}	4.1×10^{-3}	29.1
Acetone	1.6×10^{-2}	1.1×10^{-2}	1.3
Butanone	3.7×10^{-2}	0.2	63.1
Ethyl acetate	1.2×10^{-2}	0.2	2.8
Ethanol	0.7	0.2	21.4

For future reference, a collection of chain transfer constants for compounds in VAc free radical polymerisation are given later in Table 2.1.1.2. For illustration, typical values for transfer to solvent fall in the range of 10^{-3} - 10^{-4} and transfer to polymer and monomer around 2.5×10^{-4} . If a MW reduction is desired, using a CTA with $C_{tr,S} = 6 \times 10^{-4}$, as is the case for methanol (MeOH) at 60 °C, to reduce the instantaneous degree of polymerisation from 500 to 50 would require a $[MeOH]/[VAc] = 30$, according to the Mayo equation, discussed at length in Chapter 1 and given in Equation 2.1.1.1 again for reference. For clarity, in this example $\overline{X}_{n,t} = 500$, being the number average degree of polymerisation in the absence of chain transfer, $\overline{X}_n = 50$, being the number average degree of polymerisation in the presence of chain transfer, $C_{tr,S} = 6 \times 10^{-4}$ being the chain transfer constant, $[S]$ is the concentration of CTA and $[M]$ is the concentration of monomer.

$$\frac{1}{\overline{X}_n} = \frac{1}{\overline{X}_{n,t}} + C_{tr,S} \frac{[S]}{[M]} \quad (2.1.1.1)$$

The use of a CTA with a higher value for $C_{tr,S}$ would require a lower concentration to effectively reduce the MW. Using the example of transfer to *n*-dodecanethiol, where $C_{tr,S} = 223.9$ at 60 °C, for the same instantaneous reduction in the number average degree of

polymerisation, from 500 to 50, $[DDT]/[VAc] \approx 8 \times 10^{-5}$. This offers a more cost-effective approach, and, given the small amounts of CTA required, can be added to established formulations without changing other parameters such as total volume/solids content. However, as was highlighted in Chapter 1, when $C_{tr,S} \gg 1$, uncontrollable drift in $[S]/[M]$ is observed, which may add unwanted complexity to the system (requiring CTA feeds). In an ideal case, where $C_{tr,S} = 1$, no drift would be observed, and for the same reduction in the number average degree of polymerisation (500 to 50), $[S]/[M] = 1.8 \times 10^{-2}$, which is still practical.

Where one may call upon a thiol to act as a CTA in free radical polymerisation with other monomers, this is complicated by a particularly large chain transfer constant for VAc ($C_{tr,S} = 223.9$ for transfer to *n*-dodecanethiol at 333.15 K, as discussed in Chapter 1).⁶⁻⁸ This results in a dramatic decrease in MW at low conversion, however, presents the problem of uncontrollable drift to high MW as the CTA is consumed much faster than monomer. Introduction of the CTA through a continuous feed can act to minimise the influence of this drift.⁶ Also, given the magnitude of $k_{tr,S}$, issues with mixing (i.e. CTA diffusion) may begin to influence the process. Nevertheless, an important consideration is that thiols appear to reinitiate VAc polymerisation readily, demonstrating little influence on the rate of polymerisation (as seen in Chapter 1). This, coupled with the high reactivity (i.e. small concentrations leading to dramatic MW reduction), makes thiols particularly cost effective CTAs, and they are typically favoured over other species in industry. The high value for $C_{tr,S}$ means the thiol is often fed into a reaction, with a small increase in the dispersity of the MWD being an acceptable compromise.⁹⁻¹¹

It is worth noting that some influence on the rate may be observed irrelevant of the rate of reinitiation, at very high thiol loadings, due to the dependence of chain length. As discussed by Mayo (1948), during the free radical polymerisation of Sty in the presence of CCl_4 (CTA) at low degrees of polymerisation (unimers, dimers and trimers), the chain transfer constant can be variable.¹² At 76 °C, $C_{tr,S}$ was found to equal 0.0006, 0.0025 and 0.007 for unimers, dimers and trimers respectively. For higher degrees of polymerisation, this number was found to be constant at 0.0115. This led to some variation in the obtained rate data.

A number of studies have been performed demonstrating the chain transfer constants for a collection of common reagents in VAc free radical polymerisation,^{6,7,13-16} and demonstrated that those which did possess favourable chain transfer constants typically exhibited a large rate

retardation. This could be explained due to the reactivity of the PVAc radical, which often leads to the CTA derived radical being more stable, and the reinitiation step becoming slow, or instead resulting in termination of the CTA derived radical.¹⁴ Those which are quoted as being “mildly degradative” typically had chain transfer constants in the range of 10^{-3} - 10^{-4} . Some reagents were quoted as having chain transfer constants closer to unity, however, each appeared to have potential issues for industrial applicability. For example, carbon tetrachloride was found to possess $C_{tr,S} = 0.96$, however, is particularly toxic, carcinogenic, and hazardous to the environment, particularly through long-term aquatic toxicity and destruction of the ozone layer. Additionally, the introduction of chlorine into the polymer may be undesirable for particular applications. Nitromethane was another potential candidate covered by Stockmayer et al (1960), with $C_{tr,S} = 0.23$,¹⁴ however, like CCl_4 , this compound is also expected to partition poorly during emulsion polymerisation, a property deemed unattractive for future application of this work. $C_{tr,S}$ of a variety of compounds in the free radical polymerisation of VAc found in the literature are given in Table 2.1.1.2 for future reference.

Table 2.1.1.2: Collection of chain transfer agents, and their corresponding $C_{tr,S}$ values in the free radical polymerisation of vinyl acetate.

Chain transfer agent	Temp / °C	$C_{tr,S}$	Ref
<i>n</i> -Dodecanethiol	60	223.9	This work (Chapter 1)
2-Mercaptoethanol	60	260	6
<i>n</i> -butanethiol	60	48	7
Cyclohexane	60	6.59×10^{-4}	13
	60	0.01	14
Methylcyclohexane	60	2.4×10^{-3}	14
	60	1.18×10^{-3}	13
Decalin	60	4.8×10^{-3}	14
Dioxane	60	2.0×10^{-3}	14
<i>n</i> -butyl ether	60	7.6×10^{-3}	14
Methanol	60	6.0×10^{-4}	14
Ethanol	60	2.5×10^{-3}	14
<i>n</i> -Butanol	60	2.04×10^{-3}	13

<i>i</i> -Butanol	60	2.18×10^{-3}	13
<i>sec</i> -Butanol	60	3.17×10^{-3}	13
<i>tert</i> -Butanol	60	4.6×10^{-5}	13
	60	1.3×10^{-4}	14
	60	3.4×10^{-5}	15
<i>i</i> -Propanol	80	4.5×10^{-3}	17
2-Isopropoxyethanol	60	1.6×10^{-2}	18
Acetone	60	1.17×10^{-3}	13
	60	1.5×10^{-4}	14
Acetylacetone	60	1×10^{-3}	14
Butanone	60	7.38×10^{-3}	13
3-Methyl-2-butanone	60	1.18×10^{-2}	13
3-Pentanone	60	1.14×10^{-2}	13
4-Methyl-2-pentanone	60	3.45×10^{-3}	13
Cyclohexanone	60	1.8×10^{-2}	14
Acetic acid	60	1.1×10^{-4}	13
	60	1×10^{-3}	14
2-methylpropanoic acid	60	5.0×10^{-4}	13
Acetic anhydride	60	8×10^{-4}	14
Methyl formate	60	3×10^{-4}	14
Vinyl acetate	60	2.5×10^{-4}	14
	60	2.46×10^{-4}	15
Methyl acetate	60	2.5×10^{-4}	14
Ethyl acetate	50	1.2×10^{-3}	16
	60	1.1×10^{-4}	13
	60	3.3×10^{-4}	14
Ethyl trifluoroacetate	50	3.0×10^{-3}	16
Ethyl isobutyrate	50	1.60×10^{-2}	16
Ethyl 2-ethylhexanoate	50	6.50×10^{-3}	16
Ethyl methanolate	50	2.2×10^{-3}	16
Ethyl propionate	50	4.0×10^{-3}	16
Ethyl butanoate	50	4.5×10^{-3}	16
Ethyl octanoate	50	7.0×10^{-3}	16

Ethyl nonanoate	50	8.0×10^{-3}	16
Ethyl dodecanoate	50	1.05×10^{-2}	16
Ethyl octadecanoate	50	1.4×10^{-2}	16
Methyl <i>n</i> -butanoate	60	1.9×10^{-3}	14
Methyl <i>i</i> -butanoate	60	8.6×10^{-3}	14
Methyl glycolate	60	3×10^{-2}	14
Methyl lactate	60	6.4×10^{-2}	14
Ethyl lactate	60	7×10^{-2}	14
Dimethyl oxalate	60	1×10^{-4}	14
Diethyl oxalate	60	4×10^{-4}	14
Dimethyl malonate	60	1.7×10^{-3}	14
<i>i</i> -Propyl acetate	60	8×10^{-4}	14
	67.5	9×10^{-4}	14
	75	1×10^{-3}	14
<i>s</i> -Butyl acetate	60	8×10^{-4}	14
Ethylidene diacetate	60	4×10^{-3}	14
Acetaldehyde	45	5.3×10^{-2}	14
	60	6.6×10^{-2}	14
	75	7×10^{-2}	14
Propionaldehyde	60	0.10	14
<i>n</i> -Butyraldehyde	60	0.10	14
Chloral	60	0.50	14
Allyl chloride	60	0.31	14
<i>n</i> -Butyl chloride	60	1×10^{-3}	14
<i>tert</i> -Butyl chloride	60	2.6×10^{-3}	14
<i>n</i> -Butyl bromide	60	5×10^{-3}	14
<i>tert</i> -Butyl bromide	60	1.5×10^{-2}	14
<i>n</i> -Butyl iodide	60	8.0×10^{-2}	14
Dichloromethane	60	4×10^{-4}	14
1,2-Dichloroethane	60	7.2×10^{-4}	13
	60	5×10^{-4}	14
Ethylidene chloride	60	6.5×10^{-3}	14
<i>sym</i> -Tetrachloroethane	60	1.6×10^{-2}	14

Ethylidene chloride	60	0.11	14
<i>sym</i> -Tetrachloroethane	60	0.60	14
Ethylidene bromide	60	1.5×10^{-2}	14
<i>sym</i> -Tetrabromoethane	60	0.96	14
Chloroform	60	1.25×10^{-2}	13
	60	1.5×10^{-2}	14
Carbon tetrachloride	45	0.76	14
	60	0.96	14
	75	1.05	14
Methylchloroform	60	7.11×10^{-3}	13
1,1,2,2-tetrachloroethane	60	1.07×10^{-2}	13
Ethyl dichloroacetate	60	2.1×10^{-2}	14
Ethyl trichloroacetate	60	0.44	14
Acetonitrole	60	1×10^{-3}	14
Isobutyronitrile	60	1×10^{-2}	14
Dimethylformamide	60	5×10^{-3}	14
N- <i>n</i> -butylacetamide	60	4×10^{-3}	14
Di- <i>n</i> -butyl sulfide	60	2.6×10^{-2}	14
Diethyl dithioglycolate	60	1.41	14
Cyclohexene	60	6.2×10^{-2}	14
	75	7.7×10^{-2}	14
Dipentene	60	0.19	14
Allyl acetate	60	9×10^{-2}	14
Methyl oleate	60	0.10	14
Furfural	60	1.5	14
3-methylbutyn-3-ol	60	4×10^{-2}	14
Methallyl chloride	60	4×10^{-2}	14
Benzene	60	3×10^{-4}	13
	60	1.2×10^{-4}	14
	75	1.4×10^{-4}	14
Toluene	60	2.1×10^{-3}	13
	60	3.4×10^{-3}	14
Ethylbenzene	60	5.5×10^{-3}	13

	60	1×10^{-2}	14
<i>i</i> -Propyl benzene	60	9×10^{-3}	13
<i>t</i> -butyl benzene	60	3.6×10^{-4}	13
Cumene	60	1×10^{-2}	14
Fluorene	60	0.47	14
Anisole	60	1×10^{-3}	14
Phenol	60	6×10^{-2}	14
Acetophenone	60	1×10^{-2}	14
Benzoic acid	60	5×10^{-3}	14
Benzoic anhydride	60	1.3×10^{-2}	14
Ethyl benzoate	60	2.5×10^{-3}	14
Benzaldehyde	60	5.4×10^{-2}	14
	75	6×10^{-2}	14
Chlorobenzene	60	8.3×10^{-4}	13
	60	8×10^{-3}	14
Benzyl methyl ether	60	2.8×10^{-2}	14
Benzyl acetate	60	8×10^{-3}	14
Phenylacetic acid	60	4×10^{-2}	14
Benzyl chloride	60	4.5×10^{-2}	14
Benzyl cyanide	60	0.21	14
Benzoin	60	8×10^{-2}	14
Biacetyl	60	6.7×10^{-2}	14
Nitromethane	60	0.23	14
	75	0.26	14
Methyl cyanoacetate	60	0.5	14
Di- <i>n</i> -butyl disulfide	60	1.0	14
Diacetyl disulfide	60	0.29	14
α -benzyloxyacrylonitrile	60	12	19
α -benzyloxyacrylamide	60	20	19

Aldehydes have been explored as CTAs in the free radical polymerisation of VAc. Again, looking at the work of Stockmayer, acetaldehyde and propionaldehyde were shown to possess $C_{tr,S} = 0.066$ and 0.095 respectively, and did not appear to influence the rate of

polymerisation. Matsumoto *et al.* (1959) discussed how esters and aldehydes influenced the polymerisation of VAc, drawing on studies reported in previous publications.²⁰ Particularly, they concluded that the esters in the series methyl acetate, ethyl acetate, isopropyl acetate and dimethyl oxalate did not influence the rate of polymerisation, and as such, did not act as retarders. The authors found that for the linear esters, $C_{tr,S}$ increased with increasing length of the aliphatic side group, with values of 1.6×10^{-4} , 2.6×10^{-4} and 3.4×10^{-4} for methyl, ethyl and propyl acetate, respectively at 60 °C. The aldehydes discussed were acetaldehyde, butyraldehyde, crotonaldehyde and benzaldehyde. It was noted that acetaldehyde had no influence on the rate of polymerisation, however, butyraldehyde, crotonaldehyde and benzaldehyde were all retarders. $C_{tr,S}$ of 2×10^{-2} and 6.5×10^{-2} were reported for acetaldehyde and butyraldehyde, respectively. All of these species possess chain transfer constants significantly lower than what may be deemed useful to act as a CTA to reduce MW.

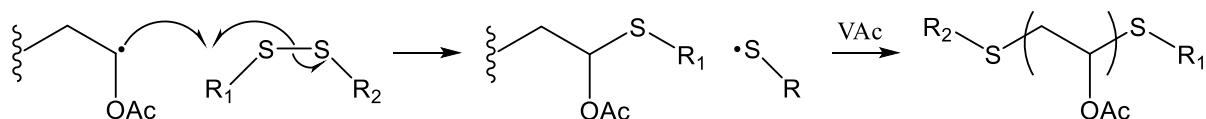
A discussion of CTAs would not be complete without a brief mention of reversible deactivation radical polymerisation (RDRP) techniques. The application of such techniques to VAc free radical polymerisation is particularly challenging due to the reactivity of the VAc radical. This leads to strong bonds with capping agents,^{21,22} making the reactivation of the chain unfavourable. Additionally, issues with transfer to other species complicates the situation, as well as around 2 % of monomer additions occurring through head to head or tail to tail additions.²³⁻²⁵ Both of these addition pathways result in the formation of a primary radical, which makes the reversibility of the deactivation even more unfavourable.²⁶ The result is a loss of control with increasing conversion, as the number of living chains slowly decreases. Many systems, with a variety of catalysts, have been trialled to control VAc polymerisation,²⁷⁻³⁰ however, only recently has good control been obtained to high monomer conversion utilising cobalt catalysts.³¹⁻³⁵ There are however some drawbacks with the use of these catalysts, most notably long inhibition periods. For example, Kaneyoshi and Matyjaszewski (2005) demonstrated inhibition of > 10 h for $\text{Co}(\text{acac})_2$ (bulk polymerisation, V-70 initiator at 30 °C, $[\text{VAc}]_0/[\text{Co}]_0/[\text{V-70}]_0 = 500/1/1$), making them less attractive industrially, despite the control they afford ($M_w/M_n < 1.2$ at $p \approx 0.6$, time = 60 h).³⁴ Additionally, the use of cobalt catalysts is problematic due to the carcinogenicity, leading to extensive efforts to outlaw its usage.

As well as a reduction in MW, the use of a CTA introduces functionality, with the introduction of Y at the ω terminus, and the reinitiating species, $X\bullet$, introducing functionality at the α terminus seen in Scheme 2.1.1.1. Given that chain transfer most commonly occurs through

proton abstraction, it is typically the initiating species which introduces the functionality, although this is not always the case, as is the case with bis-type modifiers such as disulfides, or examples such as halogenated compound such as CBr_4 or CCl_4 .³⁶ Control of end groups is a particularly active field of interest, as the functionality can influence the behaviours of the polymer, such as solubility, self-assembly,³⁷⁻³⁹ surface properties,⁴⁰⁻⁴² and rheological properties.^{43,44} Additionally, reactive functionalities may allow for post modification, which can be exploited to, for example, produce block copolymers or cyclic polymers.⁴⁵⁻⁴⁷ The reader is referred to a recent review by Kim *et al.* (2020), which gives an overview of end group chemistry and viable application areas.⁴⁸

2.1.2 The use of disulfides as chain transfer agents.

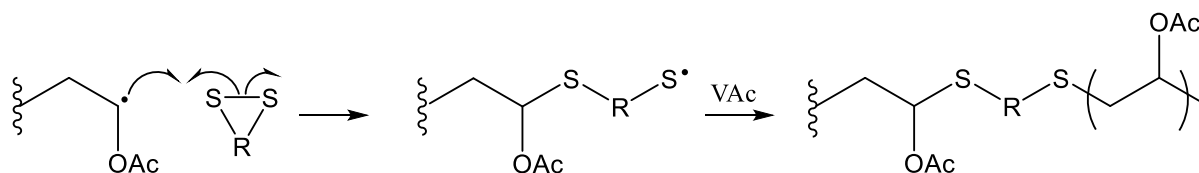
As previously alluded to, disulfides are bis-type modifiers, of the general formula RS-SR , with the labile disulfide bond a potential site for radical attack. Stockmayer *et al.* (1953) discussed the use of disulfides in VAc free radical polymerisation, initially demonstrating high levels of reactivity, expressed through chain transfer constants close to unity.⁴⁹ Specifically, di-*n*-butyl disulfide, (DBDS) $(\text{C}_4\text{H}_9\text{-S})_2$, and diethyl dithioglycolate, $(\text{C}_2\text{H}_5\text{OC(O)CH}_2\text{-S})_2$, were studied, which were demonstrated to possess $C_{tr,S}$ of 1 and 1.5 respectively. DBDS was particularly interesting, as the corresponding thioether, di-*n*-butyl sulfide had $C_{tr,S} = 0.026$, with the difference implying direct involvement of the disulfide bond in the transfer reaction. However, the rate of polymerisation was highly dependent on the concentration of disulfide employed. For example, at a benzoyl peroxide concentration of 10^{-2} M, addition of DBDS at 5.5×10^{-3} M and 2.7×10^{-2} M reduced the rate of polymerisation to 40 and 1.5 % of that of pure VAc. Given the suggested involvement of the disulfide in the reaction, the mechanism given in Scheme 2.1.2.2 was proposed. Assuming the thiyl radical is capable of reinitiation, the result is a telechelic polymer, with a thioether moiety present at both the α (reinitiating species) and ω (through chain transfer) terminus of the polymer chains.



Scheme 2.1.2.1: Proposed mechanism for the chain transfer reaction of VAc to a disulfide.

The authors went on to prove this mechanism through the use of a cyclic disulfide, as assuming the validity of the mechanism in Scheme 2.1.2.1, the thiyl radical would remain tethered to the chain, and, assuming reinitiation by this radical, would result in the

introduction of thioethers into the polymer backbone, and would not result in the same reduction in molecular weight, as per Scheme 2.1.2.2. If the reaction were to occur through proton abstraction, a similar $C_{tr,S}$ might be expected between the linear and cyclic disulfide, however, only 2 sulfur atoms per polymer chain would be expected through reinitiation by the disulfide.



Scheme 2.1.2.2: Proposed mechanism for the chain transfer reaction of VAc to a cyclic disulfide.

The authors used 1-oxa-4,5-dithia-cycloheptane (ODTCH), a cyclic disulfide with $R = -C_2H_4OC_2H_4-$, and measured $C_{tr,S} = 0.25$, however, where $[ODTCH]/[VAc] = 0.045$, the polymer was found to be composed of 7.07 wt% sulfur, correlating to a mole ratio of 0.11 of disulfide to VAc in the polymer, leading to around 9 disulfide units per chain and proving the original hypothesis. Miraculously, in the very next article in the same volume of the same journal (literally on the next page), Tobolsky and Baysal proved the same point using the same method, and the same cyclic disulfide, this time for Sty polymerisation.⁵⁰ For $[ODTCH]/[styrene] = 0.11$, the polymer was shown to contain 1.05 % sulfur, which correlated to 17.2 sulfur atoms per chain, again indicative of the mechanism presented in Scheme 2.1.2.2. In 1955, Tobolsky and Meltzer filed a patent in which they demonstrated “copolymerisation” of a vinyl monomer with cyclic disulfides, proceeding through the aforementioned mechanism.⁵¹ In the patent, experimental details for reactions with Sty, butadiene, MMA, butyl acrylate, vinyl chloride, VAc and vinylidene chloride were given, with all of the polymers shown to contain large quantities of sulfur.

Greg and Mayo later measured the transfer constants of two different linear disulfides in the bulk free radical polymerisation of styrene at 60 °C.⁵² The authors demonstrated that di-*n*-lauryl disulfide and dibenzyl disulfide both reduced the MW of Sty, with $C_{tr,S}$ of 2.3×10^{-4} and 1.0×10^{-2} respectively, although little was discussed regarding the difference in reactivity. The authors hinted that there may be a difference in the abstraction between the benzyl and alkyl hydrogen atoms, although subsequently went on to acknowledge the findings of Stockmayer regarding disulfide bond involvement. One proposition, given the involvement of the

disulfide bond, could be that the adduct thiyl radical achieves more stabilisation due to proximity to benzyl ring, and as such the bond cleaves more readily.

This was later expanded on by Pierson *et al.* (1955), who also looked at the influence of disulfides on the bulk polymerisation of Sty,³⁶ detailing the influence of the “R” groups on the reactivity of the species in chain transfer reactions. For aliphatic disulfides, the chain transfer activity was demonstrated to be quite low, for example, $C_{tr,S}$ was determined to be < 0.005 (more accuracy was not provided for each species) at 50 °C for 2-hydroxyethyl disulfide (1), 3,3'-Dithiodipropionic acid (2), Bis-(2-ethyl hexyl) disulfide (3), propyl ester of bis-(β -carboxyethyl) disulfide (4), and bis-(β -chloroacetoxyethyl) disulfide (5) respectively, with the structures given in Figure 2.1.2.3. The modification of the heteroatoms and configurations near to the disulfide did not appear to influence the chain transfer activity greatly in these compounds.

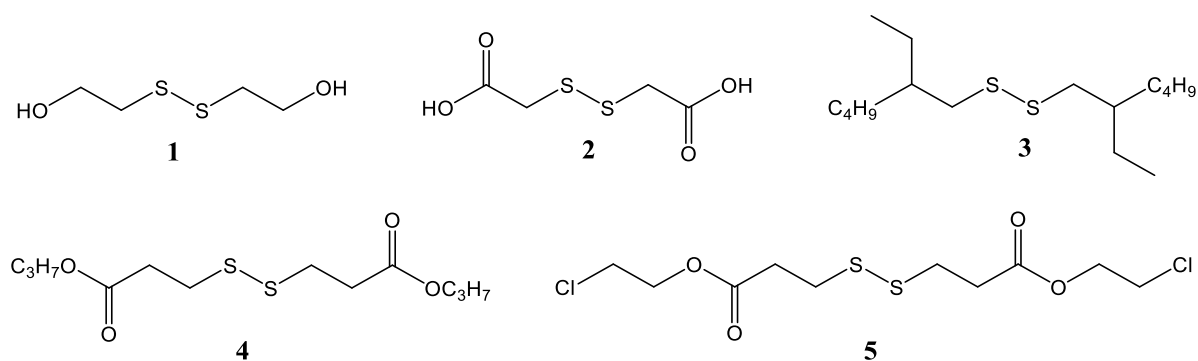


Figure 2.1.2.3: Structures of less reactive aliphatic type disulfides. Being 2-hydroxyethyl disulfide (1), 3,3'-Dithiodipropionic acid (2), Bis-(2-ethyl hexyl) disulfide (3), propyl ester of bis-(β -carboxyethyl) disulfide (4), and bis-(β -chloroacetoxyethyl) disulfide (5).

Large increases in the activity were observed when dramatically changing the functionality, however, such as the proximity of aromaticity, as with structures 6, 7, 8, 9 and 10 in Figure 2.1.2.4, which exhibited chain transfer constants of 0.06, 0.23, 0.73, 1.3 and 1.0, respectively at 50 °C. Although the exact origin of the differences was not extensively detailed, the authors simply concluded that the substitutions influence the ability of the disulfide to undergo cleavage. It is noted that the potential of transfer through the halogen atoms in 9 and 10 was not discussed. Structure 11 in Figure 2.1.2.4, a so called xanthogen, reported the highest chain transfer constant in the study of 5.3. The authors went on to demonstrate the presence of 2 end groups in polymers formed through polymerisation in the presence of carboxylic acid containing disulfides through titration, furthering the validity of the mechanism given in Scheme 2.1.2.1.

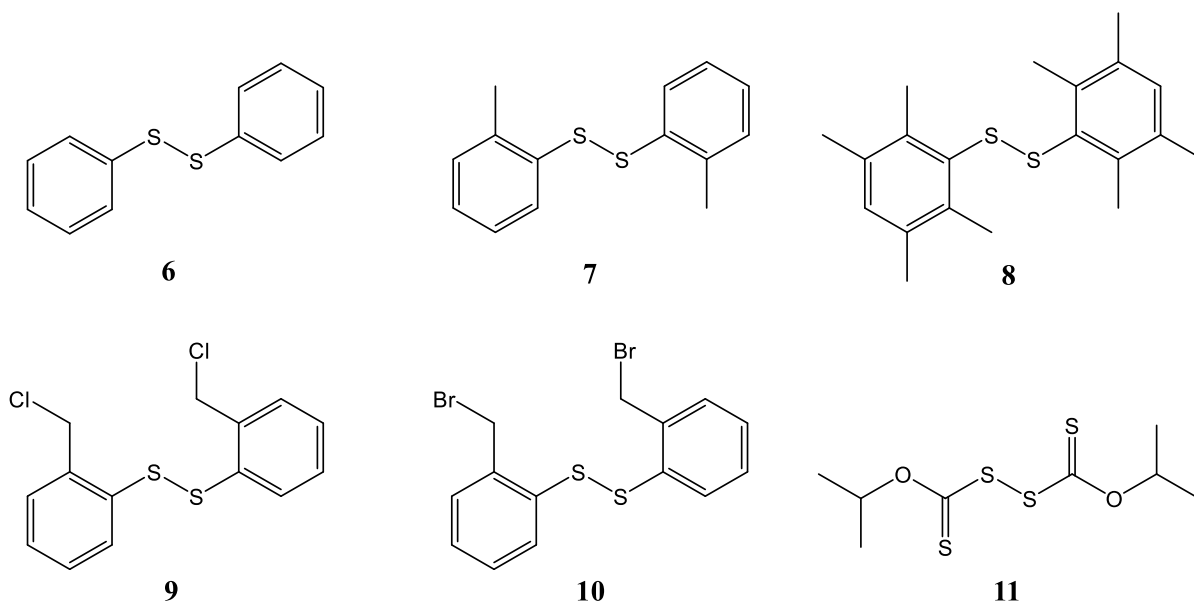
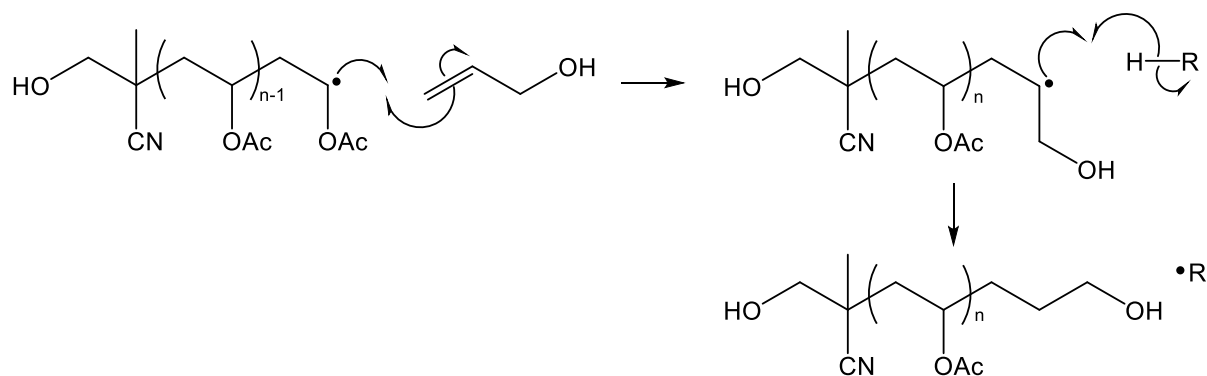


Figure 2.1.2.4: Structures of more reactive disulfides. Being diphenyl disulfide (6), di(2-methyl phenyl) disulfide (7), di(2,3,5,6-tetramethyl phenyl)disulfide(8), di(2-chloromethyl phenyl) disulfide (9), di(2-bromomethyl phenyl) disulfide (10) and di(isopropyl-xanthogen) disulfide (11).

In 1982, Otsu *et al.* polymerised VAc utilising either 4,4'-azobis(4-cyanovaleric acid) (ACVA) or azobisisobutyronitrile (AIBN), in the presence of dithiodiglycol acid, a linear disulfide with -CH₂COOH side groups (2 in Figure 2.1.2.3).⁵³ The authors were able to demonstrate through titration that, even when using AIBN (an initiator with no acid functionality), polymer chains with 2 acidic groups were produced, suggesting telechelic polymers had formed via chain transfer to the disulfide, and reinitiation by the corresponding thiyl radical.

A similar feat was later achieved by Cho *et al.* (1999), who demonstrated the production of PVAc with hydroxyl functionality at both ends of the polymer chain.⁵⁴ Here, the authors used both an initiator with alcohol functionalities (4,4'-azobiscyanopropanol, ACPROL) as well as allyl alcohol, which essentially acted as a CTA. After initiation (introduction of functionality at α terminus, the propagating PVAc would eventually undergo addition to the allyl alcohol. The resultant radical is particularly unreactive and was proposed to undergo transfer instead of propagation, suggested to be to another unit of allyl alcohol, with the net result being PVAc with OH groups at each terminus, as per Scheme 2.1.2.3 (here, the transfer step is illustrated to the generic species H-R, which may be fulfilled by allyl alcohol, VAc, PVAc, solvent or initiator). Again, chains were found to contain on average ≈ 2 hydroxyl groups per chain, and increasing the concentration of allyl alcohol decreased the MW (for example where [AA] (%) went from 0.045 to 0.450, M_n dropped from 2790 to 1900 g mol⁻¹).



Scheme 2.1.2.3: Mechanism for the reaction in the study by Cho *et al.* wherein VAc is polymerised in the presence of ACPROL and allyl alcohol, to yield PVAc with hydroxyl groups at each terminus.

Teodorescu *et al.* (2010) exploited the chain transfer activity of disulfide bonds by polymerisation of VAc in the presence of liquid polysulfides, or so called thicols.⁵⁵ These thicols are oligomeric species, with terminal thiol groups, with a backbone containing disulfide bonds. The authors discussed the prevalence of chain transfer to thiols, and therefore concluded minimal influence on the course of the polymerisation, as these were consumed before 2 % monomer conversion. The MW formed through the rest of the reaction was governed by chain transfer to the disulfide bonds, which were determined to possess $C_{tr,S} = 0.89$ by following their consumption as a function of monomer conversion.

It is worth noting that in the absence of a CTA, end groups can still be introduced by the initiating species. As will be discussed further in Chapter 3, extreme initiator concentrations are commonly used in copolymerisation of vinyl monomers with multifunctional vinyl monomers to prevent gelation, which in turn results in significant introduction of initiator derived functional groups in the polymer.⁵⁶⁻⁵⁹ In the event that polymer radicals terminate through combination (as is the case for VAc, assuming no chain transfer), the resultant polymer will have initiator residues at both ends of the chain.

2.1.3 Chapter aims.

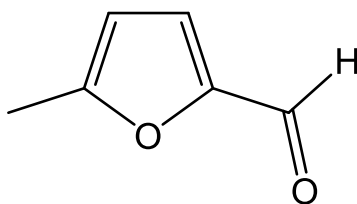
In this chapter, the aim was to explore alternative chain transfer agents to thiols for VAc free radical polymerisation, which bare chain transfer constants much closer to unity. Although Cobalt catalysts offered an interesting increased degree of control through RDRP, conventional CTAs were of greater interest herein due to the increase in industrial applicability. Disulfides were of particular interest due to the simplicity of the systems, and

the inherent production of telechelic polymers. The kinetics and mechanisms will be discussed, laying the foundation for their use in Chapters 3 and 4.

2.2 Results and discussion

2.2.1 5-methyl furfural.

One species reported by Stockmayer *et al.* (1960) to have a favourable chain transfer constant with VAc was Furfural ($C_{tr,S} = 1.5$ at 60 °C), although it was suggested to be strongly degradative.¹⁴ 5-methyl furfural (MFF, Scheme 2.2.1.1) is a compound which may be derived from biomass derived carbohydrates,^{60,61} making it attractive as a reagent not sourced from crude oil. MFF and its derivatives already find use in a variety of applications commercially, as a fragrance,^{62,63} fuel,⁶³⁻⁶⁵ and a reagent in various syntheses.^{66,67} The comparable structure to furfural (one additional methyl at the 5 position), and the favourable chain transfer constant measured for furfural means the activity of MFF was potentially very interesting.



Scheme 2.2.1.1: Structure of 5-methyl furfural (MFF).

Unfortunately, the authors did not present any conversion time data, and as such, the significance of any retardation could not be assessed. A small amount of retardation could be acceptable given the potential upsides of using a biomass derived reagent. The expectation was that the aldehyde proton would be extracted during the chain transfer reaction, and as such the CH₃ group on the furan ring was expected to contribute little to the chain transfer activity, so a chain transfer constant similar to furfural was expected.

A solution polymerisation of VAc was carried out in the presence of 1 wt% MFF to assess the significance of this retardation. As can be seen from the nuclear magnetic resonance (NMR) data displayed in Figure 2.2.1.1, very minimal conversion was observed after 3 h, and even after 24 h, a miniscule amount of polymer was observed (appearance of broad backbone polymeric CH₂ shift at \approx 1.6-1.9 ppm). The degree of conversion was too low to extract any accurate conversion time data from the NMR data, although $p < 0.01$ after 24 h. The other peaks in the spectra can be assigned as follows: the primary distributions at 2.13 and 2.04 ppm are the OCH₃ shifts of VAc and ethyl acetate (Et-OAc), respectively. The small peaks at 2.25

and 1.83 ppm are spinning side bands to the OCH₃ of Et-OAc at 2.04 ppm. The peaks at 2.35 and 1.91 ppm are spinning side bands to the OCH₃ of VAc at 2.13 ppm. The peak at 2.42 ppm is the CH₃ proton of MFF. The peak at 1.73 ppm is an unidentified contaminant. The origin of the peaks at 1.84 ppm in the 60-minute sample, 1.88 ppm in the 90-minute sample, 1.81 ppm in the 120-minute sample and 1.97 in the 150-minute sample are unknown, and seem to be unique to each spectrum. These could be contaminants during sampling, or artifacts of the analysis.

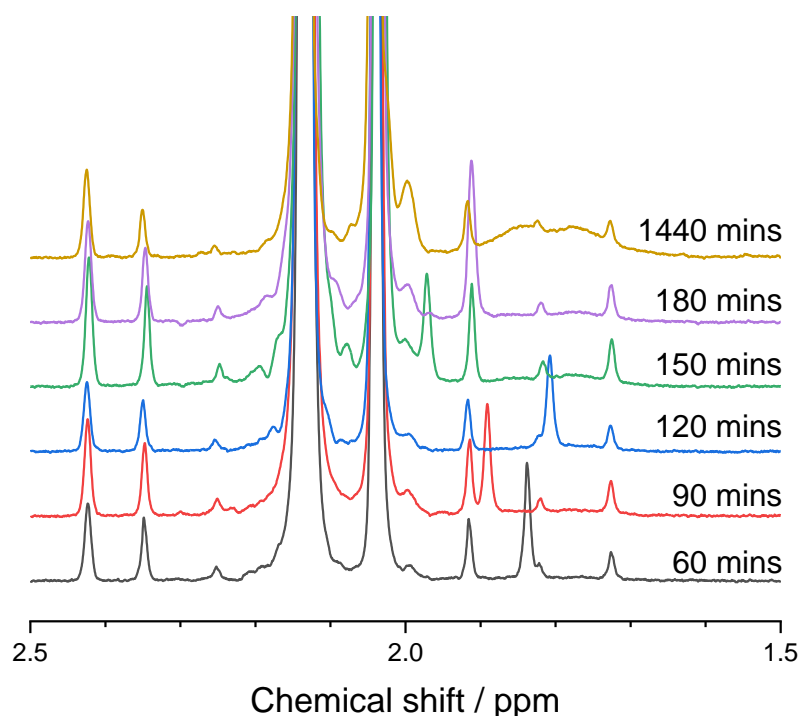


Figure 2.2.1.1: ¹H NMR (300 MHz, CDCl₃) between 1.5 and 2.5 ppm of the crude samples withdrawn from the free radical polymerisation of vinyl acetate in ethyl acetate in the presence of 1 wt% MFF wrt VAc.

The crude samples from the polymerisation were added to tetrahydrofuran (THF) to try and obtain MWDs through size exclusion chromatography (SEC). Given the miniscule conversion, only distributions for 180 and 1440 mins could be obtained, and that for 180 mins showed some noise in the signal, particularly at the high and low MW ends of the distribution. The two MWDs can be seen in Figure 2.2.1.2.

The MWD appears to shift slightly to lower MW between 180 and 1440 mins. This behaviour implies that $C_{tr,S} < 1$, which would lead to $[CTA]/[M]$ increasing with conversion, hence the shift to lower MW. $C_{tr,S}$ was determined experimentally from the SEC data using the Gilbert method discussed in Chapter 1. A plot of the natural logarithm of the number distribution, $\ln N(i)$ vs degree of polymerisation, i , can be seen in Figure 2.2.1.3. The overlaid black traces

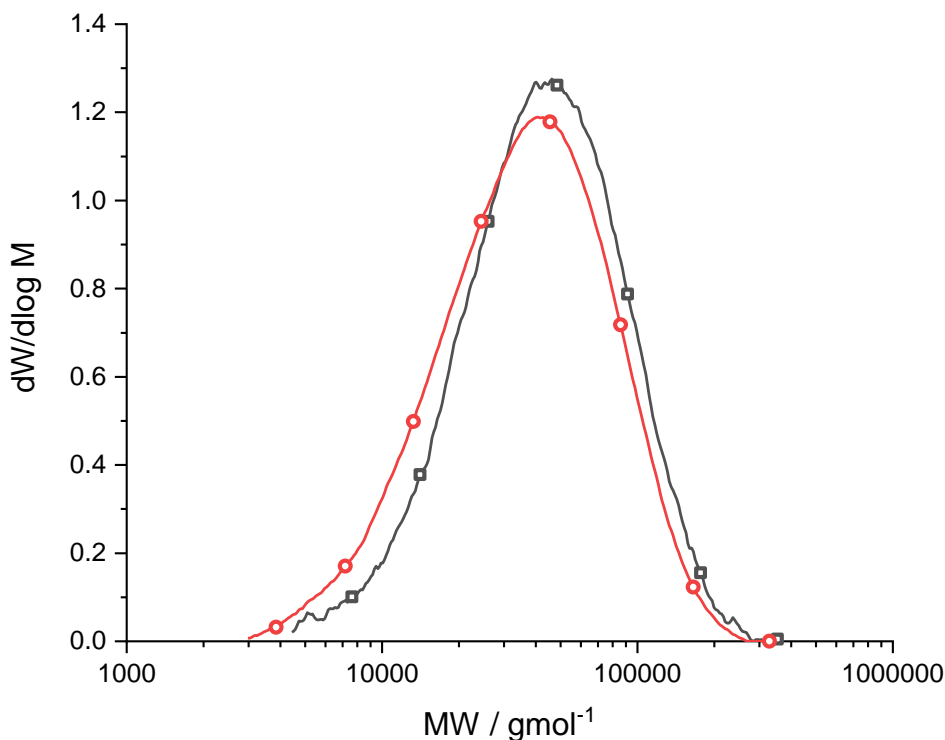


Figure 2.2.1.2: $dW/d\log M$ vs molecular weight (MW, gmol^{-1}), molecular weight distributions for the free radical polymerisation of vinyl acetate in ethyl acetate in the presence of 1 wt% MFF wrt VAc after 180 (\square) and 1440 mins (\circ).

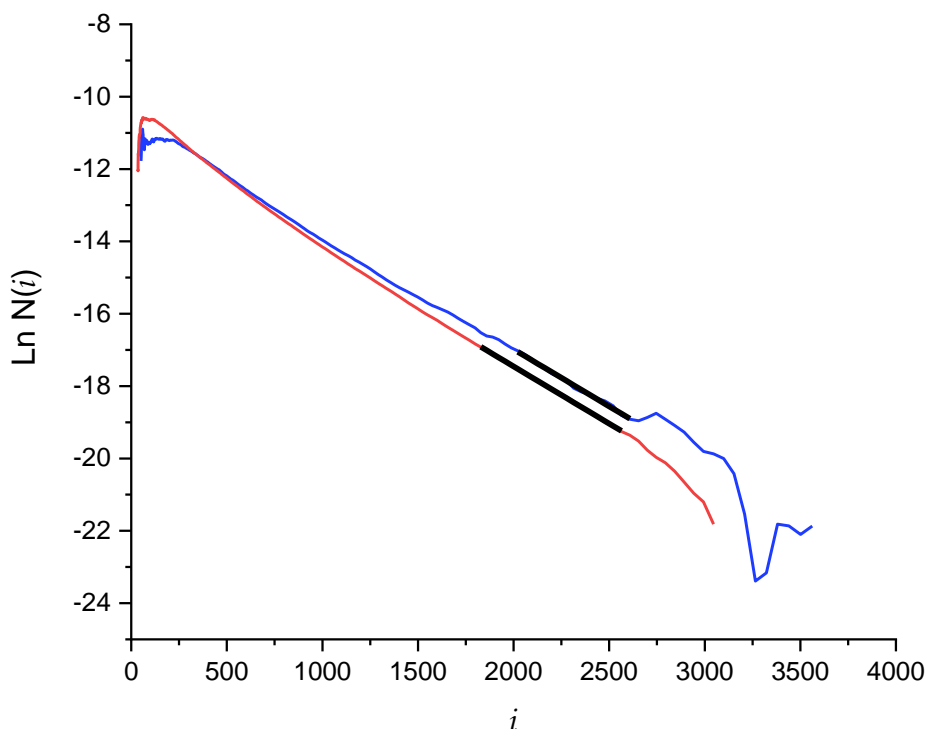
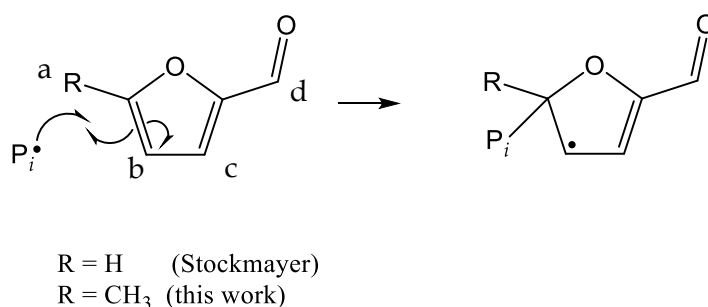


Figure 2.2.1.3: $\text{Ln } N(i)$ vs i for the samples withdrawn after 180 mins (\rightarrow) and 1440 mins (\rightarrow) during the free radical polymerisation of vinyl acetate in the presence of 1 wt% MFF. The overlaid black traces show the linear region from which the slope was extracted to calculate $C_{tr,S}$ using the Gilbert method.

are the portion of each distribution (at the high MW limit) from which the slope was extracted.

The samples at 180 and 1440 mins both yield $C_{tr,S}$ values of 0.36 (assuming $C_{tr,Solvent} = C_{tr,M} = 2.7 \times 10^{-4}$). The small shift in MW to lower degree of polymerisation (DP) can be observed here, although given the low conversion, and the fact the drift is to low DP (high MW end effected less), the similarity in the slopes of the two distributions is not unusual. It is noted that this is quite different to the value proposed by Stockmayer of 1.5 for furfural, suggesting that perhaps the methyl substituent goes some way to reduce the reactivity in chain transfer. This is not intuitive, given the expectation that aldehyde proton abstraction is the main chain transfer pathway. However, Davidenko suggested that the 5-position of a furfuryl ring is susceptible to radical attack.⁶⁸ This is demonstrated for furfural and MFF in Scheme 2.2.1.2.



Scheme 2.2.1.2: Proposed mechanism for addition to furfuryl rings, suggested by Davidenko and supported through the difference in chain transfer activity between this study and that of Stockmayer.

The retardation could therefore be explained by the low reactivity of the derived radical, with the methyl substitution at the 5-position leading to a larger steric barrier to attack, and a consequential lower value for $C_{tr,S}$. In fact, comparing the integrals of the protons a (2.42 ppm), b (6.25 ppm), c (7.18 ppm) and d (9.51 ppm), as seen in Figure 2.2.1.4 and Table 2.2.1.1, very little change is observed with increasing conversion. The integrals are normalised to proton c, although the signal to noise ratio of each of the peaks is quite low throughout, therefore, the integral values are likely not a good reference for the actual concentrations.

Table 2.2.1.1: Integral values from the 1H NMR spectra for the protons a, b, c and d defined in Scheme 2.2.1.2, with the values normalised to the integral of proton c at 7.18 ppm.

Time / mins	$\int(CH_3 - a)$ 2.42 ppm	$\int(CH - b)$ 6.25 ppm	$\int(CH - c)$ 7.18 ppm	$\int(CH - d)$ 9.51 ppm
120	2.87	0.99	1	0.96
180	3.51	1.11	1	1.11
1440	3.33	1.00	1	1.05

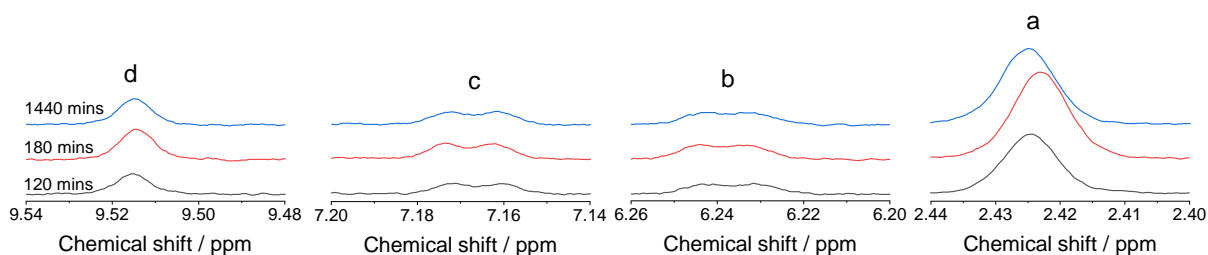


Figure 2.2.1.4: ^1H NMR shift assignments for the protons a, b, c and d from the structure in Scheme 2.2.1.2 of MFF.

Further analysis of the NMR spectra reveals the appearance of 3 new peaks in the 1440 min sample, which were not visible in any other sample. These appear at 5.55 ppm, 2.91 ppm and 2.83 ppm. The integrals of these peaks are all identical, and the shift at which they appear correlate well to the predicted shifts for the product given in Figure 2.2.1.5. This would imply favourable addition to MFF, followed by proton abstraction by the adduct radical to kill the chain.

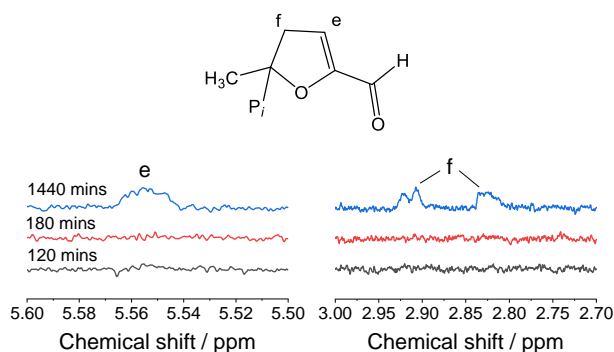


Figure 2.2.1.5: ^1H NMR shift assignments for the protons e and f, and the structure to which they correlate.

Given that this species showed such significant retardation, the origin of this difference was not explored further. It was proposed that as slow reinitiation was causing the observed retardation, introduction of a comonomer may offer an alternate species to reinitiate through. Methyl acrylate (MA) and dibutyl maleate (DBM) were trialled for this purpose. The logic here was that the MFF derived radical may then be able to reinitiate the comonomer, with the comonomer radical then cross propagating back to VAc.

Copolymerisation of VAc and DBM has been shown to produce primarily alternating copolymers ($r_{\text{VAc}} = 0.1135$, $r_{\text{DBM}} = 0.0562$).⁶⁹ In this case, assuming reinitiation through DBM, the cross propagation would be favoured. Copolymerisation with MA on the other hand, would be expected to favour homopropagation of MA ($r_{\text{VAc}} = 0.029$, $r_{\text{MA}} = 6.700$).⁷⁰ The reactions were performed at 10 wt% comonomer wrt VAc, in the presence of 1 wt% MFF wrt

VAc (total wt ratio VAc/comonomer/MFF = 100/10/1). Conversion was followed through ^1H NMR by comparison of the monomer vinylic resonances at ≈ 4.9 , 6.2 and 6.4 ppm for VAc, DBM and MA respectively, relative to the Et-OAc solvent resonance at ≈ 1.3 ppm. This solvent resonance is expected to remain unchanged, even if chain transfer to solvent occurs (transfer would likely occur through the O-CH₃ protons, changing the intensity of the shift at around 2.0 ppm). The partial monomer conversions in each reaction can be seen in Figure 2.2.1.6.

For DBM, the copolymerisation occurs as may be expected. The final partial monomer conversion of each monomer at 180 mins indicates that the polymer should contain DBM: VAc in the ratio of 1.26: 1. This is very close to that which may be expected for an alternating copolymer, as the reactivity ratios suggest, although if the reactivity ratios are valid, it may be expected that more VAc would be consumed than DBM, particularly given the difference in concentrations employed. However, given that the overall conversion is so low, the ratio is subject to significant error through NMR analysis. It is evident that during copolymerisation with MA, the rate of polymerisation is significantly faster compared to DBM, as may be expected with the acrylate which possesses a particularly high value for k_p of 27,850 L mol⁻¹ s⁻¹ at 60 °C (calculated using the Arrhenius parameters $A = 16.6 \times 10^6$ L mol⁻¹ s⁻¹ and $E_A = 17.7$ kJ mol⁻¹)⁷¹. It is also noted that homopolymerisation of methyl acrylate is heavily favoured in the copolymerisation, as the reactivity ratios predict. The MWDs as a function of time can be seen in Figure 2.2.1.7. In both cases, the distribution is seen to shift to lower MW with increasing time, again suggesting an increase in the [MFF] relative to monomer, suggesting a chain transfer constant of < 1 .

Neither of these results suggest MFF would be a viable CTA for VAc, even through use of a comonomer. With DBM, the products are limited to contain high proportions of DBM due to the alternating copolymerisation behaviour. With MA, significant proportions of MA end up in the polymer, and as such composition drift will occur, leading to the necessity of monomer feeds. At this point, the retardation was deemed too significant to justify continuing the exploration of MFF, with the optimisation of comonomer/feed rates deemed too far outside of the scope of this work. Instead, the use of disulfides was next explored.

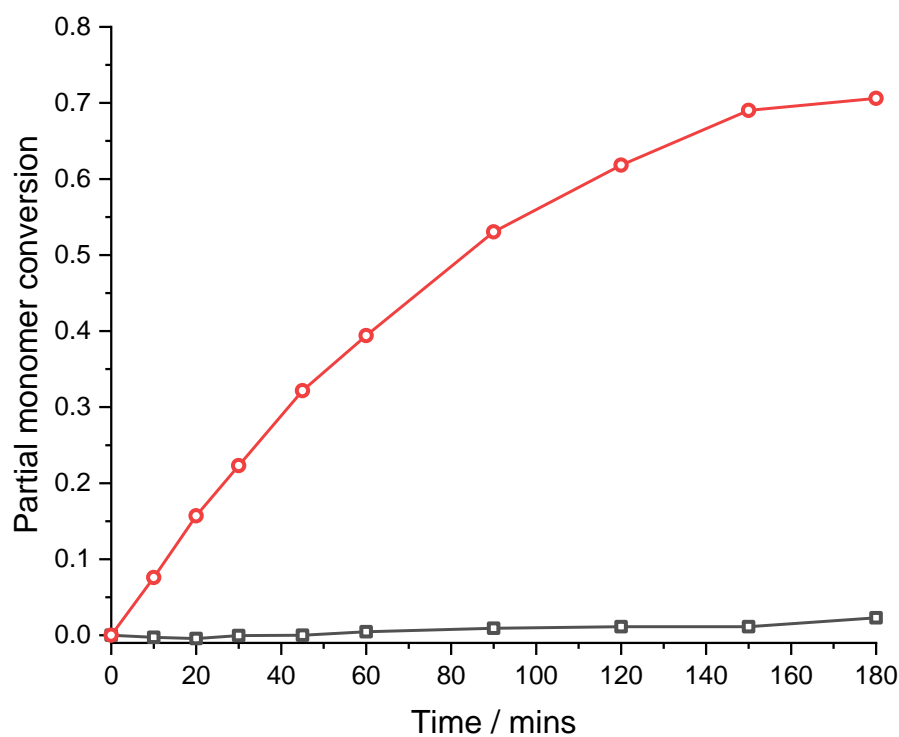
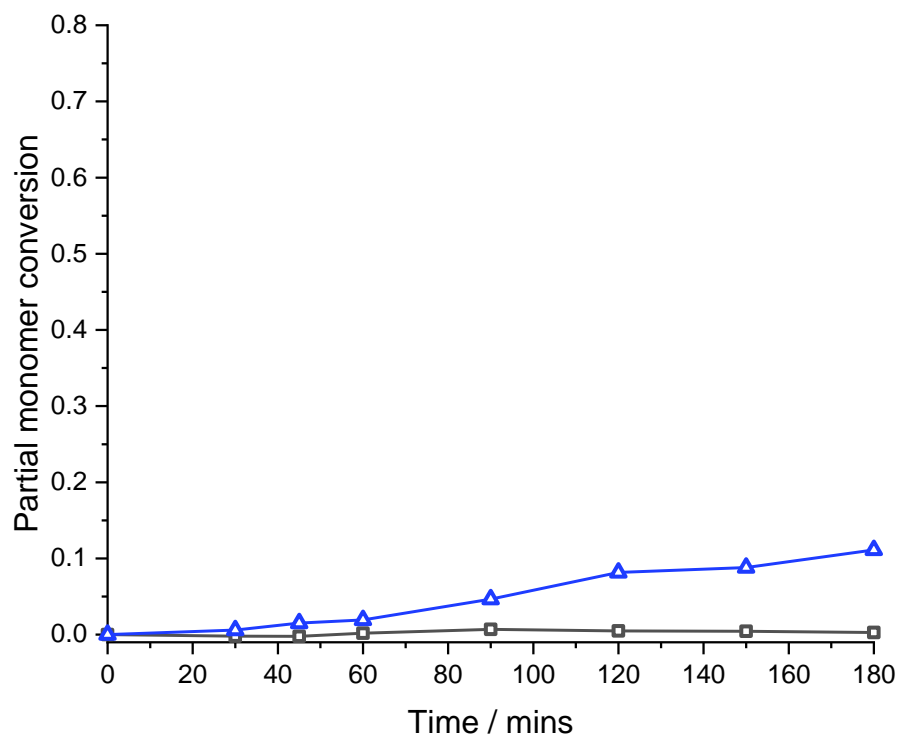


Figure 2.2.1.6: Partial monomer conversion for the copolymerisation of VAc (□) and DBM (△) (top), and the copolymerisation of VAc (□) and MA (○) (bottom), both in the presence of MFF. The weight ratios of VA/comonomer/MFF employed were 100/10/1.

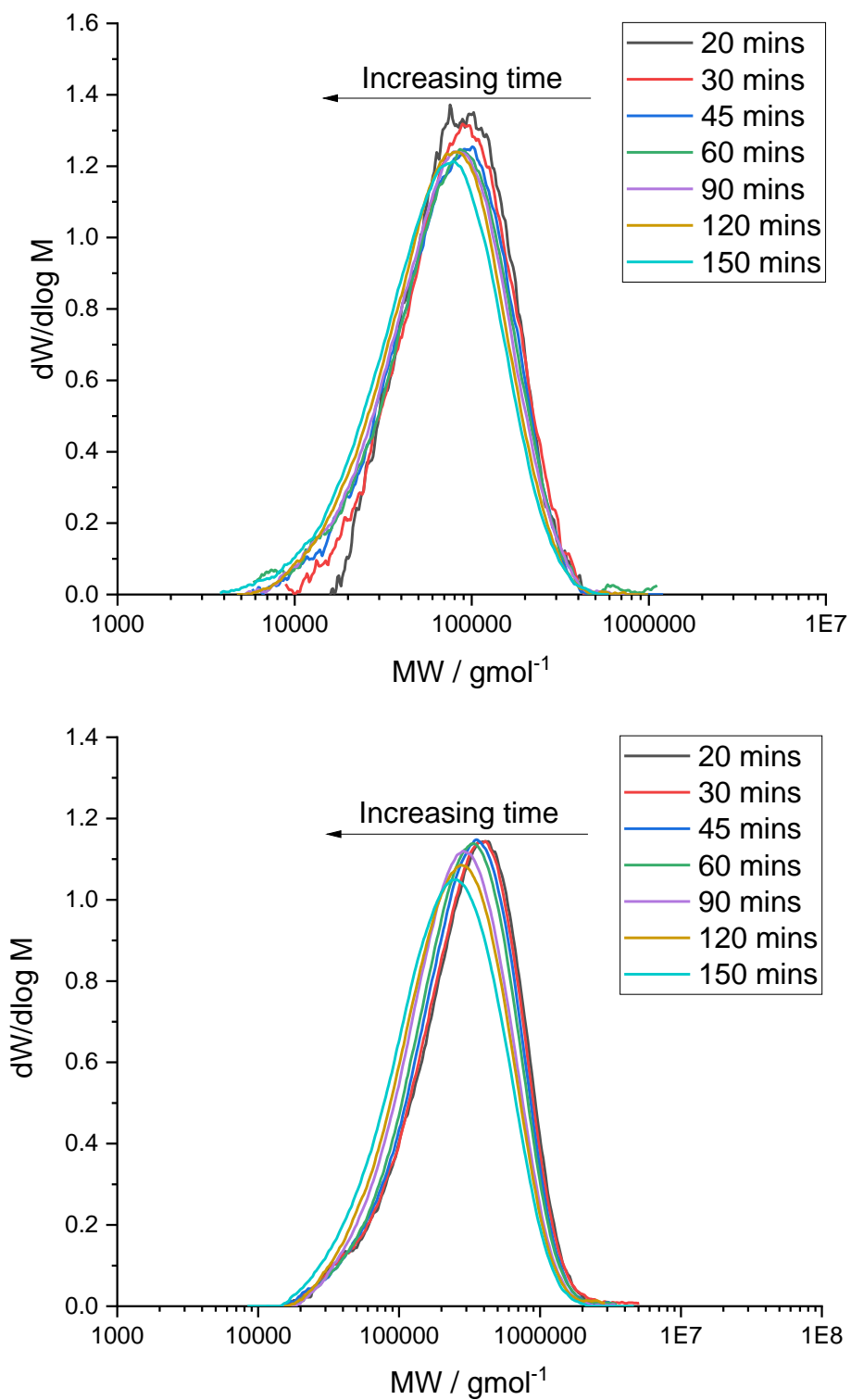
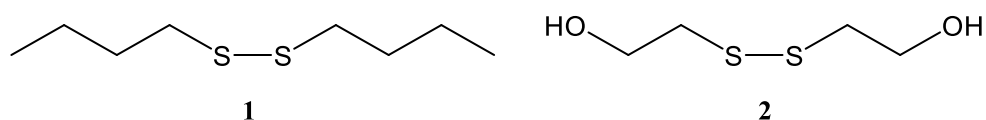


Figure 2.2.1.7: Molecular weight distributions, $dW/d\log M$ vs $MW (\text{gmol}^{-1})$, as a function of time for the copolymerisation of vinyl acetate and dibutyl maleate (top), and the copolymerisation of vinyl acetate and methyl acrylate (bottom), both in the presence of MFF. The weight ratios of VA/comonomer/MFF employed were 100/10/1.

2.2.2 Linear disulfides.

The chain transfer activity of disulfides was next evaluated, as they offered a potentially attractive chain transfer constant for VAc free radical polymerisation. The behaviour of several disulfides in the free radical polymerisation of VAc was assessed. The compounds selected, dibutyl disulfide (**1**) and 2-hydroxyethyl disulfide (**2**), can be seen in Scheme 2.2.2.1. **1** has a hydrophobic, aliphatic side chain, and **2** has a shorter side chain with an alcohol functionality. The difference in chemical functionality from the beta carbon onwards may influence the kinetics of the chain transfer/reinitiation reactions for **2** and would likely give the disulfide different partitioning behaviour to **1** when employed in a heterogenous polymerisation (such as emulsion polymerisation), which made it of interest for future applications.



Scheme 2.2.2.1: Structures of the linear disulfides used in this work, dibutyl disulfide (**1**) and 2-hydroxyethyl disulfide (**2**).

A series of solution polymerisations of VAc were first carried out in the presence of varying quantities of **1** and **2**. **1** and **2** are predicted to decrease the MW of the polymer through chain transfer. In these series, $[VAc]_0 = 8.6 \text{ M}$, $[Et-OAc]_0 = 2.1 \text{ M}$, $[AIBN]_0 = 7.7 \times 10^{-4} \text{ M}$. Solvent was used to delay the influence of increased viscosity on the rate of termination, and therefore the rate of polymerisation. Additionally, as Et-OAc can itself act as chain transfer agent ($C_{tr,S} = 3.3 \times 10^{-4}$),¹⁴ gelation due to transfer to monomer/polymer may also be delayed (to be discussed in Chapter 3), further preventing changes in the rate of termination (as [Et-OAc] is kept constant over all experiments this does not influence the measurement of $C_{tr,S}$ of the disulfides). The polymerisations were followed over time to assess the behaviour of these species as chain transfer agents. The MWDs were determined through SEC, and monomer conversion was followed gravimetrically.

It is noted that in the absence of CTA, the solution had become very viscous by 60 mins, making sampling very difficult, and the reaction was stopped to avoid any chances of thermal runaway. This behaviour was also observed for **1** where $[1]/[M] = 1 \times 10^{-4}$, 5×10^{-4} and 1×10^{-3} . At $[1]/[M] = 5 \times 10^{-3}$ and 1×10^{-2} , and in all the reactions employing **2**, the polymerisation was continued to 120 mins as solution viscosity remained low enough to allow sampling. As can be seen in Figure 2.2.2.1, the introduction of either **1** or **2** into the formulation results in a

reduction in the rate of polymerisation, which becomes more exaggerated with increasing concentration of disulfide. For example, with **1** at $[1]/[M] = 1 \times 10^{-3}$, the rate was still 92.52 % of that in the absence of disulfide, as seen in Table 2.2.2.1. This is a notable difference, but not as significant as the retardation observed by Stockmayer *et al.* for the same system.⁴⁹ Interestingly very little difference is observed in the rate at concentrations lower than this, with $[1]/[M]$ even appearing to possess a higher rate than the experiment with no CTA, although this appears to be within experimental error. When **2** was employed at the same concentration, a much more significant decrease in the rate of polymerisation was observed, with 1.55 % of the original rate being observed at $[2]/[M] = 1 \times 10^{-3}$.

Some of the experiments employing both **1** and **2** show evidence of curvature in the conversion time data, suggesting that the rate of polymerisation changes over time. In the case of $[1]/[M] = 1 \times 10^{-2}$, there appears to be an initial acceleration, followed by a decrease in rate after around 30 minutes. When $[2]/[M] = 5 \times 10^{-5}$, the rate appears to accelerate up to around 75 minutes, at which point the rate approaches that observed for the reaction run in the absence of **2**. The origin of this behaviour will be proposed in later discussions.

Table 2.2.2.1: Collated rate data for the free radical polymerisation of vinyl acetate in the presence of varying quantities of **1** and **2**. Rate % is reported relative to the experiment in the absence of S.

[S]/[M]	1 R_p / M s ⁻¹	1 Rate %	2 R_p / M s ⁻¹	2 Rate %
0	4.68×10^{-4}	100.00	4.68×10^{-4}	100.00
5.00×10^{-5}	-	-	1.01×10^{-4} ^b	21.58
1.00×10^{-4}	4.99×10^{-4}	106.62	5.29×10^{-5}	11.30
5.00×10^{-4}	4.68×10^{-4}	100.00	1.36×10^{-5}	2.91
1.00×10^{-3}	4.33×10^{-4}	92.52	7.23×10^{-6}	1.55
5.00×10^{-3}	2.88×10^{-4} ^a	61.54	-	-
1.00×10^{-2}	2.06×10^{-4} ^a	44.02	-	-

^a = R_p calculated from 30-120 mins where linear

^b = R_p calculated up to 45 mins where still linear

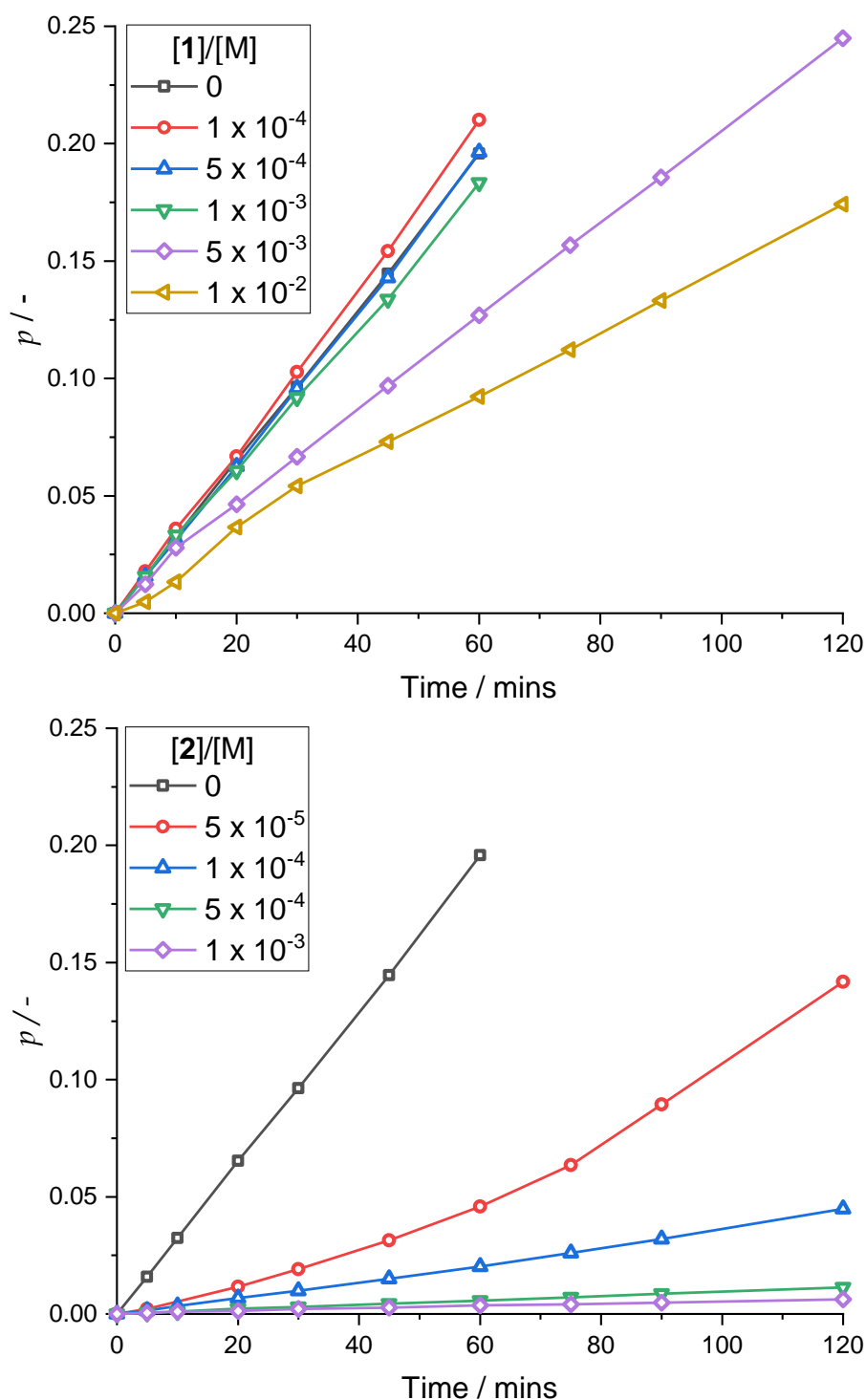


Figure 2.2.2.1: Monomer conversion, p , as a function of time (mins) for the solution polymerizations of vinyl acetate at varying concentrations of dibutyl disulfide, **1**, (top) and 2-hydroxyethyl disulfide, **2**, (bottom).

The influence of both **1** and **2** on the MWDs of the polymers produced is clear. As seen in Figure 2.2.2.2, and tabulated in Table 2.2.2.2 after 1 hour in both cases, distributions with narrow polydispersity's are produced, which decrease in MW as the concentration of

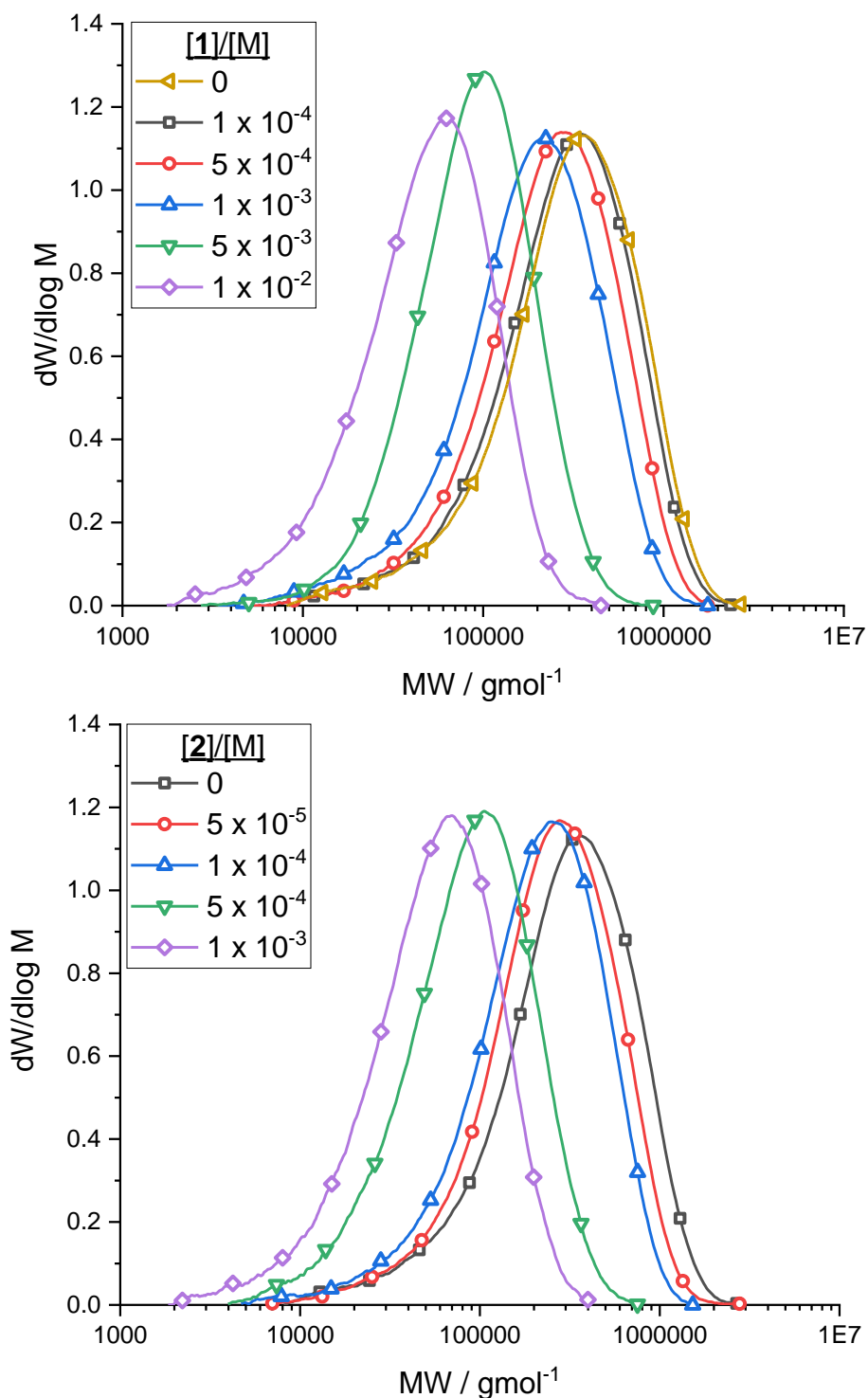


Figure 2.2.2.2: Molecular weight distributions, $dW/d\log M$ vs MW (g mol^{-1}), for the solution polymerisation of vinyl acetate in the presence of varying quantities of **1** (top) and **2** (bottom).

disulfide is increased. **2** appears to reduce the MW of the polymers produced more than **1** at the same given concentration. Again taking $[S]/[M] = 1 \times 10^{-3}$, M_n is reduced to 98,400 and 39,300 g mol^{-1} for **1** and **2** respectively from a value of 254,200 g mol^{-1} in the absence of disulfide.

Table 2.2.2.2: Collated MW data from the solution polymerisations in the presence of varying quantities of **1** and **2**, where p is monomer conversion (determined gravimetrically) and M_n , M_w and \mathcal{D}_M are the number and weight average MWs and the dispersity respectively determined through SEC analysis of the produced polymers after 1 h.

Chain transfer agent	[S]/[M]	p	$M_n / \text{g mol}^{-1}$	$M_w / \text{g mol}^{-1}$	\mathcal{D}_M
-	0	0.196	175,400	405,300	2.311
Dibutyl disulfide (1)	1.00×10^{-4}	0.210	165,000	374,400	2.270
	5.00×10^{-4}	0.196	146,800	310,400	2.115
	1.00×10^{-3}	0.183	103,700	240,700	2.322
	5.00×10^{-3}	0.127	63,500	112,000	1.763
	1.00×10^{-2}	0.092	30,400	63,000	2.071
2-Hydroxyethyl disulfide (2)	5.00×10^{-5}	0.046	156,800	325,300	2.074
	1.00×10^{-4}	0.020	123,600	270,100	2.185
	5.00×10^{-4}	0.006	57,900	113,800	1.966
	1.00×10^{-3}	0.004	34,700	72,300	2.080

The values of \mathcal{D}_M appear to decrease with increasing concentration for **2**, however, this is likely simply due to the massive reduction in rate, and therefore lower conversion of the sample after 1 h at higher concentrations. Therefore, the ratio $[\mathbf{2}]/[\text{M}]$ has much less opportunity to drift. With **1** the PDI sits quite consistently around 2-2.5, which may suggest a small amount of drift, but nowhere near the amount expected with thiols.

The low PDI observed at the reasonable degree of conversion, particularly with **1**, suggests a chain transfer constant close to unity, resulting in a very small amount of drift in a chain transfer dominated system. This can be seen when analysing the MWD as a function of time for both systems with $[\text{S}]/[\text{M}] = 1 \times 10^{-4}$ as seen in Figure 2.2.2.3.

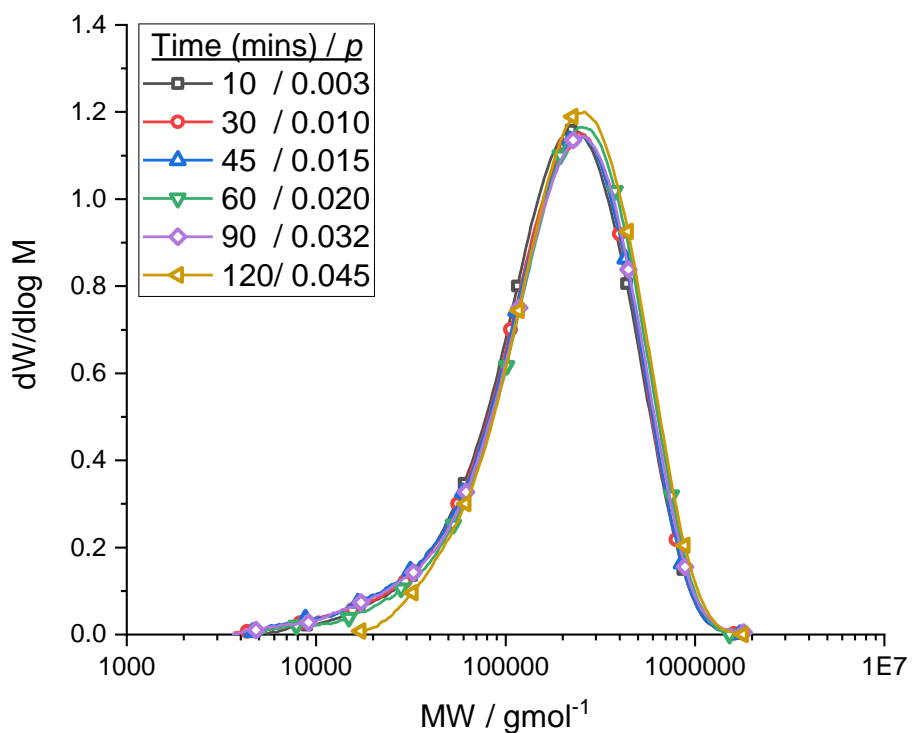
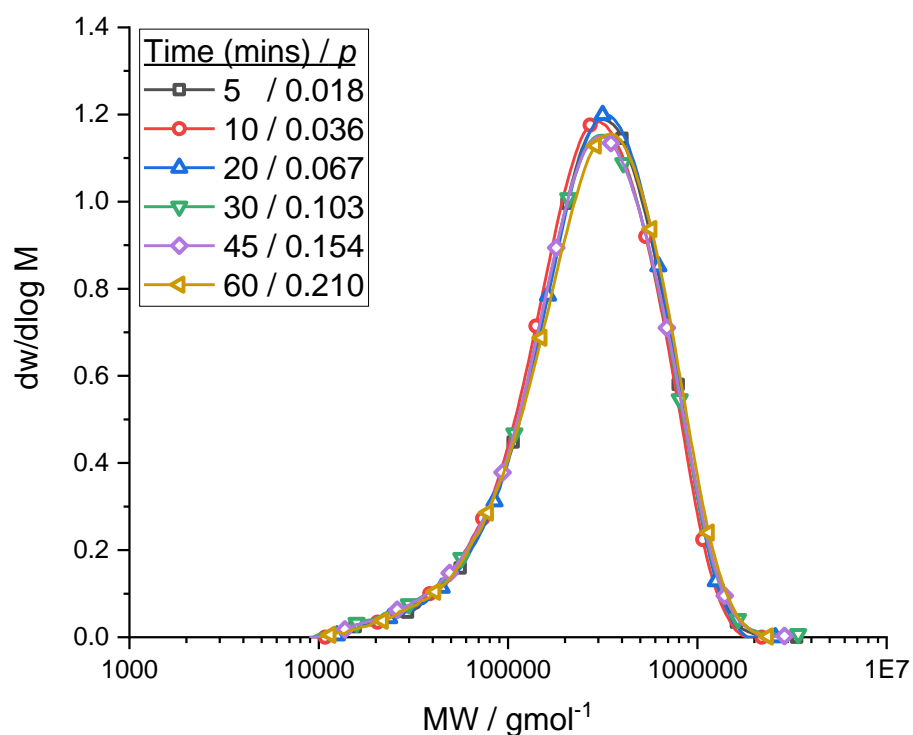


Figure 2.2.2.3: Molecular weight distributions, $dW/d\log M$ vs MW (gmol^{-1}), as a function of conversion, for the solution polymerisation of VAc in the presence of **1** (top) and **2** (bottom), both at $[S]/[M] = 1 \times 10^{-4}$. The legend details the time (mins) of the sample and the corresponding monomer conversion, p , in the form Time (mins) / p .

Due to very minimal composition drift, the MWD of a low conversion sample of polymer would provide a good instantaneous picture of how the starting $[S]/[M]$ ratio influences the MW. Therefore, both the method determined by Mayo,⁷² and Gilberts chain length distribution method (CLD),⁷³⁻⁷⁵ (both of which were discussed extensively in Chapter 1) could be applied to the data to determine a value for $C_{tr,S}$. Firstly, the MWDs of low conversion samples of the polymerisations were determined through SEC. The distribution parameters can be seen in Table 2.2.2.2 (with the exact concentration ratio's detailed). Plots of \bar{X}_n^{-1} (as originally proposed by Mayo) and $2\bar{X}_w^{-1}$ vs $[S]/[M]$ were then constructed from these low conversion samples, as seen in as seen in Figure 2.2.2.4, \bar{X}_n and \bar{X}_w being the number average and weight average degrees of polymerisation, respectively. $2\bar{X}_w^{-1}$ is used as an alternate method to determine \bar{X}_n^{-1} , given that in a chain transfer dominated system $M_w = 2M_n$.^{76,77} The origin of the fact that $M_w = 2M_n$ can be derived from the Flory-Shulz MWD, which states that the dispersity of a chain transfer dominated system is equal to $1 + p$, where p is the probability of propagation. Therefore, for polymer chains of high DP, where p approaches 1, $PDI = 2$. This is an extremely useful relation, as M_w is much less sensitive to errors during analysis of the chromatogram, and as such more reliable data may be obtained.^{78,79} These were determined by taking the number average and weight average MWs (M_n and M_w) and dividing by the mass of the repeat unit (ignoring the contribution of end groups). The slopes of the constructed plots are equal to $C_{tr,S}$ according to Mayo's method.

It is clear from the constructed data sets that linear plots can be constructed in both cases, however, one outlier can be seen for **1**, in the plot of \bar{X}_n^{-1} , despite the plot of $2\bar{X}_w^{-1}$ showing good linearity. The use of the data extracted from the plot of $2\bar{X}_w^{-1}$ is favoured here, due to the previously discussed accuracy benefits. It is noted that for the erroneous sample ($[1]/[M] = 4.98 \times 10^{-2}$), PDI is 1.731, significantly lower than a value of 2 expected for a chain transfer dominated system and is likely due to an inaccurate value for M_n . The extracted values for $C_{tr,S}$ can be seen in Table 2.2.2.3. Despite the increased accuracy expected from the $2\bar{X}_w^{-1}$ plot, the values of $C_{tr,S}$ are very consistent, with lower errors reported for $2\bar{X}_w^{-1}$ resulting from a better linear fit through the data points.

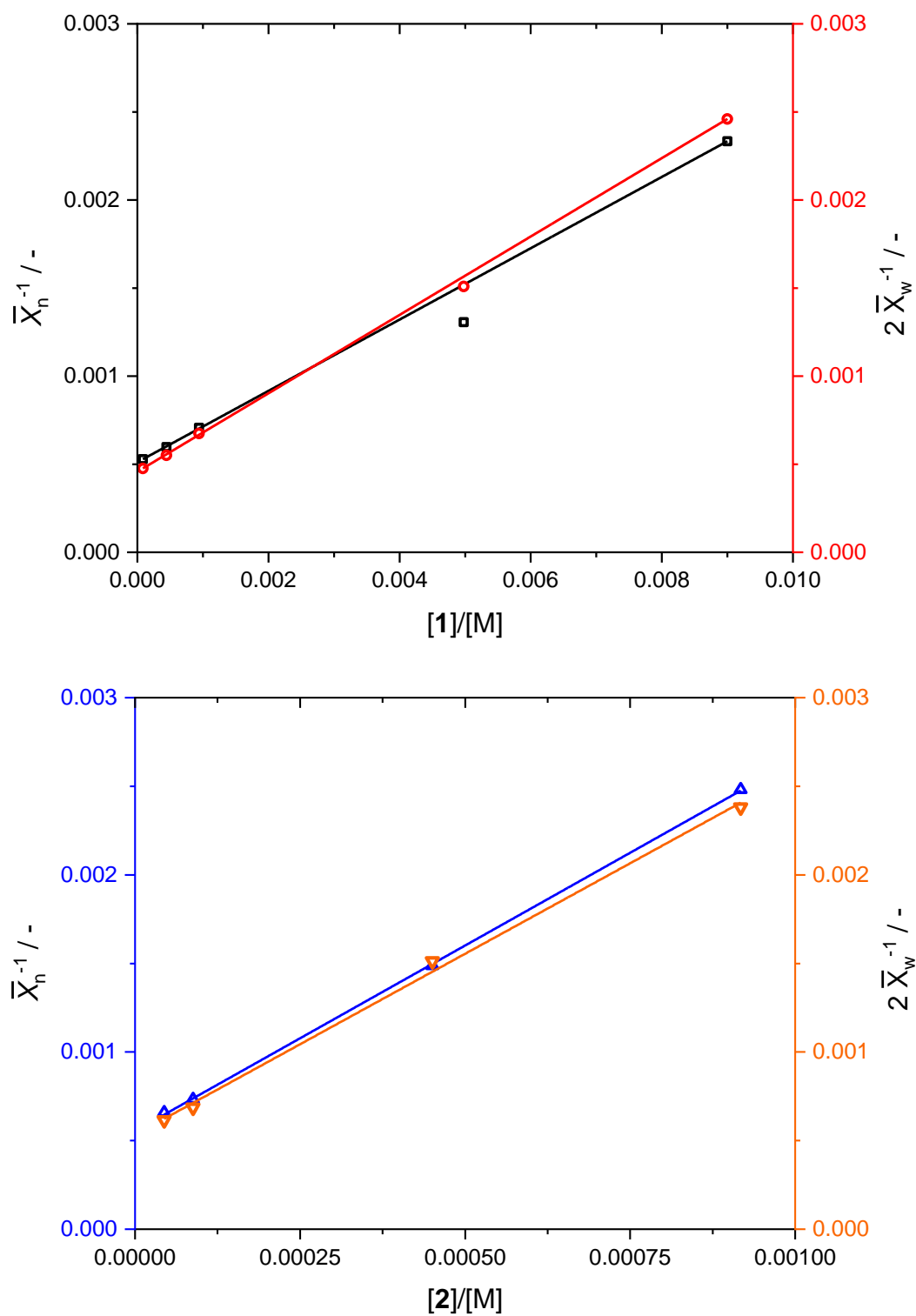


Figure 2.2.2.4: Mayo plots, showing \bar{X}_n^{-1} and $2\bar{X}_w^{-1}$ vs $[S]/[M]$ at a variety of concentrations. For **1** (top): \bar{X}_n^{-1} and $2\bar{X}_w^{-1}$ are depicted by \square and \circ respectively. For **2** (bottom): \bar{X}_n^{-1} and $2\bar{X}_w^{-1}$ are depicted by \triangle and ∇ respectively.

Table 2.2.2.3: $C_{tr,S}$ values for both **1** and **2**, determined via the Mayo method using both \bar{X}_n^{-1} and $2\bar{X}_w^{-1}$.

Disulfide	$C_{tr,S}$ (Mayo, \bar{X}_n^{-1})	$C_{tr,S}$ (Mayo, $2\bar{X}_w^{-1}$)
Dibutyl disulfide (1)	0.196 ± 0.014	0.221 ± 0.004
2-hydroxyethyl disulfide (2)	2.094 ± 0.018	2.043 ± 0.071

In the Mayo equation, the intercept is equal to $\bar{X}_{n,t}^{-1}$, that is the inverse of the degree of polymerisation in the absence of any chain transfer to the varied species, which in bulk polymerisation equates to chains terminated through bimolecular termination. However, we must also account for the prevalence of chain transfer to monomer and solvent in these reactions, given that these still occur in the absence of the varied parameter (being [disulfide]). Therefore, Equation 2.2.2.1 and 2.2.2.2 shows how the parameter $\bar{X}_{n,t}^{-1}$ may be calculated through conventional free radical polymerisation kinetics, assuming steady state conditions. Where k_t , k_p , k_d , $k_{tr,Solv}$ and $k_{tr,M}$ are the rate coefficients for termination, propagation, initiator decomposition, transfer to solvent and transfer to monomer, respectively. $[R]$, $[M]$, $[I]$ and $[Solv]$ are the concentrations of radicals, monomer, initiator, and solvent, and f is the initiator efficiency. A value for k_p of 8548 was calculated using the Arrhenius parameters $A = 1.35 \times 10^7 \text{ M}^{-1}\text{s}^{-1}$ and $E_a = 20.4 \text{ kJ mol}^{-1}$. A value for k_t of 7.31×10^8 was used, which was calculated from a value for $k_p/\sqrt{k_t}$ of 0.3162. k_d for AIBN was set at $9.67 \times 10^{-6} \text{ s}^{-1}$, with an assumed value for f of 0.7. Also $k_{tr,Solv} = k_{tr,M} = 2.317$, as reported previously.

$$\bar{X}_{n,t}^{-1} = \frac{2k_t[R] + k_{tr,Solv}[Solv] + k_{tr,M}[M]}{k_p[M]} \quad (2.2.2.1)$$

$$[R] = \left(\frac{k_d[I]f}{k_t} \right)^{\frac{1}{2}} \quad (2.2.2.2)$$

Given all experiments were performed under the same monomer, solvent and radical concentrations, a value of $\bar{X}_{n,t}^{-1} = 3.9 \times 10^{-4}$ was determined, which is in good agreement with the values extracted from the plots of $2\bar{X}_w^{-1}$ (4.5×10^{-4} and 5.3×10^{-4} for **1** and **2** respectively).

To support this data, Gilbert's CLD approach was next applied to the data. Plots of $\ln N(i)$ vs i were first constructed for the same low conversion samples as were used in the Mayo plots. These can be seen in Figure 2.2.2.5, wherein the solid black lines are the linear regions from

which the slope was extracted and was subsequently used to determine $C_{tr,S}$ using Equations 1.1.3.3.4 and 1.1.3.3.5 defined in Chapter 1. As is expected, increasing the $[S]/[M]$ ratio results in an increase in the slope at the high limit of i . The values for $C_{tr,S}$ determined from these slopes can be seen in Table 2.2.2.4. Consistent results are observed for **1**, with the values showing good agreement with those determined through the Mayo method, other than a slight anomaly in the experiment where $[1]/[M] = 9.40 \times 10^{-4}$. However, the data for **2** shows some striking differences depending on $[2]/[M]$. The values determined from the higher concentrations, where $[2]/[M] = 9.18 \times 10^{-4}$ and 4.5×10^{-4} , are in good agreement with each other, as well as in agreement with the values determined through the Mayo method. However, at lower concentrations of **2**, $C_{tr,S}$ appears to become less accurate and assumes a much larger value. This could be due to the increasing significance of chain transfer to monomer/solvent in the MW distribution.

It would therefore appear that **2** is significantly more reactive in chain transfer than **1**, given its value of $C_{tr,S}$ being roughly an order of magnitude greater. Similarly, the influence on the rate is strikingly more significant than with **1**. Stockmayer showed a similar trend in $C_{tr,S}$ for 2 disulfides with different polarity about the disulfide bond, wherein a higher value was determined for diethyl dithioglycolate compared to dibutyl disulfide (1.41 and 1 respectively), which suggests similar observations as seen here.¹⁴ However, the authors quoted the opposite rate behaviour, with diethyl dithioglycolate being quoted as “mildly degradative” and dibutyl disulfide as “strongly degradative”, although conversion time data was not provided.

The observed retardation could be due to slow reinitiation by the transfer product radical, or due to increased termination. However, thiyl radicals (as with DDT) were shown to have minimal influence on the rate of polymerisation (in Chapter 1). Due to the observations in the rate data for **2**, where the rates appear to increase over time to become essentially equal, an alternate conjecture is proposed: a build-up of transient radicals. In this scenario, the propagating radical undergoes addition to the disulfide, however, cleavage of the bond does not occur spontaneously. Instead, the rate of fragmentation is rate limiting, and may be

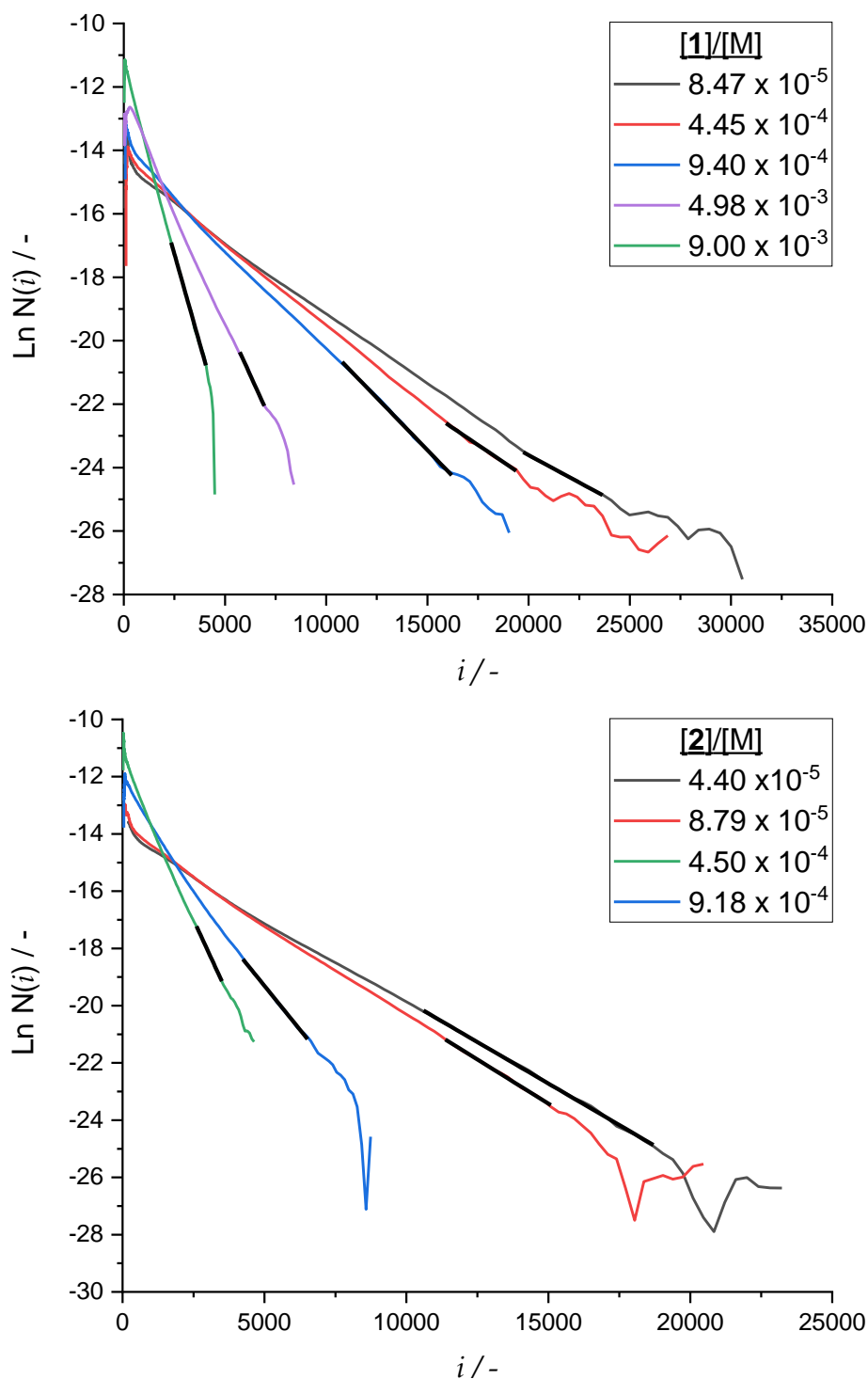


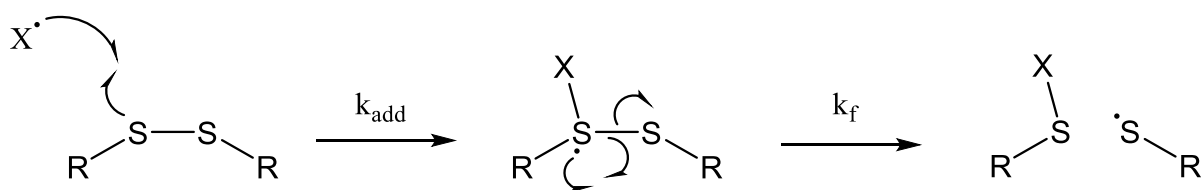
Figure 2.2.2.5: Gilbert plots of $\text{Ln } N(i)$ vs i for **1** (top) and **2** (bottom) employed at a variety of concentrations. The overlaid black lines are the linear portions from which the slope was extracted to calculate $C_{tr,S}$.

influenced by the proximity of heteroatoms, as observed through the difference in behaviour between **1** and **2**. Under these circumstances, the radical species, shown in Scheme 2.2.2.2, increases in concentration relative to the propagating radical, X. The reinitiating species is then regenerated according to the rate constant k_{frag} . Assuming the intermediate radical is

unable to reinitiate, the rate is then highly dependent on k_{frag} , with the chain length now governed by k_{add} , being the rate coefficient now measured during construction of a Mayo plot or using Gilbert CLD method, being k_{add}/k_p .

Table 2.2.2.4: $C_{tr,S}$ values determined through the Gilbert CLD approach for the low conversion samples of polymerisations of vinyl acetate performed at varying concentrations of **1** and **2**.

Disulfide	[S]/[M]	$C_{tr,S}$ (Gilbert)
Dibutyl disulfide (1)	8.47×10^{-5}	0.231
	4.45×10^{-4}	0.239
	9.40×10^{-4}	0.355
	4.98×10^{-3}	0.217
	9.00×10^{-3}	0.215
2-Hydroxyethyl disulfide (2)	4.40×10^{-5}	5.780
	8.79×10^{-5}	3.314
	4.50×10^{-4}	2.001
	9.18×10^{-4}	1.991



Scheme 2.2.2.2: Proposed mechanism of addition of a propagating radical to a disulfide.

The proposed overall reaction scheme can then be described by the steps given in Table 2.2.2.5, with the proposed key fragmentation step being step 4. In this scheme, as the concentration of the transient radical, denoted $RPSSR^*$ increases, which will occur with time, the rate of fragmentation also increases, which may explain the slow increase in rate as a function of time. This has not been studied further as part of this work, although the potential to model the kinetics may be particularly interesting for future studies. Additionally, techniques such

as electron paramagnetic resonance may allow identification of the transient radical if it is indeed formed after addition.

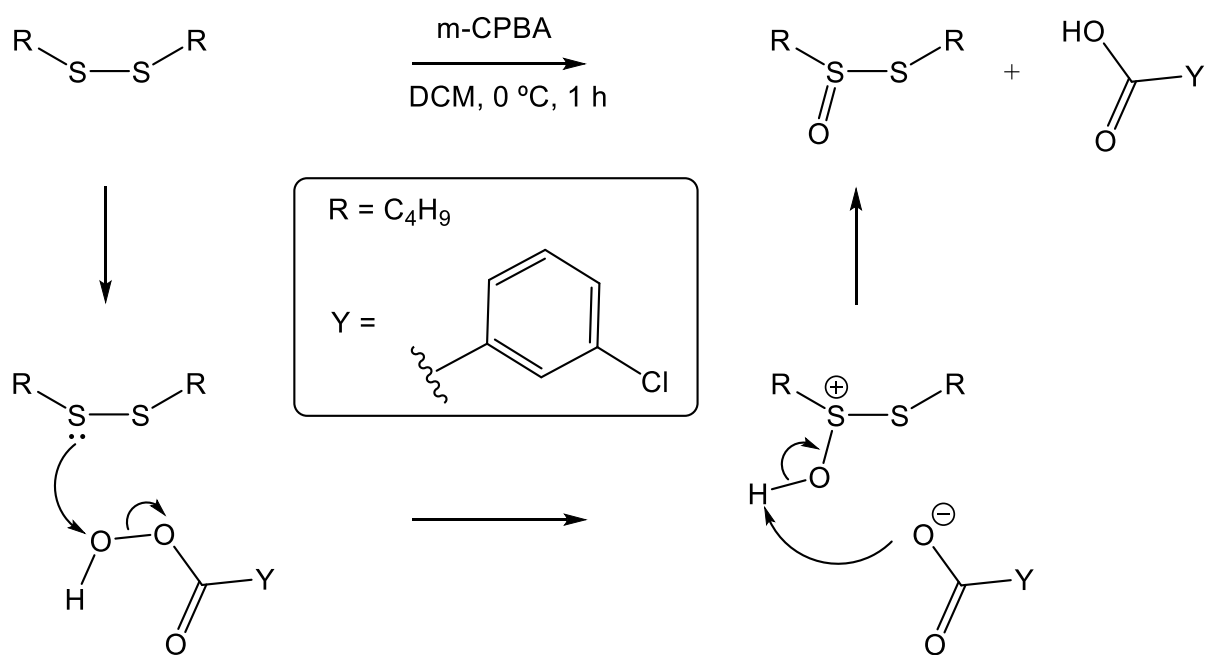
Table 2.2.2.5: Proposed kinetic scheme for the addition of VAc radicals to disulfides. The suggested addition vs chain transfer are of particular interest.

Reaction	Mechanism	Rate
Initiation	$I_2 \rightarrow 2R \cdot \rightarrow P \cdot$	$2k_{af}[I]$ (1)
Propagation	$P \cdot + M \rightarrow P \cdot$	$k_p[P \cdot][M]$ (2)
Addition	$P \cdot + RSSR \rightarrow RPSSR^*$	$k_{add}[P \cdot][RSSR]$ (3)
Fragmentation	$RPSSR^* \rightarrow PSR + RS \cdot$	$k_{frag}[RPSSR^*]$ (4)
Reinitiation	$RS \cdot + M \rightarrow P \cdot$	$k_{rein}[RS \cdot][M]$ (5)
Termination	$RS \cdot + P \cdot \rightarrow Polymer$	$k_{t1}[RS \cdot][P \cdot]$ (6)
	$RS \cdot + RS \cdot \rightarrow RSSR$	$k_{t2}[RS \cdot][RS \cdot]$ (7)
	$P \cdot + P \cdot \rightarrow Polymer$	$k_{t2}[P \cdot][P \cdot]$ (8)

2.2.3 Disulfide oxidation.

To further explore the chemistry involved in chain transfer to a disulfide, dibutyl disulfide was subjected to oxidation utilising *meta*-chloroperoxybenzoic acid (m-CPBA). Using an adapted procedure from Pratt *et al.* (2011),⁸⁰ the disulfide was converted into a thiosulfinate according to Scheme 2.2.3.1. The full experimental procedure is detailed in the experimental section. It was thought that oxidation of sulfur would influence the chain transfer behaviour, and may provide proof for the involvement of the disulfide bond, and influence the fragmentation behaviour proposed previously.

After the product was concentrated from DCM through vacuum assisted evaporation, it was analysed through ¹H NMR, as seen in Figure 2.2.3.1. Conversion to the thiosulfinate was confirmed, with a small amount of unreacted disulfide remaining (7.7 %). The product was used without further purification.



Scheme 2.2.3.1: Reaction mechanism for the conversion of dibutyl disulfide to the corresponding thiosulfinate, through oxidation by m-CPBA.

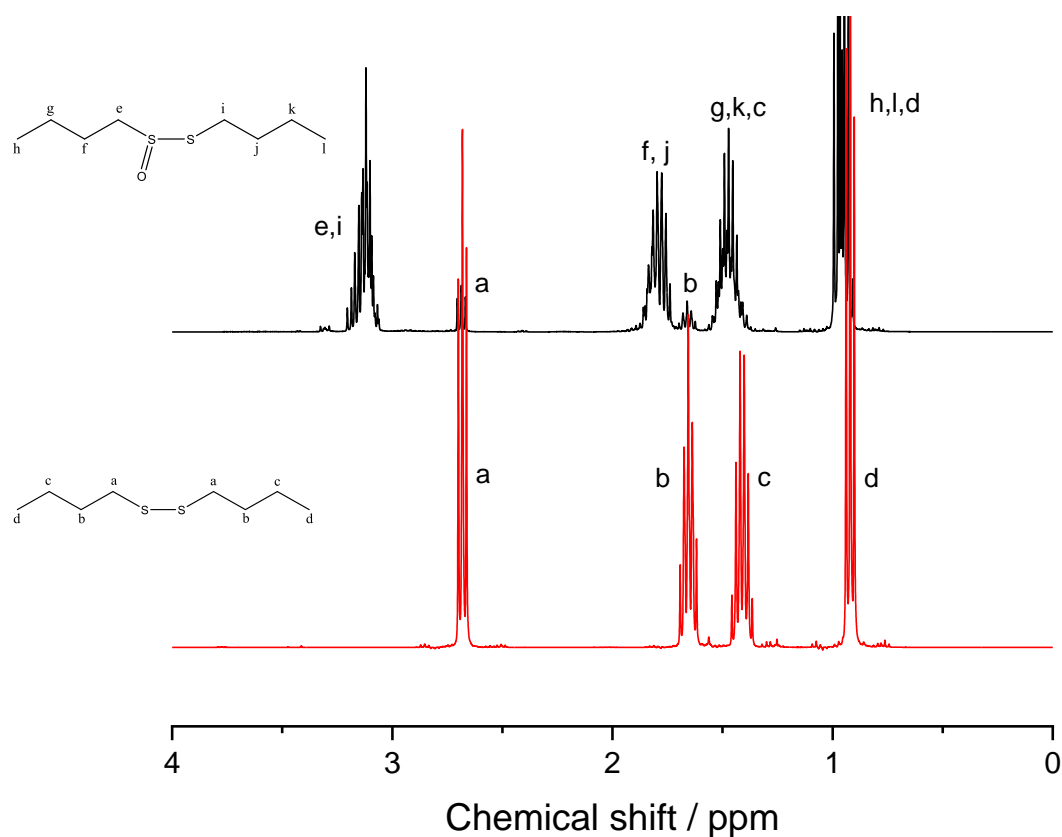


Figure 2.2.3.1: 300 MHz ^1H NMR spectra, recorded in CDCl_3 , for dibutyl disulfide (bottom, red) and the oxidation product (top, black).

A free radical polymerisation was performed at $[S]/[M] = 5 \times 10^{-3}$, where S was the corresponding thiosulfinate, adopting the same procedure as with the previous disulfides (see Experimental section), with the purity assumed to be 100 %. As can be seen on Figure 2.2.3.2, essentially no polymer is formed during the reaction, which is a striking observation when compared to the pure disulfide employed at the same concentration.

Clearly the introduction of oxygen directly to the disulfide bond dramatically changes the influence it has on the free radical polymerisation. Assuming that the addition mechanism is the same (addition to the disulfide exclusively), it suggests that the increase in polarity dramatically increases the radical stability, or delays the fragmentation. Alternatively, addition may occur resulting in localisation of the radical onto the oxygen, again changing the activity of the radical and producing the observed retardation.

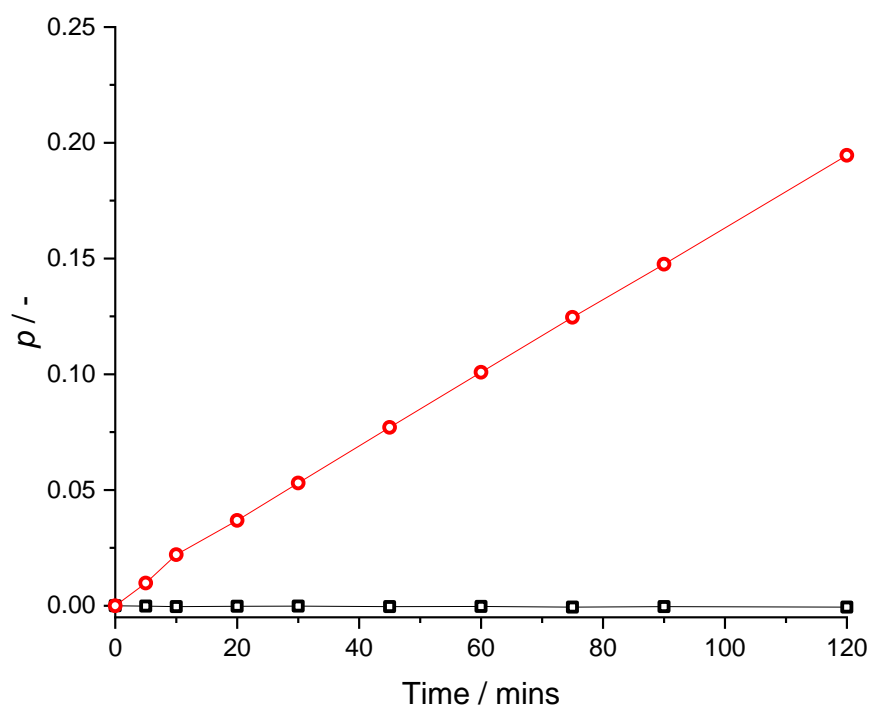
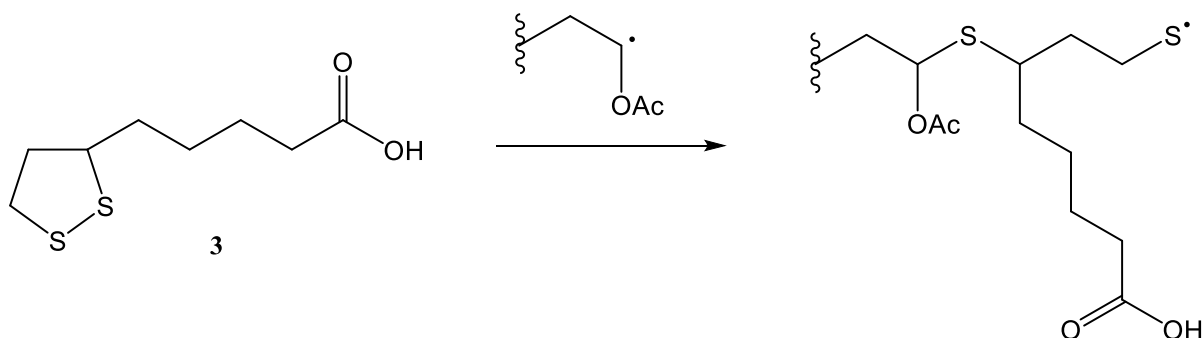


Figure 2.2.3.2: Monomer conversion, p , as a function of time (mins) for the solution polymerizations of vinyl acetate in the presence of dibutyl disulfide (○) and the oxidised thiosulfinate (□), both employed at $[S]/[M] = 5 \times 10^{-3}$.

2.2.4 Cyclic disulfide.

DL- α -lipoic acid (**3**) is an additionally very interesting compound to study in free radical polymerisation, as the disulfide is cyclic, leading to the thiyl radical formed after the breakage of the disulfide still being tethered to the polymer chain (as seen in Scheme 2.2.4.1). This radical can then undergo addition to VAc resulting in inclusion of the disulfide in the polymer backbone with thioether linkages, in a copolymerisation of sorts.^{49,50}



Scheme 2.2.4.1: Reaction mechanism for “copolymerisation” of vinyl acetate with a cyclic disulfide, DL- α -lipoic acid (**3**).

A series of free radical polymerisations were undertaken, utilising the same procedures as those applied to **1** and **2**, covering a range of disulfide to monomer ratios. As can be seen in Figure 2.2.4.1, the conversion evolution is again heavily dependent on the concentration of disulfide employed. Interestingly, for **3**, there is a significant amount of curvature in the conversion time data, which gets more pronounced for higher concentrations of **3**.

Unlike **2**, **3** possesses no heteroatoms that we expect are close enough to the disulfide bond to influence the kinetics of the fragmentation, however, shows significantly more retardation than **1**. Additionally, the curvature in the conversion time data is significantly more pronounced here. One explanation could be due to the fact that the unit is cyclic, therefore the probability of coupling to reform the disulfide bond is much more likely than with the linear disulfides, as the thiyl radicals are tethered together and kept close in space. Interestingly, looking Figure 2.2.4.2, when $[3]/[M] = 5 \times 10^{-4}$ the MWD is seen to shift to higher MW with increasing conversion, although does not appear to increase significantly in dispersity. The shift to higher MW could be due to a drift in the copolymer composition. If we assume that the rate of addition to the disulfide is comparable to that of DBDS, i.e. $k_{tr,S} = 1889 \text{ L mol}^{-1} \text{ s}^{-1}$ (using $C_{tr,S} = 0.221$ and $k_p = 8548 \text{ L mol}^{-1} \text{ s}^{-1}$), this may imply that the reactivity ratio, $r_{VAc} = 4.53$, determined by taking the ratio of $k_p/k_{tr,S}$, i.e. the ratio of the rate coefficients for

homopropagation to cross propagation, implying preferential consumption of VAc, which will result in composition drift with increasing conversion.

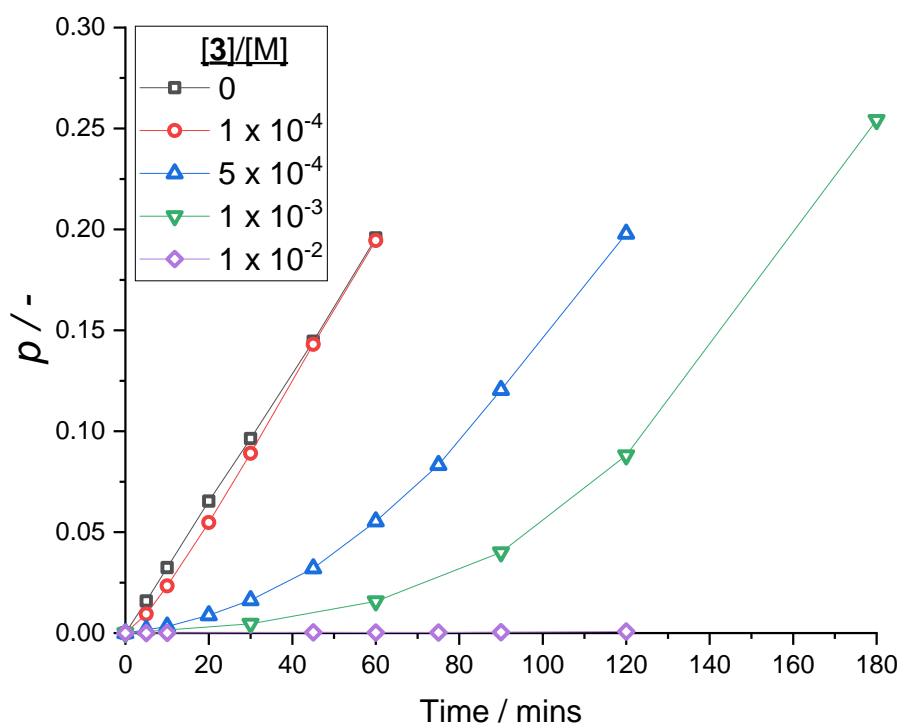


Figure 2.2.4.1: Monomer conversion, p , as a function of time (mins) for the solution copolymerisation of vinyl acetate and **3** at varying concentrations of **3**.

The corresponding reactivity ratio for a terminal disulfide radical is less trivial to determine from the data obtained here, although, if we assume that cross propagation from a terminal thiyl radical is $\geq k_p$ for VAc (due to the lack of retardation observed during chain transfer to DDT), we could estimate that the rate coefficient for addition of a thiyl radical to a disulfide bond is less than this.

Given the lack of an increase in the polydispersity, and the suggestion of reforming the disulfide bond, the increase in MW could potentially be attributed to reversible deactivation of the chain, in the event that polymer radicals undergo transfer to the disulfide, and the bond fragments, however, it reforms before cross propagation, one may envisage the reformation of the previous radical which then may propagate further.

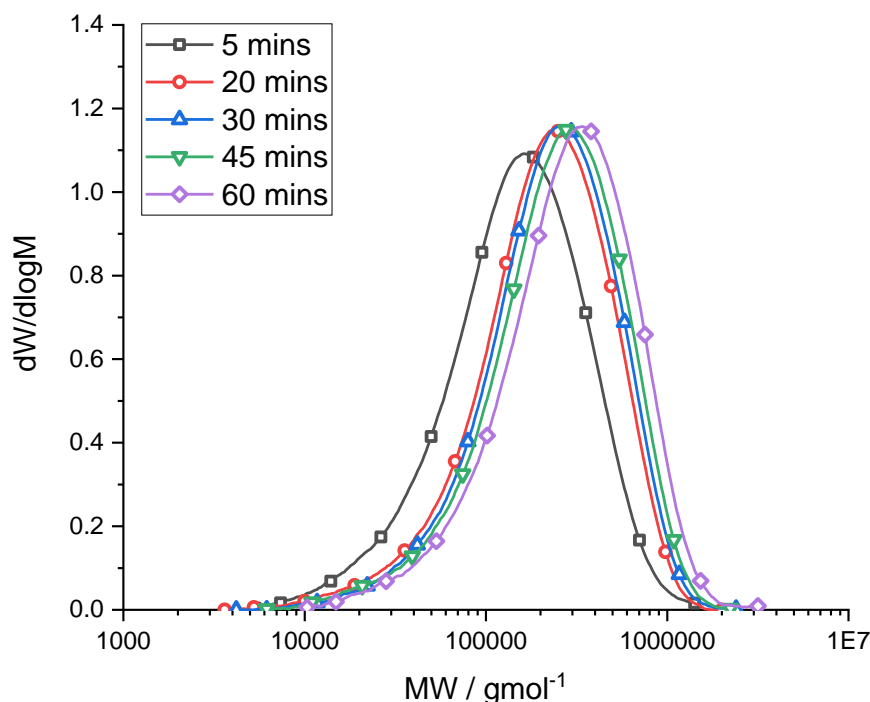


Figure 2.2.4.2: Molecular weight distributions, $dW/d\log M$ vs MW (g mol^{-1}), as a function of time, for the solution polymerisation of VAc in the presence of **3**, where $[3]/[M] = 5 \times 10^{-4}$. The legend details the time (mins) of the sample.

2.2.5 Looking at end groups: Linear disulfides.

In order to assess the end groups introduced using a disulfide as a CTA in free radical polymerisation, a reaction was performed in the presence of a high loading of dibutyl disulfide (**1**). The $[S]/[M]$ ratio was chosen to achieve $M_n = 5000 \text{ g mol}^{-1}$, predicted using a value of $C_{tr,S}$ of 0.221, as determined through the Mayo approach. Solving the Mayo equation with this in mind then yielded $[S]/[M] = 7.59 \times 10^{-2}$. The reaction was run under the same conditions as previously discussed, using this calculated $[S]/[M]$. The reaction was sampled less frequently, and was allowed to proceed for longer, to obtain enough polymer to characterise given the predicted slow rate. The conversion evolution can be seen in Figure 2.2.5.1.

Although the reaction was sampled over 240 mins, polymerisation was continued for 24 h, after which time a final monomer conversion of $p = 0.25$ was achieved. Using Equation 1.1.2.2.5, given in Chapter 1, and using a chain transfer constant of 0.221, at this degree of conversion the $[S]/[M]$ ratio would have drifted from 7.59×10^{-2} to 9.50×10^{-2} . Again, utilising the Mayo equation, this leads to an instantaneous degree of polymerisation at this conversion (and corresponding $[S]/[M]$ ratio) of $DP = 47$, drifting from a starting $DP = 58$. This drift was

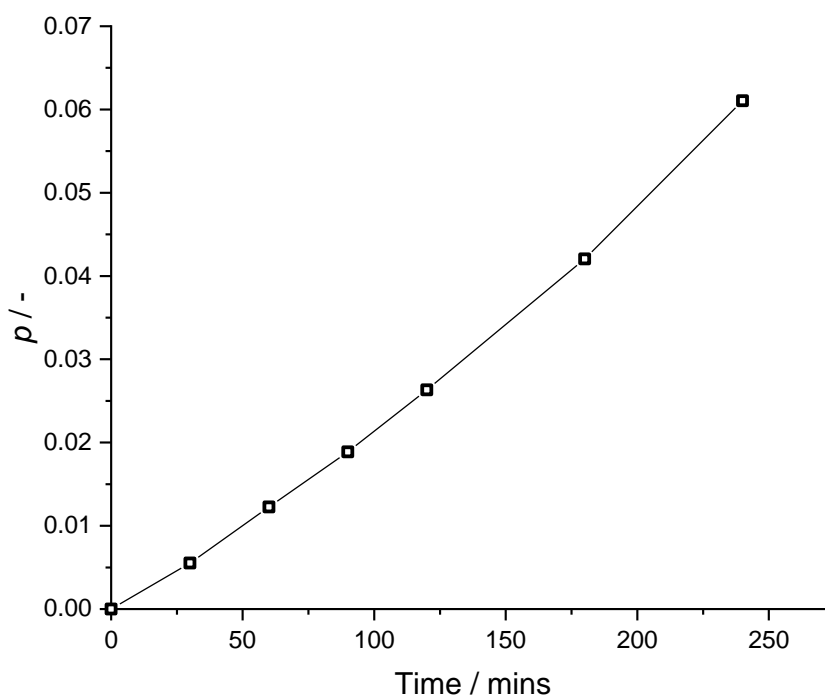


Figure 2.2.5.1: Monomer conversion, p , as a function of time (mins) for the solution polymerisation of VAc in the presence of **1**. $[1]/[M] = 7.59 \times 10^{-2}$.

deemed acceptable, and the polymer was expected to be of low enough MW to assess the end groups through mass spectrometry and ^1H NMR. The polymer at $p = 0.25$ was evaporated to constant mass under reduced pressure. This was then dissolved in a minimal amount of ethyl acetate and precipitated in pentane (cooled in a dry ice/acetone bath), before being collected by centrifugation. This precipitation was repeated once more, after which the isolated polymer was dried to constant mass under reduced pressure. The polymer was then analysed through SEC, and the corresponding MWD can be seen in Figure 2.2.5.2. M_n and M_w were equal to 5,500 and 10,000 g mol^{-1} respectively, with $\text{PDI} = 1.798$. The significantly low MWs recorded here shed doubt on the accuracy of these MW averages, particularly M_n (much more sensitive to baseline selection), as the low MW end of the distribution does not approach zero, due to overlap with the elution of some other low MW species (could be some monomer/solvent). Assuming $M_n = 2/M_w$ as before, and in the knowledge that $M_w = 10,000 \text{ g mol}^{-1}$, suggests that $M_n = 5,000 \text{ g mol}^{-1}$, as targeted.

The NMR analysis of the polymer was performed in d_6 -dimethylsulfoxide (d_6 -DMSO) and can be seen in Figure 2.2.5.3. The broad singlet at 4.78 ppm is the backbone CH , the peak at 1.97 ppm is from the side group $\text{C}(\text{O})\text{CH}_3$, and the broad peak between 1.85-1.65 ppm is the backbone CH_2 shift. The sharp singlets at 3.31 and 2.50 ppm are water and DMSO solvent

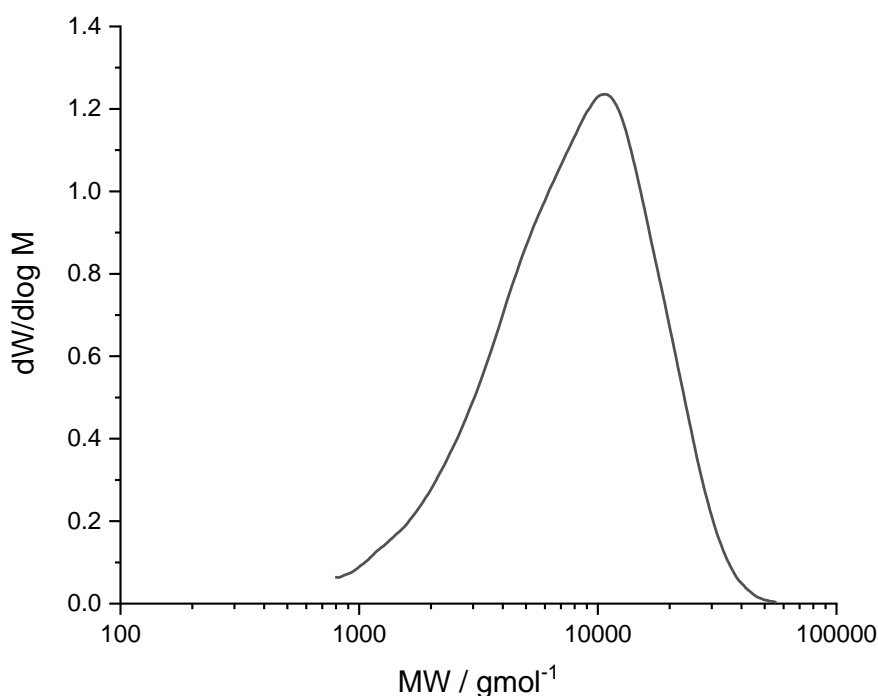


Figure 2.2.5.2: $dW/d\log M$ MWD for PVAc formed at $[1]/[M] = 7.59 \times 10^{-2}$, $p = 0.25$.

peaks, with the DMSO peak having spinning side bands at 2.33 ppm and 2.67 ppm. The small multiplet at 0.8-0.93 ppm ($\text{SCH}_2\text{CH}_2\text{CH}_2\text{CH}_3$), as well as broad unresolvable peaks in the range 1.02-1.61 ppm ($\text{SCH}_2\text{CH}_2\text{CH}_2\text{CH}_3$), and 2.56-2.73 ppm ($\text{SCH}_2\text{CH}_2\text{CH}_2\text{CH}_3$) are the disulfide aliphatic shifts, although it is noted that despite purification through precipitation there is still a significant portion of unreacted disulfide in the sample, with the peaks from free disulfide and those in the polymer overlapping too significantly to extract any information about the degree of polymerisation from these shifts. Interestingly, a small new peak appears at 5.85 ppm, which can be assigned to the penultimate backbone CH , with the carbon being bonded directly to sulfur. The analogous CH_2 bound to sulfur is not visible, although this is expected to have a comparable shift as the analogous shift in the disulfide, therefore, likely appears under the signal at 2.56-2.73 ppm. Direct comparison of the integrals of the peak at 5.85 ppm and 4.78 ppm suggests a number average degree of polymerisation = 62, which correlates to $M_n \approx 5340 \text{ g mol}^{-1}$, which is in good agreement with the SEC data, as well as the predicted value.

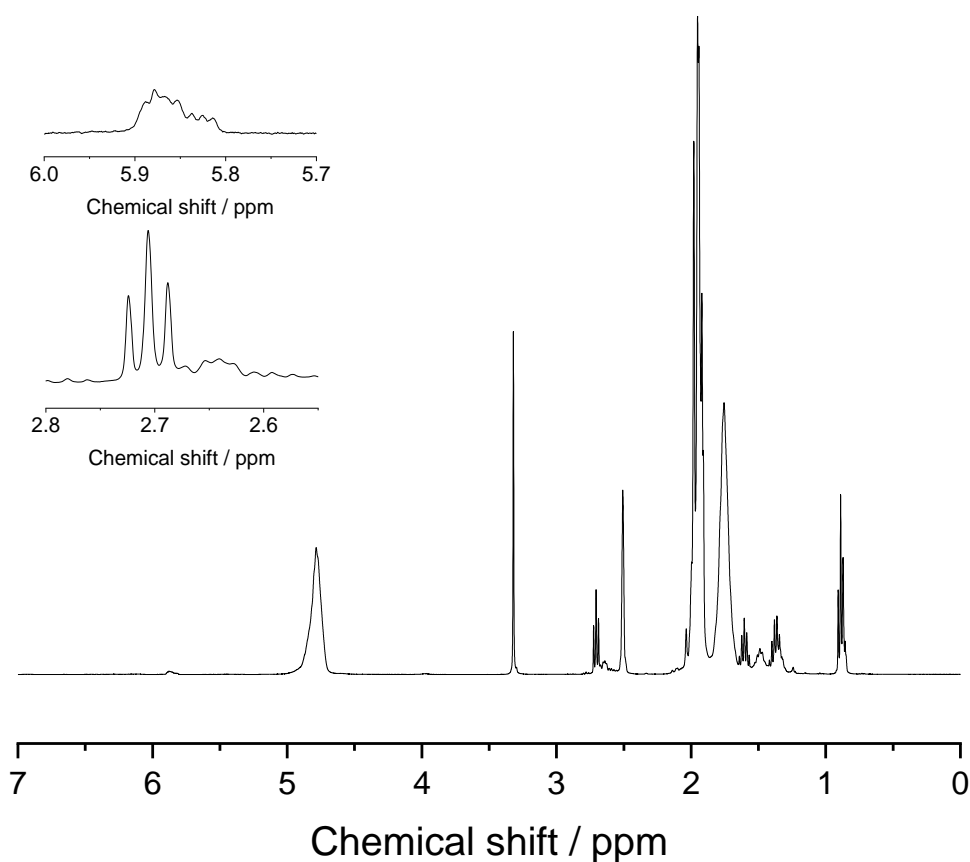


Figure 2.2.5.3: 400 MHz ¹H NMR spectra of PVAc formed at $[1]/[M] = 7.59 \times 10^{-2}$, $p = 0.25$. recorded in d₆-DMSO.

A mass spectrum was then recorded for the polymer, as can be seen in Figure 2.2.5.4. The spectrum contains a distinct pattern of intense peaks, spaced ≈ 86.04 m/z apart, which correlates to the repeat unit of PVAc (C₄H₆O₂, theoretical isotopic mass = 86.0368). The region of the distribution between $1100 < m/z < 1450$ is then highlighted, with the 4 primary peaks centred at $m/z = 1147.4788$, 1233.5158 , 1319.5519 and 1405.5883 , which correlate to masses of polymers with a degree of polymerisation of 11, 12, 13 and 14 respectively, all with two butyl thioether end groups, and a sodium counterion. Each of these m/z values correlate to the theoretical masses for the corresponding degrees of polymerisation with sub-ppm assignment errors. This is indicative of the predicted structure, i.e., proves the products in this m/z range are telechelic PVAc, with terminal thioether residues. It is noted however, that there are several other repeating distributions in the system, which could be due to some different initiating groups, or attributed to other side reactions. The full analysis of these individual distributions is outside of the scope of this work.

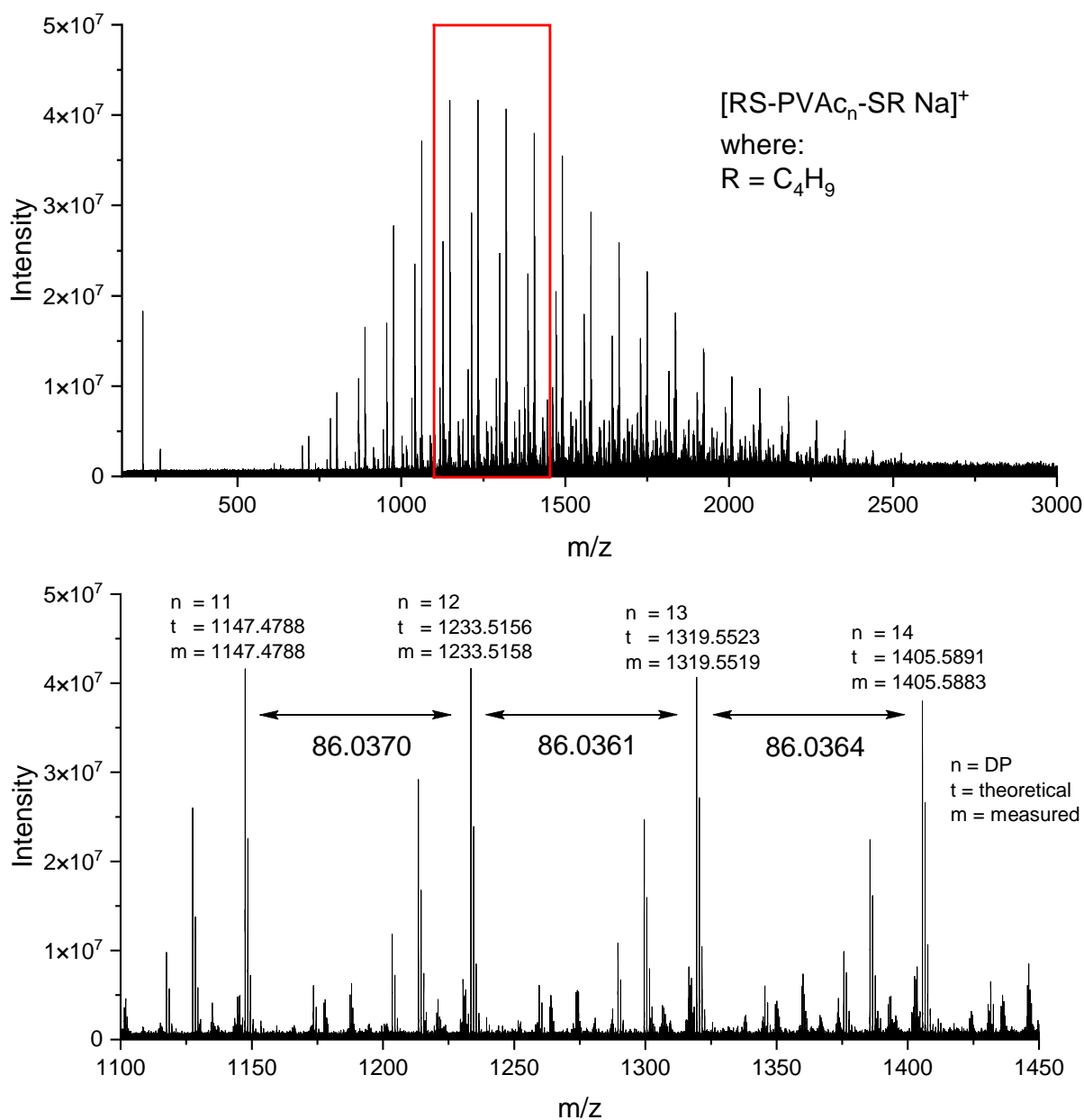


Figure 2.2.5.4: ESI mass spectrum for PVAc formed in the presence of $[1]/[M] = 7.59 \times 10^{-2}$ (top), with the highlighted red region between $1100 < m/z < 1450$ from the full spectrum then expanded (bottom). The overlaid terms n , t and m refer to the degree of polymerisation of the PVAc, the theoretical m/z assuming two butyl thioether end groups at that DP, and the experimentally measured m/z .

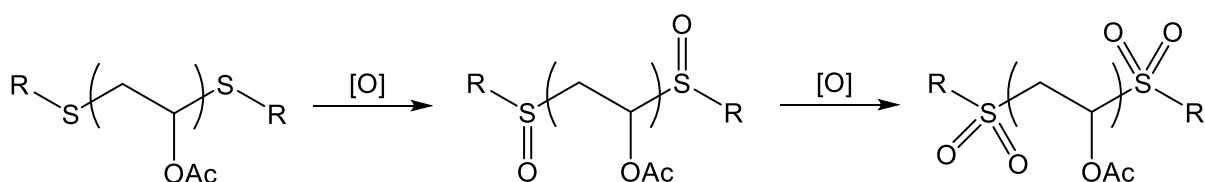
2.2.6 Conclusions and future work.

The behaviour of disulfides in the free radical polymerisation of VAc has been demonstrated, with the kinetics of these reactions demonstrated for the first time. It has been demonstrated that the use of disulfides results in telechelic polymers through addition to the disulfide and

subsequent cleavage of the bond. It was noted that the evolution of conversion did not proceed linearly, and it was suggested that this was due to the cleavage being rate limiting, which may also explain the observed retardation. For DBDS and 2-hydroxyethyl disulfide (2-HEDS), $C_{tr,S}$ of 0.221 and 2.043 were determined using the Mayo method, and $C_{tr,S}$ of 0.215 and 1.991 were determined using the Gilbert method, respectively. The favourable chain transfer constants of both of these species can facilitate minimal drift in the MWD during batch addition, particularly when compared to thiol CTAs. For DBDS, only marginal retardation was observed, and as such, this compound has huge potential in a range of applications where the MW of PVAc needs to be restricted. This CTA will be used in the subsequent chapters due to this.

However, it is noted that dibutyl disulfide does not introduce much functionality into the polymers, as would be the case for 2-HEDS, therefore, logical extensions to this work would be to expand the library of disulfides used in VAc free radical polymerisation, to those which have more functionality. Given the retardation observed for 2-HEDS, it is suggested that any disulfides bearing polar functional groups should be employed with caution, and it may be suggested that species with a significant aliphatic spacer between the disulfide bond and the polar groups be used.

Alternatively, one might conceive of methods to modify the thioether end groups produced through the use of DBDS, or other aliphatic disulfides. As an example, Hubbel *et al.* (2004)⁸¹ exposed a thioether to hydrogen peroxide, which in turn resulted in oxidation of the thioether into the corresponding sulfoxide, and then with further oxidation into the sulfone (as seen in Scheme 2.2.6.1). Application of this chemistry to the telechelic PVAc could offer an increase in the hydrophilicity of the end-groups. Additionally, if the oxidation could continue to sulfone production, the end group would bear a striking resemblance to a tosylate group, and would become a good leaving group (as discussed by Trost *et al.*),⁸² susceptible to nucleophilic substitution, allowing access to a whole range of functionalities.



Scheme 2.2.6.1: Proposed oxidation of the terminal thioether functionality to the corresponding sulfoxide and sulfone.

2.3 Experimental

Materials

Vinyl acetate (Aldrich, $\geq 99\%$) was purified by passing through a column of basic alumina, followed by vacuum assisted distillation wherein the first and final 20 vol% of the distillate was discarded. Methyl acrylate (Aldrich, 99%) and dibutyl maleate (Aldrich, 96 %) were both purified by passing through a column of basic alumina. Azobisisobutyronitrile (AIBN, from VWR) was purified by recrystallisation from methanol. *n*-Dodecanethiol (Aldrich, $\geq 98\%$), *n*-dodecane (Merck, $\geq 99\%$), Et-OAc (Merck, $\geq 99.5\%$), dibutyl disulfide (Aldrich, 97%), 2-hydroxyethyl disulfide (Aldrich, 90%), DL- α -lipoic acid (Acros Organics, $\geq 98\%$), dichloromethane (Aldrich, $\geq 99.8\%$), 3-chloroperbenzoic acid (m-CPBA, Aldrich, $\geq 70\%$), sodium carbonate (Fischer, $\geq 99.5\%$), 5-methyl furfural (MFF, Aldrich, 99%) were used without further purification.

Characterization methods

Size exclusion chromatography (SEC).

Molecular weight distributions were determined on an Agilent Infinity II MDS instrument equipped with differential refractive index (DRI), viscometry (VS), dual angle light scatter (LS) and multiple wavelength UV detectors. The system was equipped with 2 \times PLgel Mixed C columns (300 \times 7.5 mm) and a PLgel 5 μ m guard column. The eluent was THF with 0.01 % BHT (butylated hydroxytoluene). Samples were run at 1 mL min⁻¹ at 30 °C. Polystyrene standards (Agilent EasyVials) were used for calibration. Analyte samples were filtered through a PTFE filter with a 0.2 μ m pore size before injection. The *K* and α values for PVAc were determined by a triple detection SEC set-up, with light scattering and viscometry used alongside DRI. Polymer MW information of each sample was then estimated using universal calibration, utilizing the calculated Mark-Houwink-Sakurada parameters, $K = 5.01 \times 10^{-5}$ dL mol⁻¹ and $\alpha = 0.78$ for PVAc, and literature values of $K = 14.1 \times 10^{-5}$ dL mol⁻¹ and $\alpha = 0.70$ for polystyrene.⁸³

Nuclear Magnetic resonance (¹H NMR).

¹H NMR experiments were conducted on a Bruker Advance III HD 400 MHz instrument. Chloroform-*d* and dimethyl sulfoxide-*d*₆ were purchased from Sigma-Aldrich. Polymer samples were prepared to a concentration between 1 and 5 wt%. The spectral results were analysed using software from ACD laboratories.

Mass spectrometry – Acquisition and analysis performed by Bryan Marzullo.

Poly(vinyl acetate) was dissolved in methanol and diluted to a concentration of 20 μM . The sample was ionised using a nanoelectrospray (nESI) source, (in positive mode) and was subsequently analysed by a 12 T Bruker solarix FT-ICR MS. The spectra was acquired using a megaword transient (1.6 s). 100 scans were averaged to increase the signal to noise ratio. Spectra were analysed using Bruker DataAnalysis 5.0 software and the SNAP algorithm was used for peak picking.

Synthesis

Solution polymerisation of vinyl acetate in the presence of 5-methyl furfural (and comonomers) (Example reaction for copolymerisation with dibutyl maleate)

Vinyl acetate (6.06 g, 0.07 mol), 5 methyl-furfural (0.06, 5.45×10^{-4} mol) and dibutyl maleate (0.61, 2.67×10^{-3} mol) were added to a Schlenk tube. Separately, Et-OAc (6.31 g, 0.07 mol) and AIBN (0.05 g, 3.04×10^{-4} mol) were added to a Schlenk tube. Both Schlenk tubes were fitted with a magnetic stirrer and sealed with a rubber seal, before being subjected to three freeze-pump-thaw cycles, leaving the vessels under an N_2 atmosphere. The monomer and 5-methyl furfural solution was added to a 60 $^\circ\text{C}$ oil bath, and allowed to equilibrate for 5 mins, before 1 mL of the AIBN solution was injected under N_2 . Samples were removed periodically for analysis by ^1H NMR and SEC. The removed samples were immediately sealed and plunged into liquid nitrogen. For sample after 150 mins: Partial monomer conversions = 0.004 (VAc) and 0.088 (DBM). δ_{H} (400 MHz, CDCl_3): 9.51 ppm (MFF, CHO), 7.27 ppm (VAc, HHC=CH), 7.18 ppm (MFF, CHOCCH), 6.25 ppm (MFF, CH_3CCH), 6.23 ppm (DBM, HC=CH), 4.88 ppm (VAc, HHC=CH), 4.57 ppm (VAc, HHC=CH), 4.18 ppm (DBM, OCH_2), 4.12 ppm (ethyl acetate, OCH_2), 2.42 ppm (MFF, CH_3), 2.14 ppm (VAc, OCH_3), 2.04 ppm (ethyl acetate, COCH_3), 1.67 ppm (DBM, OCH_2CH_2), 1.39 ppm (DBM, CH_2CH_3), 1.26 ppm (OCH_3 , ethyl acetate), 0.94 ppm (DBM, CH_3). SEC (THF): $M_n = 34,200 \text{ g mol}^{-1}$, $M_w = 69,000 \text{ g mol}^{-1}$.

Solution polymerisation of vinyl acetate in the presence of a disulfide (Example reaction [DBDS]/[M] = 10^{-4})

In a typical reaction, vinyl acetate (68.580 g, 0.80 mol), Et-OAc (14.170 g, 0.16 mol), DBDS (0.012 g, 6.73×10^{-5} mol) and *n*-dodecane (0.104 g, 6.11×10^{-4} mol) were added to a 3 necked RBF, fitted with a PTFE temperature probe, and an air condenser with aluminium fins, sealed with a rubber septum. A magnetic stirrer bar was added, and the final neck was sealed with a

rubber septum. Separately, AIBN (0.0620 g, 3.78×10^{-4} mol) and Et-OAc (14.29 g, 0.16 mol) were added to a 20 mL crimp vial with a magnetic stirrer. The vial was crimp sealed with a PTFE crimp lid. The two vessels were then purged with N₂ for 1 h. After this time, the RBF was submersed in a 60 °C oil bath under nitrogen, with a stir speed of 750 rpm. After the reaction temperature was confirmed to be 60 °C, 3 mL of the AIBN solution was injected into the RBF under nitrogen. Samples of \approx 5 mL were then withdrawn under nitrogen at frequent intervals for analysis. The samples were immediately sealed to minimize evaporation and plunged into liquid nitrogen. A small amount of sample was retained, and the remainder was evaporated to determine conversion gravimetrically. SEC analysis was performed on the gravimetry samples after their mass had been confirmed. For the sample withdrawn after 1440 mins, $p = 0.21$, $M_n = 165,000 \text{ g mol}^{-1}$, $M_w = 374,400 \text{ g mol}^{-1}$

Synthesis of a thiosulfinate (Modified from ⁸⁰).

Dibutyl disulfide (1.839 g) was added to dichloromethane (30 mL) in a 100 mL RBF, fitted with a magnetic stir bar. To this, a solution of m-CPBA (2.35 g, mol) in DCM (mL) was added dropwise over approximately 10 minutes. A white precipitate was observed after around 80 % of the addition was completed. The reaction mixture was left to stir at 0 °C for 1 h. After this time, sodium carbonate (8.00 g, mol) was added in small portions, again over around 10 minutes, and the reaction was left to proceed for a further 1 h. The reaction mixture was then passed through a gravity filter and the filtrate was dried with MgSO₄. This was then filtered again, and the filtrate was evaporated under reduced pressure to leave a pale-yellow oil. Disulfide conversion of 92.3 % confirmed by NMR, total yield of 46 %, expected to be due to loss during filtering. The product was used without further purification. ¹H NMR (400 MHz, CDCl₃): δ 0.82-0.93 (m, 4H), 1.26-1.51 (m, 4H), 1.64-1.79 (m, 4H), 2.95-3.15 ppm (m, 4H).

Purification of polymer produced at [DBDS]/[M] = 7.59×10^{-2} .

The polymer was prepared as per the experimental description for the other disulfide reactions; however, an additional step was taken to purify the final polymer. The final reaction mixture was left open to air for 1 night to allow excess monomer and solvent to evaporate. The mixture was then concentrated under reduced pressure at 50 °C. The polymer was then dissolved in the minimum amount of Et-OAc and precipitated into pentane (> 30 fold volume excess) cooled in an acetone/dry ice bath with rigorous stirring. The precipitated polymer was collected through centrifugation. The polymer was then redissolved in the minimum amount of Et-OAc and reprecipitated into pentane cooled in an acetone/dry ice bath with

rigorous stirring. The polymer was again collected through centrifugation, and the polymer was dried under reduced pressure at 50 °C to constant mass.

2.4 References

- 1 C. Barner-Kowollik, S. Beuermann, M. Buback, R. A. Hutchinson, T. Junkers, H. Kattner, B. Manders, A. N. Nikitin, G. T. Russell and A. M. van Herk, *Macromol. Chem. Phys.*, 2017, **218**, 1600357.
- 2 M. Buback, R. G. Gilbert, R. A. Hutchinson, B. Klumperman, F. -D Kuchta, B. G. Manders, K. F. O'Driscoll, G. T. Russell and J. Schweer, *Macromol. Chem. Phys.*, 1995, **196**, 3267–3280.
- 3 R. A. Hutchinson, D. A. Paquet and J. H. McMinn, *Macromolecules*, 1995, **28**, 5655–5663.
- 4 J. L. De La Fuente and E. López Madruga, *Macromol. Chem. Phys.*, 2000, **201**, 2152–2159.
- 5 S. Beuermann, M. Buback, T. P. Davis, R. G. Gilbert, R. A. Hutchinson, O. F. Olaj, G. T. Russell, J. Schweer and A. M. Van Herk, *Macromol. Chem. Phys.*, 1997, **198**, 1545–1560.
- 6 T. Sato and T. Okaya, *Makromol. Chem.*, 1993, **173**, 163–173.
- 7 C. Walling, *J. Am. Chem. Soc.*, 1948, **70**, 2561–2564.
- 8 M. K. Donald and S. A. F. Bon, *Polym. Chem.*, 2020, **11**, 4281–4289.
- 9 Z. Sharaby, *US Patent 4931518*, 1990.
- 10 V. Chabrol, J. Batty, P. Shaw, C. Davis and M. Farrell, *WO2015145174A1*, 2015.
- 11 T. Origuchi, Y. Ikemura and H. Maki, *EP1757624B1*, 2007.
- 12 F. R. Mayo, *J. Am. Chem. Soc.*, 1948, **70**, 3689–3694.
- 13 S. R. Palit and S. K. Das, *Proc. R. Soc. Lond. A. Math. Phys. Sci.*, 1954, **226**, 82–95.
- 14 J. T. Clarke, R. O. Howard and W. H. Stockmayer, *Makromol. Chemie*, 1960, **44**, 427–447.
- 15 A. Chatterjee, K. Kabra and W. W. Graessley, *J. Appl. Polym. Sci.*, 1977, **21**, 1751–1762.
- 16 A. J. Buselli, M. K. Lindemann and C. E. Blades, *J. Polym. Sci.*, 1958, **28**, 485–498.

- 17 Z. J. A. Sunder and R. Mulhaupt, *J. Polym. Sci. A-1 Polym. Chem.*, 2002, **40**, 2085–2092.
- 18 S. Rimmer and S. Collins, *React. Funct. Polym.*, 2006, **66**, 177–186.
- 19 G. F. Meijs and E. Rizzardo, *Makromol. Chem.*, 1990, **191**, 1545–1553.
- 20 M. Matsumoto, J. Ukida, G. Takayama, T. Eguchi, K. Mukumoto, K. Imai, Y. Kazusa and M. Maeda, *Makromol. Chem.*, 1959, **32**, 13–36.
- 21 M. B. Gillies, K. Matyjaszewski, P. O. Norrby, T. Pintauer, R. Poli and P. Richard, *Macromolecules*, 2003, **36**, 8551–8559.
- 22 K. Matyjaszewski and R. Poli, *Macromolecules*, 2005, **38**, 8093–8100.
- 23 P. J. Flory and F. S. Leutner, *J. Polym. Sci.*, 1948, **3**, 880–890.
- 24 D. W. Ovenall, *Macromolecules*, 1984, **17**, 1458–1464.
- 25 F. F. Vercauteren and W. A. B. Donners, *Polymer.*, 1986, **27**, 933–998.
- 26 A. N. Morin, C. Detrembleur, C. Jérôme, P. De Tullio, R. Poli and A. Debuigne, *Macromolecules*, 2013, **46**, 4303–4312.
- 27 M. C. Iovu and K. Matyjaszewski, *Macromolecules*, 2003, **36**, 9346–9354.
- 28 Y. Champouret, U. Baisch, R. Poli, L. Tang, J. L. Conway and K. M. Smith, *Angew. Chem. Int. Ed*, 2008, **47**, 6069–6072.
- 29 M. P. Shaver, M. E. Hanhan and M. R. Jones, *Chem. Commun.*, 2010, **46**, 2127–2129.
- 30 R. Nicolaÿ, Y. Kwak and K. Matyjaszewski, *Chem. Commun.*, 2008, 5336–5338.
- 31 A. Debuigne, J. R. Caille and R. Jerome, *Angew. Chem. Int. Ed*, 2005, **44**, 1101–1104.
- 32 A. Debuigne, Y. Champouret, R. Jérôme, R. Poli and C. Detrembleur, *Chem. Eur. J.*, 2008, **14**, 4046–4059.
- 33 R. Bryaskova, C. Detrembleur, A. Debuigne and R. Jérôme, *Macromolecules*, 2006, **39**, 8263–8268.
- 34 H. Kaneyoshi and K. Matyjaszewski, *Macromolecules*, 2005, **38**, 8163–8169.
- 35 K. Santhosh, Y. Gnanou, Y. Champouret, J. C. Daran and R. Poli, *Chem. Eur. J.*, 2009,

- 15, 4874–4885.
- 36 H. M. Pierson and A. H. Weinstein, *J. Polym. Sci.*, 1955, **216**, 221–246.
- 37 K. Ito, K. Tanaka, H. Tanaka, G. Imai, S. Kawaguchi and S. Itsuno, *Macromolecules*, 1991, **24**, 2348–2354.
- 38 T. Song, S. Dai, K. C. Tam, S. Y. Lee and S. H. Goh, *Langmuir*, 2003, **19**, 4798–4803.
- 39 S. Pispas and N. Hadjichristidis, *Macromolecules*, 1994, **27**, 1891–1896.
- 40 B. Meredig, A. Salleo and R. Gee, *ACS Nano*, 2009, **3**, 2881–2886.
- 41 C. Jalbert, J. T. Koberstein, A. Hariharan and S. K. Kumar, *Macromolecules*, 1997, **30**, 4481–4490.
- 42 R. Katsumata, R. Limary, Y. Zhang, B. C. Popere, A. T. Heitsch, M. Li, P. Trefonas and R. A. Segalman, *Chem. Mater.*, 2018, **30**, 5285–5292.
- 43 P. Charlier, R. Jérôme and P. Teyssié, *Macromolecules*, 1990, **23**, 3313–3321.
- 44 D. J. Lundberg, R. G. Brown, J. E. Glass and R. R. Eley, *Langmuir*, 1994, **10**, 3027–3034.
- 45 Y. He, W. He, R. Wei, Z. Chen and X. Wang, *Chem. Commun.*, 2012, **48**, 1036–1038.
- 46 P. L. Golas, N. V. Tsarevsky, B. S. Sumerlin, L. M. Walker and K. Matyjaszewski, *Aust. J. Chem.*, 2007, **60**, 400–404.
- 47 E. D. Pressly, R. J. Amir and C. J. Hawker, *J. Polym. Sci. A-1 Polym. Chem.*, 2011, **49**, 814–819.
- 48 J. Kim, H. Y. Jung and M. J. Park, *Macromolecules*, 2020, **53**, 746–763.
- 49 W. H. Stockmayer, R. O. Howard and J. T. Clarke, *J. Am. Chem. Soc.*, 1953, **75**, 1756–1757.
- 50 A. V Tobolsky and B. Baysal, *J. Am. Chem. Soc.*, 1953, **75**, 1757.
- 51 A. Tobolsky and T. Meltzer, *US Patent 2728750*, 1955.
- 52 R. A. Gregg and F. R. Mayo, *J. Am. Chem. Soc.*, 1953, **75**, 3530–3533.
- 53 T. Otsu, M. Yoshioka and T. Tanaka, *Eur. Polym. J.*, 1992, **28**, 1325–1329.

- 54 I. Cho and J. Kim, *Polymer (Guildf)*, 1999, **40**, 1577–1580.
- 55 M. Teodorescu, P. O. Stanescu, H. Iovu and C. Draghici, *React. Funct. Polym.*, 2010, **70**, 419–425.
- 56 T. Sato, M. Hashimoto, M. Seno and T. Hirano, *Eur. Polym. J.*, 2004, **40**, 273–282.
- 57 T. Sato, K. Nomura, T. Hirano and M. Seno, *Polym. J.*, 2006, **38**, 240–249.
- 58 S. Sato, A. Ono, T. Hirano and M. Seno, *J. Polym. Sci. A-1 Polym. Chem.*, 2006, **44**, 2328–2337.
- 59 T. Sato, N. Sato, M. Seno and T. Hirano, *J. Polym. Sci. Part A Polym. Chem.*, 2003, **41**, 3038–3047.
- 60 W. Yang and A. Sen, *ChemSusChem*, 2011, **4**, 349–352.
- 61 K. Hamada, G. Suzukamo and K. Fujisawa, *US Patent 4335049*, 1982.
- 62 D. L. Kalschne, M. C. Viegas, A. J. De Conti, M. P. Corso and M. de T. Benassi, *Food Res. Int.*, 2018, **105**, 393–402.
- 63 P. Mikochik and A. Cahana, *US Patent 9108940B2*, 2015.
- 64 Y. B. Huang, Z. Yang, J. J. Dai, Q. X. Guo and Y. Fu, *RSC Adv.*, 2012, **2**, 11211–11214.
- 65 K. I. Galkin and V. P. Ananikov, *ChemSusChem*, 2019, **12**, 185–189.
- 66 H. Ban, S. Chen, Y. Zhang, Y. Cheng, L. Wang and X. Li, *Ind. Eng. Chem. Res.*, 2019, **58**, 19009–19021.
- 67 E. Zuriaga, B. Giner, M. P. Ribate, C. B. García and L. Lomba, *Environ. Toxicol. Chem.*, 2018, **37**, 1014–1023.
- 68 N. Davidenko, D. Zaldívar, C. Peniche, R. Sastre and J. San Román, *J. Polym. Sci. A-1 Polym. Chem.*, 1996, **34**, 2759–2766.
- 69 S. S. Rahdar, E. Ahmadi, M. Abdollahi and M. Hemmati, *J. Polym. Res.*, , DOI:10.1007/s10965-014-0582-5.
- 70 T. Garret and G. Park, *J. Polym. Sci. A-1 Polym. Chem.*, 1966, **4**, 2714–2717.
- 71 M. Buback, C. H. Kurz and C. Schmaltz, *Macromol. Chem. Phys.*, 1998, **199**, 1721–1727.

- 72 F. R. Mayo, *J. Am. Chem. Soc.*, 1943, **65**, 2324–2329.
- 73 P. A. Clay and R. G. Gilbert, *Macromolecules*, 1995, **28**, 552–569.
- 74 R. G. Gilbert, *Emulsion polymerisation: a mechanistic approach*, 1995.
- 75 D. Kukulj, T. P. Davis and R. G. Gilbert, *Macromolecules*, 1998, **31**, 994–999.
- 76 M. Stickler and G. Meyerhoff, *Makromol. Chem.*, 1978, **179**, 2729–2745.
- 77 O. F. Olaj, G. Zifferer, G. Gleixner and M. Stickler, *Eur. Polym. J.*, 1986, **22**, 585–595.
- 78 H. M. Kapfenstein and T. P. Davis, *Macromol. Chem. Phys.*, 1998, **199**, 2403–2408.
- 79 J. P. A. Heuts, T. P. Davis and G. T. Russell, *Macromolecules*, 1999, **32**, 6019–6030.
- 80 P. T. Lynett, K. Butts, V. Vaidya, G. E. Garrett and D. A. Pratt, *Org. Biomol. Chem.*, 2011, **9**, 3320–3330.
- 81 A. Napoli, M. Valentini, N. Tirelli, M. Müller and J. A. Hubbell, *Nature. Mater.*, 2004, **3**, 183–189.
- 82 B. M. Trost and C. A. Kalnals, *Chem. Eur. J.*, 2019, **25**, 11193–11213.
- 83 H. L. Wagner, *J. Phys. Chem. Ref. Data*, 1985, **14**, 1101–1106.
- 84 A. Ueda and S. Nagai, in *Polymer handbook, 4th ed.*; Brandup, J.; Immergut, E.H.; Grulke, E.A., Eds.; John Wiley and sons: New York, 1999.

3

Inducing branching in vinyl acetate free radical polymerisation

Abstract

The introduction of branching into polymers of vinyl acetate through copolymerisation with multivinyl monomers will be discussed. A summary of the formation of complex polymeric architectures will be provided, with a focus on the copolymerisation of vinyl monomers with multifunctional comonomers. Subsequently, the synthesis and characterisation of a series of branched copolymers of poly(vinyl acetate) will be described. The careful selection of the comonomer and chain transfer agent employed facilitates significantly better control than has been reported previously for vinyl acetate. These polymers are then subjected to alkaline saponification to produce branched poly(vinyl alcohol). The results of this process are polymers with intense brown colours, which is attributed to unsaturation in the backbone through loss of the acetate groups. This process is thought to be facilitated by the thioether end groups introduced as a result of disulfide chain transfer chemistry. Polymers with varying branch densities are prepared through variation of comonomer structure and loading.

3.1 Introduction

3.1.1 Influencing polymer architecture.

In a linear polymer, the monomeric building blocks are bonded end to end forming a flexible chain. Taking the same primary monomeric building blocks but arranging them differently in space to build a different polymer chain architecture influences the materials properties, such as solubility, solution viscosity, melt rheology, and, in the case of branched structures, benefits from the introduction of significant end group functionality.¹⁻⁶ Polymers with complex topologies find use in a range of fields, such as additives in polymer blends⁷⁻¹² and in coatings formulations.^{13,14} This makes the ability to control polymer chain architecture desirable.¹⁵⁻¹⁸

For illustration, some commonly targeted architectures can be seen in Figure 3.1.1.1. Advances in polymer synthesis control, such as the introduction of reversible deactivation radical polymerisation (RDRP) in the 1990's, has facilitated access to complex, defined polymeric architectures. Synthesis strategies which could provide more controlled and sequential assembly of the targeted architectures were then conceived, with countless reports emerging of syntheses of cyclic,¹⁹⁻²⁹ bottle brush,³⁰⁻⁴⁰ and star polymers⁴¹⁻⁴⁶ to name a few.

Focusing on free radical polymerisation, monomers with multiple vinyl end groups, also called multi vinyl monomers (MVMs), can be used to purposely introduce branch points into a polymer chain. In some of the earlier studies (1934-1935) on polymerisations of MVMs, Staudinger and Huseman copolymerised divinylbenzene (DVB) and styrene (Sty), to find that fractions of the produced polymer were insoluble, the proportion of which increased with increasing DVB concentration.⁴⁷⁻⁴⁹ This led to the authors deducing that the DVB units acted as "bridges" in the copolymer, linking together chains of poly(Sty), forming a 3D network of sorts. In 1936, Blaikie and Crozier observed similar behaviour when copolymerising vinyl acetate (VAc) with divinyl ether (DVE) in bulk, with ≈ 13 wt% DVE used wrt VAc. Similar gels were obtained, which could not be solvated in good solvents for the polymer, although underwent significant swelling, agreeing with the deductions of Staudinger and Huseman that the MVM formed bridges between adjacent chains.⁵⁰ Further expansion was provided by Norrish and Brookman (1937), who copolymerised Sty and methyl methacrylate (MMA) with a range of MVMs, including divinyl acetylene, divinyl ether, divinyl sulfide, divinyl sulfoxide

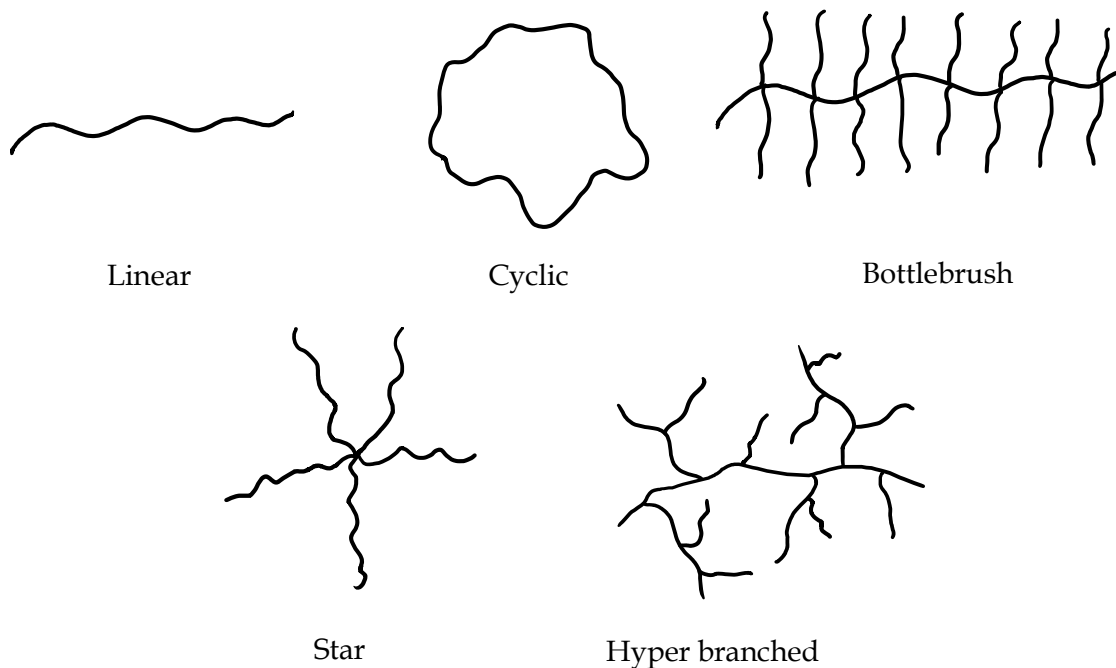


Figure 3.1.1.1: Some commonly targeted polymeric architectures.

and divinyl sulfone, demonstrating the differing cross linking capabilities of the comonomers again through solubility and swelling tests, with the differing copolymerisation behaviours being the cause of the difference in macroscopic properties.⁵¹

Building on the concept of polyfunctionality from Carothers,⁵² Flory (1941) developed a mean-field gelation theory, essentially statistically defining the feasibility of forming an infinitely large molecule in 3 dimensions during condensation polymerisation reactions.⁵³ In its generalised form, the theory predicts when gelation will occur during polymerisation of a multifunctional monomer (MM) with A type functionality, with A-A and B-B type monomers, in step-growth polymerisation, as depicted in Figure 3.1.1.2. During construction of this theory, Flory made some key assumptions to simplify the mathematics, notably that all reactive functionalities are equally reactive, all reactions occur between the complimentary functionalities (i.e. A with B in Figure 3.1.1.2), and finally, all reactions occur intermolecularly.

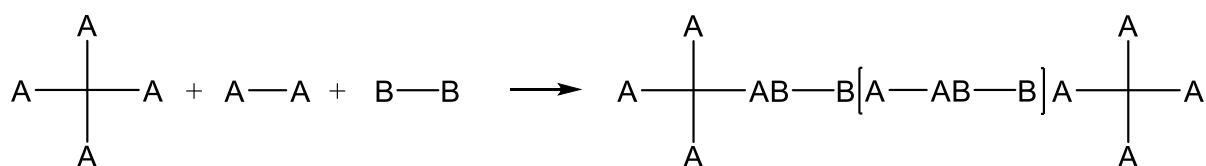


Figure 3.1.1.2: Copolymerisation of A type MM with A-A and B-B monomers according to Flory's theory.

Firstly, Flory defined the bounds of the system, starting with the definition of ρ , being the ratio of A in the MM to the total number of A units in the system:

$$\rho = \frac{f c_3}{2c_1 + f c_3} \quad (3.1.1.1)$$

Where f is the degree of functionality of the MM, being the number of functional groups (4 in the example given in Figure 3.1.1.2), c_3 is the concentration of MM and c_1 the concentration of A-A monomer. r is then defined as the ratio between the total number of A and B groups:

$$r = \frac{2c_1 + f c_3}{2c_2} = \frac{p_B}{p_A} \quad (3.1.1.2)$$

where c_2 is the concentration of B-B monomer. Therefore, $p_B = r p_A$. The theory then defines the point of gelation as the point when $\alpha > \alpha_c$, where α is defined in terms of p_A or p_B :

$$\alpha = \frac{r p_A^2 \rho}{1 - r p_A^2 (1 - \rho)} \quad (3.1.1.3)$$

or:

$$\alpha = \frac{p_B^2 \rho}{r - p_B^2 (1 - \rho)} \quad (3.1.1.4)$$

and:

$$\alpha_c = \frac{1}{f - 1} \quad (3.1.1.5)$$

Thus, after substituting in the expressions for r and ρ , one may determine that gelation occurs when:

$$p_A > \sqrt{\frac{\alpha_c}{r(\alpha_c + \rho - \alpha_c \rho)}} \quad (3.1.1.6)$$

or when:

$$p_B > \sqrt{\frac{r \alpha_c}{\alpha_c + \rho - \alpha_c \rho}} \quad (3.1.1.7)$$

Therefore, one may use the conversion of either monomer to calculate the theoretical gel point. This is even simpler when copolymerising with just an A type MM and a complimentary B-B monomer, depicted through Figure 3.1.1.3.

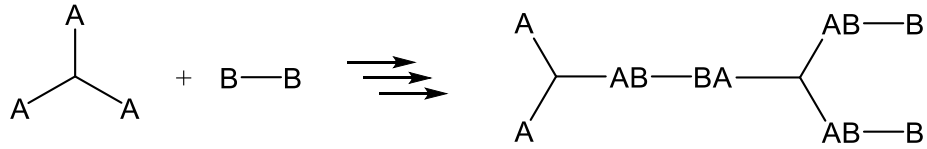


Figure 3.1.1.3: Copolymerisation of A type MM with a B-B monomer in accordance with FS theory.

In this example, this simplification leads to:

$$\alpha_c = \frac{1}{f-1} = \frac{1}{3-1} = \frac{1}{2} \quad (3.1.1.8)$$

And because all A groups are in the MM:

$$\alpha = \frac{\left(\frac{p_B^2 \rho}{r}\right)}{\left(1 - \frac{p_B^2}{r(1-\rho)}\right)} = \frac{p_B^2}{r} \quad (3.1.1.9)$$

This now leads to the much simpler scenario where gelation occurs when:

$$\frac{p_B^2}{r} > \alpha_c \quad (3.1.1.10)$$

Which can again be put in terms of both p_A and p_B :

$$p_A > \sqrt{\frac{1}{2r}} \quad (3.1.1.11)$$

or:

$$p_B > \sqrt{\frac{r}{2}} \quad (3.1.1.12)$$

This theory was later extended by Stockmayer (1944),⁵⁴ who developed the theory to apply more generally to cross linking of systems with arbitrary initial size distributions, making it applicable to vinyl/MVM polymerisations with the gel point predicted to occur according to:

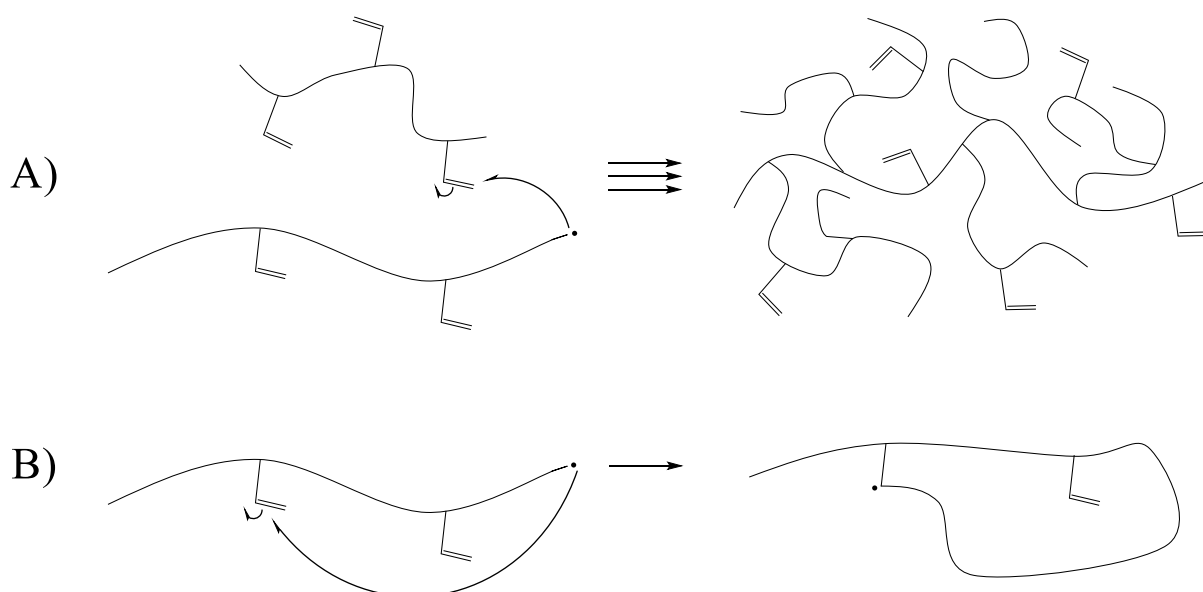
$$v_c = \alpha_c \rho (\bar{P}_w - 1) = 1 \quad (3.1.1.13)$$

Where v_c is the weight-average number of crosslinks per primary chain and α_c is the overall vinyl group conversion (where the subscript c refers to the value at gelation, where $v_c = 1$), ρ is the proportion of the total vinyl groups residing on MVM groups at the start of the reaction (as per Equation 3.1.1.1), and \bar{P}_w is the weight average degree of polymerisation of the polymer backbone assuming all branch points were cleaved. For convenience, this is often rearranged in terms of α_c :

$$\alpha_c = \left(\frac{1}{\rho}\right) \left(\frac{1}{\bar{P}_w - 1}\right) \quad (3.1.1.14)$$

The combined contributions of Flory and Stockmayer led to the statistical theory of gelation being branded “Flory-Stockmayer” (FS) theory.

During the radical copolymerisation of a vinyl monomer with an MVM, a number of pathways are available to a propagating radical, greatly increasing the complexity of the polymer’s architecture. Firstly, copolymerisation between the vinyl monomer and the MVM can occur, forming a primary polymer chain with a number of pendant vinyl groups depending on the amount of MVM used, the reactivity ratios between the two monomers, and the number of vinyl functionalities in the MVM. In the presence of these copolymers, a propagating radical could also undergo addition to a pendant vinyl group either intermolecularly or intramolecularly, as seen in Scheme 3.1.1.1.



Scheme 3.1.1.1: Potential copolymerisation processes between propagating radicals and pendant vinyl groups, both intermolecularly (A) and intramolecularly (B).

Intermolecular addition results in cross linking between 2 chains, dramatically increasing the molecular weight (MW). The dependence of the gel point (where a continuous 3D network has formed) on monomer conversion supports the logical deduction that these additions become more prevalent as the concentration of monomer decreases. Intramolecular addition yields polymers with loops, restricting the free volume occupied by the chain, however, it does not contribute to the cross linking of chains. This process relies heavily on several factors, such as the length of the primary chain, the flexibility of the chain, and the frequency of pendant groups.⁵⁵ Again, as conversion increases and the structure becomes branched due to intermolecular addition, the tendency for intramolecular addition increases as the propagating radical is more likely to be in proximity with neighbouring vinyl groups. Additionally, the reduction in monomer concentration has been shown to increase intramolecular reactions.⁵⁶ Other reactions which are scarcely considered are contributions to architecture through termination and chain transfer. In the case of termination through coupling, dramatic complexity is added if two already complex structures combine. Termination through disproportionation may add even more uncertainty to the structure, given the potential involvement of the unsaturated vinylic group in future polymerisation. Chain transfer to monomer and polymer (both inter- and intra- molecularly) add even further complication, as these can introduce additional branching into the polymer, and further influence its volume and the proximity of reactive groups.

It is important to note that FS theory assumes that all additions occur intermolecularly. If intramolecular addition is significant (as is often the case), the theoretical gel point prediction, according to FS theory, will be at much lower conversion than that observed experimentally due to consumption of pendant vinyl groups without increasing MW. As an example, in the bulk copolymerisation of DVB and Sty, where DVB is added at 1 mol% wrt Sty, Matsumoto *et al.* (1999) used FS theory to predict gelation would occur at $p = 0.04$. However, the authors were able to obtain soluble polymers up to $p = 0.22$. The authors went on to demonstrate the significance of intramolecular cyclisation through dilution of the system in toluene (dilution of 1/3), at a DVB loading of 3 mol%. The dilution was expected to increase the proportion of addition steps occurring intramolecularly. Here, a similar prediction of gelation at $p = 0.04$ is made using FS theory, however, the experimental gel point was even higher at $p = 0.39$. Comparison of the ratios of theoretical vs experimental gel point conversions of 5 and 9.6 in bulk and in solution show just how detrimental the occurrence of intramolecular reactions are on FS theory predictions.

Another key consideration is the necessity of FS theory for the functionalities to bare equal reactivity. In a simple condensation polymerisation of an A type MM and a B-B type monomer this assumption is valid, as only complimentary functionality may react. However, in free radical polymerisation this is a dramatic oversimplification, with differences in vinylic functionalities dramatically influencing reactivity, and the ability for homopropagation adding further complexity. Also, the reactivities of MVM vinyl groups may be different once one of the groups has reacted. For example, the reactivity of the vinyl bonds in divinyl benzene are different to that of the pendant vinyl bond formed after polymerisation,^{57,58} where during copolymerisation with styrene (monomer 1), *para*-DVB (monomer 2) showed reactivity ratios of $r_1 = 0.43$ and $r_2 = 0.85$, with the pendant vinyl groups (monomer 3) estimated at $r_3 = 1$.⁵⁹

Due to these inaccuracies, attempts to improve on the statistical approach of FS theory were made, and instead adopted a kinetic approach, accounting for cyclisation.^{60,61} Models have also been developed for specific systems, particularly in reversible deactivation radical polymerisations (RDRP), to predict gel points and MW/size information as a function of conversion.⁶²⁻⁶⁶ The additional control afforded by RDRP mechanisms leads to more facile prediction of the behaviour of the system. However, parameters such as variability between MVMs to produce intermolecular or intramolecular branches, copolymerisation behaviour and reactivity of pendant vinyl groups etc., make development of a universal expression particularly challenging.⁶⁷

Accurate prediction of the gel point is one thing, however, the ability to influence the experimental gel point is a useful tool during synthesis of complex molecules. Whereas it is known that addition of a chain transfer agent (CTA) will delay the onset of gelation in a polymerisation reaction, Kakurai *et al.* (1984) postulated that CTAs could prevent gel formation altogether, resulting in soluble microgels.⁶⁸ In other words: hyperbranched soluble polymer chains. Putting this proposal into context with FS theory, the gel point is defined as the point at which the weight-average number of crosslinks per primary chain, v_c , is equal to one (according to Equation 3.1.1.13). Therefore, if the average number of crosslinks per chain is reduced, then gelation may be delayed, and, if the condition $v_c < 1$ is met, may be avoided altogether. Given that v_c is a function of \bar{P}_w , introduction of a CTA, and the consequential reduction in \bar{P}_w , will achieve this goal.

This was first demonstrated for the copolymerisation of MMA and DVB.⁶⁸ CBr₄ was used as a CTA at various concentration ratios of MMA and DVB, and the authors were able to

demonstrate that the gel point could be delayed when increasing the concentration of CBr_4 . For example, fixing $[\text{DVB}]/[\text{MMA}]$ at 0.74, and using $[\text{CBr}_4]/[\text{MMA}] = 0.013$ and 0.128 resulted in gelation at 7.1 and 15.0 % conversion, respectively. At $[\text{DVB}]/[\text{MMA}] = 0.15$, and $[\text{CBr}_4]/[\text{MMA}] = 0.013$, gelation was totally prevented up to 100 % conversion. The complexity of the MW distributions (MWD) were shown to increase with increasing monomer conversion, attributed to the reaction of pendant vinyl bonds to yield more branched structures, however, soluble polymers were obtained at full conversion. The authors also demonstrate that at any given MW, the intrinsic viscosity of the polymer chains reduced at increasing reaction times, indicative of a more compact, branched structure (to be covered in later discussions). In a later study, using the same system of MMA and DVB with CBr_4 , Chen *et al.* (1985) published a more comprehensive overview, detailing a series of $[\text{DVB}]/[\text{MMA}]$, each with a range of $[\text{CBr}_4]$.⁶⁹ As may be expected, it was demonstrated that higher $[\text{DVB}]/[\text{MMA}]$ required higher amounts of CBr_4 to prevent gel formation, although again, soluble polymers were obtained at high conversions.

Sherrington *et al.* (2000)⁷⁰ repopularised this concept to produce highly branched polymers, now using thiols as the CTA. The technique, subsequently referred to as the “Strathclyde” route, was applied to the copolymerisation of MMA and but-2-ene-1,4-diacrylate (BDA), with *n*-dodecanethiol (DDT) as CTA. Notably, Sherrington pushed the limits of the theory, using particularly high mole fractions of MVM and CTA, demonstrating delay of the gel point at mol ratios of MMA/BDA/DDT of 100/10/10 to 67 % monomer conversion. Gel formation was prevented at mole ratios of 100/1/1 (89 % conversion), 100/0.5/1 (97 % conversion) and 100/2/2 (77 % conversion). It is noted that in general, soluble microgels were obtained at high conversion when $[\text{CTA}] \geq [\text{MVM}]$. The structure of the branched polymers produced were analysed using advanced size exclusion chromatography (SEC) setups (to be discussed in Section 3.1.3), which indicated that hyper-branched polymers were produced (as seen in Figure 3.1.1.1). The authors demonstrated that the branch density and length could be modified through the amount of MVM and CTA used. In the absence of DDT, macrogelation occurred rapidly, however, with some fine tuning of the relative ratios of BDA and DDT, the authors were able to avoid gel formation and go on to prove the products of this style of synthesis were highly branched.

The Strathclyde method has been demonstrated for many other monomer/MVM/CTA systems using free radical polymerisation,⁷¹⁻⁸⁰ as well as applied to heterogenous polymerisation techniques,⁸¹⁻⁸⁴ ring opening polymerisation,⁸⁵ and even extended to anionic

polymerisation.⁸⁶ There are also many recent publications which add an additional element of control to the process, exploiting RDRP techniques such as catalytic chain transfer polymerisation (CCTP),⁸⁷⁻⁹³ atom transfer radical polymerisation (ATRP),⁹⁴⁻⁹⁷ reversible addition-fragmentation chain transfer (RAFT),⁹⁸⁻¹⁰⁰ and nitroxide mediated polymerisation (NMP).¹⁰¹

Given that reduction of \bar{P}_w may delay the onset of gelation, or indeed prevent it all together, it is conceivable that the same goal may be achieved by an increase in initiator concentration. This increase in initiator concentration will reduce \bar{P}_w via an increase in the rate of termination, R_t . In fact, the aforementioned study by Chem *et al.* (1985) (copolymerisation of MMA and DVB with CBr_4) already demonstrated a delay in gelation through increasing initiator concentration. Where $[\text{MMA}] = 1.89 \times 10^{-1} \text{ M}$, $[\text{DVB}] = 6.94 \times 10^{-2} \text{ M}$ and $[\text{CBr}_4] = 1.51 \times 10^{-3}$, increasing the initiator concentration (azobisisobutyronitrile, AIBN) from 5.2×10^{-3} to $8.2 \times 10^{-2} \text{ M}$ delayed gelation from $p = 0.36$ to $p = 0.69$. Sato and co-workers have expanded on this principle over a number of publications, demonstrating the use of even higher initiator concentrations. The technique was subsequently termed “initiator-fragment incorporation radical polymerisation”, owing to the significant fraction of initiator fragments in the produced polymers.¹⁰²⁻¹⁰⁴ As an example, during the copolymerisation of DVB and N-isopropylacrylamide (NIPAm) in N,N-dimethylformamide (DMF) at 80 °C ($[\text{DVB}] = 0.15 \text{ M}$, $[\text{NIPAm}] = 0.5 \text{ M}$), a concentration of initiator (dimethyl 2,2'-azobisisobutyrate, MAIB) of 0.5 M prevented gelation entirely at full conversion ($M_n = 10,000 \text{ g mol}^{-1}$, $M_w = 104,000 \text{ g mol}^{-1}$).¹⁰³ Restricting MW through a reduction in the rate of polymerisation, R_p , was also demonstrated by Sato *et al.* (2003) through the introduction of a retarder.¹⁰⁵ In the presence of a high initiator concentration (again $[\text{MAIB}] = 0.5 \text{ M}$), DVB and ethyl styrene (Et-Sty) were copolymerised in the presence of a known retarder for DVB polymerisation (a glyoxylic oxime ether), thereby reducing R_p and consequently the MW (given that the rate of termination, R_t , was so high).

Infact, this approach was so successful at preventing gel formation that Sato later applied it to the homopolymerisation of an MVM.¹⁰⁶ Sato successfully demonstrated this concept for the homopolymerisation of divinyl adipate (DVA, a difunctional vinyl ester) in benzene at both 70 and 80 °C. For example, at $[\text{DVA}] = [\text{MAIB}] = 0.3 \text{ M}$, soluble polymer was obtained at 59 % conversion (although this was not pushed further), with $M_n = 13,800 \text{ g mol}^{-1}$ and $M_w = 88,000 \text{ g mol}^{-1}$. The complex structure was not observed through multi-detector SEC, although the branch density is expected to be extremely high, and the avoidance of gelation was striking.

A similar feat was achieved by Guan (2002), however, instead of adopting the high initiator concentration to delay/prevent gelation, the authors exploited CCTP.⁹³ In this homopolymerisation of a dimethacrylate, a cobalt porphyrin catalyst was used as a catalytic CTA, which reduces the MW through binding to the propagating radicals, promoting subsequent β -hydride elimination and the production of macromonomers. Using the cobalt catalyst (the authors measured $C_{tr,S} \approx 10^3$ for MMA), trimers of ethylene glycol dimethacrylate (EGDMA) were targeted, with the formed macromonomers going on to react to produce highly branched polymers with low dependencies of intrinsic viscosity on MW up to 70 % conversion, above which gels were formed.

A recent study by Rannard *et al.* (2020) also demonstrated the homopolymerisation of an MVM with a CTA, in this case using a thiol, and the authors were able to prevent gelation at conversion > 99%.¹⁰⁷ EGDMA was polymerised in the presence of significant concentrations of DDT, with a range of $[EGDMA]_0/[DDT]_0$ between 0.5 and 1 used, which was shown to initially produce low MW oligomeric species, with side groups bearing unreacted vinyl groups. At these ratios, the authors were targeting average degrees of polymerisation of < 2, with these dimers then undergoing further polymerisation through the unreacted vinyl functionalities of the side groups leading to highly branched polymeric products. The authors noted that $[CTA] > [MVM]$ in order to obtain soluble polymer. The necessity of short branch lengths to avoid gelation results in the introduction of significant chain end functionality through the CTA, and the structure is very dense (Mark-Houwink-Sakurada parameter α ranging from 0.283-0.340 for $[EGDMA]_0/[DDT]_0$ of 0.5 to 0.85, determined in tetrahydrofuran (THF) at 30 °C, the significance of which to be highlighted later).

Although synthesis of densely branched polymers is easy in MVM homopolymerisations, achieving a range of branch densities is not a simple task. The copolymerisation with a vinyl monomer offers a much more facile route to varying branch density, with the branch length controlled through restriction of the kinetic chain length through the aforementioned methods, being: initiator concentration, introduction of CTA, or introduction of a rate retarder.

3.1.2 Inducing branching in vinyl acetate polymerisation.

Of particular interest in this chapter is the introduction of branching into poly(vinyl acetate) (PVAc). Given the industrial relevance of both PVAc, and poly(vinyl alcohol) (PVOH), the ability to control polymer architecture could be a powerful extension to the numerous

application areas where the polymers are already commonplace. To the best of the authors knowledge, the first example of attempts to specifically introduce branching in PVAc synthesis was in a paper published by Walling in 1944. Walling demonstrated the free radical copolymerisation of VAc with an MVM, divinyl adipate (DVA),¹⁰⁸ showing that gelation was observed at lower conversion, depending on the amount of DVA employed in the copolymerisation. This suggests successful copolymerisation of DVA was achieved, and the pendant vinyl groups did indeed undergo subsequent addition. No regulation of MW was attempted however, and the relation between the intrinsic viscosity of the polymer chains and MW was not quantified.

Berry and Craig (1964) exploited the high transfer constant to polymer in VAc free radical polymerisation, performing a polymerisation of VAc in the presence of narrow MW fractions of linear PVAc.¹⁰⁹ In this way, the authors essentially used linear polymer as a CTA, where after proton abstraction,¹¹⁰ the newly produced polymeric radical could propagate, resulting in branching. Lovell *et al.* (1998) later showed through nuclear magnetic resonance (NMR) studies that this abstraction occurred almost exclusively through the acetoxy protons of the side groups. This was justified as the ratio of ultimate CH₂ protons (formed through transfer) to all backbone CH₂ protons was equal to the number of branches (if backbone abstraction were prevalent then this ratio would be greater than the number of branches as there would be less backbone CH₂ remaining). Berry and Craig were able to regulate the length of these branches through the use of toluene, which they claimed acted both as a solvent and as a CTA. Attempts were made to separate branched polymer from any lower MW linear polymer through fractional precipitation, although this approach was unlikely to yield exclusively branched polymers. The authors did report an increase in MW compared to the original linear polymer, however, the degree of grafting was not easily controlled, and significant side products were observed, limiting the scope of this approach.

Rimmer *et al.* (2005) reported the production of branched PVAc through copolymerisation of VAc with allyl carbonate monomers.¹¹¹ The structure of allyl isopropyl carbonate is given in Figure 3.1.2.1, and the isopropyl proton of the tertiary carbon is particularly susceptible to abstraction. This leads to each comonomer having the potential of introducing a branch point, much like the behaviour observed in vinyl acetate homopolymerisation, however, the rate of

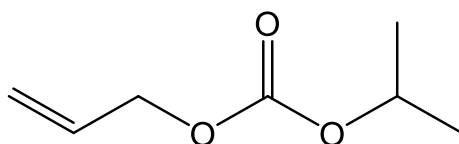


Figure 3.1.2.1: Structure of allyl isopropyl carbonate. Note the proton on the tertiary carbon of the isopropyl group is particularly susceptible to chain transfer.

proton extraction from the isopropyl groups is expected to be much greater than that from the acetate protons of VAc/PVAc. At 60 °C in solution, the reactions yielded insoluble cross-linked materials over a range of comonomer concentrations, suggesting that copolymerisation was successful, and that transfer was occurring as expected. The gelation was explained to be a result of termination via combination. Although this was not discussed, similar behaviour may be expected in the homopolymerisation of vinyl acetate at high monomer conversion, where transfer to polymer is substantial. The authors went on to obtain soluble branched polymers through adjustment of temperature, with higher temperatures favouring higher rates of transfer relative to termination. Introduction of an additional CTA (isopropanol) was also shown to prevent gel formation. It is noted that the authors found significant reductions in polymerisation rate through introduction of these comonomers, however, did manage to produce branched polymers with values of the Mark-Houwink parameter $\alpha < 0.5$, indicative of a high degree of branching (to be discussed further in Section 3.1.3).

Zeng *et al.* (2018) demonstrated a somewhat similar approach to Rimmer, through the copolymerisation of VAc with 2-(dimethylamino)ethyl methacrylate (DMAEMA) in the presence of lauryl peroxide (LPO).¹¹² DMAEMA, a so called “inimer”, bears a vinyl group capable of undergoing addition, as well as a tertiary amine capable of initiating new chains in the presence of an oxidant (the authors used LPO as both radical source and as oxidant). In this way, copolymers of VAc and DMAEMA could be produced, with each chain essentially becoming a macroinitiator, forming branch points through the DMAEMA units when polymerised in the presence of lauryl peroxide. Using this approach, the authors were able to demonstrate that in the presence of DMAEMA, the MWD shifted to higher MW, and increased in complexity as conversion increased. Interestingly, increasing [DMAEMA]/[VAc] from 0.01 to 0.02 resulted in a decrease in MW (M_n from 112,600 to 24,100), and a decrease in g' (the ratio of intrinsic viscosity of the polymer to that of linear PVAc at 200,000 g mol⁻¹) from 0.38 to 0.32, implying a more compact structure (to be discussed more later). The decrease in MW was attributed to the increase in radical generation (as DMAEMA could initiate).

Sato, building on his work in initiator-fragment incorporation radical polymerisation discussed earlier, copolymerised vinyl acetate with 1,2-polybutadiene (1,2-PB) utilising MAIB as initiator.¹¹³ The authors obtained soluble polymers at high initiator concentrations as expected, although did not push the reactions to high conversion. The reactions which avoided gelation at the highest conversion were at the concentrations: [1,2-PB] = 0.8 M, [MAIB] = 0.3 M, and [VAc] = 0.6, 0.8 and 1.2 M, all reaching 46 % conversion of monomers. The increase in [VAc] resulted in an increase in M_n from 15,000 g mol⁻¹ (for 0.6 M) to 21,000 and 58,000 g mol⁻¹ for 0.8 and 1.2 M respectively, with the increase due to an increase in the kinetic chain length. Further MW analysis of the polymers was not performed.

Stenzel and co-authors have demonstrated the synthesis of PVAc star^{114,115} and comb polymers,¹¹⁶ utilising RAFT polymerisation. As discussed in Chapter 2, these RDRP methods scarcely offer the same control for VAc as with other monomers, however, MW was shown to increase with increasing monomer conversion, albeit with an increase in the dispersity. The rates of polymerisation were also low, with 70 % monomer conversion being reached after 6 h. For the stars, tetrafunctional xanthate RAFT agents were used (therefore macromolecular design by interchange of xanthate, referred to as MADIX), which resulted in growth of PVAc from each xanthate functionality, producing 4-armed star polymers. The authors compared data obtained through GPC with conventional calibration to that obtained through dual detection with a viscometer. They demonstrated that with conventional calibration, the evolution of MW with conversion deviated significantly from the theoretical value, however, use of dual detection gave a much more consistent fit. This was used as proof for the star like architecture, although the authors did not report the relation between the intrinsic viscosity and the MW, or any Mark-Houwink parameters to further this explanation.

For the comb polymers, PVAc precursors were modified through a multistage process to convert the acetate side groups into xanthate groups capable of undergoing MADIX/RAFT. From this, PVAc could be polymerised, producing comb polymers through a “grafted from” mechanism, although the authors noted some linear polymer chains produced at moderate conversion, as well as high MW shoulders in the distributions, which were attributed to polymers formed through termination. The complexity of the multistage synthesis, as well as the shortcomings in the results, beg the question as to whether this approach is a viable method to produce higher order structures of PVAc. Later, Taton *et al.* (2008) copolymerised VAc with divinyl adipate (an MVM to be discussed later), in the presence of a MADIX agent.¹¹⁷ The authors obtained very complex distributions during the copolymerisation, although did

not analyse the architecture, and instead simply commented on the lack of gel formation or shifting in the retention time of the produced polymers. For example, fixing the mol % of DVA at 6 mol% in the presence of only 1 mol% of CTA resulted in gelation. However, increasing to 4 mol% CTA yielded soluble polymer, with $M_n = 6,500 \text{ g mol}^{-1}$ and $M_w = 16,000 \text{ g mol}^{-1}$ at 94 % total conversion of vinyl groups. Other authors have noted similar results with self-condensing vinyl copolymerisation, exploiting RAFT/MADIX polymerisation with VAc.^{118,119} Essentially a RAFT/MADIX agent bearing a vinylic bond is used as CTA, thereby reducing the MW of PVAc, whilst offering an alternate site susceptible to addition.

Sherrington and Baudry (2006) applied the previously discussed “Strathclyde” methodology to the production of branched PVAc, employing a tri-functional allyl comonomer, 1,3,5-triallyl-1,3,5-triazine-2,4,6(1H,3H,5H)-trione (TTT), and a range of thiol CTAs.¹²⁰ Soluble polymers were obtained when CTA’s were employed, and the branching behaviour was shown to change as the ratios of VAc/TTT/CTA were adjusted. The authors noted very broad MWDs, and slow polymerisation times. The branched PVAc was converted to branched PVOH through alkaline saponification. To prove the architecture was unaffected by the saponification, i.e. the branches were resistant to the process, the PVOH was then acetylated. The authors found striking similarity between the MWDs of the reacetylated PVOH and the original branched PVOH, suggesting resistance to saponification under their experimental conditions.

Despite this, it is important to consider some points of contention in this study. Firstly, the viability of using TTT as a comonomer may not be optimal, due to potential poor copolymerisation with VAc (as is the case in most copolymerisation’s with VAc). Poor copolymerisation will result in a drift in the copolymer composition, and would complicate the MWD and broaden the dispersity in branching as polymerisation progresses. Although conversion vs time data was not discussed, slow polymerisation times are also a potential consequence of poor copolymerisation, and this may be confirmed by the long polymerisation times (48 h) and use of two initiator additions (one additional shot added after 24 h) utilised by the authors. The potential for TTT to act as a radical transfer species was also discussed due to the presence of allylic H atoms which may undergo proton abstraction. However, the authors proposed that this was unlikely due to the high loading of TTT and the presence of thiol CTAs in the system, as this would likely result in oligomeric species exclusively.

The second big issue with this system is the use of a thiol CTA, due to the large chain transfer constant, $C_{tr,S}$, expected with vinyl acetate. The magnitude of $C_{tr,S}$ (≈ 223.9), as discussed in detail in Chapter 1, leads to an uncontrollable composition drift to higher MW with increasing conversion. This will likely result in macrogellation over a wider range of compositions, even at low/moderate monomer conversion, and, if soluble polymers are obtained, the distributions will be very broad. This may go some way to explain the breadth of the distributions observed (up to $D_M = 48$ in some cases) and the irregularities of the shapes of the distributions. Given the magnitude of $C_{tr,S}$, one may be forgiven for questioning how the authors managed to obtain any soluble polymer at all at the degrees of conversion obtained in the study, however, solvent selection was noted to be of particular importance. At a mole ratio of VAc/TTT/ME = 100/3/10, reactions performed in ethyl acetate ($C_{tr,S} = 3.3 \times 10^{-4}$)¹²¹ yielded macro gels, and in ethanol ($C_{tr,S} = 2.5 \times 10^{-3}$)¹²¹ yielded microgels of which MW information could not be acquired. However, performing the same reaction in 2-isopropoxy ethanol ($C_{tr,S} = 1.6 \times 10^{-2}$)¹²² prevented gel formation. The difference in the chain transfer constants between the solvents is a clear factor, and contributes to the hindrance of gel formation. This approach to producing branched PVAc, and the corresponding branched PVOH, is particularly attractive, however, clear improvements are possible with comonomer and CTA selection.

Han and Zhang copolymerised VAc with small amounts of allyl methacrylate (up to 0.01 mol% wrt VAc) in methanol.¹²³ Given the low amounts of MVM used, a minimal increase in MW was observed (M_n and M_w increased from 118,000 and 316,000 to 123,000 and 394,000 g mol⁻¹ for no comonomer and 0.01 mol% comonomer respectively).

3.1.3 Branched polymer characterisation.

One key consideration in this chapter is how branched polymers may be differentiated from their linear counterparts. The most common technique to achieve this is SEC. The technique functions based on the separation of molecules by hydrodynamic volume (V_H). This is achieved by flowing polymer solutions through columns packed with porous material, where larger chains are excluded more from these pores and pass through the column faster. At the end of the column, a concentration detector, such as differential refractive index (DRI) or ultraviolet (UV), is used to determine the amount of material at each elution volume, which in conventional SEC is then compared to the elution volume of narrow MW standards of known MW.

Stockmayer and Zimm (1949)¹²⁴ derived how the dimensions of a polymer chain changes through the introduction of branching. The authors discussed this in terms of the mean square radius gyration of a chain, R^2 , which for a linear chain can be described as:

$$R_{linear}^2 = \frac{b^2 N}{6} \quad (3.1.3.1)$$

Where b is a characteristic length of a segment of the polymer being a function of the length and flexibility of its bonds (the so called Kuhn length), and N is the number of segments per chain. Through introduction of one branch point, this becomes:

$$R_{branched}^2 = \frac{b^2}{N} \sum_v \left[\left(\frac{N_v^2}{2} \right) - \left(\frac{N_v^3}{3N} \right) \right] \quad (3.1.3.2)$$

Where N_v is the number of segments in the v th chain, and where v runs from 1 to f , with f being the functionality of the branch unit.

The authors went on to derive expressions for the radius of gyration of polymers with 2 and 3 branches individually, before arriving at a more general expression to describe materials with branch units distributed at random. It became apparent that two polymers of the same MW, but with different degrees of branching, possessed different molecular density. More specifically, the higher the degree of branching, the higher the density, i.e. lower R^2 , and therefore, the lower the contribution to the solution viscosity. The parameter, g , was defined as the ratio of R^2 of a linear and branched polymer:

$$g = \frac{R_{branched}^2}{R_{linear}^2} \quad (3.1.3.3)$$

Therefore, when comparing an analyte polymer and a polymer known to be linear of the same MW (of the same chemical functionality), if $g = 1$, the analyte polymer is linear, and if $g < 1$, the analyte polymer is branched.

Zimm and Thurmond (1952)¹²⁵ went on to confirm this by analysing a series of copolymers of DVB and Sty, utilising multidetector SEC. These copolymers are expected to contain a high degree of branches due to the two vinyl groups per molecule of DVB. The authors demonstrated that for polymers of the same MW but different degrees of long chain branches, V_H was measurably different. A visual depiction of this is provided in Figure 3.1.3.1, wherein two polymer chains of identical MW but different molecular densities are shown. These findings are huge drawbacks for conventional SEC analysis. In the case where a set of

standards of different chemistries are used to calibrate the system, the analyte polymer will elute at a different elution volume despite being at the same MW as the standard. Also, even if the analyte is of the same chemical functionality as the standard, but different architecture, the difference in the radius of gyration, and therefore the hydrodynamic volume will be different. As an example of this, the schematic in Figure 3.1.3.1 shows two polymer chains of the same MW and functionality, however different architecture. The star polymer (depicted in red) has a higher molecular density, therefore a lower hydrodynamic volume, and will be retained more by the column, which through comparison with the conventional calibration will be assumed to be of lower MW. With the addition of, for example, a viscosity detector, it would become clear that in fact the linear polymer has a significantly higher intrinsic viscosity relationship to MW, and the linearity of its structure could be inferred compared to the branched analogue.

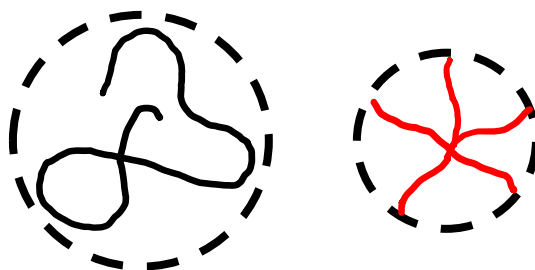


Figure 3.1.3.1: Depiction of the hydrodynamic volume of a linear (black) and star (red) polymer of the same MW.

In Chapter 1, the theory of universal calibration for SEC was introduced, and how this may be exploited to achieve accurate MW information despite differing molecular densities arising from the analyte polymer having a different architecture or a different interaction with the solvent compared to the standards used. This relies on the simple deduction, discussed by Benoit *et al.*,¹²⁶ and exploiting the Einstein viscosity law, that the product of the intrinsic viscosity, $[\eta]$, and MW of a chain is a measure of V_H :

$$V_H = [\eta] \cdot MW \quad (3.1.3.4)$$

Given that SEC separates by V_H , the use of a viscosity detector alongside the concentration detector can give accurate MW data. The system is first calibrated through determination of the elution volume of narrow MW standards, as with conventional GPC, however, the additional viscosity detector allows the construction of a calibration of the form $\log([\eta] \cdot MW)$ vs elution volume. The viscosity detector is typically a capillary bridge viscometer (the reader is referred to an excellent summary by Haney for specifics),¹²⁷ which is used to determine the

specific viscosity through the inlet pressure (IPr) and the differential pressure (DPr) of the capillary bridge:

$$\text{Specific viscosity} = \frac{4DPr}{IP - 2DPr} \quad (3.1.3.5)$$

Then the specific viscosity is reduced to $[\eta]$ by division of the concentration of polymer:

$$[\eta] = \frac{\text{Specific viscosity}}{\text{concentration}} \quad (3.1.3.6)$$

The concentration of polymer at a given elution volume is determined through the use of a concentration detector. The overall concentration of the polymer distribution can be determined through a user defined concentration. This concentration is then used to calculate the refractive index increment, dn/dc (for DRI detector), or molar extinction (for UV detector), based on the intensity of the signal at the detector. Alternatively, either of these parameters (depending on the detector in use) can be defined by the user and the concentration can be determined in reverse. UV detectors are typically less versatile, as clearly the polymer needs to absorb strongly to obtain a good signal response, which limits its application. Once the concentration of the distribution is known, each elution volume may be assigned a concentration, and therefore its $[\eta]$ can be calculated.

During analysis of an analyte sample, each elution volume is compared to the universal calibration to determine $\log([\eta] \cdot MW)$, and the measured value of $[\eta]$ is then used to calculate MW. This is useful knowledge for analysis for linear polymers, as the use of calibrants of the same chemical functionality and architecture is no longer required. The measured $[\eta]$ and calculated MW can then be used to construct a Mark-Houwink-Sakurada (MHS) plot from the MHS equation:

$$[\eta] = K MW^\alpha \quad (3.1.3.7)$$

Where K and α are the MHS parameters. Plotting on a log scale facilitates trivial extraction of α , being the slope, and $\log K$, being the intercept.

$$\log[\eta] = \log K + \alpha \log MW \quad (3.1.3.8)$$

Being the slope of this plot, α gives a good indication of the molecular density. Comparing linear polymers of different chemistries, changes in the slope reflect differences in the solvent/polymer interaction, with poorly solvated chains adopting more compact globule

arrangements, and consequently showing a weaker dependence of $[\eta]$ on MW, and therefore a lower value of α .

α is also particularly useful when discriminating between two polymer chains of the same chemical functionality, but with different architecture. Remembering that when increasing branching, an increase in molecular density is observed, and therefore $[\eta]$ will decrease at a given MW. In fact, with more compact branched structures, it would be logical to assume that a lower dependence of $[\eta]$ on MW will be observed, and as such comparing α of a branched polymer to a linear polymer of the same chemical functionality should reveal information on the extent of branching.

However, Castignolles *et al.* (2007)¹²⁸ elegantly pointed out that universal calibration is not without its flaws. The authors discussed that during separation of some complex branched polymers, a specific elution volume may contain a distribution of MWs and architectures, and as such a distribution of intrinsic viscosities, which may not be trivial to deconvolute. However, comparison of α (determined over a broad range of elution volumes) between a branched polymer and its linear counterpart is still a useful tool to quantify the molecular density differences.

Additional detectors can be added inline to provide further information, or increase the accuracy of the MW/structural determination. For example, light scattering detectors are often included in addition to viscosity and DRI detectors, which allows the direct measurement of MW, without relying on the validity of the universal calibration. The Mark-Houwink-Sakurada parameters can be determined in much the same way, plotting $\log[\eta]$ vs $\log MW$, with direct measurement of MW leading to increased validity of the plot. It is often the case that light scattering detectors are very sensitive to noise/contamination, and can often over exaggerate the contributions of the high MW side of the distribution, so the use is not necessarily always an improvement over the universal calibration.

3.1.4 Experimental aims.

The primary aim of the experimental section of this chapter is to improve on a strategy for branched poly(vinyl acetate), through copolymerisation with MVMs in the presence of a CTA. The copolymerisation behaviour with a selection of MVMs is demonstrated, and the molecular density is tuned through the relative concentrations of VAc, MVM and CTA. How TTT influences the rate of polymerisation, and which alternate comonomers may be used to prevent retardation is also discussed. We used dibutyl disulfide (DBDS) as CTA, where $C_{tr,S}$

is significantly closer to unity ($C_{tr,S} = 0.221$ at 60 °C, as measured in Chapter 2) than previous works, minimising composition drift. Equations 3.1.4.1-3.1.4.3 show a reminder of the equation derived by Smith,¹²⁹ discussed in Chapter 1, detailing how the concentration ratio of CTA to monomer changes as a function of monomer conversion. The normalised, unitless form shown in Equation 3.1.4.3 is then plotted in Figure 3.1.4.1, and it should become obvious that employment of DBDS results in the ratio of [CTA]/[M] undergoing significantly less drift compared to a thiol (as was used by others), and as such, narrower, more defined MWDs can be expected.

$$\frac{[S]}{[M]} = \frac{[S]_{p=0}}{[M]_{p=0}} (1 - p)^{C_{tr,S}-1} \quad (3.1.4.1)$$

$$\frac{s}{m} = \left(\frac{[S]}{[S]_{p=0}} \right) \left(\frac{[M]}{[M]_{p=0}} \right)^{-1} \quad (3.1.4.2)$$

$$\frac{s}{m} = (1 - p)^{C_{tr,S}-1} \quad (3.1.4.3)$$

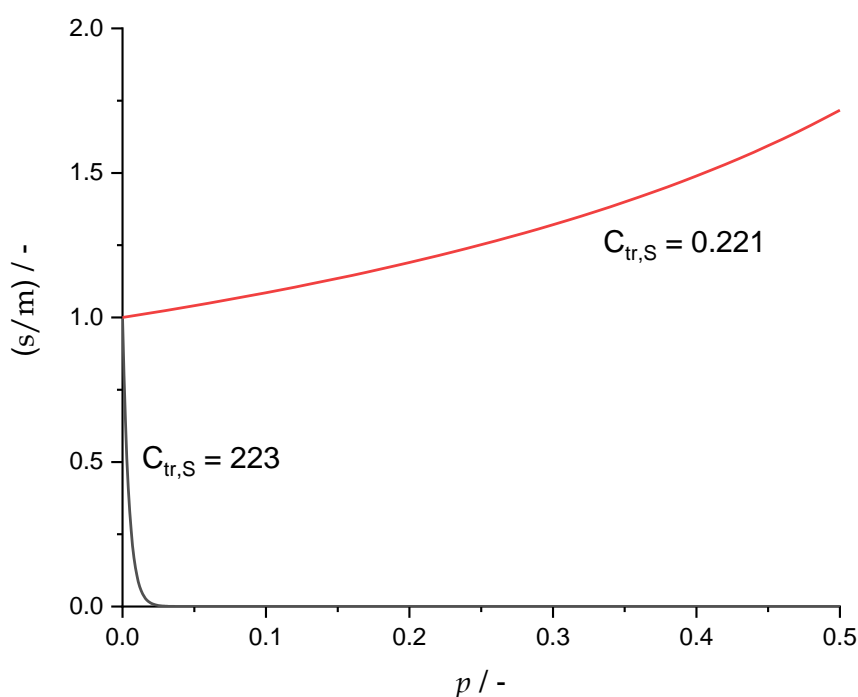


Figure 3.1.4.1: Plot of the normalised ratio, s/m , defined in Equation 3.1.5.3, demonstrating how s/m changes as a function of monomer conversion when $C_{tr,S} = 223$ (—) and 0.221 (—).

An additional consequence of the use of disulfide CTAs in these studies is the expectation of thioether groups being introduced at the end of every branch (see Figure 3.1.4.2 for expected structure after copolymerisation with a difunctional MVM), which may facilitate the synthesis of highly functional hyper branched polymers in future work, opening the doors to further applications.

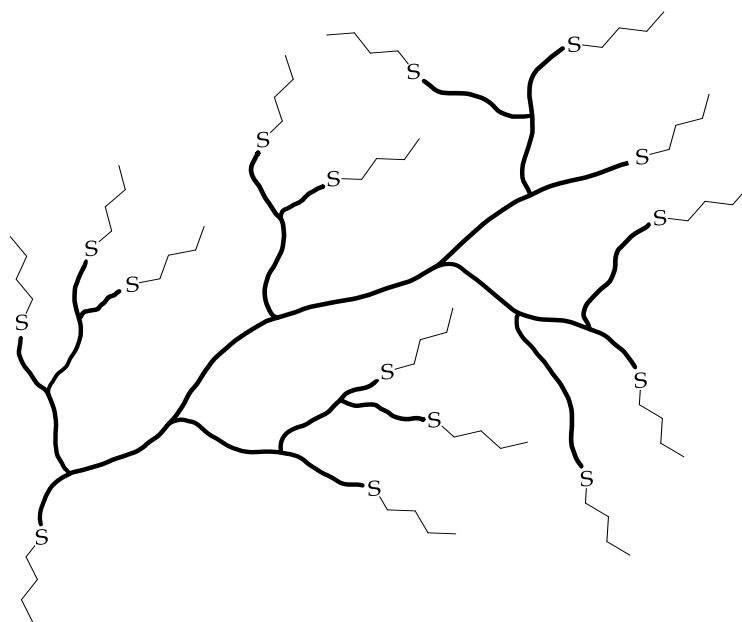


Figure 3.1.4.2: Predicted structure of branched PVAc, formed through copolymerisation with a difunctional MVM in the presence of a CTA, DBDS.

3.2 Results and discussion

3.2.1 1,3,5-triallyl-1,3,5-triazine- 2,4,6(1H,3H,5H)-trione (TTT).

Firstly, a series of free radical copolymerization's of VAc and TTT (structure as seen in Figure 3.2.1.1) were performed, in the presence of DBDS. The amount of DBDS was fixed at 1 mol% wrt VAc and the comonomer concentration varied to assess the behaviour of the copolymerisation. Solution polymerisations were performed at the mole ratios of

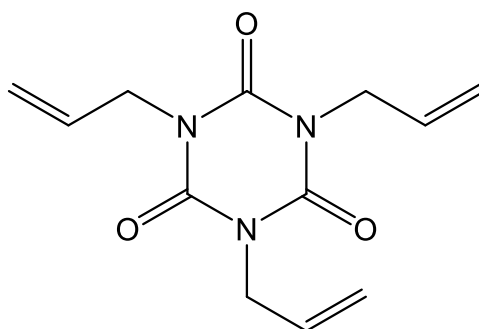


Figure 3.2.1.1: Chemical structure of 1,3,5-triallyl-1,3,5-triazine-2,4,6(1H,3H,5H)-trione (TTT).

VAc/DBDS/TTT = 100/1/X where X = 0.0, 0.1, 0.5, 1.0, 2.0 and 5.0. The polymerizations were performed at 60 °C, using AIBN as initiator at a concentration of 7.7×10^{-4} M (see experimental section for full procedure).

As can be seen in Figure 3.2.1.2, the rate of conversion dramatically decreases with increasing concentration of TTT. Taking the slopes after any inhibition periods shows the rate of polymerisation decreases to 75.96 %, 42.52 %, 39.65 % and 18.15 % of the rate in the absence of TTT for X = 0.1, 0.5, 1.0 and 2.0 respectively, as seen in Table 3.2.1.1. This behaviour suggests that propagation and cross-propagation from a terminal TTT radical is rate limiting. Reactivity ratios were reported by Roth and Church to be $r_{VAc} = 0.91$ and $r_{TTT} = 0.75$ at 60 °C, however, the low reactivity of the allyl terminal unit would make termination and chain transfer likely once a TTT unit has been added.¹³⁰ This may imply that a significant proportion of the branch points will be at the end of a chain, with the two terminal pendant vinyl groups undergoing copolymerisation, instead of these being in the chain.

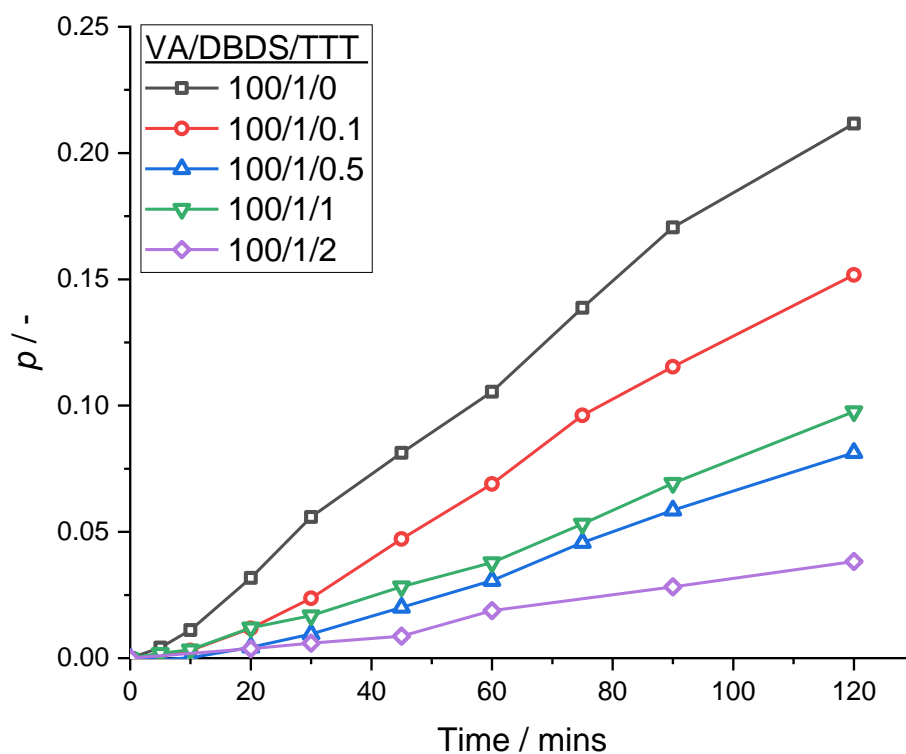


Figure 3.2.1.2: Monomer conversion, p , vs time (mins) for the free radical solution copolymerisation of vinyl acetate and TTT in the presence of DBDS. The ratios of VAc/DBDS/TTT are detailed in the figure legend.

Table 3.2.1.1: Rate of polymerisation, R_p for the free radical copolymerisation of VAc and TTT in the presence of DBDS. R_p is determined by fitting a linear relation to the conversion time data points and extracting the slope. The Rate % is calculated relative to the experiment performed at VAc/DBDS/TTT = 100/1/0.

VAc/DBDS/TTT	$R_p / \text{M s}^{-1}$	Rate %
100/1/0.0	6.28×10^{-5}	100.00
100/1/0.1	4.77×10^{-5}	75.96
100/1/0.5	2.67×10^{-5}	42.52
100/1/1.0	2.49×10^{-5}	39.65
100/1/2.0	1.14×10^{-5}	18.15

The MWD of the polymers after 120 mins reaction time can be seen in Figure 3.2.1.3, along with the corresponding Mark-Houwink plots. M_n and M_w , being the number and weight average MWs, as well as K and α , being the Mark-Houwink parameters, can be seen in Table 3.2.1.2.

A very particular procedure was undertaken to determine the value for α , which allowed consistent analysis of the acquired data. Firstly, SEC data was obtained for each sample, in CHCl_3 , and the MW was estimated using universal calibration, using a known concentration of polymer in the sample (for calculation of the intrinsic viscosity). The MW vs $[\eta]$ plot was then analysed between the MW values where the intensity of the $dW/d\log M$ distribution was greater than 50 % of the maximum in the $dW/d\log M$ distribution. Equation 3.1.3.7 (the MHS equation) was fitted to this region, allowing the extraction of K and α . These K and α values are then used to recalculate $[\eta]$ at each MW, showing how the fitted parameters correlate with the experimental data. The displayed plots of MW vs $[\eta]$ are cut off below DP = 150, as to ensure that both the signal is intense enough to give reliable data, and to avoid any inaccuracies deduced from a non-constant value for Flory's characteristic ratio at low MW. Additionally, at low MW, contributions of the end groups to V_H , as well as the response of the differential refractive index detector introduce more uncertainty in MW determination. The high MW end of the plot was cut off at the MW at which the intensity of the $dW/d\log M$ distribution dropped below 5 % of the maximum to account for low polymer concentrations and consequentially noisy data points.

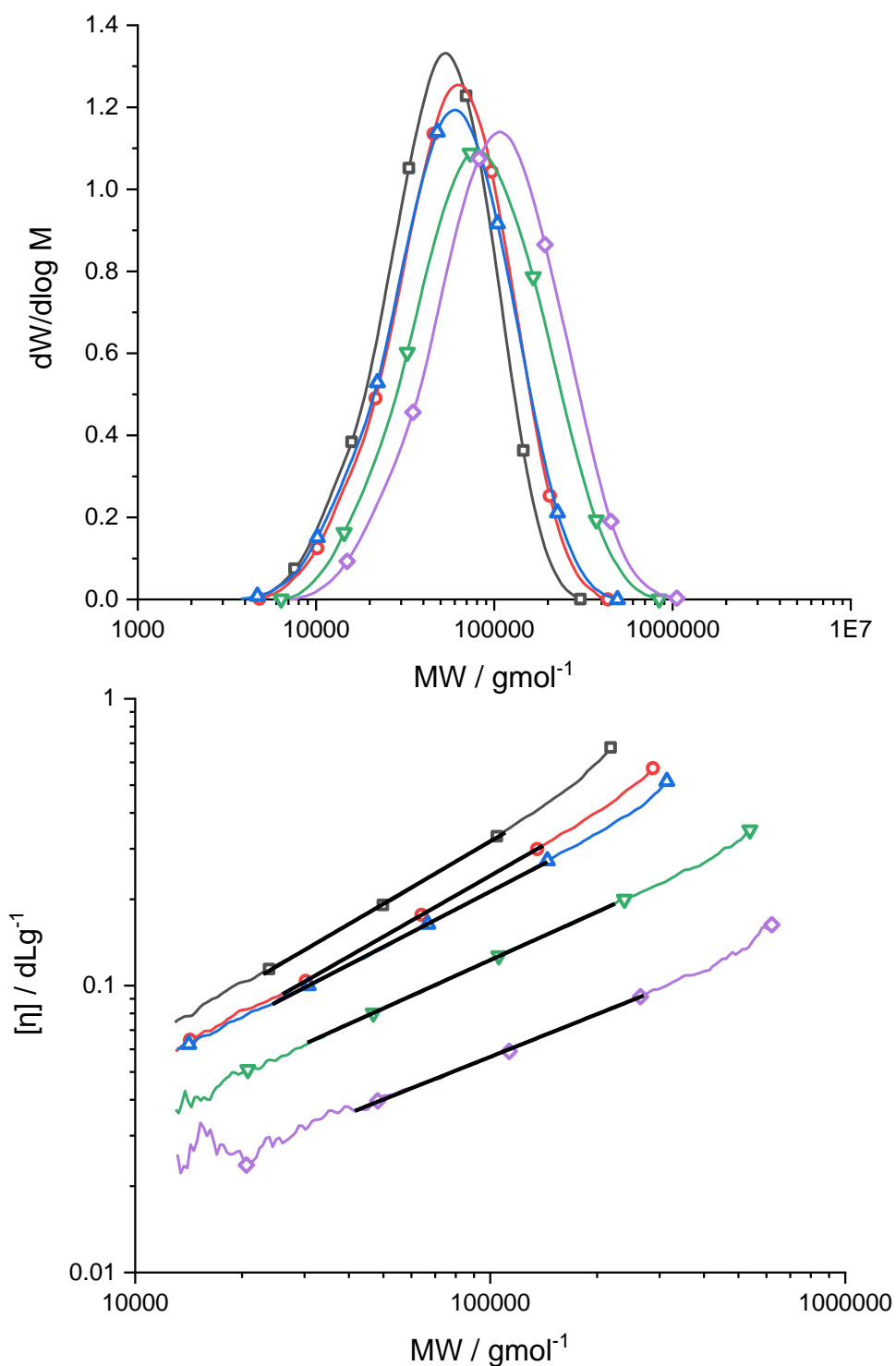


Figure 3.2.1.3: $dW/d\log M$ vs MW (g mol^{-1}) MW distributions (top) and the Mark-Houwink plots of intrinsic viscosity, $[\eta]$ (d Lg^{-1}), vs MW (g mol^{-1}) (bottom) for the 120 mins samples taken during the free radical solution copolymerisation of vinyl acetate and TTT in the presence of DBDS. Mol ratios $\text{VAc/DBDS/TTT} = 100/1/X$ where $X = 0.0$ (\square), 0.1 (\circ), 0.5 (\triangle), 1.0 (∇) and 2.0 (\diamond). The solid black lines show the fitted regions from which α and K were extracted.

Table 3.2.1.2: Monomer conversion, p , number average and weight average MWs (M_n and M_w respectively) and the Mark-Houwink parameters K and α for the 120 mins samples in the series of copolymerisation's of VAc with TTT in the presence of DBDS.

VA/DBDS/TTT	p	M_n / gmol ⁻¹	M_w / gmol ⁻¹	$K \times 10^5$	α
100/1/0.0	0.21	36,100	58,200	7.635	0.724
100/1/0.1	0.15	41,800	71,200	7.129	0.706
100/1/0.5	0.08	40,100	72,000	13.274	0.641
100/1/1.0	0.10	56,600	108,200	19.679	0.559
100/1/2.0	0.04	71,900	134,600	19.134	0.494

Increasing the TTT concentration results in a shift in the MWD to higher MW (shown by an increase in M_n and M_w), which provides evidence that TTT acts like a branching agent. An increase in M_n from 36,100 to 71,900 g mol⁻¹ through introduction of 2 mol% TTT wrt VAc demonstrates this. M_w appears slightly more sensitive to an increase in TTT, where a rise from 58,200 to 134,600 g mol⁻¹ can be observed. The relationships between MW and $[\eta]$ are essentially linear throughout, implying a relatively uniform branch density.

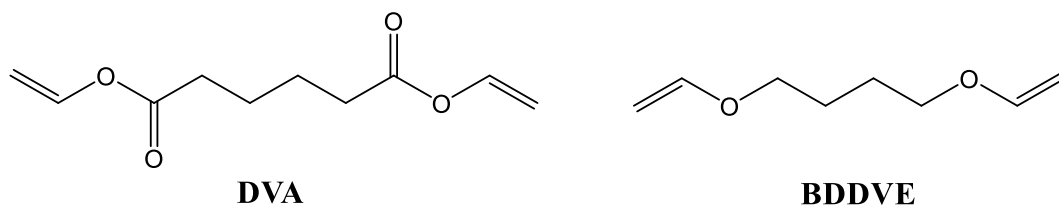
Comparing to the study by Sherrington, the distributions seen here are more monomodal, however, are formed at much lower monomer conversion, with the previous study providing no data at lower monomer conversion, so comparison between these two sets of work is not valid. But it is important to emphasise that the lack of substantial drift in [CTA] when employing disulfides vs thiols will maintain a much more defined branched architecture. In fact, given that $C_{tr,S}$ is lower than 1 for dibutyl disulfide, the drift will result in more chain transfer at increasing conversion, meaning polymers produced at higher conversions will undergo more chain transfer, further hindering gelation through a decrease in \bar{P}_w .

Looking at the Mark-Houwink plots, and the data extracted therein, an increase in the mol % of TTT results in a decrease in α , which may be observed through a decrease in the slope in the plot of $[\eta]$ vs MW on a log-log scale, seen in Figure 3.2.1.3. The fact that overall monomer conversion decreases as TTT increases, yet α still decreases, suggests copolymerisation of pendant vinyl groups even at low conversion. Although this could instead be explained through a decrease in kinetic chain length between branches, due to the low reactivity of the allyl group toward propagation. This would lead to a more compact structure and reflect a decrease in α . If neither of these arguments were true, α may be expected to increase as TTT increases when taking samples at a fixed time, as monomer conversion is lower. Interestingly,

K varies quite considerably between the samples, which can be visualised by different intercepts on the Mark-Houwink plots. This is unexpected behaviour, as the architecture at infinitely low MW should be the same linear structure in all cases, therefore, these plots should be expected to intersect in this range. If inclusion of TTT is present across the full MW range, then perhaps an explanation for this observation is a difference in the interaction between the solvent and the polymer, which is more exaggerated at low MW (where the significance of, for example, 1 repeat unit per chain, is greater), resulting in a difference in the hydrodynamic volume (due exclusively to different interactions and not due to molecular architecture). Alternatively, this could be due to the reliance of MW on the validity of the universal calibration, with this potentially being solved through the use of light scattering data for absolute MW determination.

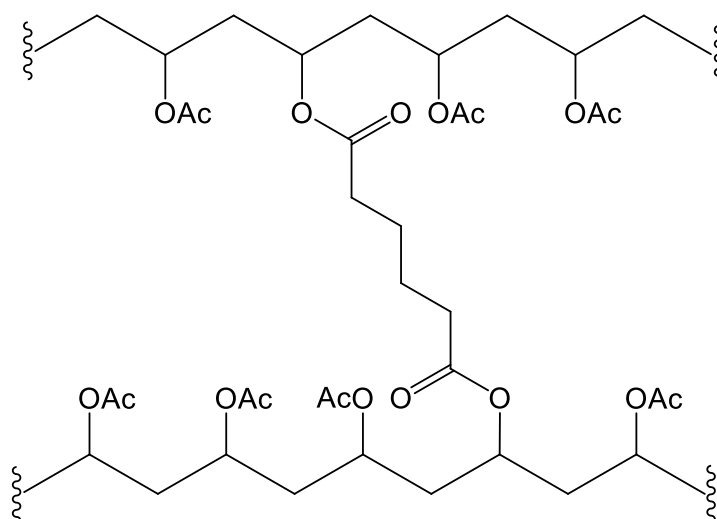
3.2.2 Alternate comonomer proposal.

With the aim of improving this system, and the corresponding copolymerisation, two different multifunctional comonomers were trialled, divinyl adipate (DVA) and 1,4-butanediol divinyl ether (BDDVE), both of which can be seen in Scheme 3.2.2.1.



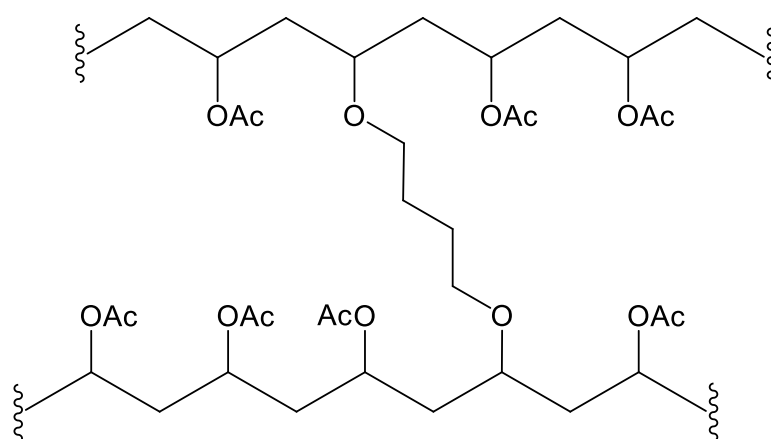
Scheme 3.2.2.1: Chemical structures for divinyl adipate (DVA) and 1,4-butanediol divinyl ether (BDDVE).

DVA is a divinyl ester, possessing the same vinyl functionality as VAc with a short butyl linker. As such this monomer would be expected to copolymerise well with VAc and have little to no influence on the rate of polymerisation. Walling reported that the rate of polymerisation remained virtually unchanged when increasing the concentration of DVA in the copolymerisation.¹⁰⁸ Breitenbach and Gleixner (1976) found reactivity ratios of $r_{\text{VAc}} = 0.99$ and $r_{\text{DVA}} = 0.79$ which would confirm this suggestion, with a slight tendency for favourable cross propagation from a terminal DVA radical, although the copolymer composition with these reactivity ratios is not expected to drift significantly.¹³¹ Taton *et al.* (2008) also proposed equal reactivity of both vinyl groups in the copolymerisation.¹¹⁷ DVA would be expected to cross link according to Scheme 3.2.2.2, with the linkages formed through ester bonds.



Scheme 3.2.2.2: Branched structure of the copolymer of VAc and DVA.

BDDVE, contains two vinyl ether functionalities. Although copolymerisation data with BDDVE could not be found, Mayo *et al.* (1948) demonstrated the copolymerisation of VAc with ethyl vinyl ether (EVE), measuring reactivity ratios of $r_{VAc} = 3.0$, $r_{EVE} = 0$, with the authors suggesting that EVE retards the polymerisation. The reported numbers show a tendency to favour homopropagation of VAc over cross propagation, and a high tendency for cross propagation from a terminal vinyl ether radical, which may lead to some composition drift during polymerisation, resulting in an increase in branch density at higher monomer conversion. The anticipated branching structure is given in Scheme 3.2.2.3, with the branches being formed through ether linkages, which are likely more stable towards hydrolysis/saponification compared to the ester linkages introduced with DVA.



Scheme 3.2.2.3: Branched structure of the copolymer of VAc and BDDVE.

To illustrate the predicted copolymer composition, the copolymer equation was used to produce the plot seen in Figure 3.2.2.1. The equation was derived through the work of Mayo

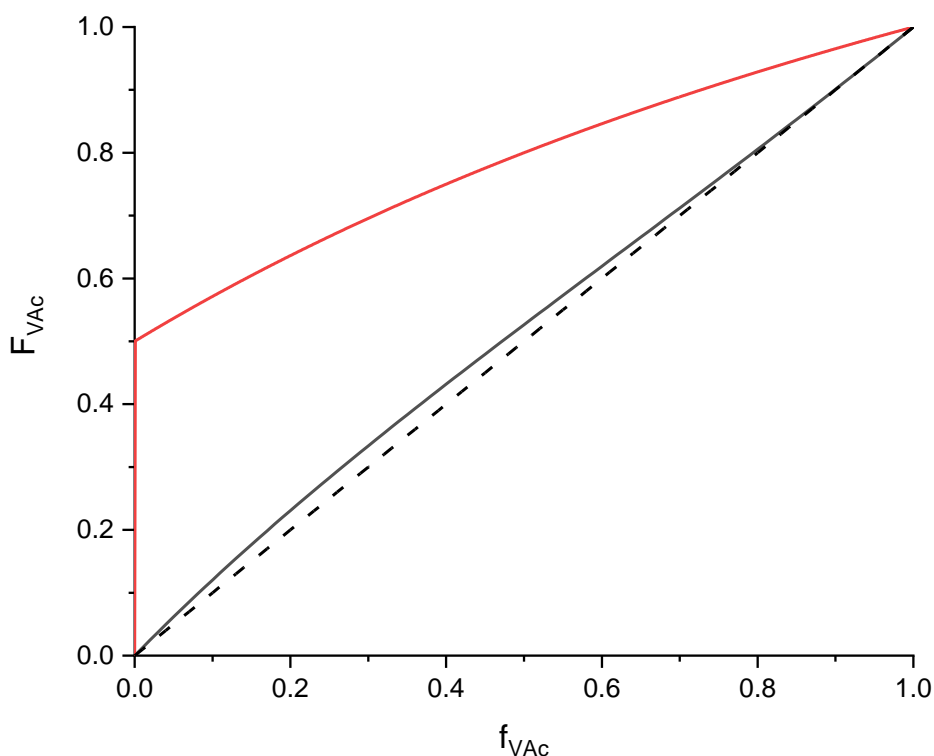


Figure 3.2.2.1: Copolymer composition plot, constructed from Equation 3.2.2.1, where F_{VAc} (fraction of VAc in the polymer) is plotted against f_{VAc} (fraction of VAc in the monomer mixture), where $r_{VAc} = 0.99$ and $r_{DVA} = 0.79$ (—), and where $r_{VAc} = 3.0$ and $r_{EVE} = 0$ (—). The dotted black line shows the ideal case where $r_1 = r_2 = 1$ (---).

and Lewis (the given equation is the modified form expressing concentrations as mole fractions),¹³² as seen in Equation 3.2.2.1. In this equation F_1 and F_2 are the mole fractions of monomer 1 and 2 in the polymer, r_1 and r_2 are the reactivity ratios for monomer 1 and 2, defined as the ratio of the rate coefficients of homopropagation (k_{11} or k_{22})/cross propagation (k_{12} or k_{21}), as seen in Equation 3.2.2.2, and f_1 and f_2 are the mole fractions of monomer 1 and 2 in the feed respectively. In short, the equation shows how much of a monomer will be in the polymer, based on the reactivity ratios and the molar proportions of each monomer in the feed. This is an instantaneous picture, and begins to highlight the potential for composition drift when there is a large discrepancy between the reactivity ratios in a copolymerisation. In the experiments detailed in this chapter, $f_{VAc} > 0.95$ in all cases, however, even at these values, for the case of EVE, it is evident that a higher proportion of VAc is included in the polymer than EVE. As such, with increasing conversion, the parameter f_{VAc} will decrease. This results in an increasing inclusion of comonomer at higher conversions, which in the context of these studies may result in an increase in the branch density, and perhaps the probability of gel formation. This effect is still present for DVA, however, it is clear that the effect is much less pronounced, with a smaller difference in the reactivity ratios observed. It is worth considering

that this drift to higher comonomer inclusion may be cancelled out due to the drift in VAc/CTA, resulting from $C_{tr,s} < 1$, meaning the probability of producing insoluble polymer is still likely to be low.

$$F_1 = 1 - F_2 = \frac{r_1 f_1^2 + f_1 f_2}{r_1 f_1^2 + 2f_1 f_2 + r_2 f_2^2} \quad (3.2.2.1)$$

$$r_1 = \frac{k_{11}}{k_{12}} \quad \text{and} \quad r_2 = \frac{k_{22}}{k_{21}} \quad (3.2.2.2)$$

3.2.3 Divinyl adipate (DVA).

A series of copolymerisation's between VAc and DVA were performed, in the presence of DBDS. The conversion time data can be seen in Figure 3.2.3.1. A significantly lower dependence of the rate of polymerisation on the concentration of comonomer can be seen than that observed for TTT. Here, the rate of polymerisation is seen to slowly decrease with increasing DVA concentration at a fixed DBDS concentration of 1 mol% (discounting any inhibition periods). The rate decreases to 92.52 %, 87.90 % and 83.28 % of that in the absence of DVA for 0.5, 1.0 and 3.0 mol % DVA respectively, as seen in Table 3.2.3.1. This implies that

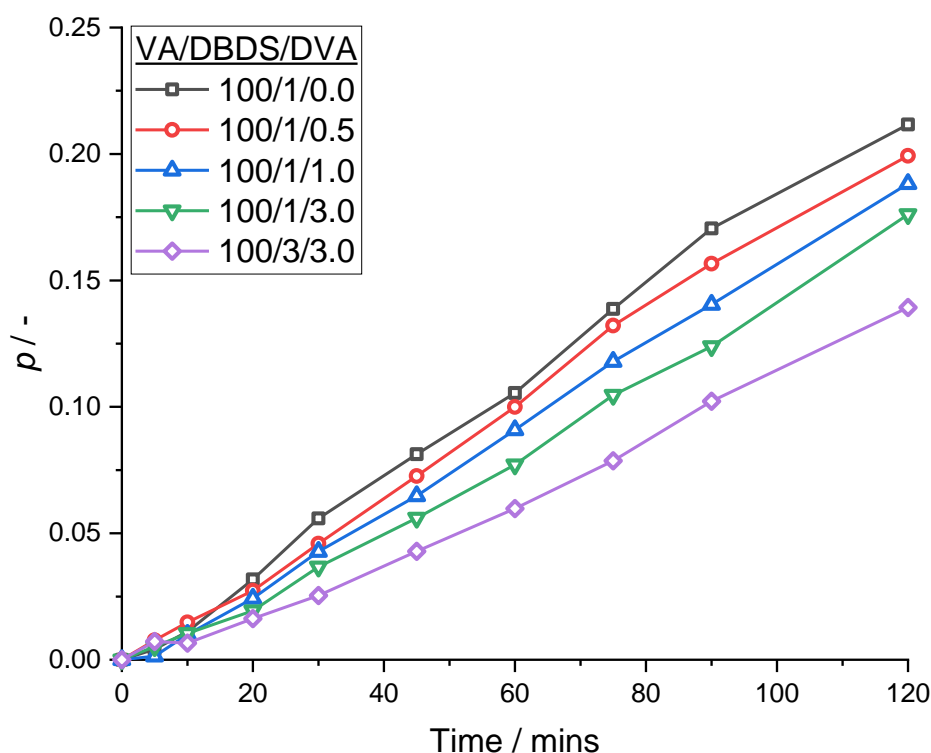


Figure 3.2.3.1: Monomer conversion, p , vs time (mins) for the free radical solution copolymerisation of VAc and DVA in the presence of DBDS. The ratios of VAc/DBDS/DVA are detailed in the figure legend.

Table 3.2.3.1: Rate of polymerisation, R_p for the free radical copolymerisation of VAc and DVA in the presence of DBDS. The Rate % is calculated relative to the experiment performed at VAc/DBDS/DVA = 100/1/0.

VAc/DBDS/DVA	$R_p / \text{M s}^{-1}$	Rate %
100/1/0.0	6.28×10^{-5}	100.00
100/1/0.5	5.81×10^{-5}	92.52
100/1/1.0	5.52×10^{-5}	87.90
100/1/3.0	5.23×10^{-5}	83.28
100/3/3.0	4.18×10^{-5}	66.56

copolymerisation occurs, and as is suggested by the reactivity ratios, cross propagation from a terminal DVA unit is slightly slower than homopropagation, which may explain the reduction in rate given the low concentrations of DVA, reducing the likelihood of homopropagation.

Direct comparison with the data obtained for TTT can be made for the experiments employing 0.5 and 1.0 mol% comonomer, where the rates of polymerisation are 5.81×10^{-5} and 5.52×10^{-5} M s^{-1} for DVA and 2.67×10^{-5} and 2.49×10^{-5} M s^{-1} for TTT respectively. Increasing DBDS to 3 mol% at 3 mol% DVA does result in a decrease in the rate of polymerisation, however, this behaviour is expected due to mild retardation by DBDS discussed in Chapter 2.

Following the same procedures as those discussed for TTT, SEC data gathered on the polymers was analysed. The MWDs, and Mark-Houwink plots can be seen in Figure 3.2.3.2. The parameters extracted from the MWDs, and the Mark-Houwink parameters can be seen in Table 3.2.3.2. A similar trend is observed as with TTT, wherein an increase in the concentration of DVA results in an increase in MW, although for DVA the dependence of MW

Table 3.2.3.2: Monomer conversion, p , number average and weight average MWs (M_n and M_w respectively) and the Mark-Houwink parameters K and α for the 120 mins samples in the series of copolymerisation's of VAc with DVA in the presence of DBDS.

VAc/DBDS/DVA	p	M_n / gmol^{-1}	M_w / gmol^{-1}	$K \times 10^5$	α
100/1/0.0	0.21	36,100	58,200	7.635	0.724
100/1/0.5	0.20	40,200	72,900	11.455	0.679
100/1/1.0	0.19	44,100	86,500	15.389	0.644
100/1/3.0	0.18	54,700	191,700	48.978	0.520
100/3/3.0	0.14	24,700	46,900	21.135	0.598

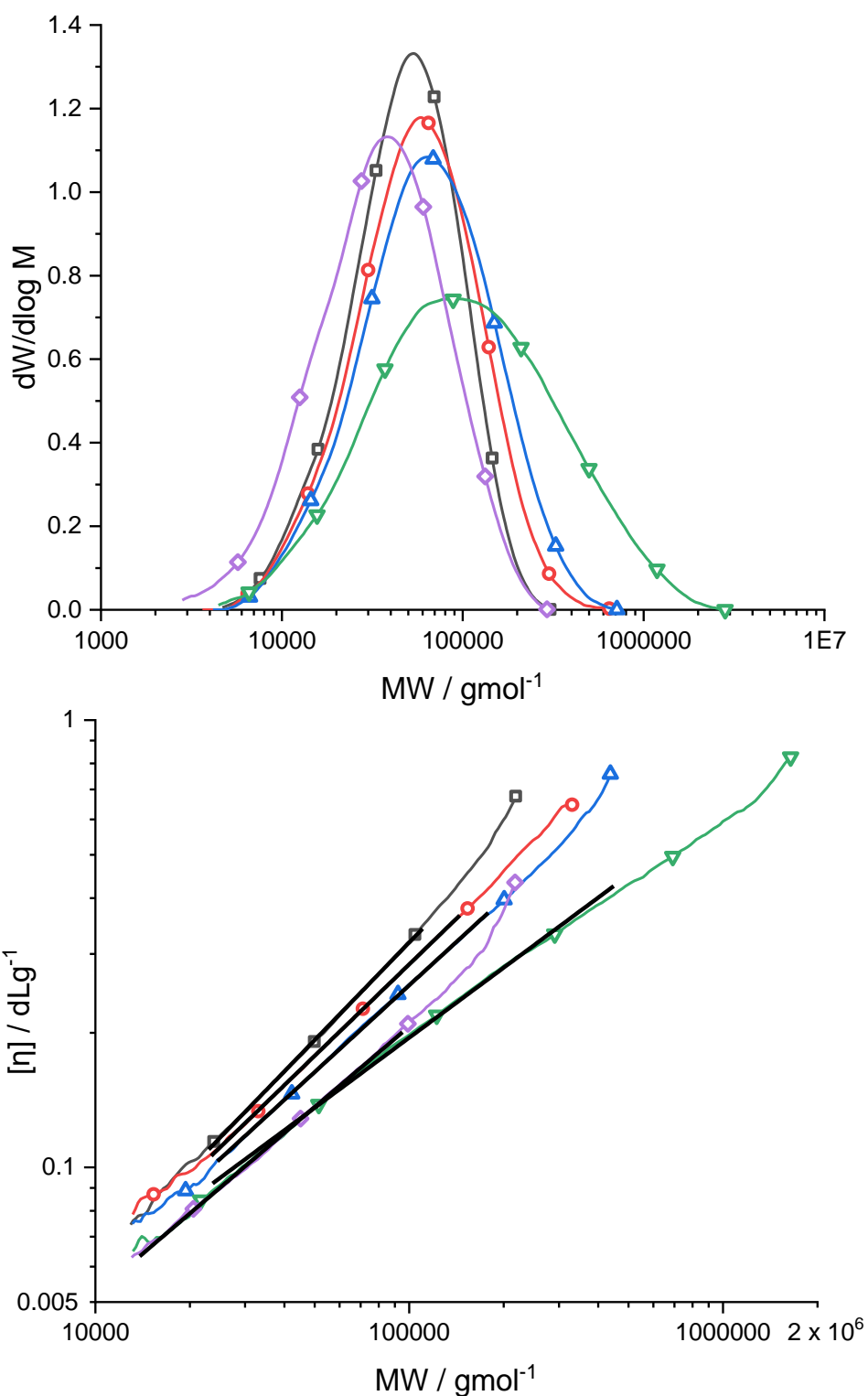


Figure 3.2.3.2: $dW/d\log M$ vs MW (g mol^{-1}) MW distributions (top) and the Mark-Houwink plots of intrinsic viscosity, $[\eta]$ (dL g^{-1}), vs MW (g mol^{-1}) (bottom) for the 120 mins samples taken during the free radical solution copolymerisation of vinyl acetate with DVA in the presence of DBDS. Mole ratio VAc/DBDS/DVA = 100/1/0 (\blacksquare), 100/1/0.5 ($\color{red}\circ$), 100/1/1.0 ($\color{blue}\blacktriangle$), 100/1/3.0 ($\color{green}\blacktriangledown$) and 100/3/3.0 ($\color{purple}\blacklozenge$).

on comonomer concentration appears to be less significant. A minimal effect is seen on M_n

until 3 mol% DVA wrt VAc is used, however M_w is seen to increase steadily with increasing DVA. Comparison between 1 and 3 mol% DVA shows a huge jump in M_w from 86,500 to 191,700 g mol^{-1} , as well as a jump in M_n from 44,100 to 54,700 g mol^{-1} . It is also noted that the distribution is visibly wider in the case of 3 mol% DVA, which may signify an increase in the dispersity of the polymers, which may be expected when higher MW polymers are synthesised, due to branching becoming more significant. Assuming equal reactivities of DVA and VAc, the increase from 1 to 3 mol% DVA sees the number of DVA groups jump from 1 in 100 units to around 1 in 33 units, justifying the dramatic increase in MW.

Direct comparison between the polymers produced at 0.5 and 1 mol% comonomer wrt VAc for TTT and DVA show some interesting differences. In both cases, M_n and M_w are slightly higher for copolymerisation with TTT, and the values for α are slightly lower. For example, for 1.0 mol% DVA, M_n and M_w are 44,100 g mol^{-1} and 86,500 g mol^{-1} respectively, with $\alpha = 0.644$, however, for 1.0 mol% TTT M_n and M_w are 56,600 g mol^{-1} and 108,200 g mol^{-1} respectively, with $\alpha = 0.559$. This is likely simply due to the fact that TTT has three vinyl groups at which polymerisation can occur, whereas DVA only has two. This in theory would result in more branches introduced per unit of comonomer copolymerised, which results in a higher MW. Additionally, the increase in the number of branches increases the molecular density and is reflected through a decrease in α . This is more evidence to suggest that copolymerisation with pendant vinyl groups occurs even at low monomer conversion, sufficient to provide a measurable increase in branching. For VAc/DBDS/DVA = 100/1/1.0, the reaction was allowed to proceed for 24 h, after which time the VAc conversion had reached $p = 0.57$. The MWDs were measured at various degrees of conversion in the first 2 h and compared to that after 24 h. MWDs and Mark-Houwink plots as a function of conversion can be seen in Figure 3.2.3.3, and the corresponding parameters are seen in Table 3.2.3.3.

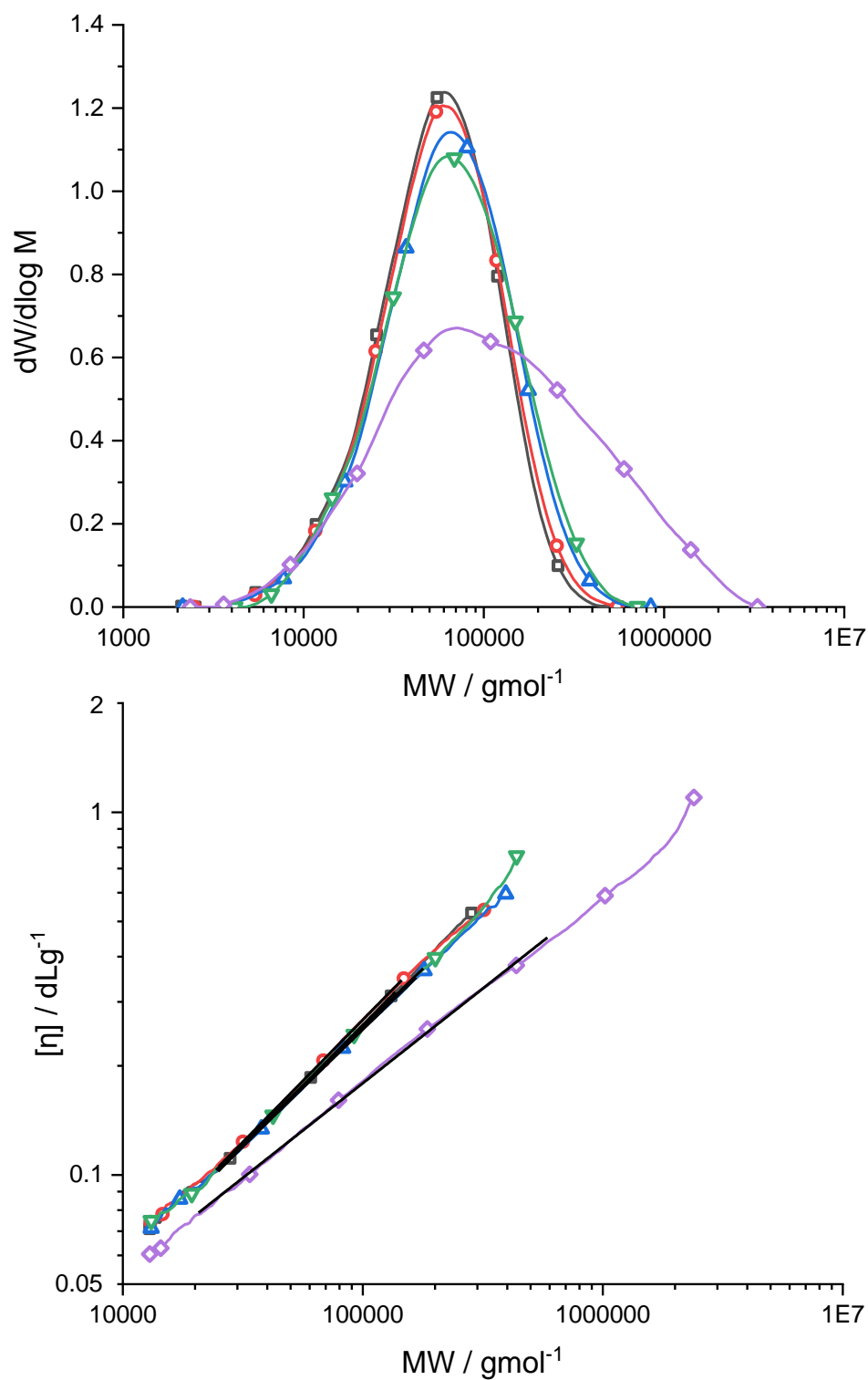


Figure 3.2.3.3: $dW/d\log M$ vs MW (g mol^{-1}) MW distributions (top) and the Mark-Houwink plots of intrinsic viscosity, $[\eta]$ (dL g^{-1}), vs MW (g mol^{-1}) (bottom) for samples taken during the free radical solution copolymerisation of vinyl acetate and DVA in the presence of DBDS. Mol ratio VAc/DBDS/DVA = 100/1/1. Data is shown for monomer conversions of 0.02 (\square), 0.06 (\circ), 0.12 (\triangle), 0.18 (∇) and 0.57 (\diamond). The solid black lines in the Mark-Houwink plots show the fitted regions from which α and K were extracted.

Table 3.2.3.3: Monomer conversion, p , and the corresponding MW distribution parameters M_n and M_w being the number average MW and the weight average MW, and the Mark-Houwink parameters K and α for samples withdrawn from the copolymerisation where VAc/DBDS/DVA = 100/1/1.0.

Time/mins	p	M_n / gmol ⁻¹	M_w / gmol ⁻¹	$K \times 10^5$	α
20	0.02	38,800	69,200	11.593	0.670
45	0.06	39,900	73,200	11.425	0.674
75	0.12	40,000	76,300	15.070	0.645
120	0.18	44,100	86,500	15.389	0.644
1440	0.57	51,400	240,500	43.914	0.522

It becomes apparent that the distribution formed is very dependent on the degree of monomer conversion, particularly at high conversion. The values for M_n , M_w and α show a very weak dependence on p in the first 120 mins, with a very slow drift to higher MW and slight decreases in α . This supports the original hypothesis that any composition drift would be insignificant given how close the reactivity ratios are to unity. However, the sample analysed at $p = 0.57$ shows a dramatic increase in M_w and reduction in α compared to the sample at $p = 0.18$. As the polymer concentration increases, and monomer concentration decreases, the likelihood of reactions with polymer increases. This will occur through addition to pendant vinyl groups, but also through transfer to polymer (particularly due to the prevalence for acetate proton extraction). To assess the significance of transfer to polymer on the MWD at moderate conversion, the reaction in the absence of comonomer was analysed as a function of conversion (VAc/DBDS/DVA = 100/1/0.0). Clearly, addition to pendant vinyl groups could not occur in this case, and therefore any dramatic jump in MW could be attributed to transfer.

The MW parameters are summarised in Table 3.2.3.4, and the MWD and Mark-Houwink plots as a function of monomer conversion can be seen in Figure 3.2.3.4. The MWD is seen to slowly shift to lower MW, which can be ascribed to the fact that $C_{tr,S} < 1$ for transfer to DBDS. No notable broadening in the MWD or change in intrinsic viscosity as a function of MW is observed, and indeed α remains essentially unchanged even at $p = 0.66$. This observation suggests that the contributions of transfer to polymer to the MWD at intermediate conversion

Table 3.2.3.4: Monomer conversion, p , and the corresponding MW distribution parameters M_n and M_w being the number average MW and the weight average MW, as well as the Mark-Houwink parameters K and α for the samples from the homopolymerisation of VAc with 1 mol% DBDS.

Time/mins	p	M_n /gmol ⁻¹	M_w /gmol ⁻¹	$K \times 10^5$	α
45	0.08	38,500	62,100	7.458	0.724
75	0.14	38,100	62,400	8.111	0.718
120	0.21	36,100	58,200	7.635	0.724
1440	0.66	28,700	48,400	7.898	0.721

values, such as those observed here after 24 h reaction time, is minimal, and instead the increase in $[\text{DBDS}]/[\text{M}]$ plays a much more significant role on the control of the MW produced. This supports the hypothesis that the increase in MW observed in the higher conversion sample in the copolymerisation with DVA is as a result of the consumption of pendant vinyl groups.

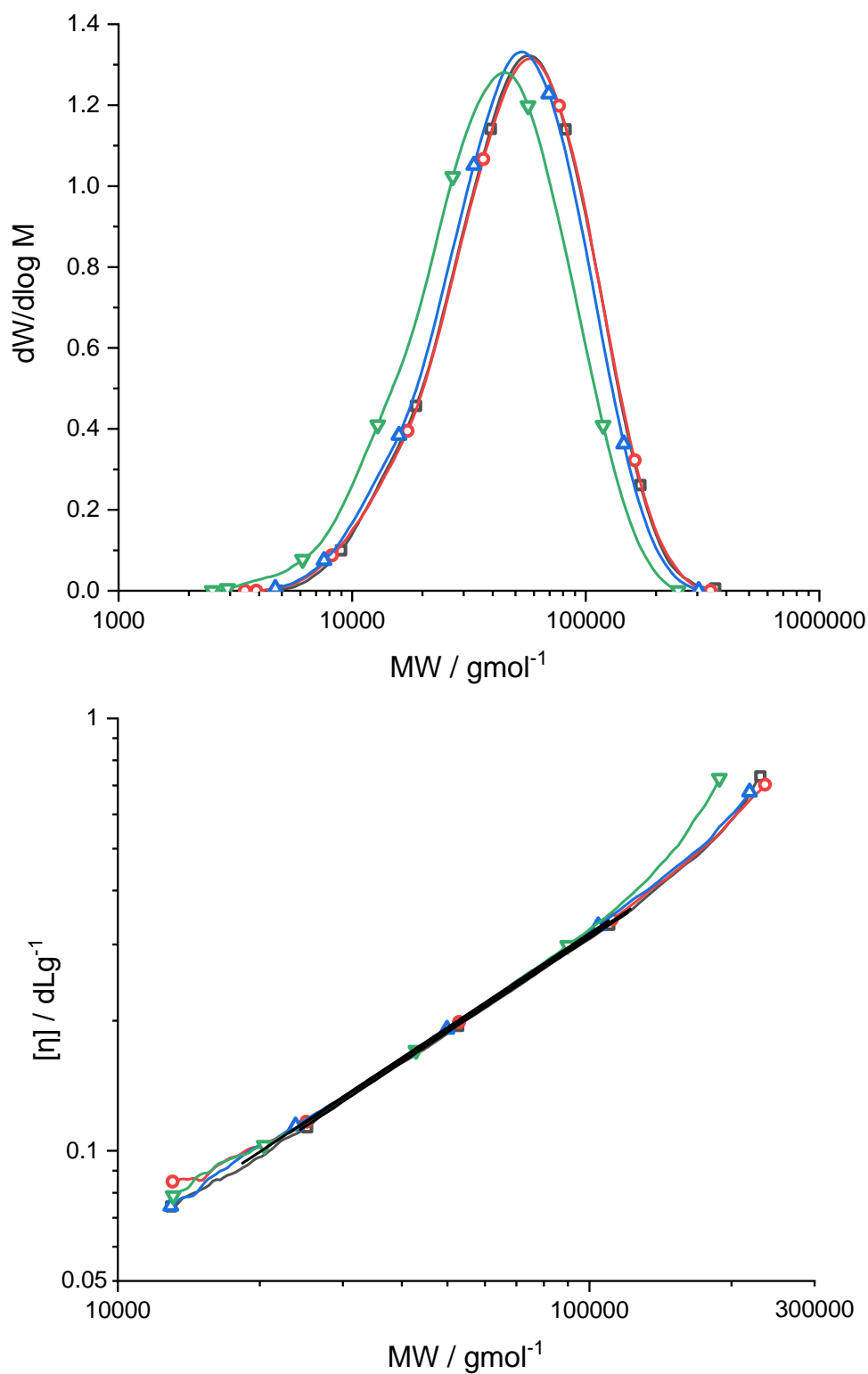


Figure 3.2.3.4: $dW/d\log M$ vs MW (g mol^{-1}) MW distributions (top) and the Mark-Houwink plots of intrinsic viscosity, $[\eta]$ (dL g^{-1}), vs MW (g mol^{-1}) (bottom) for samples taken during the free radical solution polymerisation of vinyl acetate in the presence of 1 mol% DBDS. Data is shown for monomer conversions of 0.08 (\square), 0.14 (\circ), 0.22 (\triangle) and 0.66 (∇). The solid black lines show the fitted regions from which α and K were extracted.

3.2.4 1,4-Butanediol divinyl ether (BDDVE).

BDDVE was also trialled as an MVM in the copolymerisation with VAc. The conversion evolution can be seen in Figure 3.2.4.1, with the rate data displayed in Table 3.2.4.1. The influence of copolymerisation on the rate of polymerisation appears to be more significant than that observed in the case of DVA, most evident where VAc/DBDS/BDDVE = 100/1/3.0 and 100/3/3.0. The acceleration of the rate between 60 and 90 mins was unexpected, as one may argue this could be due to drift in monomer concentrations, although the differences in reactivity ratios seen here will not cause this behaviour. Additionally, the rate after 90 mins returns back to that comparable before 60 mins, suggesting this is simply an error in measurement or local temperature increase in these reactions. The rates for these two experiments were calculated over the first 20 minutes of polymerisation. Additionally, where VAc/DBDS/BDDVE = 100/1/1.0, the rate in the first 20 mins appears to be much faster than that observed over the subsequent 100 mins, and as such, the rate was calculated from 20-120 mins. Taking the rate in the 100/1/1.0 reaction as an example, it becomes clear that the decrease in rate for BDDVE ($4.34 \times 10^{-5} \text{ M s}^{-1}$) is an intermediate between that observed for

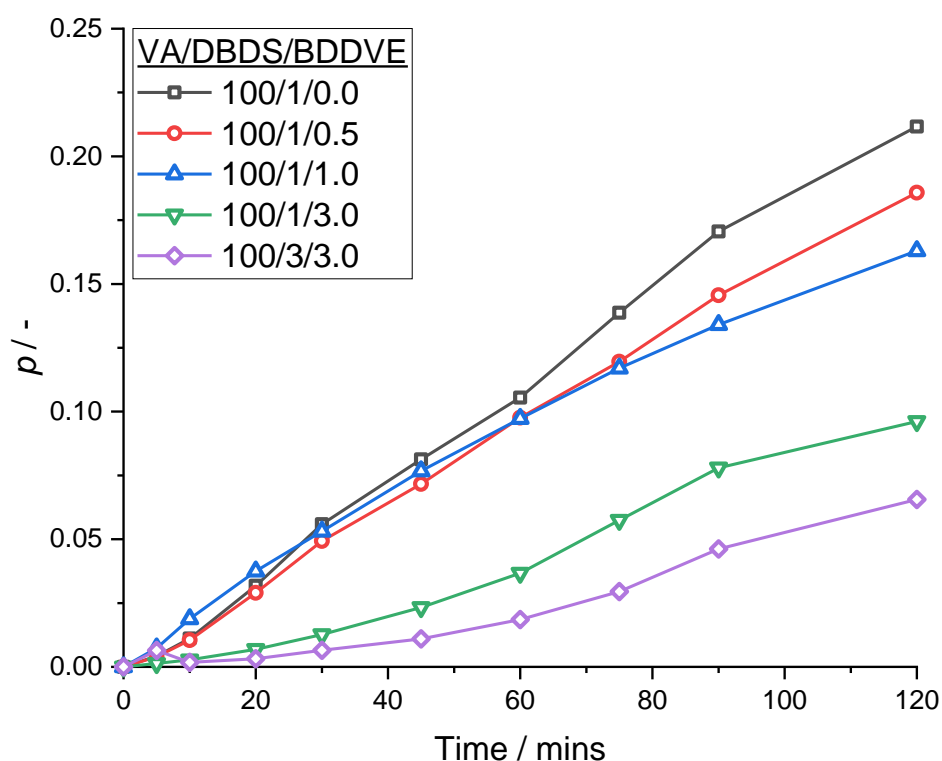


Figure 3.2.4.1: Monomer conversion, p , vs time (mins) for the free radical solution copolymerisation of vinyl acetate and BDDVE in the presence of DBDS. The ratios of VAc/DBDS/BDDVE are detailed in the figure legend.

Table 3.2.4.1: Rate of polymerisation, R_p for the free radical copolymerisation of VAc and BDDVE in the presence of DBDS. The Rate % is calculated relative to the experiment performed at VAc/DBDS/DVA = 100/1/0. (^a - Rate calculated between 20-120 mins, ^b - Rate calculated between 0-20 mins).

VAc/DBDS/BDDVE	R_p /Ms ⁻¹	Rate %
100/1/0.0	6.28×10^{-5}	100.00
100/1/0.5	5.06×10^{-5}	80.57
100/1/1.0 ^a	4.34×10^{-5}	69.11
100/1/3.0 ^b	1.15×10^{-5}	18.31
100/3/3.0 ^b	5.29×10^{-6}	8.42

TTT (2.49×10^{-5} M s⁻¹) and DVA (5.52×10^{-5} M s⁻¹). This suggests faster propagation from a terminal BDDVE radical with VAc than from a terminal TTT radical, with DVA being fastest as expected.

The MWDs for the samples withdrawn after 120 mins can be seen in Figure 3.2.4.2, along with the Mark-Houwink plots. It becomes clear that the MWD is much less dependent on the concentration of comonomer, when compared to the equivalent data from TTT and DVA. As seen in Table 3.2.4.2, M_n and M_w remain virtually unchanged after the addition of 1 mol% BDDVE, where the other comonomers show more significant increases. When 3 mol% BDDVE is employed, M_n still remains virtually unchanged, however, M_w jumps from 58,200 to 88,600, suggesting an increase in branching. This observation is echoed by a less significant drop in α up to 1 mol% comonomer. In fact, with BDDVE, α only changes from 0.724 to 0.695, where DVA and TTT drop to 0.644 and 0.559 respectively. At 3 mol% a larger drop in α is observed

Table 3.2.4.2: Monomer conversion, p , number average and weight average MWs (M_n and M_w respectively) and the Mark-Houwink parameters K and α for the 120 mins samples in the series of copolymerisation's of VAc with BDDVE in the presence of DBDS.

VAc/DBDS/BDDVE	p	M_n /gmol ⁻¹	M_w /gmol ⁻¹	$K \times 10^5$	α
100/1/0.0	0.21	36,100	58,200	7.635	0.724
100/1/0.5	0.19	33,500	56,400	10.228	0.704
100/1/1.0	0.16	37,100	61,200	9.842	0.695
100/1/3.0	0.10	35,300	88,600	17.770	0.626
100/3/3.0	0.07	16,600	31,500	13.029	0.650

to 0.626, although this is still considerably higher than the value of 0.520 observed for DVA at the same concentration.

As with DVA, increasing the loading of DBDS to 3 mol% at 3 mol% BDDVE results in a dramatic reduction in M_n and M_w , and α increases to 0.650, indicative of an increase in chain transfer reactions, shortening the length of branches. Both M_n and M_w are lower than that seen for DVA at the same loading, and α is higher, supporting the hypothesis that the initial copolymerisation of the MVM, or copolymerisation of pendant vinyl groups in the DVA reactions is more favourable than for BDDVE.

As with DVA, the reaction where VAc/DBDS/BDDVE = 100/1/1.0 was allowed to proceed for 24 h, and the MW data was compared against samples formed before 2 h reaction time. For BDDVE, the 24 h sample correlated to a monomer conversion of $p = 0.55$. The data can be seen in Figure 3.2.4.3 and is summarised in Table 3.2.4.3. Unlike DVA very little change was observed in either the MWD or the Mark-Houwink-Sakurada relation between MW and $[\eta]$. As conversion increases, the general trend up to 120 mins is a slight increase in MW and a corresponding marginal decrease in α . After 24 h, MW decreases slightly overall, and additionally a decrease in α is observed. This is an interesting observation and shows strikingly different behaviour to the DVA copolymerisation. Given the predicted lower reactivity of the BDDVE, it may be expected that the pendant vinyl groups will also be less reactive than those for DVA. This may result in the degree of branching not being fully realised until much higher conversion than obtained here. It was initially expected that BDDVE would be significantly more sensitive to conversion, given the prediction from the reactivity ratios that the copolymer composition would drift to include increasing amounts of the comonomer at higher conversion. However, if the introduced pendant vinyl groups remain mostly unreacted, the observed influence of monomer conversion on the MW parameters is justified up to the conversion measured here.

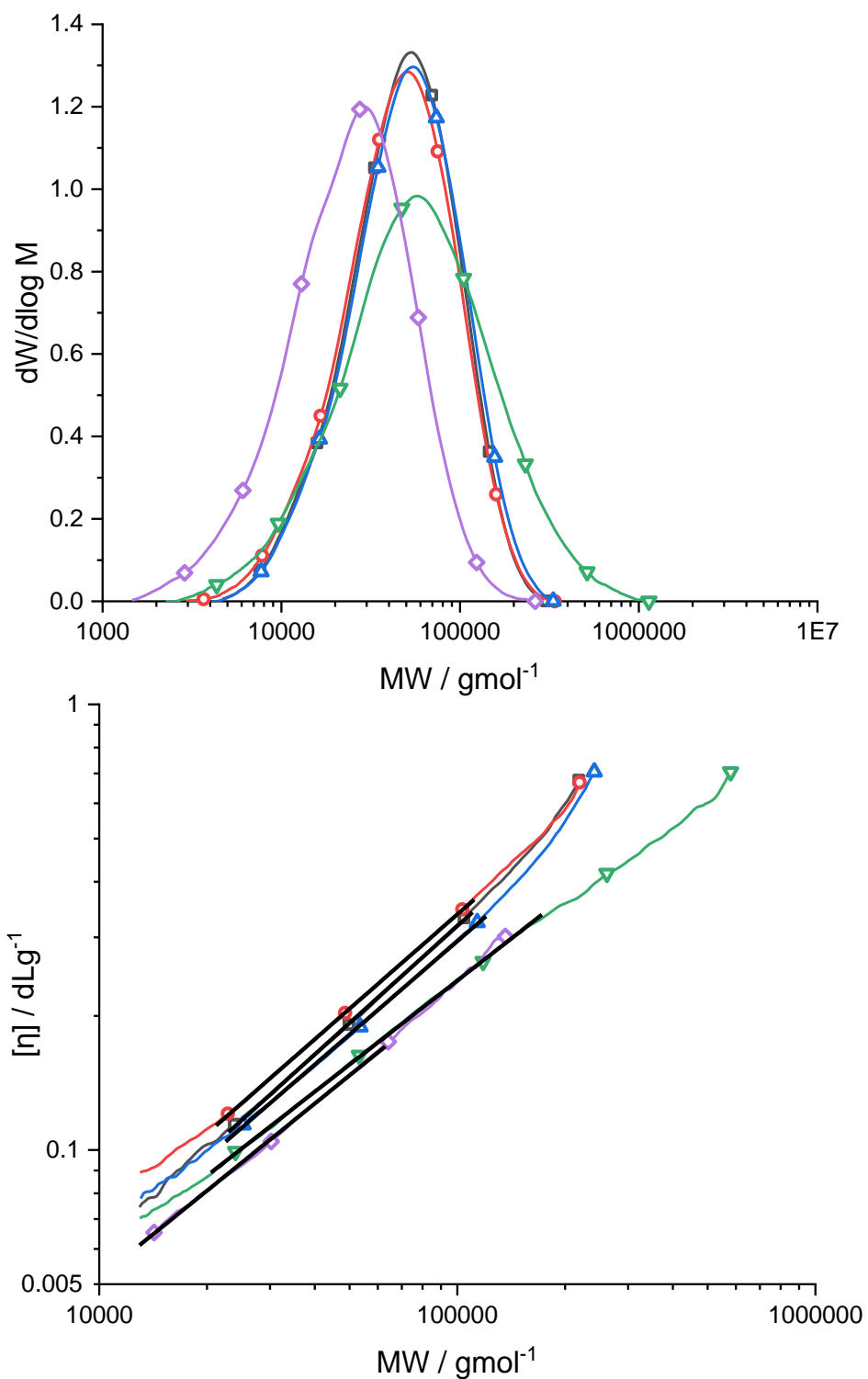


Figure 3.2.4.2: $dW/d\log M$ vs MW (g mol^{-1}) MW distributions (top) and the Mark-Houwink plots of intrinsic viscosity, $[\eta]$ (dL g^{-1}), vs MW (g mol^{-1}) (bottom) for the 120 mins samples taken during the free radical solution copolymerisation of vinyl acetate with BDDVE in the presence of DBDS. Mole ratio VAc/DBDS/DVA = 100/1/0 (\blacksquare), 100/1/0.5 (\bullet), 100/1/1.0 (\blacktriangle), 100/1/3.0 (\blacktriangledown) and 100/3/3.0 (\blacklozenge).

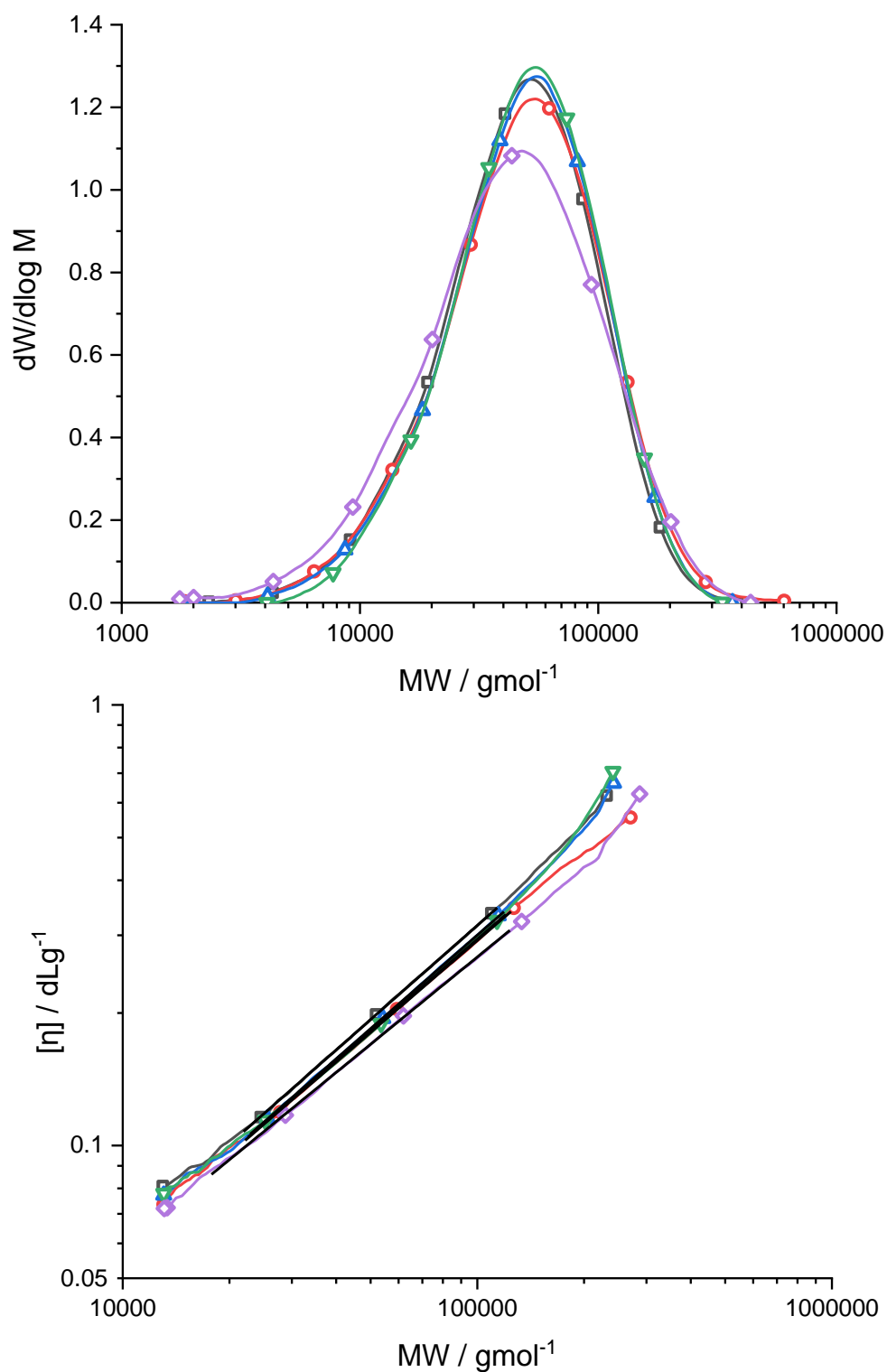


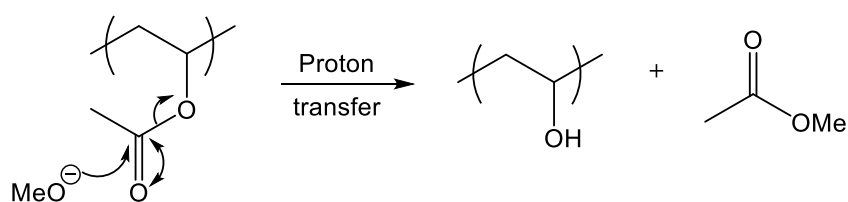
Figure 3.2.4.3: $dW/d\log M$ vs MW (g mol^{-1}) MW distributions (top) and the Mark-Houwink plots of intrinsic viscosity, $[\eta]$ (dL g^{-1}), vs MW (g mol^{-1}) (bottom) for samples taken during the free radical solution copolymerisation of vinyl acetate and BDDVE in the presence of DBDS. Mol ratio VAc/DBDS/BDDVE = 100/1/1. Data is shown for monomer conversions of 0.04 (\square), 0.08 (\circ), 0.12 (\triangle), 0.16 (∇) and 0.55 (\diamond). The solid black lines in the Mark-Houwink plots show the fitted regions from which α and K were extracted.

Table 3.2.4.3: Monomer conversion, p , and the corresponding MW distribution parameters M_n and M_w being the number average MW and the weight average MW, and the Mark-Houwink parameters K and α for samples withdrawn from the copolymerisation where VAc/DBDS/BDDVE = 100/1/1.0.

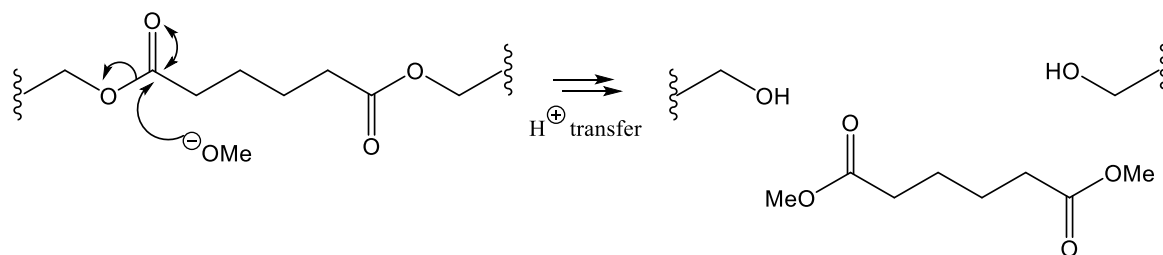
Time/mins	p	M_n /gmol ⁻¹	M_w /gmol ⁻¹	$K \times 10^5$	α
20	0.04	33,100	58,100	8.906	0.710
45	0.08	34,300	63,600	10.044	0.693
75	0.12	35,000	60,600	8.945	0.705
120	0.16	37,100	61,200	9.842	0.695
1440	0.55	28,500	59,100	13.725	0.658

3.2.5 Saponification and reacetylation of branched PVAc.

The saponification of the branched PVAc to PVOH was an interesting avenue to explore, given the widespread applications of poly(vinyl alcohol). Subjecting the produced PVAc's to alkaline saponification would result in conversion of the acetate side groups to the alcohol analogues, as shown in Scheme 3.2.5.1, whilst simultaneously cleaving any branches formed through labile linking groups, such as the ester linkages formed through transfer to monomer or polymer. This same saponification was expected to break the ester linkages introduced through copolymerisation with DVA, as per Scheme 3.2.5.2, however, the vinyl ether linkages of BDDVE were expected to be more resistant. Subsequent reacetylation regenerates PVAc, which would allow solvation in organic solvents, facilitating trivial analysis through SEC and NMR, and direct comparison to the original products before hydrolysis. In the case of copolymerisation with DVA, given that the branches are expected to break, the resulting MWDs may reveal more information on the distribution of branches. In the cases of copolymerisation with BDDVE, cleavage of the ether linkages is not expected unless under catalysis by strong acids (sufficient to protonate the ether). This should therefore be a viable alternative to TTT if branched PVOH is the desired product.



Scheme 3.2.5.1: Mechanism for the alkaline saponification of PVAc in methanol.



Scheme 3.2.5.2: Proposed mechanism for the saponification of the linkages of DVA. This reaction is likely to occur in both polymer and monomer.

The final samples of the copolymerisation's were evaporated to remove excess monomer and solvent. The polymer was then dissolved in the minimum amount of acetone, and precipitated into a large excess of *n*-pentane cooled in an acetone/dry ice bath. This purification step was expected to remove any unreacted DBDS/comonomer, although some resonances of both DBDS and comonomer were still detected, as will be discussed below. After extensive drying, NMR spectra of the polymers were analysed to offer some comparison before and after the process. The samples chosen for these experiments were the 24 h samples of the blank experiment (VAc/DBDS/comonomer = 100/1/0), and the reactions containing 1 mol% of DVA or BDDVE wrt to VAc (VAc/DBDS/comonomer = 100/1/1). The NMR's of the polymers before hydrolysis can be seen in Figure 3.2.5.1.

The broad singlet at 4.78 ppm can be assigned to the backbone CH, the peak at 1.97 ppm is from the side group C(O)CH₃, and the broad peak between 1.85-1.65 ppm is the backbone CH₂ shift for PVAc. The sharp singlets at 3.31 and 2.50 ppm are water and DMSO solvent peaks, with the DMSO peak having spinning side bands at 2.33 ppm and 2.67 ppm. The small quartet at 4.04 ppm and the triplet at 1.17 ppm are the CH₂ and CH₃ shifts of residual ethyl acetate, with the C(O)CH₃ protons expected at 1.99 ppm overlapping with the corresponding proton in the PVAc side group. The peak at 4.04 from ethyl acetate also overlaps with an unknown impurity in the pure DBDS reagent. In the region of 1.87-2.05 ppm there are some additional features in each spectrum, arising from the analogous backbone protons close to, or in, the comonomer units. This added complexity results in the creation of new environments which cannot be resolved. All spectra show a small multiplet at 0.8-0.93 ppm (SCH₂CH₂CH₂CH₃), as well as broad unresolvable peaks in the range 1.02-1.61 ppm (SCH₂CH₂CH₂CH₃), and 2.56-

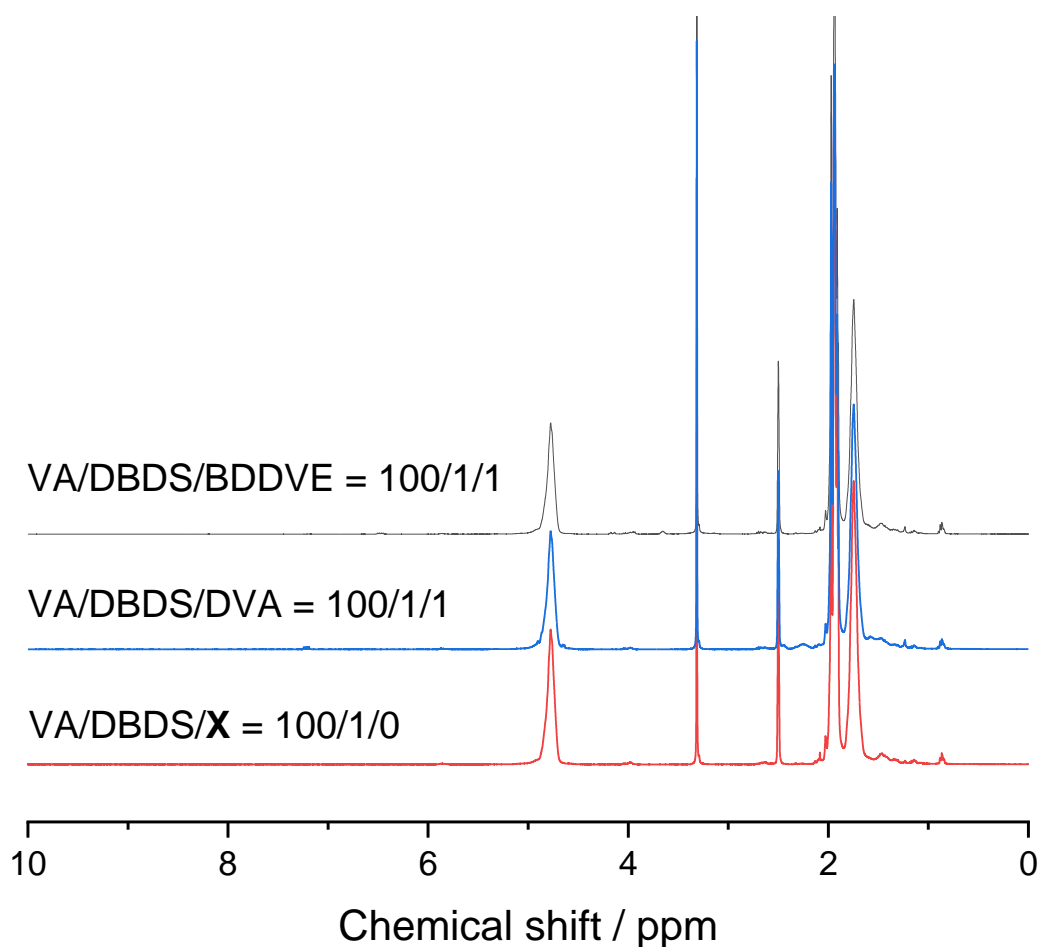


Figure 3.2.5.1: 400 MHz ^1H NMR spectra, recorded in d_6 -DMSO, for the polymers isolated from the reactions in the presence of 1 mol% DBDS wrt VAc, with no comonomer (bottom), 1 mol% DVA (middle) and 1 mol% BDDVE (top).

2.73 ppm ($\text{SCH}_2\text{CH}_2\text{CH}_2\text{CH}_3$) which are the disulfide aliphatic shifts. It should be noted that there is overlap between those in the polymer and in unreacted disulfide broadening the resonances. All spectra also show a small peak at 5.85 ppm which is expected to be due to the penultimate backbone CH (with the carbon being bonded to sulfur through chain transfer), with the adjacent CH_2 potentially the cause of some small additional complexity at around 2.10 ppm, although this overlaps with the PVAc $\text{C}(\text{O})\text{CH}_3$. Importantly, the backbone CH peak at 4.78 ppm is well resolved, and is expected to shift upon saponification.

For the BDDVE copolymer, the peaks at 6.48, 4.16 and 3.95 ppm are vinyl groups from unreacted BDDVE monomer, with an additional triplet at ≈ 4 ppm from the OCH_2 of the monomer, with the expected $\text{CH}_2\text{CH}_2\text{CH}_2\text{CH}_2$ shifts at around 1.78 ppm unresolvable due to overlap with the PVAc backbone CH_2 . A relatively broad peak can be observed at 3.65 ppm, which is assigned to the OCH_2 polymer protons from the comonomer, along with a small

broad bump overlapping with the water peak at 3.14 being the backbone CH of the comonomer unit in the polymer.

In the DVA copolymer, the additional peaks at 2.45 and 2.25 ppm are the C(O)CH₂CH₂ side group resonance from the comonomer in the monomer and polymer, respectively. The anticipated C(O)CH₂CH₂ shift from the comonomer at 1.75 ppm cannot be seen (resides under the intense PVAc CH₂ backbone shift), although an increase in intensity at 1.58 ppm could be assigned to the equivalent protons in the polymer, although poorly resolved. The peak at 7.22 ppm is a DVA vinyl resonance, with the other vinyl peaks at \approx 4.90 ppm and 4.64 ppm overlapping with the polymeric backbone CH of PVAc. The introduced backbone CH and CH₂ are expected to overlap with those of VAc, and are irresolvable given the similarity of the environments.

The polymers were then saponified utilising the same reaction conditions described in the literature.^{114,120} As discussed in the experimental section, the polymers were refluxed overnight in a solution of NaOH in methanol, during which time an off white solid precipitated out of solution (PVOH). The polymer was collected through centrifugation and dried at 50 °C under reduced pressure to constant mass. It was noted that after drying all of the polymers showed a dark orange colouration. This was an unexpected observation, with PVOH typically taking a much lighter colour. Given that this colouration was observed for polymers with and without comonomer, the reactivity of the thioether end groups during the saponification reaction was questioned, with the colour suggesting some unsaturation/conjugation. The same saponification protocol was applied to PVAc formed in the absence of disulfide (solution polymerisation in ethyl acetate in the absence of CTA discussed in Chapter 2, [M]/[Solvent] higher than for the copolymerisation's, exact quantities detailed in experimental section of Chapter 2), and the product was a white solid. This was also compared to commercial PVOH (albeit the synthesis route is not known), Mowiol 6-98, which possessed a similar white appearance. Images of each of the described samples can be seen in Figure 3.2.5.2. These PVOH's produced in the absence of disulfide possess a significantly lighter (white) colour. Similar yellow colouration was observed by Taton *et al.* (2008) when using Xanthate CTA's, however, the authors exclusively attributed this to transesterification on the xanthate moieties, and the NMR spectra are cut off above 5.0 ppm, so comparisons cannot be made above this region.¹¹⁷

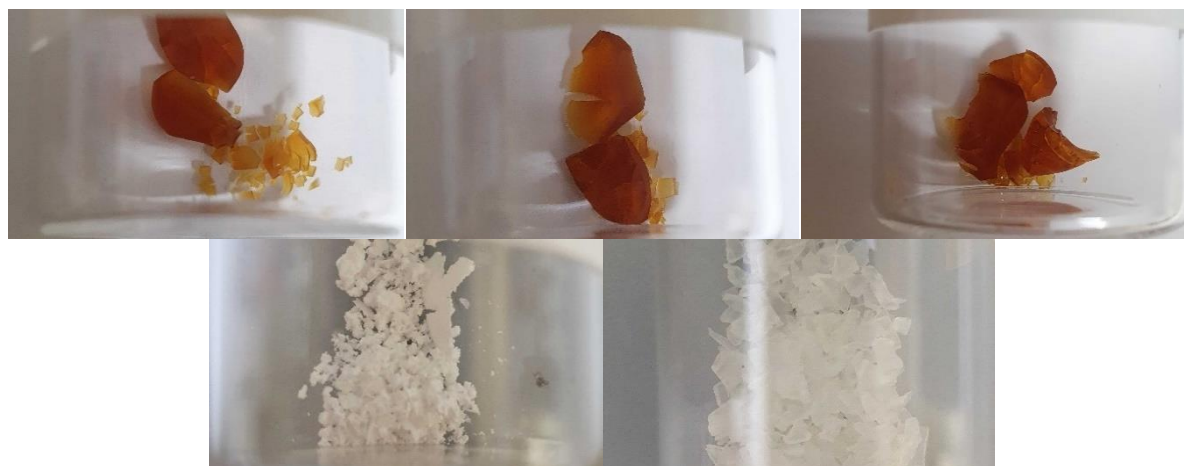


Figure 3.2.5.2: Isolated and dried PVOH. DVA (100/1/1) (top left), No comonomer (100/1/0) (top centre), BDDVE (100/1/1) (top right), No CTA or comonomer (100/0/0) (bottom left) and commercial PVOH (Mowiol 6-98, $M_w = 47,000$) (bottom right).

The saponified polymers were then again analysed through ^1H NMR, and the spectra can be seen in Figure 3.2.5.3. In all cases, disappearance of the singlet at 1.97 ppm (C(O)CH₃ of side group) suggests total removal of the acetate groups from the polymer chains. Additional support for this hypothesis is the shifting of the backbone CH resonance from 4.78 to 3.84 ppm. The backbone CH₂ resonance also shifts from 1.65-1.85 ppm to 1.11-1.70 ppm. The three new peaks which appear at 4.68, 4.51 and 4.26 ppm are the newly formed side group OH protons, with three resonances arising from differences in tacticity.¹³³ The peaks at 4.68, 4.51 and 4.26 correlate to the mm, mr and rr triads, being isotactic, heterotactic and syndiotactic respectively.¹³³ The relative intensities of these triads (mm/mr/rr) are 20.3/49.7/30.0, 21.3/49.1/29.6 and 21.6/49.1/29.3 for BDDVE, DVA and no comonomer respectively, which are essentially equal within the error of NMR, and are in line with those previously reported.^{133,134} The sharp singlets at 3.3 and 2.5 ppm are water and DMSO, and singlets at 4.11 and 3.16 ppm are due to the OH and CH₃ protons of residual methanol respectively.

The BDDVE copolymer has evidence of an additional peak at 6.49 ppm, being a vinyl shift from unreacted monomer, with the other vinyl shifts visible at 4.18 and 3.95 ppm, although these are poorly resolved. A small triplet is visible at 3.66 ppm, attributed to the OCH₂ polymer protons from the comonomer, which is significantly more defined after hydrolysis.

The DVA copolymer has an addition broad triplet at 2.30 ppm, with peaks in this region previously assigned as C(O)CH₂CH₂ side group resonances, with both monomer and polymer signals identified for PVAc previously (2.45 and 2.25 ppm respectively). Only one signal is present in PVOH, and is slightly shifted, suggesting this may be due to the creation of an

alternative environment. Interestingly, a new sharp resonance appears at 3.57 ppm, which may be assigned to the methyl ester protons of dimethyl adipate resulting from DVA saponification. A similar shift may be expected in the other spectra, due to methyl acetate liberation after saponification of the acetate side groups of PVAc, although the compound is significantly more volatile hence the lack of signal.

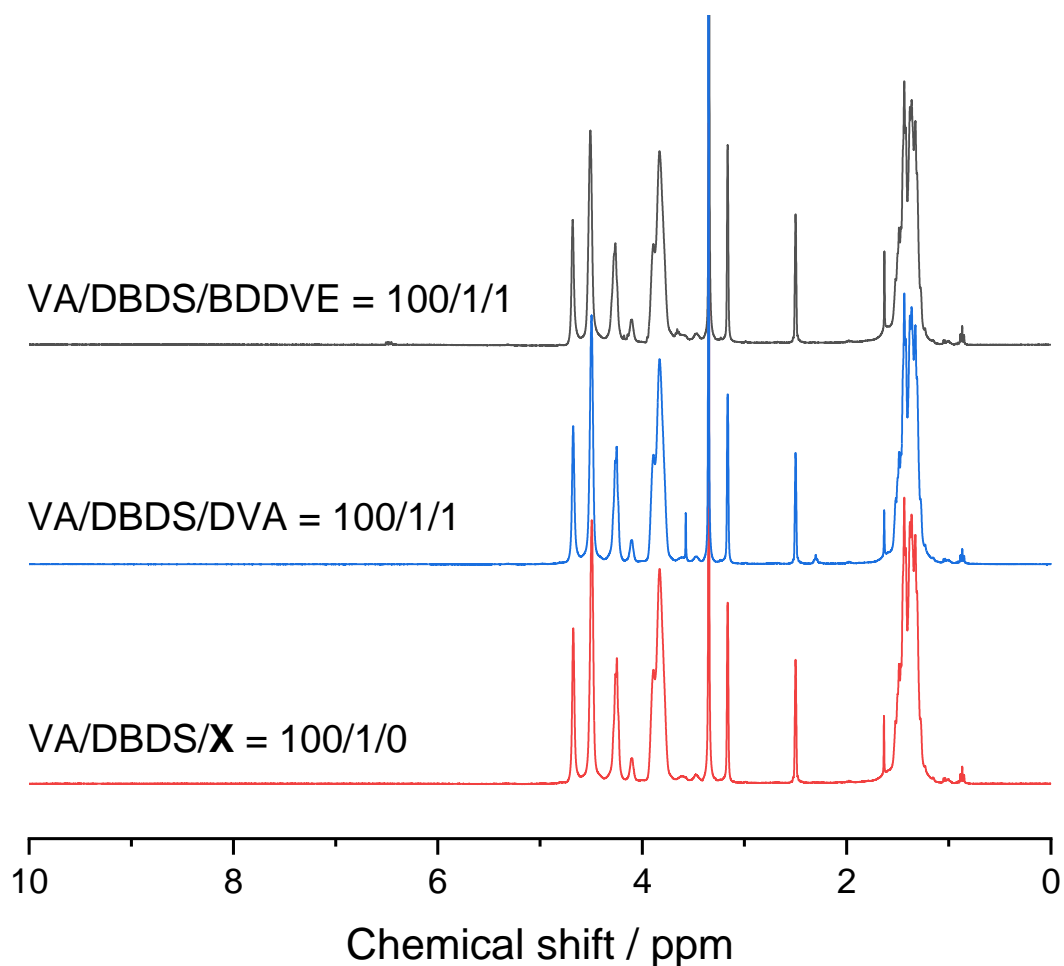


Figure 3.2.5.3: 400 MHz ^1H NMR spectra, recorded in d_6 -DMSO, for the polymers isolated from the reactions in the presence of 1 mol% DBDS wrt VAc, with no comonomer (bottom), 1 mol% DVA (middle) and 1 mol% BDDVE (top).

The sample where VAc/DBDS/X = 100/1/0 was then compared to the sample produced in the absence of DBDS detailed in Chapter 2 and mentioned previously during the colour comparison, i.e. VAc/DBDS/X = 100/0/0. Although the experimental conditions were slightly different (as discussed previously, and detailed in the experimental), the hydrolysis products did not show any colouration in this sample, so the PVOH NMR was a useful comparison. The combined NMR spectra are given in Figure 3.2.5.4.

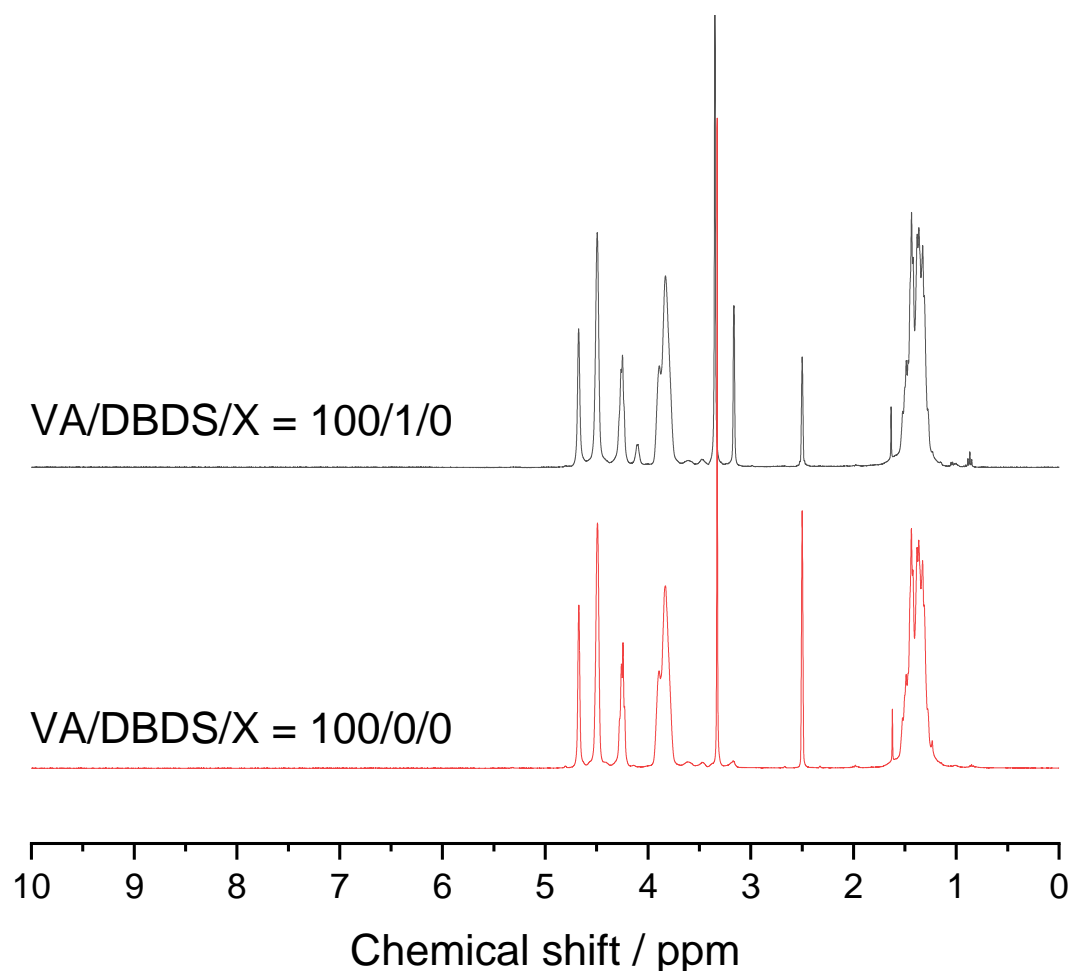


Figure 3.2.5.4: 400 MHz ^1H NMR spectra, recorded in d_6 -DMSO, for the polymers isolated from the hydrolysis of the PVAc formed in the presence of 1 mol% DBDS wrt VAc, with no comonomer (top), and in the absence of both DBDS and comonomer (bottom).

The spectra are strikingly similar, with the only differences being the lack of the disulfide shifts, and significantly lower intensity of the methanol shifts at 3.16 ppm and 4.10 ppm in the absence of DBDS and comonomer. No obvious explanation for the change in colour was provided by these NMR spectra, however, this is not overly surprising given the MW of the polymers. If indeed this transformation occurs due to some modification from the end groups, then the intensity of these newly created environments is likely very low at this MW. As such, an analogous hydrolysis was performed on the low MW VAc homopolymer formed in Chapter 2 in solution ($[\text{DBDS}]/[\text{M}] = 7.65 \times 10^{-2}$, $M_n = 5,500 \text{ gmol}^{-1}$). The corresponding ^1H NMR spectra can be seen in Figure 3.2.5.5. Before saponification, the same main PVAc shifts are observed, as is seen in the case of the higher MW polymers, i.e. shifts of polymeric CH and CH_2 resonances at 4.78 and 1.85-1.65 ppm, as well OCH_3 at 1.98 ppm. Given the significantly higher loading of DBDS, the disulfide signals appear much more intensely here, with a small multiplet at 0.8-0.93 ppm ($\text{SCH}_2\text{CH}_2\text{CH}_2\text{CH}_3$), as well as broad unresolvable peaks in the

range 1.02-1.61 ppm ($\text{SCH}_2\text{CH}_2\text{CH}_2\text{CH}_3$), and 2.56-2.73 ppm ($\text{SCH}_2\text{CH}_2\text{CH}_2\text{CH}_3$) which are the disulfide aliphatic shifts, however, there is significant overlap between the comparable resonances in the polymer (thioether adjacent) and in unreacted disulfide, broadening the resonances. The small complex multiplet in the range 3.92-4.07 is an unidentified contaminant present in the pure DBDS reagent, as well as some residual ethyl acetate, as reported previously. The peak at 5.86 ppm is again attributed to the penultimate backbone **CH** (with the carbon being bonded to sulfur through chain transfer). Again, the shifts at 2.5 ppm and at 3.32 ppm are DMSO and water, respectively.

Saponification leads to the same shifts in the polymeric resonances as discussed previously. The disulfide shifts interestingly essentially disappear during this process, with the most notable and resolvable resonance being that at 2.56-2.73 ppm. The small peak at 0.87 ppm is likely due to residual pentane from the purification of the polymer. Closer inspection of the distribution reveals some subtle complexity, particularly in the region of 7.5 - 4 ppm. Shown in Figure 3.2.5.5, the region between 7.5 and 5 ppm shows the generation of a number of environments with very low intensity, which cannot be seen in the high MW samples. Additionally, the multiplet centred around 5.85 ppm and assigned to the terminal backbone **CH** bound to sulfur, disappears. The shift at which these environments resonate, combined with change in colour, suggested that the saponification process introduced some amount of unsaturation into the backbone.

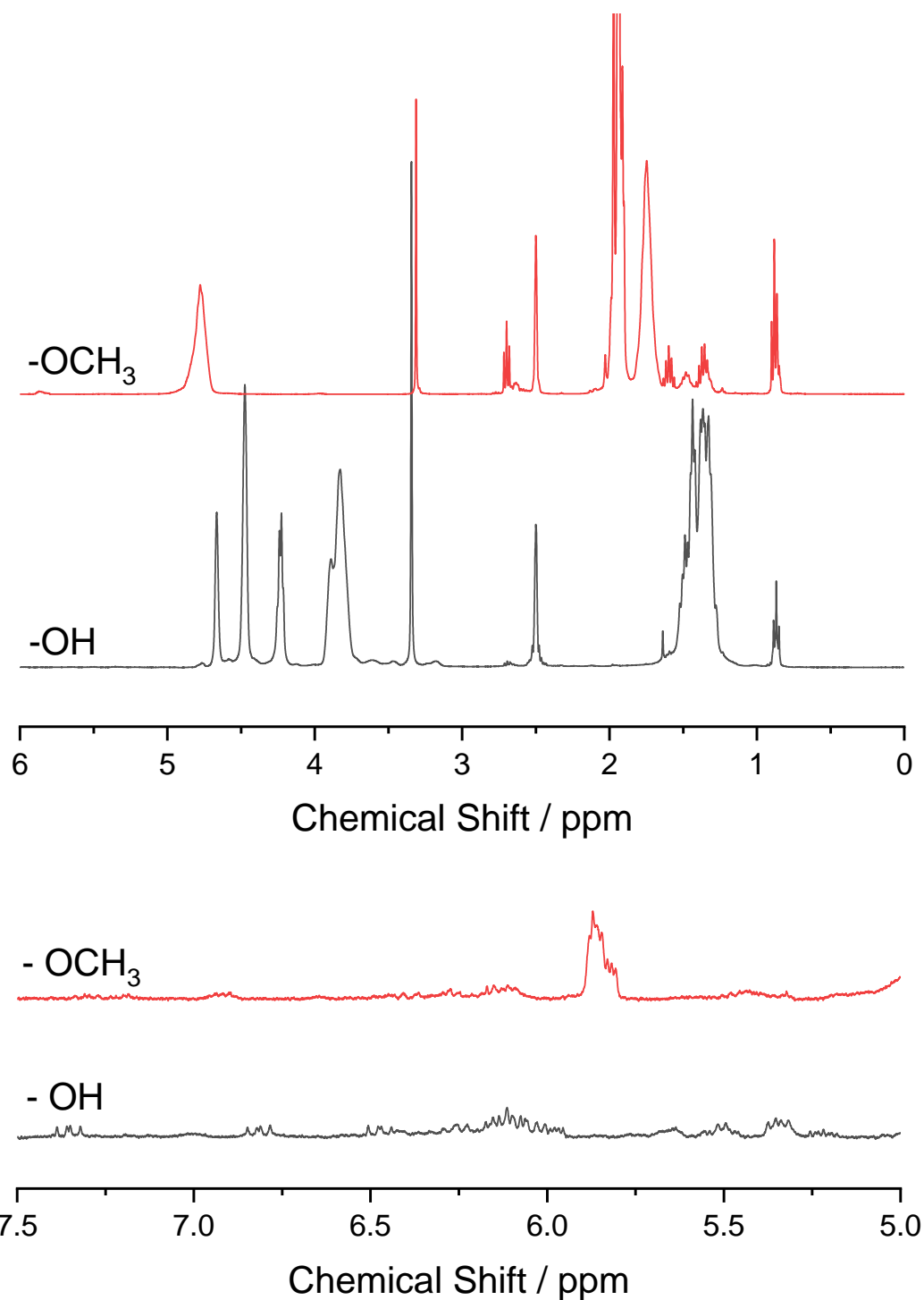


Figure 3.2.5.5: 400 MHz ¹H NMR spectra, recorded in d₆-DMSO, for the PVOH formed through saponification of low MW PVAc (solution polymerisation with [DBDS]/[VAc] = 7.65 × 10⁻²) between 6-0 ppm (top), with the spectra between 7.5 ppm and 5 ppm highlighted (bottom).

The region between 5-4 ppm, shown in Figure 3.2.5.6, also shows an increase in complexity. This region contains the shifts for the OH protons, and nuances are observed around 4.75 and 4.6 ppm, which are not seen in the higher MW samples. The proximity to the OH protons

suggest a small change in environment near some OH protons, and it is suggested to be those in proximity to the proposed unsaturation. An additional caveat could simply be the shifting of the CH proton next to the end group after hydrolysis, although assignment of the specific shift of this proton is not possible.

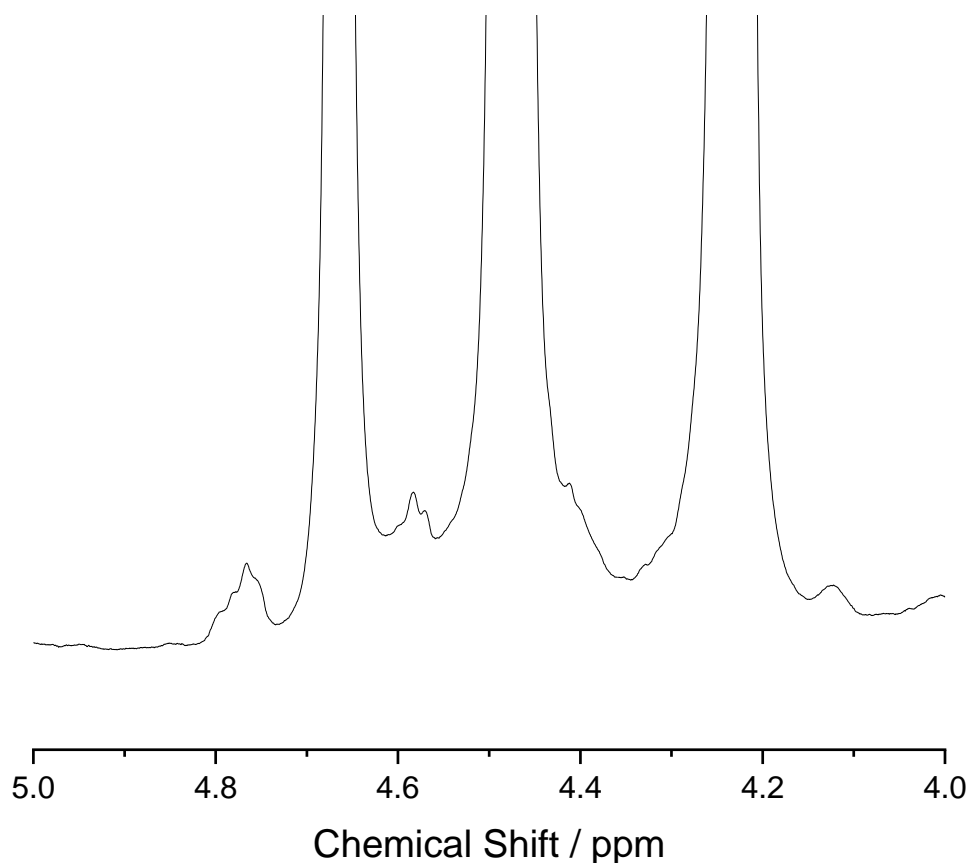


Figure 3.2.5.6: 400 MHz ¹H NMR spectra between 5.0 and 4.0 ppm, recorded in d₆-DMSO, for the PVOH formed through saponification of low MW PVAc (solution polymerisation with [DBDS]/[VAc] = 7.65 × 10⁻²).

This proposal for the unsaturation in the backbone of VAc has been reported by others, under different conditions or with different end groups. It has been demonstrated that during mass spectrometry experiments, fragmentation of PVAc occurs through loss of acetic acid, yielding unsaturated products.^{135,136} Loss of acetic acid is also observed at temperatures in the range of 300-400 °C, again yielding highly unsaturated products.¹³⁷ The difference in this study is the relatively mild conditions (65 °C, catalytic NaOH), which may be facilitated by the end group. Iriuchijima *et al.* (1973) discussed the possibility of aldehyde formation in sulfides wherein the alpha carbon bears a group susceptible to hydrolysis, such as an acetate group.¹³⁸ This terminal aldehyde likely sits in the enol form, introducing one unsaturated bond, and in the

case of PVAc may encourage the elimination of neighbouring acetate groups, introducing conjugation.

Similar unsaturation has been demonstrated when introducing particularly good leaving groups through chain transfer reactions. For example, Matyjasczewski and Iovu observed unsaturation formed through dehydration of penultimate acetate groups during alkyl iodide assisted controlled radical polymerisation of VAc, wherein the leaving group ability of iodide promoted the elimination reaction.¹³⁹ In their work, peaks residing at ≈ 9.58 and 9.53 ppm were assigned to the acidic proton in acetic acid, and an aldehyde proton thought to be at the end of the chain. The authors also demonstrated a small quartet at around 9.48 ppm, which was assigned to the aldehyde proton in acetaldehyde, and a very weak multiplet around 9.41 ppm which was assigned to an aldehyde proton adjacent to an unsaturated C=C bond. Similar assignments may be possible in this region in the spectra recorded for the low MW PVAc, formed in the presence of DBDS. The general assignment is given in Figure 3.2.5.7. The authors also observed very similar peaks as seen in this study in the range 5.5 ppm to 6.7 ppm, which

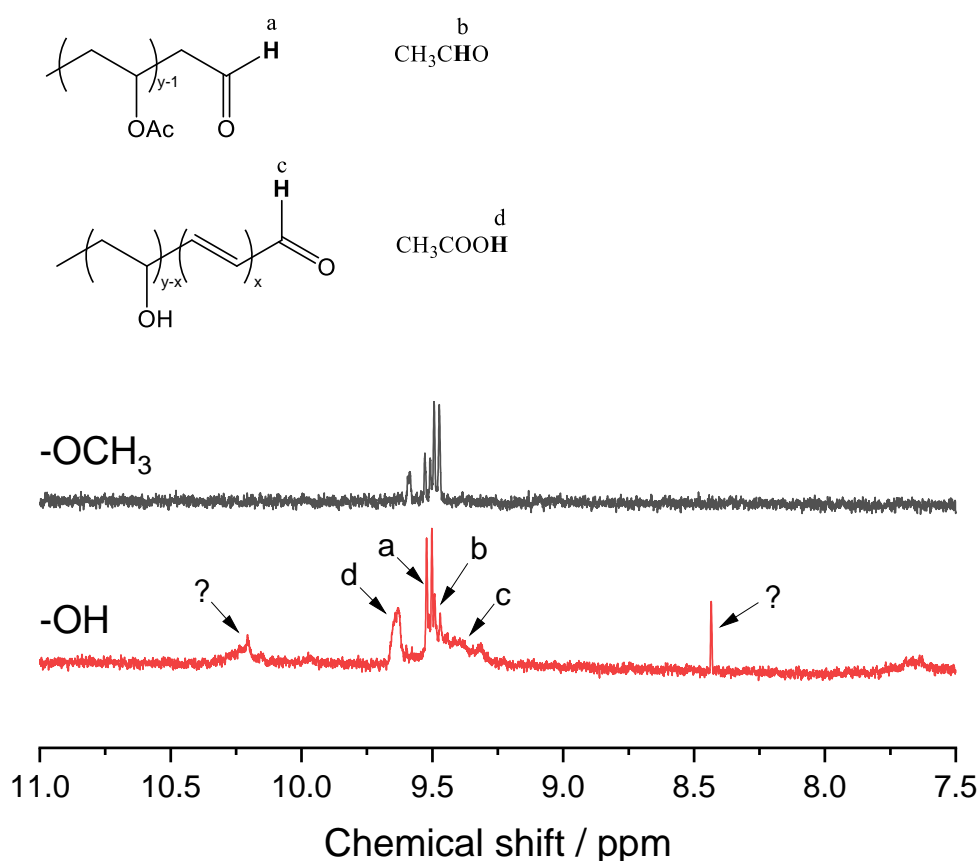


Figure 3.2.5.7: 400 MHz ^1H NMR spectra between 7.5 and 11.0 ppm, recorded in d_6 -DMSO, for the PVOH (bottom, red) formed through saponification of low MW PVAc (top, grey) (solution polymerisation with $[\text{DBDS}]/[\text{VAc}] = 7.65 \times 10^{-2}$).

were arbitrarily assigned to the protons residing on unsaturated carbons. Interestingly, before saponification the polymer also shows a shift at around 9.5 ppm, as was reported in the study by Matyjasczewski and Iovu, suggesting that the thioether promotes aldehyde formation without the need for the saponification conditions. However, given that the PVAc does not contain colour, and has less complexity in the unsaturated region, the loss of acetate to form unsaturation is not expected. The formation of the aldehyde may also be supported through the aforementioned loss of resonances from the thioether protons. If this mechanism does indeed proceed through these means, the liberated butanethiol is expected to be volatile enough to leave during drying.

The strong colouration could therefore be attributed to the conjugation in the backbone. Very interestingly, Psittacofulvin, the structure of which is given in Figure 3.2.5.8, looks to be of very similar structure to that proposed in Figure 3.2.5.7, and is thought to be the chromophore in yellow/red regions in feathers of some parrot species.¹⁴⁰

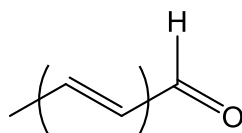
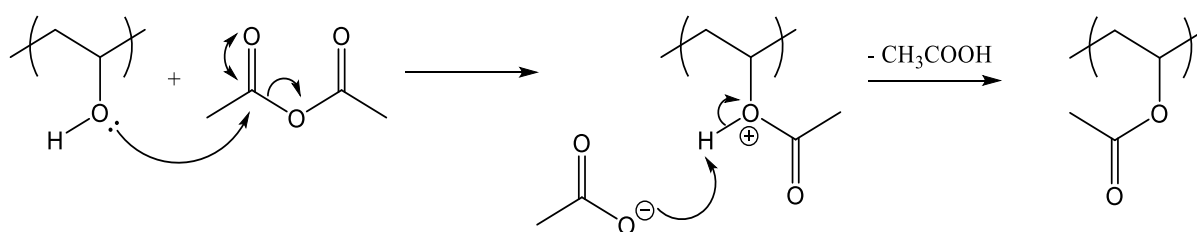


Figure 3.2.5.8: General structure of Psittacofulvin.

Acetylation of the PVOH samples was achieved through reaction with acetic anhydride. According to Scheme 3.2.5.3. The polymer was not particularly soluble in pyridine initially, however, around 30 minutes after addition of the acetic anhydride the polymer entered solution, presumably due to partial acetylation increasing the solubility. After 20 h the polymer solution was concentrated under reduced pressure and the residue was dissolved in a minimum amount of acetone. The polymer was then precipitated into cold water, isolated,



Scheme 3.2.5.3: Mechanism for the acetylation of poly(vinyl alcohol) to poly(vinyl acetate) utilising acetic anhydride.

and dried under reduced pressure to constant mass. The dark brown colour obtained after hydrolysis was retained after reacetylation, as can be seen in the images in Figure 3.2.5.9.



Figure 3.2.5.9: Isolated and dried PVAc, formed after acetylation of PVOH. DVA (100/1/1) (left), No comonomer (100/1/0) (centre), and BDDVE (100/1/1) (right).

The NMR spectra for the acetylated polymers can be seen in Figure 3.2.5.10. Total disappearance of the OH shifts at 4.68, 4.51 and 4.26 ppm suggest reacetylation was successful.

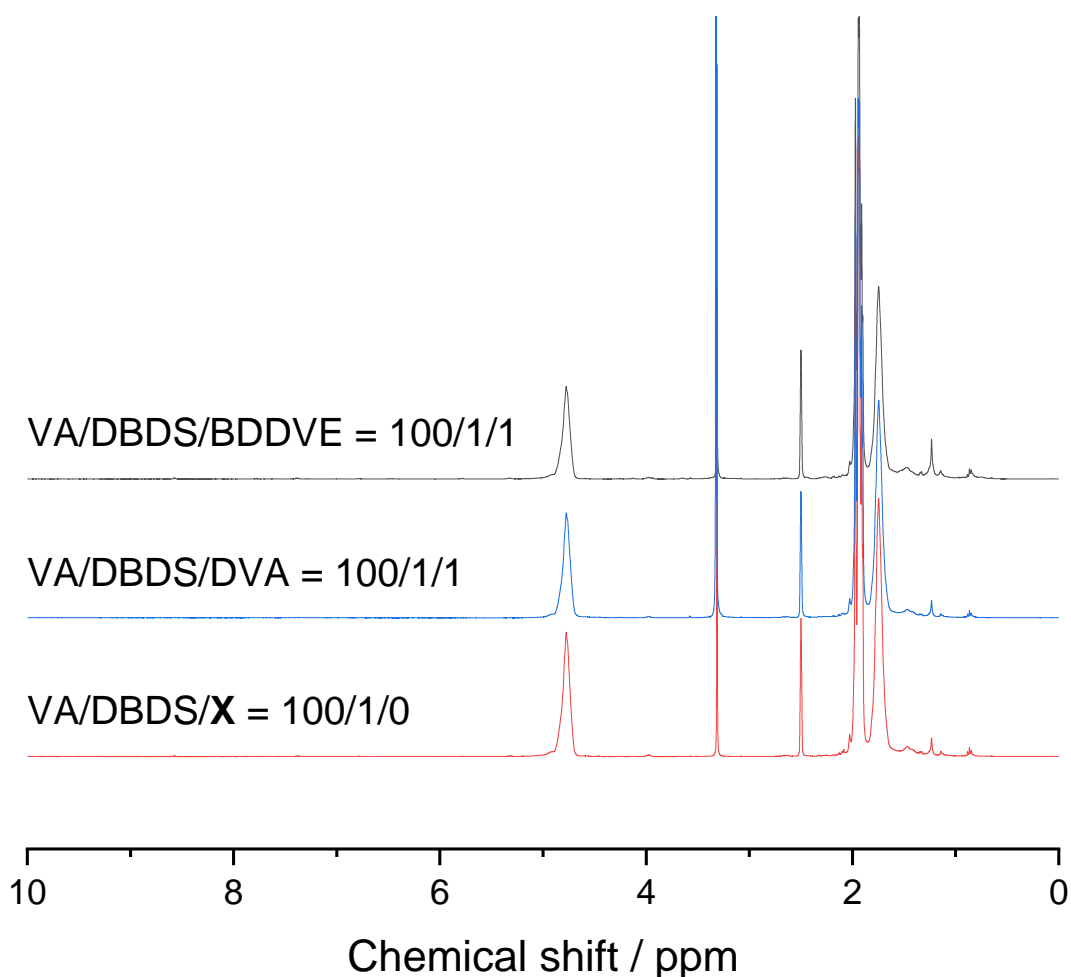


Figure 3.2.5.10: 400 MHz ^1H NMR spectra, recorded in $\text{d}_6\text{-DMSO}$, for the PVAc samples reacetylated from the PVOH samples, from the polymers isolated from the reactions in the presence of 1 mol% DBDS wrt VAc, with no comonomer (bottom), 1 mol% DVA (middle) and 1 mol% BDDVE (top).

This is confirmed through the shifting of the backbone CH_2 resonances from 1.11-1.70 back to 1.65-1.85 ppm, as well as the backbone CH shifting from 3.84 back to 4.78 ppm. The aforementioned complexity above ≈ 5 ppm, due to the aldehyde end group and the occurrence of backbone unsaturation cannot be seen in these samples, however, this is again most likely due to the MW of the polymer being too high. Reacetylation of the low MW PVOH was not performed here.

The MWDs of the PVAc before hydrolysis and after reacetylation are now compared. For simplicity in the subsequent discussions, those polymers analysed before hydrolysis are deemed to be in state "A", and those after hydrolysis and subsequent reacetylation in state "B". The summarised MW information can be seen in Table 3.2.5.1, the MWDs can be seen in Figure 3.2.5.11, and the Mark-Houwink-Sakurada plots in Figure 3.2.5.12. Firstly, taking the blank experiment, where VAc/DBDS/comonomer = 100/1/0, we actually see a slight shift in MW after reacetylation to higher MW. This is unexpected, as we would either expect the distribution to look identical to before hydrolysis, or potentially have a slightly lower MW through cleavage of any branches formed through transfer to polymer. The copolymer with DVA shows a decrease in MW, particularly in M_w , and a resultant narrowing of the distribution. Given that the DVA linkages were expected to be break during the saponification process, this behaviour conforms with the prediction. However, it is worth noting that the

Table 3.2.5.1: MW distribution parameters M_n and M_w being the number average MW, the weight average MW, and the Mark-Houwink parameters K and α for the polymers before hydrolysis (reaction state A) and after hydrolysis and subsequent acetylation (reaction state B).

Comonomer	Reaction state	M_n /gmol ⁻¹	M_w /gmol ⁻¹	$K \times 10^5$	α
None	A	26,300	48,700	7.196	0.731
	B	34,600	68,400	16.845	0.653
DVA	A	35,100	222,700	54.325	0.520
	B	31,000	140,900	69.454	0.536
BDDVE	A	26,800	57,400	11.959	0.681
	B	30,200	177,000	95.631	0.503

relationship between $[\eta]$ and MW does see a significant change. The absolute value of $[\eta]$ increases at a given MW, however the slope of the plot stays comparable. Also, there is a

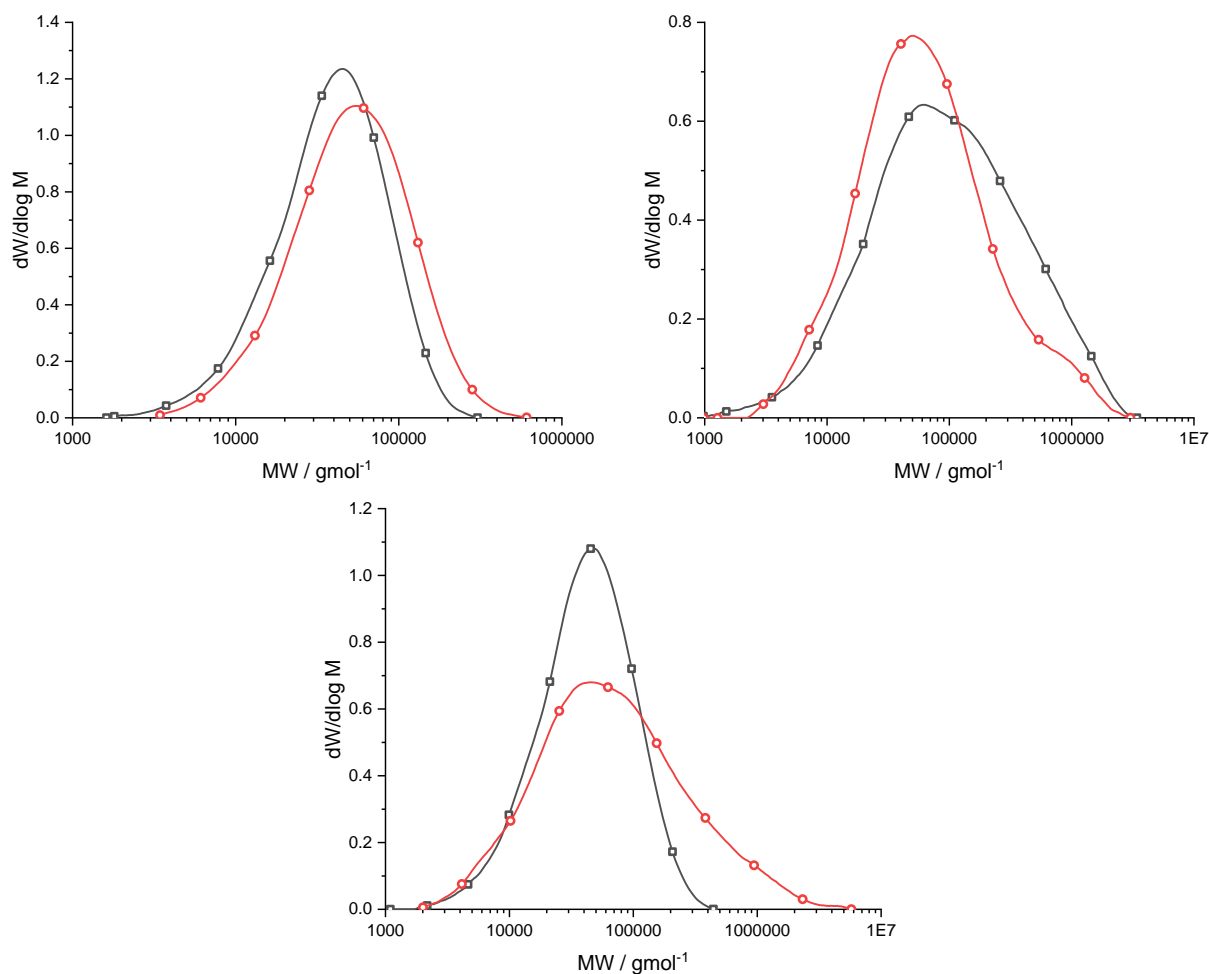


Figure 3.2.5.11: $dW/d\log M$ vs MW (g mol^{-1}) MW distributions for the reactions before hydrolysis (\square) (Reaction state A) and after reacetylation (Reaction state B) (\circ). The reactions shown are that without comonomer (top left), with 1 mol% DVA (top right) and with 1 mol% BDDVE (bottom centre).

noticeable dip in $[\eta]$ at the high MW limit. The copolymer of BDDVE shows the opposite behaviour, wherein a dramatic increase in the MW of the polymer, particularly in M_w , and a corresponding increase in the breadth of the distribution is observed. Additionally, a decrease in the slope of the $[\eta]$ vs MW plot is observed, quantified by a dramatic drop in α .

All of these behaviours suggest that the interconversion between the acetylated and hydrolysed forms does not proceed as one might expect. If we consider the proposal that the hydrolysis reaction produces unsaturation in the backbone, this may explain the observed behaviours. During the reacetylation process, a reaction temperature of 115°C is used and the reaction is operated under nitrogen, so there is a possibility for radical generation and subsequent initiation. For example, if any unreacted AIBN remained in the polymer, this could generate radicals, and subsequently initiate through an unsaturated group. If some of

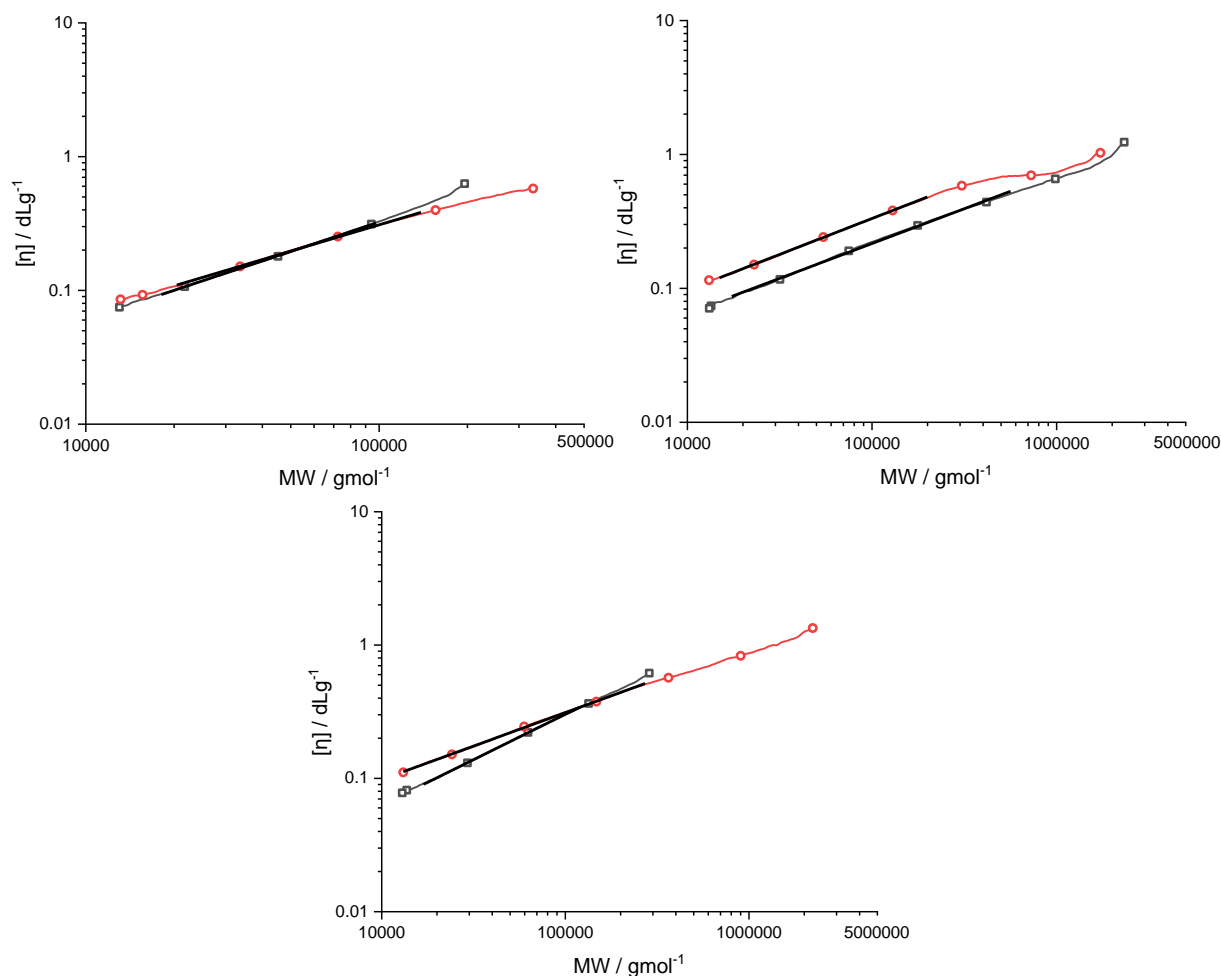


Figure 3.2.5.12: Mark Houwink plots of $[\eta]$ (dL g^{-1}) vs MW (g mol^{-1}) for the reactions before hydrolysis (\square) (Reaction state A) and after reacetylation (Reaction state B) (\circ). The reactions shown are that without comonomer (top left), with 1 mol% DVA (top right) and with 1 mol% BDDVE (bottom centre).

these radicals undergo propagation or bimolecular termination, an increase in the MW would be observed, as well as a reduction in α . This increase in MW appears more exaggerated in the case of BDDVE. This could be due to the copolymer with BDDVE retaining unreacted pendant vinyl groups from the copolymerisation, which may also contribute. As the branches are not expected the break in the BDDVE copolymer, this appears a reasonable explanation for the observed behaviour.

The behaviour of the DVA copolymer is more difficult to justify, as it shows the opposite behaviour. Although a reduction in MW is expected due to the lability of the branch points, a corresponding increase in α is also expected, which is observed but only marginally. An increase in $[\eta]$ is observed, which does suggest a less dense structure however, so the proposal for this case is likely a blend of two competing effects. Cleavage of the arms reduces MW and

increases α , whilst coupling of chains increases MW and decreases α . The deconvolution of these phenomena is not trivial with this data, and the complexity of the $dW/d\log M$ distribution may support this hypothesis.

Despite the lack of clarity in this mechanism, what is certain is that the interconversion is not a trivial process, and perhaps the use of disulfide CTAs is not ideal if branched PVOH is targeted. However, analysis of the branched PVOH in aqueous GPC may prove otherwise, particularly for the BDDVE copolymer, although this was outside of the scope of this work.

3.2.6 Conclusions and future work.

The copolymerisation of vinyl acetate with a collection of multi-functional-vinyl monomers has been demonstrated, in the presence of dibutyl disulfide. The MW of the produced polymers has been shown to be a function of the comonomer used, and the concentration it is employed at. In the case of TTT, improvements over previous work has been made through employment of DBDS, which has a chain transfer constant closer to unity when compared to the previously employed thiol CTAs. BDDVE was also shown to influence the MW and degree of branching, albeit less so than TTT, likely due to lower functionality. BDDVE also showed a slightly lower influence on the rate of polymerisation compared to TTT. DVA was the most promising candidate for industrial applicability, given the low influence on the rate of polymerisation, and measurable increases in MW and increases in the measured degree of branching. It was noted however, that for DVA a huge increase in MW occurred at moderate conversion, behaviour which was not observed at a comparable degree of conversion for BDDVE. It was deduced that this was simply a result of increased reactivity of DVA, leading to less remaining pendant vinyl groups at moderate conversion.

Obvious extensions to this work would be to take the copolymerisations to full conversion, to ascertain if gelation would occur given further polymerisation of pendant vinyl groups, and also to determine the corresponding gel points. Following the concentration of pendant vinyl groups as a function of monomer conversion would beautifully demonstrate any discrepancies in the reactivity ratios between the monomers. Increasing the loadings of both MVM and CTA will increase the branch density even further and would be another logical extension of the data reported here. Additionally, modifications of the thioether end groups, or use of different disulfide CTAs, may allow access to highly functional branched polymers, which opens the doors to a range of application areas.

3.3 Experimental

Materials

Vinyl acetate (VAc, Aldrich, $\geq 99\%$) was purified by passing through a column of basic alumina, followed by vacuum assisted distillation, wherein the first and final 20 vol% of the distillate was discarded. Azobisisobutyronitrile (AIBN, VWR) was purified by recrystallisation from methanol. 1,3,5-triallyl-1,3,5-triazine-2,4,6(1H,3H,5H)-trione (TTT, Aldrich, 98%) and divinyl adipate (DVA, TCI chemicals, $> 99\%$) were added to ethyl acetate before being passed through a column of basic alumina to remove any inhibitors. 1,4-Butanediol divinyl ether (BDDVE, Aldrich, 98 %) was passed through a column of basic alumina undiluted for the same purpose. Ethyl acetate (Merck, $\geq 99.5\%$), dibutyl disulfide (DBDS, Aldrich, 97 %), methanol (VWR, $\geq 99.8\%$), acetone (Aldrich, $\geq 99.5\%$), anhydrous pyridine (Alfa Aesar, $> 99.5\%$), acetic anhydride (Aldrich, $\geq 99\%$) and sodium hydroxide (NaOH, Fischer) were used without further purification.

Characterization methods

Size exclusion chromatography (SEC).

MWDs were determined on an Agilent Infinity II MDS instrument equipped with differential refractive index (DRI) and viscometry (VS) detectors. The system was equipped with 2× PLgel Mixed C columns (300×7.5 mm), and a PLgel 5 μm guard column. Samples of ≈ 3 mg mL⁻¹ (measured precisely) were run in CHCl₃ at 1 mL min⁻¹ at 30 °C. Analyte samples were filtered through a poly(tetrafluoroethylene) (PTFE) filter with a 0.2 μm pore size before injection. Polymer MW information was estimated using universal calibration. The universal calibration was generated from narrow MW standards of methyl methacrylate (Agilent EasyVials). Use of the DRI detector allowed concentration assignment to each chunk of the distribution, using the precise analytical concentration of polymer in the sample. The intrinsic viscosity was then determined at each elution volume by taking the measured specific viscosity from the viscosity detector and reducing it by the concentration of polymer at that elution volume. The molecular weight was then determined by comparing the elution volume to the universal calibration, giving $\log([\eta] \cdot MW)$, and MW determined will the use of the measured $[\eta]$. As discussed in the text, the Mark-Houwink-Sakurada plots were constructed using a precise methodology. The MW range between which the $dW/d\log M$ signal exceeded 50 % of the maximum was used to determine the parameters K and α from the relation between MW

(from the universal calibration) and $[\eta]$. The data for intrinsic viscosity was cut off below $DP = 150$, and above the MW at which the $dW/d\log M$ signal went below 5 % of the maximum. In the Mark-Houwink plots displayed in this chapter, the solid black lines correlate to the linear fit constructed from the extracted Mark-houwink parameters, over the region from which they were extracted.

Nuclear Magnetic Resonance (NMR).

NMR spectra were recorded on a Bruker Advance III HD 400 MHz in d_6 -DMSO. The pulse angle was 30° , the acquisition time was 4.09 s, the relaxation delay was 1 s, and the number of scans was 128 for each sample.

Synthesis

Production of branched PVAc: Solution copolymerization of vinyl acetate with a multifunctional monomer in the presence of DBDS (example quantities for copolymerisation with DVA, employing mol ratio VAc/DBDS/DVA = 100/1/1).

In a typical reaction, vinyl acetate (15.000 g, 0.17 mol), ethyl acetate (60.000 g, 0.68 mol), dibutyl disulfide (0.320 g, 1.74×10^{-3} mol) and DVA (0.334 g, 1.67×10^{-3} mol) were added to a 3 necked round bottomed flask (RBF), fitted with a PTFE temperature probe and an air condenser with aluminium fins, sealed with a rubber septum. A magnetic stirrer bar was added, and the final neck was sealed with a rubber septum. Separately, AIBN (0.057 g, 3.47×10^{-4} mol) and ethyl acetate (14.280 g, 0.16 mol) were added to a 20 mL crimp vial with a magnetic stirrer. The vial was crimp sealed with a PTFE crimp lid. The two vessels were then purged with N_2 for 1 h. The RBF was then submersed in a $60^\circ C$ oil bath under nitrogen, with a stir speed of 750 rpm. After the reaction temperature was confirmed to be $60^\circ C$, 3 mL of the AIBN solution was injected into the RBF under nitrogen. Samples of ≈ 5 mL were then withdrawn under nitrogen at frequent intervals for analysis. The samples were immediately sealed to minimize evaporation and plunged into liquid nitrogen. A small amount of sample was retained (≈ 1 mL), and the remainder was evaporated to determine conversion gravimetrically. SEC analysis was performed on the evaporated gravimetry samples. For the sample withdrawn after 1440 mins, $p = 0.66$, $M_n = 35,100 \text{ g mol}^{-1}$, $M_w = 222,700 \text{ g mol}^{-1}$, $K = 5.43 \times 10^{-4} \text{ dL mol}^{-1}$ and $\alpha = 0.520$. δ_H (400 MHz, d_6 -DMSO): 7.22 ppm (DVA, HC=CH), 5.85 ppm (penultimate CH after transfer, CHS), 4.78 ppm (PVAc, backbone CH), 2.73-2.56 ppm (SCH₂CH₂), 2.45 ppm (DVA, C(O)CH₂CH₂), 2.25 ppm (pDVA, C(O)CH₂CH₂) 2.05-1.87 ppm (addition copolymer backbone CH₂ shifts), 1.97 ppm (PVAc, COCH₃), 1.85-1.65 ppm (PVAc, backbone CH₂), 1.61-

1.02 ppm (m, SCH₂CH₂CH₂CH₃, 0.93-0.8 ppm (m, SCH₂CH₂CH₂CH₃). pDVA backbone peaks unresolvable from PVAc equivalents.

Saponification of (branched) PVAc.

PVAc (0.6 g, 7.0×10^{-3} mol acetate groups), NaOH (0.014 g, 3.5×10^{-4} mol) (5 mol% relative to acetate groups if pure PVAc) and methanol (20 mL) were added to a 50 mL RBF fitted with a magnetic stirrer and reflux condenser. The solution was refluxed at 65 °C, and after around 10 minutes an off-white precipitate was observed. The reaction was left overnight under reflux, after which the precipitate was collected through centrifugation. The supernatant was removed and the solid was allowed to dry under vacuum at 50 °C overnight to constant mass. The resultant polymer was dark orange in colour. Example analysis given for reaction of the polymer formed in the reaction where VAc/DBDS/Comonomer = 100/1/1, $p = 0.66$. After saponification: δ_{H} (400 MHz, d₆-DMSO): 4.68 ppm (PVAc, OH, mm triad), 4.51 ppm (PVAc, OH, mr triad), 4.26 ppm (PVAc, OH, rr triad), 3.84 ppm (PVAc, backbone CH), 3.57 ppm (s, dimethyl adipate, OCH₃), 2.30 ppm (t, dimethyl adipate, C(O)CH₂), 1.11-1.70 ppm (PVAc, backbone CH₂),

Reacetylation of PVOH

PVOH (0.20 g, 4.5×10^{-3} mol OH groups if pure PVOH) and anhydrous pyridine (15.71g, 0.20 mol) were added to a 50 mL RBF fitted with a magnetic stirrer. To this, a solution of acetic anhydride (0.69 g, 6.8×10^{-3} mol) in anhydrous pyridine (7.86 g, 0.10 mol) was added dropwise over 10 mins (equating to ≈ 1.5 eq. acetic anhydride to OH groups). The RBF was then fitted with a reflux condenser, and the system flushed with N₂ for 10 mins. The solution was then refluxed for 20 hours under nitrogen with a stir speed of 300 rpm. After cooling, the reaction mixture was concentrated under vacuum. The resultant product was dissolved into acetone and precipitated into cold water. The product was filtered cold to yield PVAc, and was dried under vacuum at 50 °C to constant mass. Example analysis given for reaction of the polymer formed in the reaction where VAc/DBDS/Comonomer = 100/1/1, $p = 0.66$. After saponification and subsequent reacetylation: $M_n = 31,000$ g mol⁻¹, $M_w = 140,900$ g mol⁻¹, $K = 6.95 \times 10^{-4}$ dL mol⁻¹ and $\alpha = 0.536$. δ_{H} (400 MHz, d₆-DMSO): 4.78 ppm (PVAc, backbone CH), 1.97 ppm (PVAc, COCH₃), 1.85-1.65 ppm (PVAc, backbone CH₂).

3.4 References

- 1 C. Schubert, C. Osterwinter, C. Tonhauser, M. Schömer, D. Wilms, H. Frey and C. Friedrich, *Macromolecules*, 2016, **49**, 8722–8737.
- 2 C. J. G. Plummer, A. Luciani, T. Q. Nguyen, L. Garamszegi, M. Rodlert and J. A. E. Manson, *Polym. Bull.*, 2002, **49**, 77–84.
- 3 J. R. Dorgan, D. M. Knauss, H. A. Al-Muallem, T. Huang and D. Vlassopoulos, *Macromolecules*, 2003, **36**, 380–388.
- 4 T. H. Mourey, S. R. Turner, M. Rubinstein, J. M. J. Fréchet, C. J. Hawker and K. L. Wooley, *Macromolecules*, 1992, **25**, 2401–2406.
- 5 C. J. Hawker and J. M. J. Fréchet, *J. Chem. Soc. Perkin Trans. 1*, 1992, 2459–2469.
- 6 M. G. McKee, G. L. Wilkes, R. H. Colby and T. E. Long, *Macromolecules*, 2004, **37**, 1760–1767.
- 7 A. Gopala, H. Wu, J. Xu and P. Heiden, *J. Appl. Polym. Sci.*, 1999, **71**, 1809–1817.
- 8 D. Schmaljohann, P. Pötschke, R. Hässler, B. I. Voit, P. E. Froehling, B. Mostert and J. A. Loontjens, *Macromolecules*, 1999, **32**, 6333–6339.
- 9 P. L. Carr, G. R. Davies, W. J. Feast, N. M. Stainton and I. M. Ward, *Polymer (Guildf)*., 1996, **37**, 2395–2401.
- 10 C. M. Nunez, A. L. Andrady, R. K. Guo, J. N. Baskir and D. R. Morgan, *J. Polym. Sci. A-1 Polym. Chem.*, 1998, **36**, 2111–2117.
- 11 D. J. Massa, K. A. Shriner, S. R. Turner and B. I. Voit, *Macromolecules*, 1995, **28**, 3214–3220.
- 12 Y. H. Kim and O. W. Webster, *Macromolecules*, 1992, **25**, 5561–5572.
- 13 M. Johansson, E. Malmstrom and A. Hult, *Prog. Org. Coatings*, 1993, **31**, 619–624.
- 14 D. Schmaljohann, B. I. Voit, J. F. G. A. Jansen, P. Hendriks and J. A. Loontjens, *Macromol. Mater. Eng.*, 2000, **275**, 31–41.
- 15 D. A. Tomalia, A. M. Naylor and W. A. Goddard, *Angew. Chem. Int. Ed. Engl.*, 1990, **29**,

- 138–175.
- 16 K. Inoue, *Prog. Polym. Sci.*, 2000, **25**, 453–571.
 - 17 G. Jannerfeldt, L. Boogh and J. A. E. Månson, *Polymer (Guildf.)*, 2000, **41**, 7627–7634.
 - 18 A. Asif and W. Shi, *Eur. Polym. J.*, 2003, **39**, 933–938.
 - 19 C. W. Bielawski, D. Benitez and R. H. Grubbs, *Science.*, 2002, **297**, 2041–2044.
 - 20 A. J. Boydston, Y. Xia, J. A. Kornfield, I. A. Gorodetskaya and R. H. Grubbs, *J. Am. Chem. Soc.*, 2008, **130**, 12775–12782.
 - 21 S. Honda, T. Yamamoto and Y. Tezuka, *Nat. Commun.*, 2013, **4**, 1574.
 - 22 N. E. Kamber, W. Jeong, S. Gonzalez, J. L. Hedrick and R. M. Waymouth, *Macromolecules*, 2009, **42**, 1634–1639.
 - 23 Z. Li, L. Qu, W. Zhu, J. Liu, J. Q. Chen, P. Sun, Y. Wu, Z. Liu and K. Zhang, *Polymer.*, 2018, **137**, 54–62.
 - 24 B. A. Laurent and S. M. Grayson, *J. Am. Chem. Soc.*, 2006, **128**, 4238–4239.
 - 25 F. M. Haque and S. M. Grayson, *Nat. Chem.*, 2020, **12**, 433–444.
 - 26 B. Zhang, H. Zhang, Y. Li, J. N. Hoskins and S. M. Grayson, *ACS Macro Lett.*, 2013, **2**, 845–848.
 - 27 B. J. Ree, T. Satoh and T. Yamamoto, *Polymers.*, 2019, **11**, 163.
 - 28 H. Iatrou, N. Hadjichristidis, G. Meier, H. Frielinghaus and M. Monkenbusch, *Macromolecules*, 2002, **35**, 5426–5437.
 - 29 S. Honda, T. Yamamoto and Y. Tezuka, *J. Am. Chem. Soc.*, 2010, **132**, 10251–10253.
 - 30 H. Gao and K. Matyjaszewski, *J. Am. Chem. Soc.*, 2007, **129**, 6633–6639.
 - 31 C. Hou, J. Hu, G. Liu, J. Wang, F. Liu, H. Hu, G. Zhang, H. Zou, Y. Tu and B. Liao, *Macromolecules*, 2013, **46**, 4053–4063.
 - 32 M. Brett Runge, C. E. Lipscomb, L. R. Ditzler, M. K. Mahanthappa, A. V. Tivanski and N. B. Bowden, *Macromolecules*, 2008, **41**, 7687–7694.

- 33 D. Lanson, F. Ariura, M. Schappacher, R. Borsali and A. Deffieux, *Macromolecules*, 2009, **42**, 3942–3950.
- 34 P. Chen, C. Li, D. Liu and Z. Li, *Macromolecules*, 2012, **45**, 9579–9584.
- 35 I. Gadwal, J. Rao, J. Baettig and A. Khan, *Macromolecules*, 2014, **47**, 35–40.
- 36 K. L. Beers, S. G. Gaynor, K. Matyjaszewski, S. S. Sheiko and M. Moeller, *Macromolecules*, 1998, **31**, 9413–9415.
- 37 H. G. Börner, D. Duran, K. Matyjaszewski, M. Da Silva and S. S. Sheiko, *Macromolecules*, 2002, **35**, 3387–3394.
- 38 J. Bolton and J. Rzaev, *Macromolecules*, 2014, **47**, 2864–2874.
- 39 M. B. Runge, S. Dutta and N. B. Bowden, *Macromolecules*, 2006, **39**, 498–508.
- 40 M. B. Runge and N. B. Bowden, *J. Am. Chem. Soc.*, 2007, **129**, 10551–10560.
- 41 J. Xia, X. Zhang and K. Matyjaszewski, *Macromolecules*, 1999, **32**, 4482–4484.
- 42 X. Zhang, J. Xia and K. Matyjaszewski, *Macromolecules*, 2000, **33**, 2340–2345.
- 43 H. Gao and K. Matyjaszewski, *Macromolecules*, 2006, **39**, 3154–3160.
- 44 S. Abrol, P. A. Kambouris, M. G. Looney and D. H. Solomon, *Macromol. Rapid Commun.*, 1997, **18**, 755–760.
- 45 H. T. Lord, J. F. Quinn, S. D. Angus, M. R. Whittaker, M. H. Stenzel and T. P. Davis, *J. Mater. Chem.*, 2003, **13**, 2819–2824.
- 46 G. Zheng and C. Pan, *Polymer (Guildf.)*, 2005, **46**, 2802–2810.
- 47 H. Staudinger and W. Heuer, *Ber. Dtsch. Chem. Ges.*, 1934, **67**, 1164–1172.
- 48 H. Staudinger and E. Husemann, *Ber. Dtsch. Chem. Ges.*, 1935, **68**, 1618–1634.
- 49 H. Staudinger and E. Husemann, *ibid*, 1935, **68**, 1618–1634.
- 50 K. G. Blaikie and R. N. Crozier, *Ind. Eng. Chem.*, 1936, **28**, 1155–1159.
- 51 R. G. W. Norrish and E. F. Brookman, *Proc. R. Soc. Lond.*, 1937, **A163**, 205–220.
- 52 W. H. Carothers, *Trans. Faraday Soc.*, 1936, **32**, 39–49.

- 53 P. J. Flory, *J. Am. Chem. Soc.*, 1941, **63**, 3083–3090.
- 54 W. H. Stockmayer, *J. Chem. Phys.*, 1944, **12**, 125.
- 55 K. Dusek, *Adv. Polym. Sci.*, 1986, **78**, 1–59.
- 56 H. Gao, W. Li and K. Matyjaszewski, *Macromolecules*, 2008, **41**, 2335–2340.
- 57 R. H. Wiley and G. L. Mayberry, *J. Polym. Sci.*, 1960, **42**, 491–500.
- 58 G. Schwachula, *J. Polym. Sci. Polym Symp.*, 1975, **53**, 107–112.
- 59 P. W. Kwant, *J Polym Sci Polym Chem Ed*, 1979, **17**, 1331–1338.
- 60 N. A. Dotson, C. W. Macosko and M. Tirrel, *Synthesis, Characterisation, and theory of polymeric networks and gels. Plenum Press: New York*, 1992.
- 61 S. Zhu and A. E. Hamielec, *Markomol. Chem., Macromol. Symp.*, 1993, **69**, 247–256.
- 62 R. Wang, Y. Luo, B. G. Li and S. Zhu, *Macromolecules*, 2009, **42**, 85–94.
- 63 J. C. Hernández-Ortiz, E. Vivaldo-Lima, M. A. Dubé and A. Penlidis, *Macromol. Theory simul.*, 2014, **23**, 429–441.
- 64 J. C. Hernández-Ortiz, E. Vivaldo-Lima, M. A. Dubé and A. Penlidis, *Macromol. Theory simul.*, 2014, **23**, 147–169.
- 65 H. Gao, P. Polanowski and K. Matyjaszewski, *Macromolecules*, 2009, **42**, 5925–5932.
- 66 I. Bannister, N. C. Billingham and S. P. Armes, *Soft Matter*, 2009, **5**, 3495–3504.
- 67 J. L. Mann, R. L. Rossi, A. A. A. Smith and E. A. Appel, *Macromolecules*, 2019, **52**, 9456–9465.
- 68 H. Chen, K. Ishizu, T. Fukutomi and T. Kakurai, *J. Polym. Sci. A-1 Polym. Chem.*, 1984, **22**, 2123–2130.
- 69 H. Chen, Y. M. Won, K. Ishizu and T. Fukutomi, *Polym. J.*, 1985, **17**, 687–692.
- 70 N. O. Brien, A. Mckee, D. C. Sherrington, A. T. Slark and A. Titterton, *Polymer.*, 2000, **41**, 6027–6031.
- 71 O. Eckardt, B. Wenn, P. Biehl, T. Junkers and F. H. Schacher, *React. Chem. Eng.*, 2017, **2**,

- 479–486.
- 72 S. V. Kurmaz, N. V. Fadeeva, E. I. Knerelman, G. I. Davydova, V. I. Torbov and N. N. Dremova, *J. Polym. Res*, 2019, **26**, 153.
- 73 D. L. Popescu and N. V. Tsarevsky, *Macromol. Rapid Commun.*, 2012, **33**, 869–875.
- 74 D. L. Popescu and N. V. Tsarevsky, *Aust. J. Chem.*, 2012, **65**, 28–34.
- 75 L. Wang, W. Huang, S. Wang, Y. Cui, P. Yang, X. Yang and J. V. M. Weaver, *J. Appl. Polym. Sci.*, 2015, **132**, 1–8.
- 76 S. A. Kurochkin, M. A. Silant'Ev, E. O. Perepelitsyna and V. P. Grachev, *Eur. Polym. J.*, 2014, **57**, 202–212.
- 77 F. Isaure, P. A. G. Cormack and D. C. Sherrington, *Macromolecules*, 2004, **37**, 2096–2105.
- 78 A. T. Slark, D. C. Sherrington, A. Titterton and I. K. Martin, *J. Mater. Chem.*, 2003, **13**, 2711–2720.
- 79 F. Isaure, P. A. G. Cormack and D. C. Sherrington, *J. Mater. Chem.*, 2003, **13**, 2701–2710.
- 80 P. A. Costello, I. K. Martin, A. T. Slark, D. C. Sherrington and A. Titterton, *Polymer.*, 2002, **43**, 245–254.
- 81 R. Baudry and D. C. Sherrington, *Macromolecules*, 2006, **39**, 1455–1460.
- 82 Y. Liu, J. C. Haley, K. Deng, W. Lau and M. A. Winnik, *Macromolecules*, 2008, **41**, 4220–4225.
- 83 H. Yong, Y. Miao, A. Sigen, D. Quan, A. Ivankovic, K. Singh, J. Zhang, D. Zhou and W. Wang, *Polym. Chem.*, 2019, **10**, 885–890.
- 84 M. Chisholm, N. Hudson, N. Kirtley, F. Vilela and D. C. Sherrington, *Macromolecules*, 2009, **42**, 7745–7752.
- 85 N. T. Nguyen, K. J. Thurecht, S. M. Howdle and D. J. Irvine, *Polym. Chem.*, 2014, **5**, 2997–3008.
- 86 S. Habibu, N. M. Sarih and A. Mainal, *RSC Adv.*, 2018, **8**, 11684–11692.
- 87 C. J. Atkins, D. K. Seow, G. Burns, J. S. Town, R. A. Hand, D. W. Lester, N. R. Cameron,

- D. M. Haddleton and A. M. Eissa, *Polym. Chem.*, 2020, **11**, 3841–3848.
- 88 N. M. B. Smeets, M. W. Freeman and T. F. L. McKenna, *Macromolecules*, 2011, **44**, 6701–6710.
- 89 S. Camerlynck, P. A. G. Cormack, D. C. Sherrington and G. Saunders, *J. Macromol. Sci. Part B Phys*, 2005, **44**, 881–895.
- 90 S. V. Kurmaz and E. O. Perepelitsina, *Russ. Chem. Bull. Int. Ed.*, 2006, **55**, 835–844.
- 91 S. V. Kurmaz, E. O. Perepelitsina, M. L. Bubnova and G. A. Estrina, *Mendeleev Commun.*, 2004, **14**, 125–127.
- 92 S. V. Kurmaz, V. P. Grachev, I. S. Kochneva, E. O. Perepelitsina and G. A. Estrina, *Polym. Sci. Ser. A*, 2007, **49**, 884–895.
- 93 Z. Guan, *J. Am. Chem. Soc.*, 2002, **124**, 5616–5617.
- 94 E. Hasan, S. Furzeland, D. Atkins, D. J. Adams and J. V. M. Weaver, *Polym. Chem.*, 2012, **3**, 625–627.
- 95 T. Zhao, H. Zhang, D. Zhou, Y. Gao, Y. Dong, U. Greiser, H. Tai and W. Wang, *RSC Adv.*, 2015, **5**, 33823–33830.
- 96 I. Bannister, N. C. Billingham, S. P. Armes, S. P. Rannard and P. Findlay, *Macromolecules*, 2006, **39**, 7483–7492.
- 97 F. Isaure, P. A. G. Cormack, S. Graham, D. C. Sherrington, S. P. Armes and V. Büttin, *Chem. Commun.*, 2004, **4**, 1138–1139.
- 98 J. L. Mann, A. K. Grosskopf, A. A. A. Smith and E. A. Appel, *Biomacromolecules*, 2020, **Article**, DOI: 10.1021/acs.biomac.0c00539.
- 99 M. Luzon, C. Boyer, C. Peinado, T. Corrales, M. Whittaker, L. Tao and T. P. Davis, *J. Polym. Sci. A-1 Polym. Chem.*, 2010, **48**, 2783–2792.
- 100 M. Yan, Y. Huang, M. Lu, F. Y. Lin, N. B. Hernández and E. W. Cochran, *Biomacromolecules*, 2016, **17**, 2701–2709.
- 101 R. I. Komendant, E. O. Perepelitsina and S. A. Kurochkin, *IOP Conf. Ser. Mater. Sci. Eng.*, 2019, **525**, 1.

- 102 T. Sato, K. Nomura, T. Hirano and M. Seno, *Polym. J.*, 2006, **38**, 240–249.
- 103 T. Sato, N. Higashida, T. Hirano and M. Seno, *J. Polym. Sci. A-1 Polym. Chem.*, 2004, **42**, 1609–1617.
- 104 T. Sato, M. Hashimoto, M. Seno and T. Hirano, *Eur. Polym. J.*, 2004, **40**, 273–282.
- 105 T. Sato, N. Sato, M. Seno and T. Hirano, *J. Polym. Sci. Part A Polym. Chem.*, 2003, **41**, 3038–3047.
- 106 T. Sato, Y. Arima, M. Seno and T. Hirano, *Macromolecules*, 2005, **38**, 1627–1632.
- 107 S. R. Cassin, P. Chambon and S. P. Rannard, *Polym. Chem.*, 2020, **11**, 7637–7649.
- 108 C. Walling, *J. Am. Chem. Soc.*, 1945, **67**, 441–447.
- 109 G. C. Berry and R. G. Craig, *Polymer.*, 1964, **5**, 19–30.
- 110 D. Britton, F. Heatley and P. A. Lovell, *Macromolecules*, 1998, **75**, 2828–2837.
- 111 S. Rimmer, S. Collins and P. Sarker, *Chem. Commun.*, 2005, 6029–6031.
- 112 N. Zeng, Y. Yu, J. Chen, X. Meng, L. Peng, Y. Dan and L. Jiang, *Polym. Chem.*, 2018, **9**, 3215–3222.
- 113 S. Sato, A. Ono, T. Hirano and M. Seno, *J. Polym. Sci. A-1 Polym. Chem.*, 2006, **44**, 2328–2337.
- 114 M. H. Stenzel, T. P. Davis and C. Barner-Kowollik, *Chem. Commun.*, 2004, 1546–1547.
- 115 J. Bernard, A. Favier, L. Zhang, A. Nilasaroya, T. P. Davis, C. Barner-Kowollik and M. H. Stenzel, *Macromolecules*, 2005, **38**, 5475–5484.
- 116 J. Bernard, A. Favier, T. P. Davis, C. Barner-Kowollik and M. H. Stenzel, *Polymer.*, 2006, **47**, 1073–1080.
- 117 J. Poly, D. James Wilson, M. Destarac and D. Taton, *Macromol. Rapid Commun.*, 2008, **29**, 1965–1972.
- 118 J. Schmitt, N. Blanchard and J. Poly, *Polym. Chem.*, 2011, **2**, 2231–2238.
- 119 X. Zhou, J. Zhu, M. Xing, Z. Zhang, Z. Cheng, N. Zhou and X. Zhu, *Eur. Polym. J.*, 2011, **47**, 1912–1922.

- 120 R. Baudry and D. C. Sherrington, *Macromolecules*, 2006, **39**, 5230–5237.
- 121 J. T. Clarke, R. O. Howard and W. H. Stockmayer, *Makromol. Chemie*, 1960, **44**, 427–447.
- 122 S. Collins, *PhD Thesis, Univ. Sheff.*
- 123 H. Han and J. Zhang, *J. Appl. Polym. Sci.*, 2013, **130**, 4608–4612.
- 124 B. H. Zimm and W. H. Stockmayer, *J. Chem. Phys.*, 1949, **17**, 1301–1314.
- 125 C. D. Thurmond and B. H. Zimm, *J. Polym. Sci.*, 1952, **8**, 477–494.
- 126 Z. Grubisic, P. Rempp and H. Benoit, *Polym. Lett.*, 1967, **5**, 753–759.
- 127 M. A. Haney, *J. Appl. Polym. Sci.*, 1985, **30**, 3037–3049.
- 128 M. Gaborieau, R. G. Gilbert, A. Gray-Weale, J. M. Hernandez and P. Castignolles, *Macromol. Theory Simulations*, 2007, **16**, 13–28.
- 129 W. V. Smith, *J. Am. Chem. Soc.*, 1946, **68**, 2059–2064.
- 130 R. W. Roth and R. F. Church, *J. Polym. Sci.*, 1961, **55**, 41–48.
- 131 J. W. Breitenbach and G. Gleixner, *Monatshefte für Chemie*, 1976, **107**, 1315–1326.
- 132 F. R. Mayo and F. M. Lewis, *J. Am. Chem. Soc.*, 1944, **66**, 1594–1601.
- 133 T. Moritani, I. Kuruma, K. Shibatani and Y. Fujiwara, *Macromolecules*, 1972, **5**, 577–580.
- 134 N. Nomura, K. Shinoda, A. Takasu, K. Nagata and K. Inomata, *J. Polym. Sci. A-1 Polym. Chem.*, 2013, **51**, 534–545.
- 135 S. Collins and S. Rimmer, *Rapid Commun. Mass Spectrom.*, 2004, **18**, 3075–3078.
- 136 M. S. Giguère and P. M. Mayer, *Int. J. Mass Spectrom.*, 2004, **231**, 59–68.
- 137 B. Rimez, H. Rahier, G. Van Assche, T. Artoos, M. Biesemans and B. Van Mele, *Polym. Degrad. Stab.*, 2008, **93**, 800–810.
- 138 S. Iriuchijima, K. Maniwa and G. Tsuchihashi, *J. Am. Chem. Soc.*, 1974, **96**, 4280–4283.
- 139 M. C. Iovu and K. Matyjaszewski, *Macromolecules*, 2003, **36**, 9346–9354.
- 140 J. E. Barnsley, E. J. Tay, K. C. Gordon and D. B. Thomas, *R. Soc. open sci.*, 2018, **5**, 172010.

4

Disulfide chain transfer agents in the soap free emulsion polymerisation of vinyl acetate

Abstract

An overview of the emulsion polymerisation of vinyl acetate is given, with a particular focus on the complications afforded by the nuances of the monomer. The soap free emulsion polymerisation of vinyl acetate is then demonstrated through copolymerisation with surfmers. The need for effective chain transfer agents is discussed, and the use of dibutyl disulfide is then explored, yielding latexes with controllable molecular weight distributions. The size and stability of these latexes is shown to be greatly influenced by the amount of disulfide employed, as well as the comonomer used. These latexes are then tested as stabilisers in the suspension polymerisation of vinyl chloride.

4.1 Introduction

4.1.1 Application of VAc/VOH polymers: Influencing the S-PVC morphological control.

One of the applications of vinyl acetate (VAc)/vinyl alcohol (VOH) polymers is as a stabiliser in the suspension polymerisation of vinyl chloride (VCM).¹ The suspension polymerisation of VCM offers a unique challenge due to two main reasons.² Firstly, at atmospheric conditions, VCM is a toxic gas, meaning polymerisation must occur under pressure to ensure it stays liquid at polymerisation temperatures. Typically, pressures of ≈ 10 bar are used at temperatures between 40 - 70 °C.³ Variation of temperature is used to influence the average molecular weight of the poly(vinyl chloride) (PVC).⁴ The toxicity and state of the monomer under atmospheric conditions leads to the requirement that all of the monomer is removed before the polymer can be used for subsequent applications.

The second key feature in the production of PVC through suspension polymerisation (S-PVC), is the inherent insolubility of PVC in VCM. This results in the formation of nano aggregates inside a polymerising droplet, which are thought to be stabilised through chloride ions in the early stages of polymerisation ($p < 0.1$ % where p is monomer conversion).⁵⁻⁷ As conversion increases, typically between $1\% < p < 5\%$, the surface area of these aggregates exceeds that for which the free chloride can stabilise and aggregation occurs, forming primary particles within the droplet.⁵ Additionally, at around $p = 2\%$, a membrane begins to form around the droplet, thought to be a graft copolymer between PVC and the stabiliser (to be discussed later).⁸ Between $5\% < p < 30\%$, the primary PVC particles within the droplet grow through both aggregation and polymerisation into a continuous network. Between $50\% < p < 70\%$ the network increases to such an extent that PVC particles exist throughout the polymerising droplet, with the size and distribution of these particles influenced greatly by their stability.⁹ By this stage of conversion, the particles are very closely packed and their diffusion is limited, with the voids between particles being rich in monomer. Continued polymerisation ultimately leads to polymerisation of monomer in the voids between the aggregates, and consequently a loss of porosity. The infilling of the voids causes a pressure drop within the polymerising droplet due to the density difference between VCM and PVC, which results in the aforementioned membrane collapsing in on the droplet, filling in the pores and also reducing porosity. A schematic demonstrating this process is given in Figure 4.1.1.1.

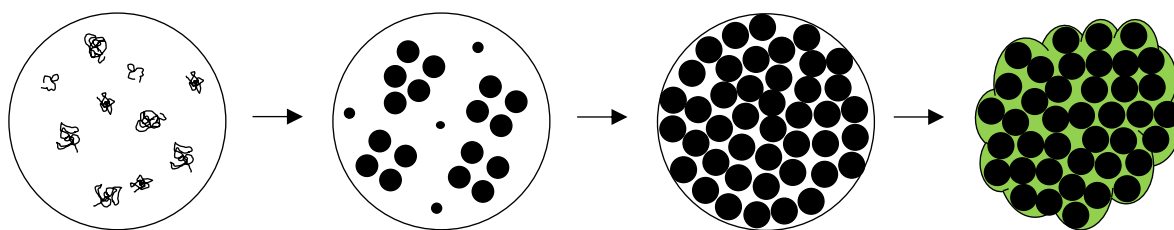


Figure 4.1.1.1: Schematic representation of the suspension polymerisation of VCM.

The pressure drop in the droplets is reflected by an overall pressure drop in the reactor, and as such this stage of polymerisation is very distinct to the operator. The polymerisation is often halted at this point, as this can allow the voids between the particles to be retained, leading to a final granule with high porosity. This porosity is vital as it facilitates the removal of unreacted toxic monomer, as well as the incorporation of processing aids/plasticisers. Proceeding to higher conversion also results in more side-reactions, such as transfer to polymer (both intra and intermolecular) due to lower monomer concentrations, and these structural “defects” significantly influence the thermal stability of the final polymer. One such side reaction which dramatically influences thermal stability is HCl elimination yielding backbone unsaturation.^{10,11} In fact, compounds are very commonly introduced to aid thermal stability of PVC, with many commercial grades suffering from significant degradation at low temperature (120 °C in some cases) without added stabilisers,^{12,13} the incorporation of which is easier for highly porous granules.

PVAc/PVOH copolymers are used as stabilisers in S-PVC synthesis, with the role they play depending on the relative ratio of PVAc to PVOH in the copolymer. Typically, these copolymers are produced by the solution polymerisation of vinyl acetate (VAc), with the polymers being selectively hydrolysed to different degrees to dictate the stabilising role.^{7,14,15} Copolymers with a high degree of hydrolysis (DH) are often referred to as primary stabilisers, and are more water soluble, typically playing the role of stabilising the interface of the VCM emulsion droplet. Droplet, and thus granule size, can be tuned through reduction of the interfacial tension between VCM/Water. Adsorption and later chemisorption of the PVAc/PVOH stabiliser provides steric colloidal stabilisation. Ormondroyd (1987) discussed the observation of a skin which formed during polymerisation at the interface of the growing PVC granules,⁸ which was shown by Davidson and Witenhafter (1980) to be a graft copolymer between PVOH and PVC.⁷ As previously discussed, the skin can fold during the pressure drop within the droplet, however the stiffness of the skin can hinder this, and therefore the stabiliser used is thought to be a key parameter in dictating not only the final shape and size,

but also the porosity of the granules.¹⁵ Copolymers with low DH are less water soluble, and as a result are likely to partition more into polymerising droplet, influencing the stability and size of the precipitating primary PVC particles formed during polymerisation within each droplet.⁹ In reality, a combination of both types of stabiliser are typically employed, to give a combined effect.

In this chapter polymers of vinyl acetate produced through emulsion polymerisation were of particular interest and their applicability as stabilisers in S-PVC synthesis is explored. Emulsion polymerisation is of great importance commercially, allowing polymerisation of hydrophobic monomers in water. The lack of toxic, polluting solvents aside, the particularly high heat capacity of water facilitates heat dissipation, a feature very attractive on industrial scale polymer production. Additionally, the latex polymers can be formulated to much higher solid contents than comparable solution polymerisations, and maintain low overall viscosities making processing and transport of products much more viable. The synthesis of these VAc latexes will be discussed, and the necessity to regulate the molecular weight emphasised. A range of the produced latexes will then be trialled as stabilisers in S-PVC synthesis to assess the influence on the granules produced.

4.1.2 Emulsion polymerisation of vinyl acetate.

4.1.2.1 Emulsion polymerisation introduction

The mechanism of emulsion polymerisation was outlined by Harkins in the 1940s.^{16,17} As the name indicates, the reaction mixture is an emulsion of monomer in water, stabilised by a surfactant. A simplified schematic of the process can be seen in Figure 4.1.2.1.1. Micelles are present when a surfactant is used above its critical micelle concentration (CMC), and become swollen in monomer via transport through the water phase from surfactant stabilised monomer droplets. A water-soluble initiator is used to produce aqueous radicals, which can initiate monomer in the water phase. Propagation of this aqueous oligoradical (bearing an initiator residue) results in the chain becoming increasingly surface active, and at a critical degree of polymerisation, denoted z (a function of the monomer and the initiator residue), the chain (now referred to as a z -mer) may undergo entry into a monomer swollen micelle. We then refer to the object as a primary latex particle. The micelle has undergone nucleation. Typically, the number of micelles will be between 10^{18} - 10^{21} L⁻¹, with a diameter of around 2-

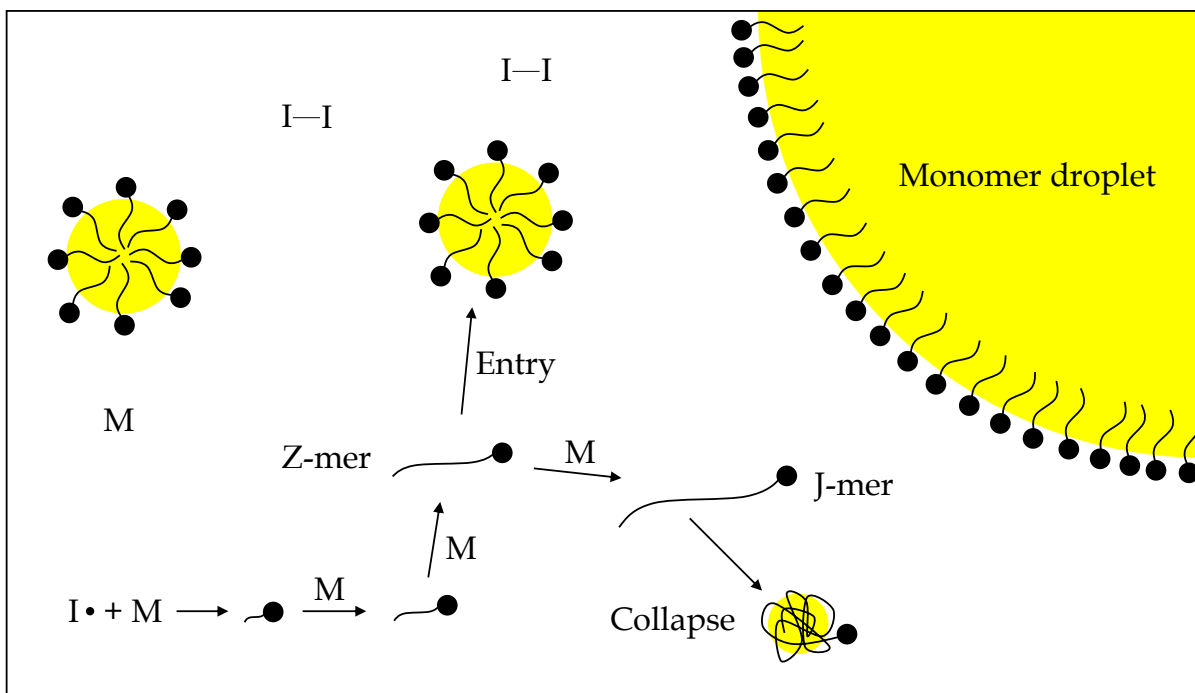


Figure 4.1.2.1.1: General mechanistic steps involved in particle formation/entry in emulsion polymerisation.

3 nm, and the number of monomer droplets are of the order of $10^{10} - 10^{12} \text{ L}^{-1}$ with diameters of around $10 \mu\text{m}$.¹⁸ Therefore, the total surface area of micelles far exceeds that of monomer droplets, which led to Harkins discounting arguments for monomer droplet entry.

Maxwell *et al.* (1991) proposed that this entry process could be assumed to be diffusion controlled, allowing the rate of entry into particles to be determined through calculation of the rate of formation of a z-mer in the water phase.¹⁹ The processes involved in z-mer formation, and the corresponding rates are given in Table 4.1.2.1.1. Assuming initiation step (2) in Table 4.1.2.1.1 is fast and not rate limiting, and both termination and propagation are chain-length independent, z could be estimated for persulfate derived oligomers through Equation 4.1.2.1.1, where R is the ideal gas constant, T is temperature and $[M]_{aq}$ is the concentration of monomer in the water phase (the importance of which will be highlighted in Section 4.1.2.2). The numerator of the right-hand side of the equation (23 kJ mol^{-1}) is the predicted minimum free energy of the lyophobic polymer (ΔG^{hyd}) required to make the chain surface active, based on the knowledge of that for the sulfate anion. The degree of polymerisation at which this free energy is achieved is a function of the hydrophobicity. For styrene this leads to a prediction for z of 2-3 at 50°C , which was verified experimentally in the same paper.¹⁹ Equation 4.1.2.1.1 has also been applied to other monomers at 50°C , for example for methyl methacrylate this number is around 4-5, whereas for vinyl acetate this is predicted

Table 4.1.2.1.1: Aqueous free radical reactions possible before radical entry, and their corresponding rates. k_d , k_i , k_p , k_t and k_{tr} are the rate coefficients for initiator decomposition, propagation of an initiator radical, propagation of a polymer radical, termination and chain transfer respectively, f is the initiator efficiency, I_2 is initiator, M is monomer, XY is any species capable of acting as a chain transfer agent, $T \bullet$ is any aqueous radical, p_{init} is the particle entry rate coefficient, N_p is the number of particles per unit volume and N_A is Avogadro's number. Importantly, all concentrations refer to those in the water phase only.

Reaction	Mechanism	Rate
Initiation	$I_2 \rightarrow 2I \bullet$	$2k_d f [I_2]$ (1)
	$I \bullet + M \rightarrow IM \bullet$	$k_i [I \bullet] [M]_{aq}$ (2)
Propagation	$IM_{i-1} \bullet + M \rightarrow IM_i \bullet, i < z$	$k_p [IM_{i-1} \bullet] [M]_{aq}$ (3)
Termination	$IM_i \bullet + T \bullet \rightarrow P, i < z$	$k_t [IM_i \bullet] [T \bullet]$ (4)
Transfer	$IM_i \bullet + XY \rightarrow IM_i X + Y \bullet, i < z$	$k_{tr} [IM_i \bullet] [XY]$ (5)
Entry	$IM_z + Particle \rightarrow entry$	$p_{init} N_p / N_A$ (6)

as 8.²⁰ More generally, the entry rate coefficient for initiator derived radicals, p_{init} could be described through Equation 4.1.2.1.2,

$$z \approx 1 - \frac{23 (kJ mol^{-1})}{RT \ln [M]_{aq}} \quad (4.1.2.1.1)$$

$$p_{init} = \left(\frac{2k_d f [I] N_A}{N_p} \right) \left(\frac{2\sqrt{f k_d [I] k_t}}{k_p [M]} + 1 \right)^{1-z_{crit}} \quad (4.1.2.1.2)$$

The number of latex particles will slowly increase as more micelles are nucleated, until no free micelles remain. After entry, the radical is now in a monomer rich phase, and is compartmentalised from other radicals, which can result in fast overall polymerisation rates and can facilitate access to higher molecular weights than can be achieved through homogenous polymerisation methods. The monomer concentration in the nucleated micelle (now referred to as a latex particle) is kept constant whilst monomer droplets are still present, via diffusion through the water phase at a rate much faster than the rate of polymerisation, R_p , leading to R_p being constant in the presence of monomer droplets. In fact, R_p can be determined via Equation 4.1.2.1.3, where \bar{n} is the average number of radicals per particle, N_p is the number of particles per unit volume of water, k_p is the rate coefficient for propagation, $[M]_p$ is the concentration of monomer in the particle phase, and N_A is Avogadro's number. It becomes clear that due to the compartmentalisation of radicals, the number of radicals per

particle (\bar{n}) is of paramount importance to the polymerisation rate, and the rate is also seen to increase linearly with N_p .

$$R_p = \frac{N_p k_p [M]_p}{N_A} \bar{n} \quad (4.1.2.1.3)$$

Smith and Ewart provided the quantification of emulsion polymerisation kinetics, specifying the differences under 3 different limits of \bar{n} , in accordance with the mechanism of nucleation outlined by Harkins.^{21,22} For clarity, a particle containing a propagating radical will be referred to as “active” herein. The first two cases assume instantaneous termination of polymer radicals after entry into an active particle. This can be justified when considering that the rate coefficient for termination between two polymeric radicals, k_t , is particularly high ($2.4 \times 10^8 \text{ dm}^3 \text{ mol}^{-1} \text{ s}^{-1}$ for VAc at 333.15 K determined from experimental data in Chapter 1), and the rate of termination, R_t , is second order with respect to radical concentration, $[P \bullet]$, (as seen in Equation 4.1.2.1.4).

$$R_t = 2k_t[P \bullet]^2 \quad (4.1.2.1.4)$$

Compartmentalisation of the polymeric radicals results in a high $[P \bullet]$ after entry into an active particle. The influence of particle size on R_t and the corresponding lifetime of a radical, τ , can be seen in Table 4.1.2.1.2, wherein R_t is calculated for 2 radicals in a particle of a given volume, assuming bulk kinetics. This leads to the approximation that in small particles termination after entry can be deemed instantaneous, therefore a particle may contain only one radical or no radicals, so called “zero-one”. Given the statistical nature of radical entry, the active and inactive periods in any given particle are essentially equal, leading to the average number of radicals per particle, $\bar{n} = 0.5$, the limit defined by case 2 in the Smith-Ewart theory. After entry into a vacant particle, the radical is in a monomer rich environment, and in the absence of chain transfer may propagate freely until a new radical enters. It is worth noting that when

Table 4.1.2.1.2: Influence of particle size on R_t where 2 radicals are isolated within the particle. Using $k_t = 2.4 \times 10^8 \text{ dm}^3 \text{ mol}^{-1} \text{ s}^{-1}$ (determined in Chapter 1 for VAc at 333.15 K).

Particle Diameter / nm	$[P \bullet] / \text{M}$	$R_t / \text{M s}^{-1}$	τ
10	6.4×10^{-3}	1.93×10^4	0.33 μs
100	6.4×10^{-6}	1.93×10^{-2}	0.33 ms
1,000	6.4×10^{-9}	1.93×10^{-8}	0.33 s
10,000	6.4×10^{-12}	1.93×10^{-14}	330 s

the particle becomes large, R_t becomes small, and as such termination may not be considered instantaneous, which can lead to $\bar{n} > 0.5$. As a direct example, the difference in R_t between a 10 nm particle and a 1000 nm particle is 12 orders of magnitude (1.93×10^4 to 1.93×10^{-8}).

If the propagating radical is particularly prone to chain transfer and exit of chain transfer derived radicals is faster than the entry rate, then this leads to $\bar{n} < 0.5$, case 1 in Smith-Ewart theory. In the event a radical enters a vacant particle (a particle without a radical), it may propagate freely in a monomer rich environment, leading to fast polymerisation and high molecular weight. When termination cannot be considered as instantaneous, which is observed in large particles or particles with high viscosity (where k_t is low), and assuming that aqueous termination and radical exit are also insignificant, $\bar{n} > 0.5$, the limit defined in Smith-Ewart theory as case 3.

Due to the effects of compartmentalisation, Smith-Ewart deduced the dependence of the number of particles on the concentration of emulsifier and initiator, and consequently on the rate of polymerisation. Given that the kinetics rely on the validity of the Harkins model, it is logical to deduce that as the emulsifier concentration increases, and therefore the number of micelles increases, the number of particles will also increase. Given the direct dependence of R_p on N , the rate will also increase. In fact, the authors deduced orders of reaction with respect to initiator, I , and emulsifier, S , as defined in Equation 4.1.2.1.5.

$$R_p \propto N_p \propto [I]^{\frac{2}{5}}[S]^{\frac{3}{5}} \quad (4.1.2.1.5)$$

This relation was initially validated for the emulsion polymerisation of styrene, although was not universally applicable due to the assumptions that the area of occupancy of an emulsifier at the polymer/water interface would be comparable to that at the air/water interface, which becomes increasingly invalid with polymers with lower polymer/water interfacial tensions.

It is important to emphasise that in the Smith-Ewart quantification of the kinetics of emulsion polymerisation, polymerisation is assumed to occur almost exclusively in the polymer particles, and not in the water phase, which may be valid for hydrophobic monomers, however for more hydrophilic monomers, such as VAc, this may not be a satisfactory assumption.

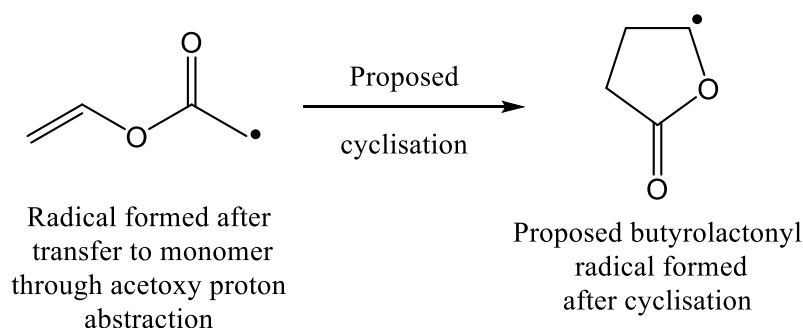
4.1.2.2 Emulsion polymerisation of vinyl acetate

Patsiga *et al.* (1960) demonstrated the differences between the emulsion homopolymerisation of VAc and styrene (Sty) at 60 °C, with batch addition of the respective monomers to a PVAc seed latex.²³ A sample of PVAc seed latex was first coagulated with concentrated salt solutions (10 % NaCl or MgSO₄) and the coagulum was filtered. It was found that around 4 % of the polymer present in the seed latex remained in the supernatant, suggesting water soluble PVAc. This was an interesting initial observation and suggested that a considerable amount of polymerisation occurred in the water phase. The authors then went on to vary the seed latex concentration in the batch polymerisations of VAc and Sty, finding that the rate of polymerisation depended on the number of particles roughly to the 1.0 and 0.2 power for Sty and VAc respectively. This behaviour suggests polymerisation of Sty occurs almost exclusively in the particle phase, in line with Smith-Ewart theory, however, further suggests that significant polymerisation occurs in the water phase for VAc (in contradiction with Maxwell's predictions).

Later work by Motoyama *et al.* (1962) supported this, demonstrating a very weak dependence of the rate of the emulsion polymerisation of VAc on the surfactant concentration, with the exponent ≈ 0 (sodium lauryl sulfate, SLS, between 0 and 8.5×10^{-3} M, [ammonium persulfate] = 2×10^{-3} M) and no jump observed above or below the CMC,²⁴ an observation also later reported by others,^{25,26} again in direct contradiction to the behaviour expected in Smith-Ewart theory. Sty followed the expected behaviour, with extremely slow polymerisation below the CMC ($R_p \approx 0.04$ %/min at [SLS] $\leq 4.8 \times 10^{-3}$ M), however a huge jump was observed above the CMC ($R_p \approx 0.76$ %/min at [SLS] = 6.9×10^{-3} M), with the CMC estimated at [SLS] $\approx 5.9 \times 10^{-3}$ M as the midpoint in the rate transition. This lack of dependence of the rate of polymerisation on the emulsifier concentration in VAc emulsion polymerisation suggested that the Harkins picture of Micellar nucleation may not be a valid for VAc emulsion polymerisation. This deduction was not necessarily surprising, given the numerous reports in the literature and patents in much earlier years of the emulsion polymerisation of VAc in the presence of polyvinyl alcohol stabilisers, or other non-ionic species, which clearly did not micellise.²⁷⁻³¹

Patsiga *et al.* took this deduction to new heights in 1970, formulating a model for VAc emulsion polymerisation.²⁶ In accordance with the work of Motoyama, the rate of polymerisation in their study was found to be independent of soap concentration. They also found the rate was dependant on initiator concentration to the first power ([potassium

persulfate] = 2×10^{-4} to 2×10^{-3} M). This high value may be attributed to transfer to monomer which will be discussed later. In seeded polymerisations the rate of polymerisation was found to depend on initiator and particle concentration to the 0.8 and 0.2 power, respectively. The authors' model was formulated around four assumptions to explain the observed behaviour: 1) polymerization is initiated in the water phase, with the formed polymer being stabilised by soap adsorption, 2) the aqueous radical propagates until a degree of polymerisation of 50-200 units before entering a pre-existing particle, 3) chain transfer to monomer in the particle phase results in a monomeric radical which cyclises to form a butyrolactonyl radical (Scheme 4.1.2.2.1), which readily desorbs from the particle phase, and finally, 4) termination occurs through combination between this butyrolactonyl radical and a propagating radical in the water phase. It was assumed that using these deductions, kinetic equations were formulated and integrated, with these integrated equations matching experimental rate observations convincingly. The proposed cyclisation was later discredited by Starnes *et al.*,³² as its presence was not detected by end group analysis of PVAc, although Gilbert later discussed that the reduction of radical activity after transfer to monomer led to aqueous termination after exit and not reinitiation and subsequent re-entry,³³ explaining why the model still showed good agreement with experimental results.



Scheme 4.1.2.2.1: Demonstration of the radical formed after transfer to monomer, and the proposed cyclisation to form a butyrolactonyl radical.

In order to understand why this might be the case, it is important to discuss the water solubility of VAc relative to other monomers polymerised through emulsion polymerisation. As can be seen in Table 4.1.2.2.1, the water solubility of VAc at 50 °C is over 100 times higher than that of styrene, and more than 3 times higher than methyl methacrylate. This high concentration of monomer in the water phase, combined with high k_p (discussed in chapter 1), leads to high rates of polymerisation in the water phase, and may consequently result in continued propagation of an aqueous oligoradical beyond z-crit.

Table 4.1.2.2.1: $[M]_{\text{aq,sat}}$, being the saturated monomer concentration in water at 50 °C for some monomers commonly polymerised through emulsion polymerisation.

Monomer	$[M]_{\text{aq,sat}} / M$ (50 °C)	Reference
Vinyl acetate	5.0×10^{-1}	123
Methyl methacrylate	1.5×10^{-1}	124
<i>n</i> -Butyl acrylate	6.4×10^{-3}	125
Styrene	4.3×10^{-3}	126
<i>n</i> -Butyl methacrylate	2.5×10^{-3}	127

If this aqueous oligoradical propagates to a critical degree of polymerisation, termed j , before undergoing entry, the chain becomes so insoluble that it precipitates forming a new primary particle, so called homogenous nucleation. The fact that there is a marginal dependence on the emulsifier concentration later led to the deduction that stabilisers, be them polymeric or surfactant, adsorb to the surface of particles after nucleation instead of influencing nucleation itself, and thereby preventing flocculation.³⁴ The high water solubility and prevalence of homogenous nucleation also leads to long nucleation periods, as significant surface area of particles is required to effectively capture oligoradicals before propagating to j -mers, which can lead to relatively broad particle size distributions.

This nucleation pathway was discussed in a publication by Whitby *et al.* (1955),³⁵ building on work by Hohenstein and Mark (1946),³⁶ with the authors arriving at the deduction that latex particles were formed through precipitation of aqueous chains after reaching a critical degree of polymerisation. Fitch and co-authors later reported the aqueous polymerisation of methyl methacrylate, also in the absence of micelles.³⁷ From this, Fitch and Tsai developed the quantitative picture of the process,³⁸ which was later furthered by Hansen and Ugelstad³⁹⁻⁴¹ (leading to the theory often being referred to as HUFT theory, later beautifully summarised by Gilbert⁴²). The formed particles are stabilised in part by the initiator residues, as well as a build-up in charge due to a difference in the dielectric constant between the polymer and water phase, and adsorption of any surfactant (be that added surfactant, or surface-active oligomers formed through aqueous transfer/termination). These small particles can then grow either through polymerisation, facilitated by diffusion of monomer into the particles through the water phase, or through flocculation with other small particles. Flocculation will occur until sufficient colloidal stability is achieved (Section 4.1.3). Homogeneous nucleation is

expected to continue until the size and number of particles (effectively total surface area of particles) is large enough to capture all newly formed radicals.

4.1.2.3 Chain transfer in vinyl acetate emulsion polymerisation

It is also important to consider the susceptibility of PVAc radicals to undergo chain transfer to both monomer and polymer, as has been covered extensively in previous chapter, and how this influences the emulsion polymerisation. The monomeric radical produced after transfer to monomer is so water soluble that radical exit occurs rapidly (leading to average number of radicals per particle < 0.5).^{26,43} Supporting this, Friis and Nyhagen (1973) found that during a vinyl acetate emulsion polymerisation, at a total solids content (TSC) of 30 %, in the presence of 1.8 wt% sodium lauryl sulfate wrt VAc, the initiator (potassium persulfate) dependence exponent on the rate of polymerisation was 0.5, however the initiator concentration had no influence on the number of particles (supporting the theory of homogenous nucleation),⁴⁴ an observation seen independently by others spanning a range of potassium persulfate concentrations at 50 °C ($1.2 \times 10^{-4} - 3 \times 10^{-2}$ M over the included studies).^{45,46} This suggests that \bar{n} increased when increasing the initiator concentration. If we assume zero-one kinetics, i.e. instantaneous termination after entry, then $\bar{n} = 0.5$. In systems where radical exit occurs, $\bar{n} < 0.5$. For illustration, at a low initiator concentration, let $\bar{n} = x$, where $0 < x < 0.5$. Increasing the initiator concentration in this system will increase \bar{n} to some value in the range $x < \bar{n} < 0.5$. This explains the observed dependence on initiator concentration, which would not be observed in the absence of exit, where $\bar{n} = 0.5$, independent of initiator concentration. The authors also noted that the same increase in radical concentration resulted in no change in the limiting viscosity (molecular weight) of the polymers produced. As the number of particles remained essentially equal, and the monomer concentration in these particles can be assumed to be equal, this suggests transfer as the dominant termination mechanism.

Another deviation from Smith-Ewart theory is that the rate of polymerisation remains almost constant during interval 3 in VAc emulsion polymerisation, wherein the concentration of monomer in the particles slowly decreases.⁴⁷ Zollars demonstrated the disappearance of monomer droplets from around 20 % monomer conversion, however a constant reaction between 20 and 80% monomer conversion.⁴⁸ Gilbert *et al.* (1996) discussed that this was due to the high rate of transfer, as both the transfer rate and polymerisation rate are dependent on monomer concentration and, assuming transfer almost always leads to exit and termination, these effects essentially cancel each other.³³ Therefore, as the concentration of monomer in the particle phase depletes, chains grow slower but live proportionally longer. In other words,

$[M]_p \bar{n}$, being the product of the monomer concentration in the particle phase and the average number of radicals per particle, remains essentially constant, as $[M]_p$ decreases \bar{n} increases proportionally.

Transfer to polymer is also important in emulsion polymerisation, particularly at high instantaneous monomer conversion, that is at high polymer concentrations in the particle phases. For VAc this has been shown to occur predominantly through abstraction of the acetoxy protons of the side groups.⁴⁹ This influences polymer chain architecture and the corresponding molecular weight distribution. The effect is exaggerated during semi-batch monomer addition, as demonstrated by El-Aasser *et al.* (1983).⁵⁰ The authors utilised the same recipe, changing the addition method of monomer, with batch addition in one experiment, and in the other semi-batch addition over 4.5 h (although conversion time data was not provided). The final molecular weight distributions were measured and in the case of batch addition, a broad distribution was obtained (PDI = 14.7), attributed to transfer to polymer at high conversion. However, semi batch addition yielded a bimodal molecular weight distribution, with a high molecular weight fraction attributed to transfer to polymer throughout polymerisation due to high instantaneous monomer conversion throughout. Lovell *et al.* (2000) explored semi batch addition further, observing a gradual increase in the mol% branches as a function of conversion during starved monomer addition, however during faster feeds, and therefore lower instantaneous conversion, the cumulative mol% of branches was greatly reduced (attributed to more transfer to monomer and exit).

Often however, monomer starved conditions are desirable to reduce the risks of thermal runaway, or during copolymerisation to minimise composition drift. Additionally, little tailoring of the molecular weight distribution can be achieved through feed rate alone. In order to reduce the significance of transfer to polymer under monomer starved conditions, and to further influence the molecular weight of the formed polymers, a chain transfer agent (CTA) can be used. This is not necessarily a trivial addition however, as a CTA can dramatically influence the course of the polymerisation. Fujita *et al.* (1982) demonstrated the influence of thiol chain transfer agents on the emulsion polymerisation of styrene.⁵¹ After nucleation, a feed of *n*-dodecanethiol (DDT) was started, and was shown to have no influence over the rate of polymerisation at 4.37×10^{-5} mol/g of monomer. However, adding *n*-butanethiol at the same time at a comparable concentration (4.33×10^{-5} mol/g of monomer) dramatically reduced the rate. The authors explained this behaviour by considering that the transfer products had very different water solubility, with the radical formed through transfer

to butanethiol readily desorbing from the particle into the water phase. It should be noted that desorption of radicals leads to increased aqueous termination and may affect latex stability due to the occurrence of depletion flocculation (to be discussed in Section 4.1.3.4), or trigger additional nucleation events, which may explain the increase in particle number observed in the study when using more hydrophilic CTA's.

As discussed in Chapter 2, a wide range of reagents cause significant retardation in VAc polymerisation, and as such selection of a CTA is not trivial. Litt *et al.* (1970) suggested a low concentration of acetaldehyde (8×10^{-3} M) had no influence on the rate of emulsion polymerisation of VAc, and could reduce the molecular weight.²⁶ Expanding on this, De Bruyn noted that only a marginal reduction in rate was observed at high concentrations (up to 0.3 M acetaldehyde).²⁰ The author did not quote any size data, although concluded that the minimal retardation given the dramatically high concentration of acetaldehyde used suggested this was not the origin of retardation observed in other studies, instead attributing the behaviour to dissolved oxygen.

Data from a study by Ferguson *et al.* (2003) suggests no influence on the particle size of PVAc homopolymer particles produced with 0.1 and 1.0 wt% DDT wrt VAc when producing seed latexes through starve fed emulsion polymerisation.⁵² The authors discussed that extensive branching was observed in the absence of CTA, resulting in no molecular weight information being obtainable, however, DDT effectively reduced the extent of this branching behaviour. \bar{X}_n of 280 and 151, and \bar{X}_w of 3500 and 760 were measured for 0.1 and 1.0 wt% DDT in the feeds respectively, indicative of effective molecular weight reduction. The authors did not provide the distributions, however the dispersity (M_w/M_n) was notably high, (12.5 and 5.0 for 0.1 and 1% DDT respectively), which may be attributed to the dramatically large value for $C_{tr,S}$ of 223, resulting in continual drift in the $[S]/[M]$ ratio in each particle. This would result in some chains proceeding to high molecular weight, and having a higher branch density than others (through transfer to polymer), resulting in a broad molecular weight distribution. DDT is by far the most widely used CTA for VAc emulsion polymerisation, most likely due to the absence of retardation and the hydrophobicity preventing significant exit from latex particles after transfer inspite of the large value of $C_{tr,S}$. In fact, in applications where narrow molecular weight distributions or mild branching are not an issue, this may be beneficial as costs can be reduced through the need for small amounts of CTA. Despite this, very little work has been performed demonstrating the behaviours of other chain transfer agents, with $C_{tr,S}$ closer to unity, on VAc emulsion polymerisation.

There are some reports of reversible deactivation radical polymerisation (RDRP) techniques applied to VAc emulsion polymerisation, which facilitates the production of much narrower molecular weight distributions. Nomura *et al.* (2012) demonstrated that control of molecular weight could be achieved through iodine transfer-radical polymerisation and reversible addition-fragmentation chain transfer (RAFT) emulsion polymerisation of VAc.⁵³ Monomer addition was performed batch-wise, and the authors were able to obtain molecular weight distributions in the absence of CTA, with $M_n = 88,500 \text{ g mol}^{-1}$ and $M_w = 469,000 \text{ g mol}^{-1}$ at a monomer conversion (p) > 0.99. Addition of 1 mol% of ethyl iodoacetate (EIA) resulted in effective reduction of molecular weight, to $M_n = 10,600 \text{ g mol}^{-1}$ and $M_w = 31,800 \text{ g mol}^{-1}$, with an associated reduction in the dispersity. Further increasing to 2 mol% EIA reduced M_n to 9,600 g mol^{-1} and M_w to 21,100 g mol^{-1} . The RAFT agents **A** and **B** given in Figure 4.1.2.3.1 were also demonstrated at a variety of concentrations, with 2 mol % yielding polymers of $M_n = 4,900 \text{ g mol}^{-1}$ and $4,700 \text{ g mol}^{-1}$ and $M_w = 9,500 \text{ g mol}^{-1}$ and 6500 g mol^{-1} for **A** and **B**, respectively. Utilisation of **B** at 2 mol% also resulted in a reduction in the final particle size from 86 nm to 58 nm compared to the experiment in the absence of CTA, although the origin of this behaviour was not discussed, and no other size data was reported. Zhao *et al* (2012) noticed similar behaviour during the RAFT emulsion polymerisation of VAc, and attributed the reduction in size to increased hydrophobicity of the initiating species, leading to more micellar nucleation, and lower value of j compared to in the absence of RAFT agent (wherein homogenous nucleation dominates).⁵⁴

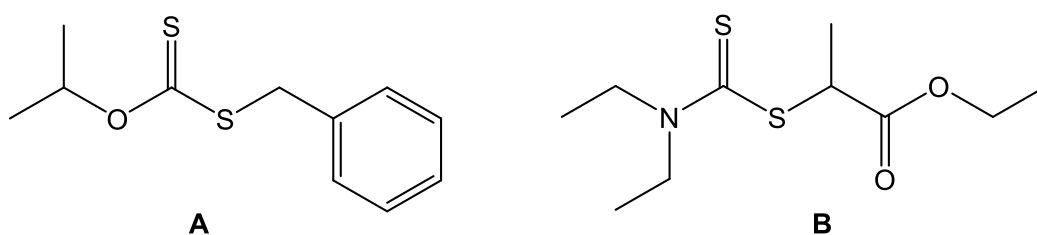


Figure 4.1.2.3.1: Examples of some of the RAFT agents used in the study by Nomura to control the emulsion polymerisation of VAc.

Copolymerisation with more hydrophobic monomers is commonplace in VAc emulsion polymerisation for the same reasons, particularly for coatings and adhesives applications. In particular copolymerisation with *n*-butyl acrylate or vinyl neodecanoate (Trade name VEOVA 10) is common, with the comonomer also improving water resistance and modifying the film forming temperature.^{55,56} Those particles which do form through homogenous nucleation are also more stable, as the increased hydrophobicity leads to easier adsorption of surfactant.^{57,58} The molecular weight distribution can have a big influence on film formation and the films

properties,⁵⁹⁻⁶⁵ and as such there is also interest in the application of chain transfer agents to the emulsion copolymerisation's, for which thiols are by far the most prevalent.^{66,67}

Suzuki *et al.* (2006) studied the influence of dibutyl disulfide (DBDS) on the kinetics of vinyl pivalate (VPiv) emulsion polymerisation, noting a reduction in size with increasing [DBDS], as well as a reduction in MW using potassium persulfate as initiator.⁶⁸ For example, the authors noted that an increase in [DBDS]/[VPiv] from 1.2×10^{-5} to 5.0×10^{-2} resulted in a decrease in particle diameter from 31 nm to 11 nm, and a reduction in the number average degree of polymerisation from 1250 to 160. Interestingly, the authors hypothesised that the reduction in size was due to DBDS acting as a cosurfactant, and in turn increasing the number of micelles. They also justified a reduction in the rate of polymerisation by significant radical exit after chain transfer, which is likely true, although the potential of retardation by chain transfer was not discussed.

To the best of the authors knowledge, disulfides have not been used in VAc emulsion polymerisation, and given their favourable chain transfer constants ($C_{tr,S} = 0.221$ for transfer to dibutyl disulfide at 60 °C, as determined in Chapter 2), this was of particular interest.

4.1.2.4 Soap-free emulsion polymerisation of vinyl acetate

The aforementioned process of homogenous nucleation has been discussed for VAc in the presence of surfactant, however this process is very similar in the absence of surfactant, so called "soap-free" emulsion polymerisation. Soap-free emulsion polymerisation is a particularly attractive technique for applications such as coatings and adhesives, wherein surfactant migration during drying can negatively influence properties such as water resistance and adhesion.^{69,70} The lack of surfactant may limit the colloidal stability, leading to coagulation of small particles, so called coagulative nucleation.⁷¹⁻⁷⁴ Priest (1952) demonstrated this through polymerisation of vinyl acetate in water (VAc/Water = 0.058) in the absence of any surfactant, using potassium persulfate as initiator.⁴⁵ Fixing the potassium persulfate concentration at 2.5 mM, yet increasing the temperature from 51 °C to 70 °C, decreased the particle diameter from 410 nm to 280 nm. This was explained by a decrease in chain length due to increased termination, resulting in an increase in the relative number of sulfate end-groups per particle. Increasing the concentration of initiator may logically have the same effect, however the author noted that variability in particle size was observed, attributed to competing effects of increased sulfate end-groups per particle vs increased electrolyte concentration. The increase in electrolyte concentration will reduce the size of the electrical

double layer, consequently influencing stability and size (to be discussed later). It is important to consider that a reduction in molecular weight may be observed when increasing the initiator concentration, therefore decoupling of molecular weight and particle size through radical flux alone is a challenging prospect.

More control over this process may be achieved through the use of reactive surfactants. These can take the form of an “inisurf” (combination of an initiator and surfactant),⁷⁵⁻⁷⁸ a “transurf” (combination of chain transfer agent and surfactant),⁷⁹⁻⁸¹ or a “surfmer” (combination of monomer and surfactant), which possesses functionality capable of providing stability to the colloidal dispersion. Given they are chemically bound to the surface of the latex particle, stability is provided without the risks of migration during drying. Also, functionality of the latex particle can be influenced through the selection of the reactive surfactant, and often stability is improved, and latexes can be made dispersible after drying due to a lack of desorption. Surfmers are of particular interest here, as the functionality introduced through the use of inisurfs and transurfs often cannot be varied significantly without influencing polymerisation rate or molecular weight distributions.⁸²

Originally referred to as “vinyl soaps”, the first syntheses of surfmers were reported by Medalia *et al.* (1957), who produced a range of carboxylic acid type monomers, with styrenic, acrylophenone and acrylamido vinylic functionalities.⁸³ However, since their conception, development of a wide range of surfmers with different stabilising functionalities, including examples without charged groups, and different vinyl group functionalities have been developed and used to good effect,⁸⁴⁻⁸⁹ although very few studies have looked into emulsion copolymerisation of surfmers with VAc, likely due to VAc copolymerising poorly with most vinyl monomers,

El-Aasser and co-workers reported the emulsion copolymerisation of VAc with a surfmer, sodium dodecyl allyl sulfosuccinate, comparing its behaviour to the hydrogenated equivalent (lacking a vinylic bond, referred to simply as surfactant herein) over a series of publications,⁹⁰⁻⁹² reinforcing the fact that molecular surfactants can undergo desorption from the particle surface, however surfmers cannot. The structures of both the surfmer and the corresponding surfactant are given in Figure 4.1.2.4.1, and it was noted that both the CMC and the interfacial tension with water were comparable between the surfmer and the surfactant, and as such the differences in behaviour were due to covalent attachment of the stabiliser. Notably, increasing the concentration of surfmer reduced the rate of polymerisation, however increasing the

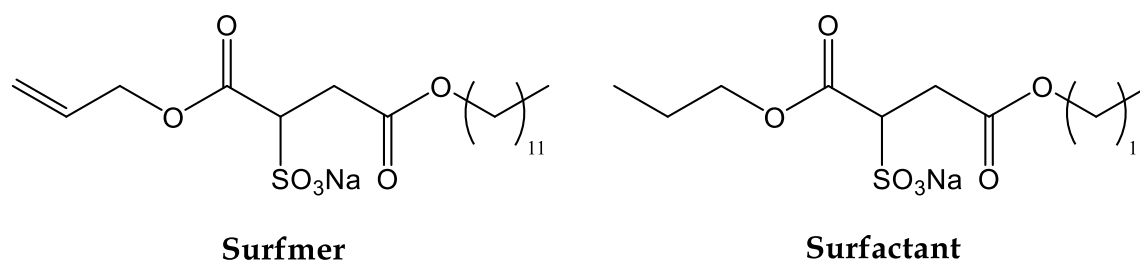


Figure 4.1.2.4.1: Structure of the surfmer and surfactant used in the studies by El-Aasser and coworkers.⁹⁰⁻⁹²

concentration of the surfactant increased the rate of polymerisation slightly. The size of the particles produced decreased with increasing surfmer and surfactant concentration, with the surfmer appearing to decrease particle size more effectively. For example, at a concentration of 16.7 mM of surfmer, a particle size of 114 nm was obtained, compared to 214 nm for the surfactant at the same concentration. The reduction in rate observed for the surfmer, in spite of a reduction of particle size, was attributed to the copolymerisation rate being slower than homopolymerisation, and some chain transfer through abstraction of the allylic hydrogen of the surfmer. The important conclusion was that covalent attachment of the surfmer prevented desorption, and as such smaller particle sizes were obtained at the same concentration as the surfactant. The covalent attachment has also been shown to increase some material properties, with Shaffei *et al.* (2008)⁹³ demonstrating that PVAc latexes produced with bis(2-ethylhexyl) maleate (BEHM) were stronger adhesives than corresponding latexes produced with PLURONIC F108, a commercial polymeric stabiliser. The adhesives produced with BEHM had a shear strength of 120 kg/cm² vs 87 kg/cm² for PLURONIC F108 latexes at the same loading, with the difference again being attributed to the covalent attachment of the stabiliser.

In a recent patent by Chabrol *et al.* (2015), the synthesis of latexes of vinyl esters was discussed through copolymerisation with a surfmer.⁹⁴ A number of comonomers were suggested, with the sodium salts of 2-acrylamido-2-methyl-1-propanesulfonic acid (Na-AMPS) and 3-allyloxy-2-hydroxypropane sulfonate (Na-AHPSA) being two examples, wherein semi batch monomer addition was used to force statistical copolymerisation and reduce monomer

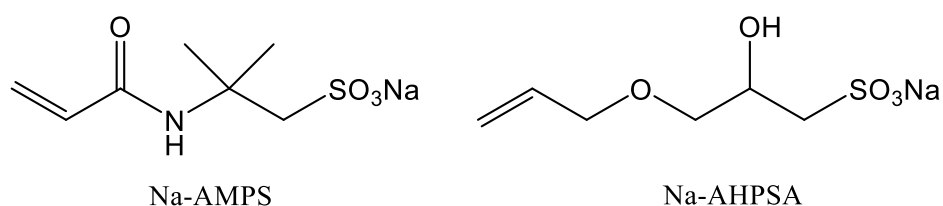


Figure 4.1.2.4.2: Structures of the sodium salts of 2-acrylamido-2-methyl-1-propanesulfonic acid (Na-AMPS) and 3-allyloxy-2-hydroxypropane sulfonate (Na-AHPSA).

pooling. Kinetic data was not provided, however the authors noted good stability could be achieved in PVAc latexes with up to 2 wt% comonomer for the above-mentioned surfmers at 35 % TSC, with particle sizes in the range of 200-500 nm depending on comonomer loading.

The soap free emulsion copolymerisation of VAc and butyl acrylate has been demonstrated with a variety of surfmers, with Zhang *et al.* (2013) using Na-AMPS to achieve latexes with good stability. Although specific details on the VAc/BA ratios were not included, the authors obtained particles with an average diameter of 390.7 nm, and PDI of 0.251, at a total solids content of 38.39 with 0.5 wt% Na-AMPS. Increasing the loading of Na-AMPS to 1.5 % dramatically reduced the particle size to 143.7 nm and PDI to 0.075. Interestingly, further increasing the loading of Na-AMPS to 2 wt% began to increase the particle size (178 nm) and the PDI (0.086), which was explained by an increase in water soluble polymer contributing to depletion flocculation. Xiao *et al.* (2016) also demonstrated the use of acrylic acid as a surfmer, however again neglected to detail the VAc/butyl acrylate ratio, or other experimental details. The authors found that increasing the concentration of acrylic acid in the semi batch monomer feed from 0.5 to 1 % resulted in a reduction in particle diameter from ≈ 575 nm to ≈ 335 nm.

Sun *et al.* (2007) demonstrated the synthesis of a class of maleate surfmers, the structures of which are given in Figure 4.1.2.4.3.⁹⁵ These surfmers were then utilised in the semi batch emulsion polymerisation of vinyl acetate-butyl acrylate-vinyl neodecanoate-hexafluorobutyl methacrylate in the mol ratio 65-15-10-10. Around 6% of the total monomer was added batchwise, and the remainder was fed in over 3 h 15. Stable latexes were obtained using ≈ 1 wt% hexadecyl(trimethyl)ammonium bromide (CTAB, a commercial molecular surfactant), which was added in the same fashion as the monomer (6% batch, remainder fed), with a particle diameter of 229 nm and PDI = 0.03. Replacing CTAB with the maleate surfmers, also at 1 wt%, resulted in a general decrease in particle size with increasing poly(ethylene glycol) units (n). The diameter decreased to 225.5, 204 and 206 nm for n = 3, 9 and 15 respectively. The key observation was that the latexes formed with the surfmers showed superior stability,

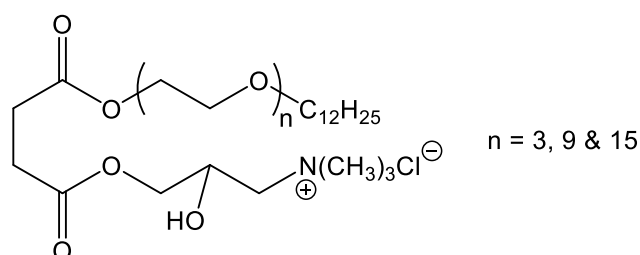


Figure 4.1.2.4.3: Structure of the maleate derived monomer synthesised in the work by Sun *et al.*

where in the presence of 1 M MgSO_4 flocculation was avoided. At the same $[\text{MgSO}_4]$ the latex with CTAB underwent significant destabilisation. The surfmer latexes also showed superior freeze/thaw stability, with stability maintained after 5 cycles, behaviour again not observed for CTAB where irreversible coagulation was observed. Both behaviours can again be attributed to covalent attachment of the stabiliser.

4.1.2.5 A note on (P)VAc hydrolysis

The acetate group of (P)VAc is particularly susceptible to hydrolysis, and as such, any aqueous formulations must be designed in such a way to minimise this. The hydrolysis is actually slowest under mildly acidic conditions, with the minimum in the rate occurring at $\text{pH} \approx 4.5$.⁹⁶ Typically, pH values of 4.5-7 are used, mediated through the introduction of a buffer, most commonly sodium bicarbonate, which regulates a drop in pH due to liberation of acetic acid during hydrolysis. It is however important to consider that the use of buffers typically increases the ion concentration and the corresponding ionic strength of the water phase, and as such may influence the particle size and colloidal stability if significant concentrations are required to regulate pH.

4.1.3 Colloidal stability.

4.1.3.1 General challenge

Preventing aggregation/coagulation of latex particles is a key consideration when preparing colloidal formulations. A colloidal dispersion which will be used as a coating is of little use if after 1 week of storage the system collapses. In order to prevent such behaviour, an energy barrier can be provided which must be overcome before particles can aggregate. For example, electrostatic charges about the surface of the particle, or the introduction of a steric barrier, can counteract the attractive Van Der Waals forces (VDW) that two particles experience when in proximity. Both will be discussed herein.

4.1.3.2 DLVO theory

Derjaguin and Landou,⁹⁷ Verwey,⁹⁸ and Overbeek⁹⁹ are all credited with major contributions to the theory used to describe the interactions between particles which are stabilised electrostatically (DLVO theory). Importantly, the interactions between two particles approaching close in space are a balance between attractive VDW forces and electrostatic/coulombic repulsion. Electrostatic repulsion occurs due to the presence of surface charge, which is present on latex particles implicitly due to a difference in dielectric

constant between the polymer and water phases. Charged initiators and comonomers also contribute, and an electrical double layer is formed when in a fluid, with a layer of counter ions closely bound to the surface of the particle (the so-called stern layer), and a more diffuse layer surrounding this (the thickness of which is referred to as the Debye length). When inside this double layer, the repulsive potential (V_r) at any given point is described by equation 4.1.3.2.1, where V_0 is the potential of the surface, H is the distance from the surface, r is the radius of the particle and $1/k$ is the Debye length.

$$V_r = V_0 \frac{H}{r} e^{-k(H-r)} \quad (4.1.3.2.1)$$

The attractive VDW force was proposed by Hamaker,¹⁰⁰ and can be determined using Equation 4.1.3.2.2, where A is the Hamaker constant, r is the particle radius, and H is the interparticle separation (when $H \ll 2r$). It is worth noting that the Hamaker constant changes as the surface charge of the particle changes.

$$V_a = -\frac{Ar}{12H} \quad (4.1.3.2.2)$$

DLVO theory describes the mathematics of the energy potential between two particles as a function of the distance between them. At long distances, the particles feel weak attraction through VDW forces. However, as the distance between them is reduced, the repulsive potential increases and a balance between the two opposing potentials is reached. When particles with overlapping double layers get too close in space, a dramatic increase in ion concentration leads to a large osmotic pressure, forcing the particles apart. The combination of these effects can be illustrated when considering the total potential energy between two particles as a function of the distance between them. As seen in Figure 4.1.3.2.1, combination of the attractive VDW interactions and the electrostatic repulsive forces results in a combined potential energy which is dependent on the particle separation. As the distance between the particles slowly decreases, the potential passes through an initial minimum, denoted the secondary minimum. Here, the particles are weakly held close in space, a phenomenon often coined "flocculation", wherein separation of the particles is relatively low in energy. As the two particles get closer, the electrostatic repulsion becomes increasingly dominant, and a large energy barrier is observed, which if overcome, the potential energy becomes dominated by the VDW attraction and a dramatic drop in potential into the so-called primary minimum is seen. Particles which are at this separation are strongly bound to each other, a process referred to as coagulation. The energy barrier to coagulation is the main measure of the stability of the

colloidal dispersion and can be influenced through the selection of electrostatic stabiliser employed.

Introduction of salt into the system reduces the magnitude of this energy barrier by contracting the electrical double layer with a higher saturation of ions screening the charge of each particle. Additionally, the increase in ions in the fluid reduces the osmotic pressure observed when particles approach. The use of a comonomer which can contribute to stability is an alternative strategy to achieve colloidal stability.

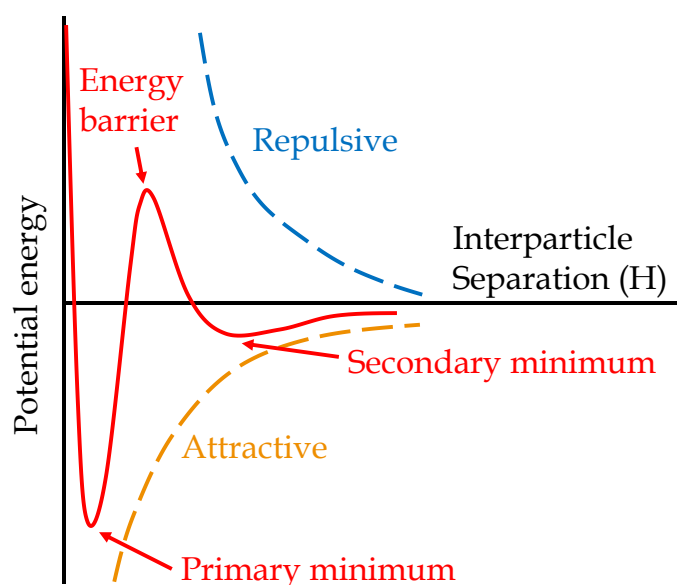


Figure 4.1.3.2.1: The potential energy of two lyophobic colloids at short distances, as a function of the interparticle separation.

4.1.3.3 Steric stabilisation

Another route to achieve colloidal stability is to introduce a steric barrier around the particles, a process which was described at length by Napper and co-workers in the 1960/70's.¹⁰¹⁻¹⁰⁵ This is often achieved through the use of polymeric stabilisers, which wrap around the particle and introduce a physical bumper of sorts. Alternatively, copolymerisation with a water-soluble monomer could yield particles with covalently bound hairs extruding from the surface of the particle. When two sterically stabilised particles approach, the chains of the stabiliser become intertwined, which results in repulsion through two collaborative effects. Firstly, during entanglement, the concentration of chains in the interstitial space dramatically increases, creating a large osmotic pressure which contributes to the repulsion. Additionally, a decrease in the degrees of freedom of these chains provides entropic justification for the particle's repulsion.

4.1.3.4 Other causes of instability – depletion/bridging flocculation

Asakura and Oosawa developed a theoretical description for depletion,^{106,107} which was later covered comprehensively in an excellent book by Lekkerkerker and Tuinier.¹⁰⁸ When free water soluble polymer is present in a colloidal dispersion, sometimes flocculation is observed. The interaction between the polymer and the particle phase dictates the mechanism through which this occurs, however the outcome is the same. If a favourable interaction is present, the polymer may adsorb to the particle surface, however, if below the saturation area of the particles, bridging between particles can occur, promoting aggregation. In the event that the polymer does not adsorb to the particle surface, due to an unfavourable interaction, the displacement of the polymer from the interface results in a polymer “depleted” area as two particles approach, which may force particles together resulting in flocculation. This is important to consider in polymerisations wherein significant water-soluble polymer is formed in situ, either via poor copolymerisation with charged comonomers, or in systems with significant aqueous termination/transfer.

4.1.4 Key aims of chapter.

In this chapter the primary aim was to synthesise latexes of PVAc using surfmers, for use in S-PVC synthesis. The exploration of DBDS as a chain transfer agent in the emulsion polymerisation of VAc is presented, as the lack of viable chain transfer agents for VAc emulsion polymerisation made this of particular interest. A series of latexes are presented with control over molecular weight, and influences of comonomers discussed, all with the goal of producing more cost-effective stabilisers for S-PVC synthesis.

4.2 Results and discussion

4.2.1 Soap free emulsion polymerisation of vinyl acetate.

In order to synthesise latexes for use as stabilisers in S-PVC synthesis, a simple formulation was conceived. The recipe is outlined in Table 4.2.1.1. The target solids content of the formulation was set to 20 %, with VAc and Na-AMPS (0.5 mol% wrt VAc) fed linearly into the reaction over 2 h. Semi-batch addition was chosen for two reasons: to prevent monomer pooling (minimising the risk of thermal runaway during any future scale up), and to force a more statistical copolymerisation between VAc and Na-AMPS, although blocky Na-AMPS regions were still expected, given that $r_{VAc} = 0.05$ and $r_{Na-AMPS} = 11.6$.¹⁰⁹ NaPS was added batchwise at 1 wt% wrt total VAc and the polymerisation was performed at 60 °C. As

discussed previously, pH control was necessary to minimise hydrolysis. A series of polymerisations were performed in the presence of different buffers at different concentrations, assessing the influence of each species and concentration on the latex stability and pH, with the goal of achieving a pH of 4.5 – 7.0 whilst maintaining good latex stability.

Table 4.2.1.1: Reagent quantities for the modified soap free emulsion copolymerisation of VAc and Na-AMPS.

Reagent	Amount (g)	
Water	157.00	
Buffer	Varied	
Sodium persulfate	0.40	
Water	4.00	
VAc	40.00	} Fed linearly over 2 h
Na-AMPS	0.60	} Fed linearly over 2 h
Water	5.00	

Initially, the role of sodium citrate was tested, which was expected to buffer the pH in the range 3.0-6.2 depending on the concentration used. As seen in Table 4.2.1.2, at the concentrations tested, initial pH values of 3.7 and 3.8 were obtained, with little variation observed when the concentration was increased. When $[\text{sodium citrate}]_{\text{aq}} = 2.2 \times 10^{-3}$ and 4.4×10^{-3} M (referring to the initial concentration in the water phase), the initial latexes both had a pH of 3.7, which fell to 3.0 and 3.1 after 4 months, respectively. This reduction could be attributed to liberation of acetic acid after side group hydrolysis. However, both latexes remained stable after this time. Increasing the concentration to 8.9×10^{-3} M increased the final pH to 3.8 and again the initial latex was stable, however this stability was short-lived, with notable coagulation after 4 months, and the pH dropping to 3.5 after this time. It is important to consider that the total concentration of sodium is already rather high in the absence of buffer, due to the use of both NaPS and Na-AMPS (final total $[\text{Na}]$ in total volume in the absence of buffer, $[\text{Na}]_{\text{tot}} = 0.020$ M). Therefore, adding more electrolyte in the form of buffer potentially further compresses the electrical double layer, influencing stability.

Table 4.2.1.2: pH recorded directly after polymerisation and after 4 months, as well as observations of the latex stability after 4 months for a series of buffer compositions and concentrations.

Buffer	[Buffer] _{aq} / M	Original pH	4-month pH	4-month observation
Sodium Citrate	8.9 × 10 ⁻³	3.8	3.5	Coagulation
	4.4 × 10 ⁻³	3.7	3.1	Stable
	2.2 × 10 ⁻³	3.7	3.0	Stable
Sodium Bicarbonate	2.3 × 10 ⁻²	6.1	5.1	Coagulation
	1.1 × 10 ⁻²	5.6	4.7	Coagulation
	8.5 × 10 ⁻³	5.5	4.6	Stable
	5.7 × 10 ⁻³	5.2	4.0	Stable

Given the pH was still too low at 8.9 × 10⁻³ M sodium citrate, logic would dictate that an increase in concentration would be needed, however given that stability was already such a problem ([Na]_{tot} = 0.027 M) this buffer system was discounted.

A range of sodium bicarbonate concentrations were also tested with more promising results. In the range of 8.5 × 10⁻³ and 2.3 × 10⁻² M, pH values between 5.5 and 6.1 were obtained immediately after polymerisation, and the pH remained above 4.5 after 4 months. For a concentration of 5.7 × 10⁻³ M the starting pH was seen to drop from 5.2 to 4.0 after 4 months of storage. Notably for [sodium bicarbonate]_{aq} ≥ 1.1 × 10⁻² M, the latexes observed after 4 months had significant coagulum. A concentration of 8.5 × 10⁻³ M appeared to show the most promise, with a good balance of long-term stability and maintenance of the targeted pH range.

In order to follow the influence of these changes in buffer composition on the emulsion polymerisation kinetics, samples were withdrawn during polymerisation. These samples were analysed via gravimetry to determine the VAc monomer conversion, and the size evolution was followed by dynamic light scattering (DLS). The conversion time evolution for the reactions can be seen in Figure 4.2.1.1. The cumulative VAc conversion appears to evolve linearly with the feed rate of monomer after around 60 mins, and only very slight deviations

are observed where $[\text{sodium citrate}]_{\text{aq}} = 8.9 \times 10^{-3}$, where the cumulative conversion appears to evolve faster, albeit within the range of experimental error. The effect is slightly more exaggerated when looking at the instantaneous conversion as a function of time. Importantly, all reactions are seen to achieve high values of instantaneous conversion during polymerisation, with all reactions reaching values of $\approx 90\%$ by 60 mins. As mentioned previously, this is important to minimise the chances of monomer pooling and subsequent thermal runaway, as well as maintaining a consistent ratio of Na-AMPS/VAc.

Little difference is observed in the size of the particles during the change of the buffer concentration. The particle size evolution, as seen in Figure 4.2.1.2, is essentially identical in the sodium citrate series, with final values of around 160 nm achieved in all cases, with $\text{PDI} \leq 0.05$. In this series, $[\text{Na}]_{\text{tot}}$, accounting for buffer, initiator, and Na-AMPS, varies from 2.2×10^{-2} to 2.7×10^{-2} M, therefore may not influence the final size significantly, however, the compression of the electrical double layer likely leads to the long-term instability for $[\text{sodium citrate}]_{\text{aq}} = 8.9 \times 10^{-3}$, $[\text{Na}]_{\text{tot}} = 2.7 \times 10^{-2}$. In the sodium bicarbonate series, at $[\text{sodium bicarbonate}]_{\text{aq}} 2.3 \times 10^{-2}$ M a higher size of 181 nm is observed, which generally decreases as the concentration decreases. Here $[\text{Na}]_{\text{tot}}$ spans a higher range of 2.5×10^{-2} M – 3.8×10^{-2} M, and therefore may be more influential during polymerisation and during storage. This dependence of size on the buffer concentration during synthesis could be explained by an increase in the interfacial tension between the polymer/medium, promoting coagulation of smaller particles at low conversion, enhanced by the compression of the double layer.^{71,72} Notably, $\text{PDI} \leq 0.03$ in all cases, suggesting low dispersity in particle size independent of $[\text{sodium bicarbonate}]_{\text{aq}}$.

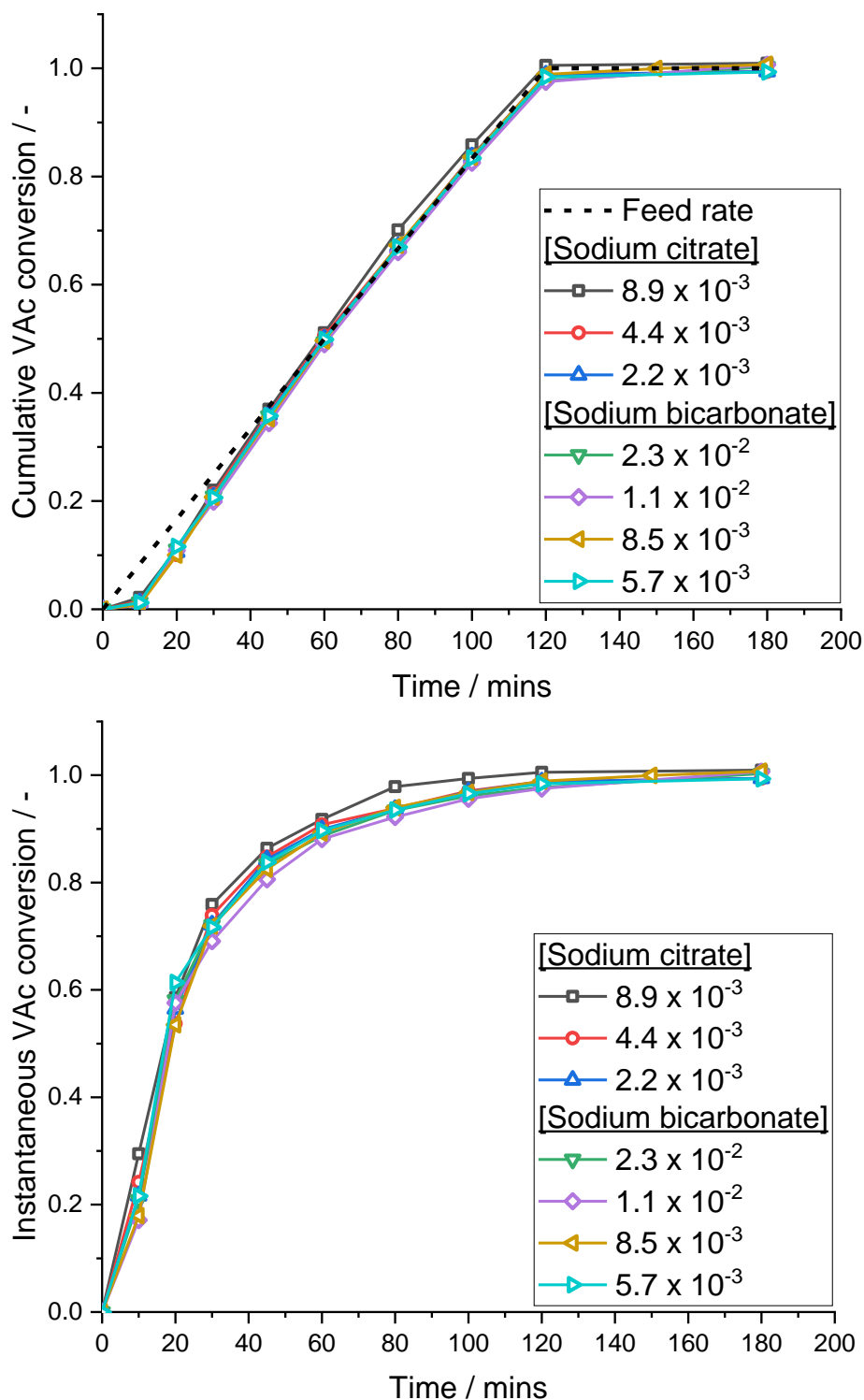


Figure 4.2.1.1: Cumulative (top) and instantaneous (bottom) VAc conversion (top) for the semi-batch soap free emulsion copolymerisation of VAc and Na-AMPS (0.5 mol% wrt VA) in the presence of varying concentrations of buffer. Conversion was determined gravimetrically. Note the black dashed line in the top plot is the theoretical max conversion, based on the feed rate of VAc.

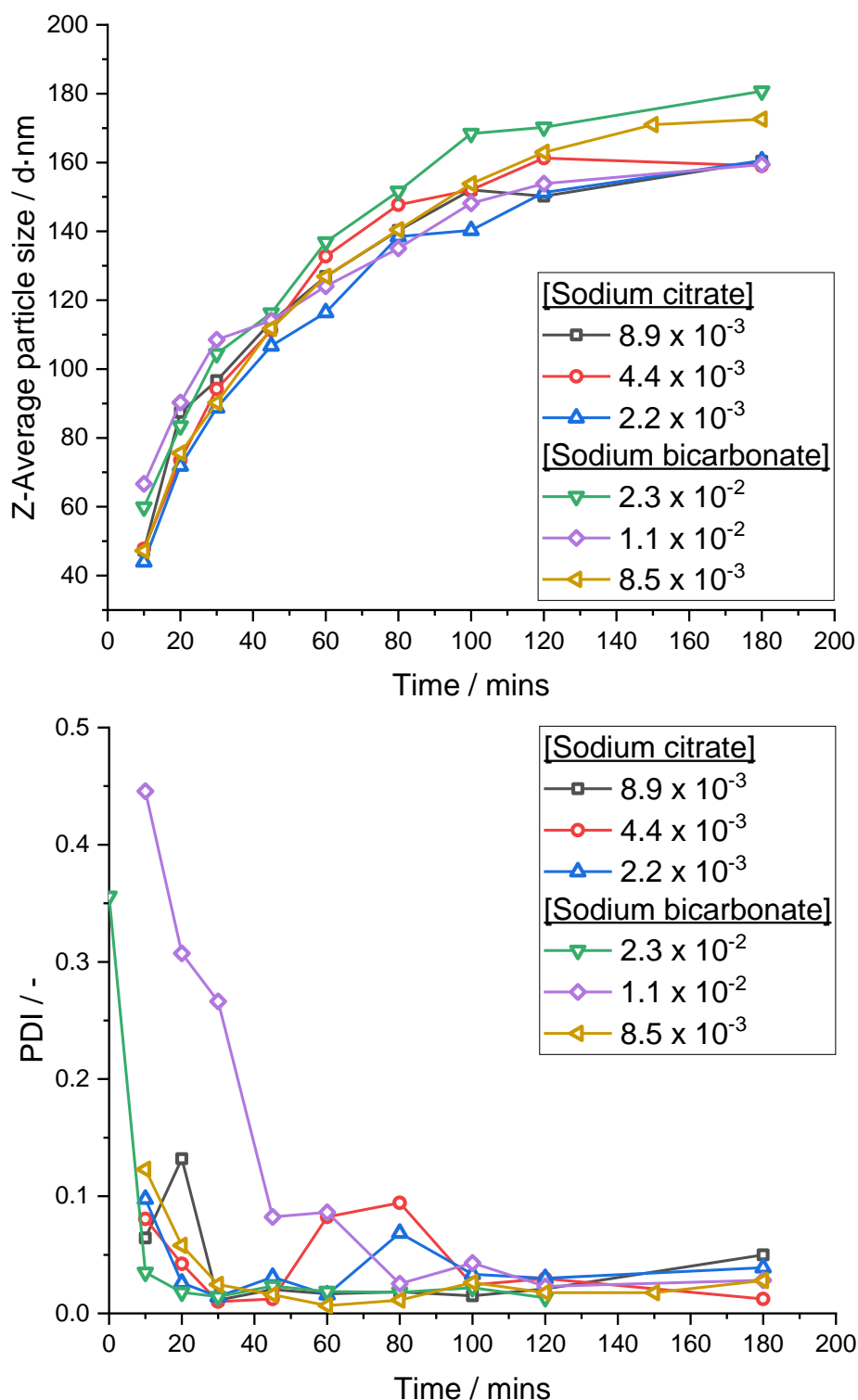


Figure 4.2.1.2: Z-average particle size (d · nm) (top) and PDI (bottom) vs time for the semi-batch soap free emulsion copolymerisation of VAc and Na-AMPS (0.5 mol% wrt VA) in the presence of varying concentrations of buffer. Data determined through DLS in water.

Figure 4.2.1.3 shows a plot of Z-average particle size vs the cube root of cumulative VAc conversion ($p^{1/3}$). Given that conversion progresses through an increase in volume of the particles, one might expect that if all particles grow at the same rate, a linear increase in the particles volume will occur as a function of monomer conversion. This will result in a linear relation in particle size (diameter being proportional to the cube root of particle volume) and the cube root of monomer conversion. The plot appears to show a slight slope change at $p^{1/3} = 0.59$ (corresponding time of 30 mins and conversion of 0.21), however relatively linear progression before and after this point. This slight increase in slope could infer some marginal aggregation, as the reported average size includes some flocculated particles. However, this could also be due to slow nucleation, with the first 2 data points showing a slower evolution in size due to continuous particle nucleation, hence slower growth per particle. This then phases out as conversion increases. It is also worth considering that the lower conversion points have a higher dispersity, and as such the absolute value of Z-average particle size may be erroneous.

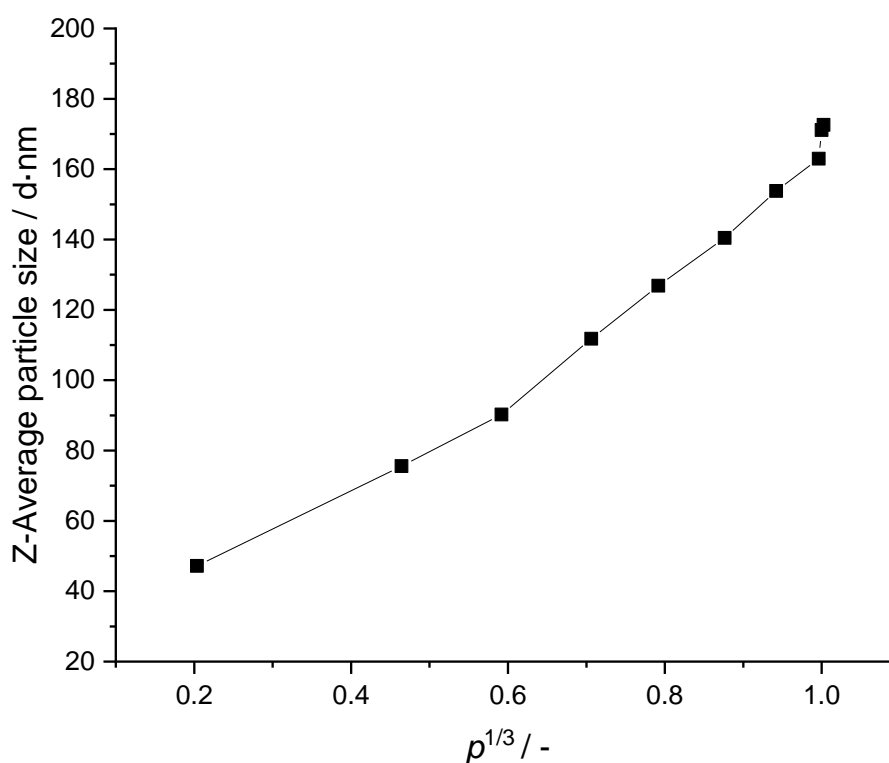


Figure 4.2.1.3: Z-average particle size (d · nm) vs $p^{1/3}$ for the semi-batch soap free emulsion copolymerisation of VAc and Na-AMPS (0.5 mol% wrt VAc) in the presence of varying concentrations of buffer. Size determined through DLS in water. $p^{1/3}$ determined gravimetrically.

Despite the observed stability in the latex, it is worth noting that gelation of the polymer chains in the particles is observed in all cases. Molecular weight distributions could not be

obtained, inevitably due to transfer to polymer resulting from the high instantaneous monomer conversions observed here (as discussed in the introduction). In order to reduce the influences of transfer to polymer, and therefore the number of branches per chain, a chain transfer agent can be introduced. To prove the potential issues of using a CTA with an extremely high chain transfer constant, $C_{tr,s}$, DDT was added to the formulation at 1 wt% wrt VAc (≈ 0.43 mol% wrt VAc). At this concentration in homogenous polymerisation, polymers of $DP_n \approx 1$ are expected utilising Equation 4.2.1.1, i.e. spontaneous transfer (determined using $C_{tr,s} = 223$). Even if partitioning is accounted for when translating this to emulsion polymerisation, one might expect the concentration of DDT in the particle phase to be even higher relative to VAc, as some VAc will partition into the water phase, and as such instantaneous transfer after entry.

$$\frac{1}{DP_n} \approx C_{tr,s} \frac{[S]}{[M]} \quad (4.2.1.1)$$

Looking at the conversion evolution (Figure 4.2.1.4), the absolute slope of the cumulative conversion is comparable (rate of polymerisation of 0.9 %/min in both cases), although a slight inhibition period appears to offset the plot marginally. Consequently, the instantaneous and cumulative conversions appear slightly lower in the presence of DDT. Given the lack of retardation observed during solution studies of VAc free radical polymerisation in the presence of DDT, it is not expected to be due to this. Minamino *et al.* (1982) also observed no influence on the rate for the emulsion polymerisation of styrene with DDT due to a lack desorption of DDT derived radicals due to the low water solubility.⁵¹ It may be argued that desorption from PVAc latexes may be faster given the higher hydrophilicity of the polymer, or indeed that short oligomeric PVAc may undergo desorption and therefore reduce the rate.

Alternatively, the small amount of DDT which may exist in the water phase, combined with the large value of $C_{tr,s}$ could contribute to some aqueous transfer before particle entry. This would reduce the radical entry rate into the particle phase and consequently a small reduction in the rate of polymerisation would be observed. Having said this the rates of polymerisation between 20 mins and 120 mins are $3.34 \times 10^{-4} \text{ Ms}^{-1}$ and $3.23 \times 10^{-4} \text{ Ms}^{-1}$ with and without DDT so the reduction in rate is very marginal and could simply be error in measurement. Analysis of the particle size evolution and PDI as a function of time (Figure 4.2.1.5) shows very similar behaviour with and without DDT. The final particle sizes of 166 nm and 164 nm and PDI's of 0.018 and 0.033 with and without DDT respectively are essentially identical and are well within experimental error.

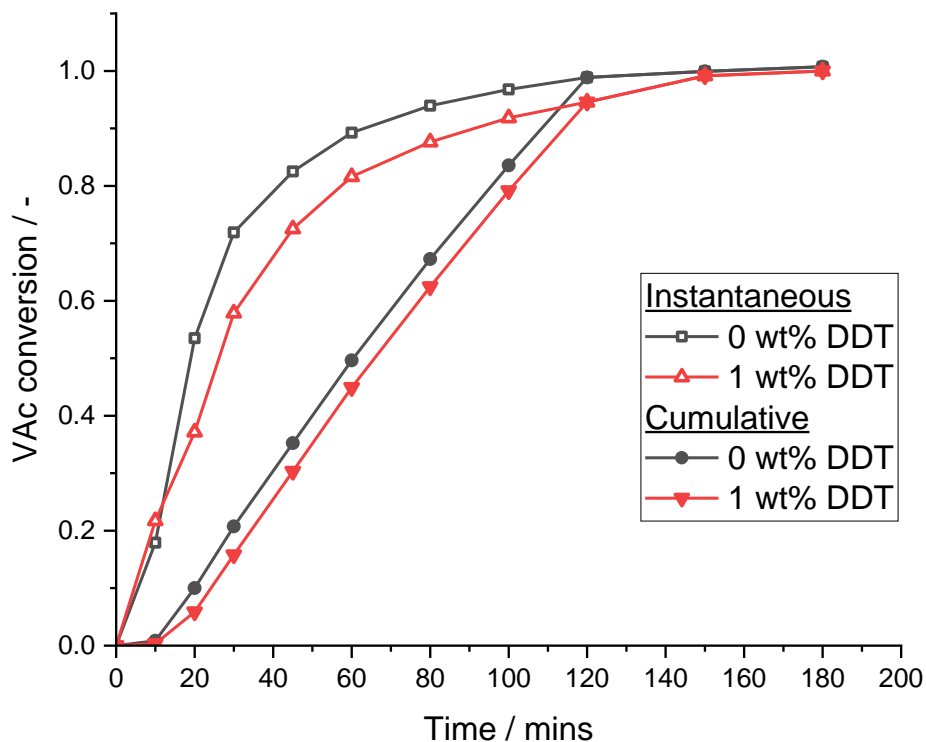


Figure 4.2.1.4: Cumulative and instantaneous VAc conversion vs time for the semi-batch soap free emulsion copolymerisation of VAc and Na-AMPS (0.5 mol% wrt VAc), with and without DDT.

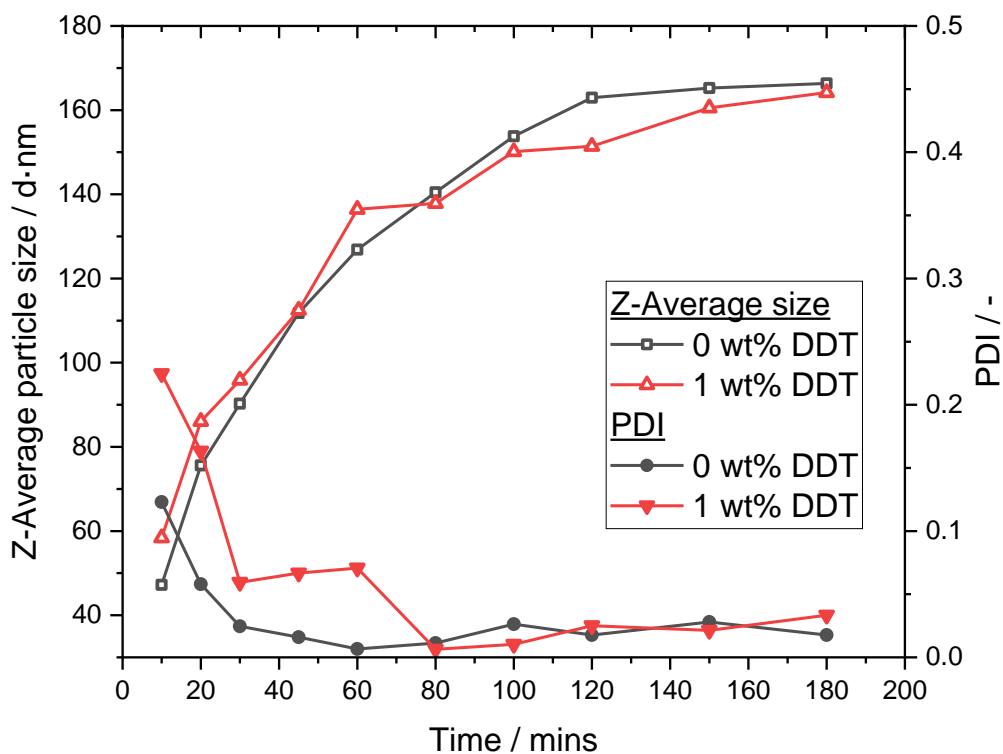


Figure 4.2.1.5: Z-Average particle size and PDI vs time for the semi-batch soap free emulsion copolymerisation of VAc and Na-AMPS (0.5 mol% wrt VAc), with and without DDT.

Both latexes were imaged through scanning electron microscopy (SEM) and can be seen in Figure 4.2.1.6. Interestingly, the particle size distribution in both cases appears relatively broad, despite the narrow PDI reported through DLS of 0.018 and 0.033 without and with DDT, respectively. This behaviour is not unexpected given the water solubility of the monomer likely leading to a long nucleation period. Very little difference between the two images is noted, albeit in the case of DDT some evidence of material which looks like it may have undergone film formation on the SEM sample stub is present, which could be explained through the presence of some low molecular weight material in the sample, although this is far from conclusive.

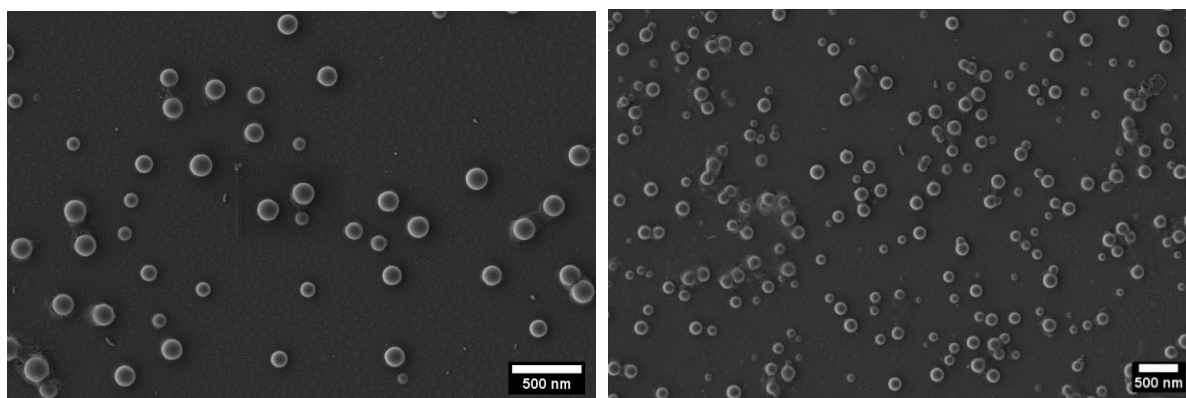


Figure 4.2.1.6: SEM image of the final latex produced during the soap free emulsion copolymerisation of VAc and Na-AMPS (0.5 mol% wrt VAc) in the presence 8.5×10^{-3} M sodium bicarbonate, without (left) and with (right) 1 wt% DDT in the feed. (Scale bars = 500 nm).

Importantly, molecular weight distribution data was still not obtainable for the latex formed in the presence of 1 wt% DDT, suggesting a significant gel content in the particles was still present. It is proposed that this is due to a significant amount of transfer to polymer still being prevalent, given an expected dramatic drift in $[DDT]/[M]$ in the particles. Even by feeding the DDT into the reactor with VAc, the large value of $C_{tr,S}$ essentially leads to spontaneous transfer after radical entry (assuming the presence of DDT in the particle), which may lead to an oscillating concentration of DDT in the particle phase. Significantly increasing the $[DDT]$ may allow access to soluble polymer, however the distribution is still expected to be broad due to composition drift. This may also increase the amount of aqueous transfer, which could contribute to depletion flocculation which can dramatically affect the latex stability, although the low water solubility of DDT likely means this is not a dominant effect. Implementation of a chain transfer agent with $C_{tr,S}$ closer to unity, such as dibutyl disulfide (DBDS), may allow access to polymers with tuneable molecular weight distributions.

4.2.2 Disulfide chain transfer agents in VAc emulsion polymerisation.

DBDS was expected to partition primarily into the particle phase during polymerisation due to the expected low water solubility. Unlike DDT, the concentration of CTA in the particles was not expected to deplete, as $C_{tr,S} = 0.221$ (determined in Chapter 2), and as such, feeding in the CTA should more aptly maintain a consistent concentration ratio in the particles.

As can be seen in Figure 4.2.2.1, increasing the [DBDS] in the feed appears to marginally decrease the rate of polymerisation, with $[DBDS]/[VAc] = 4.76 \times 10^{-3}$ being an anomaly showing cumulative and instantaneous conversion comparable with no DBDS. Due to the hydrophilicity of the transfer derived radical, one could argue that both radical exit and aqueous transfer and termination would result in a reduction in \bar{n} . Nucleation was observed between 9-12 minutes in all cases, after which time the conversion evolution is seen to proceed linearly. The rates of conversion detailed in Table 4.2.2.1 were calculated from the slopes of the conversion plots between 10 and 120 minutes in all cases, where all plots showed high degrees of linearity. All other variables, including the concentrations of buffer, initiator and comonomer were kept constant. The total volume of VAc/DBDS fed into the reactor was kept constant, hence why the feed rate of VAc in moles slightly decreases as the amount of DBDS in the feed increases. The marginal decrease in the rate could be due to the mild retarding effect discussed in Chapter 2, although the reduction was so insignificant that it was not considered an issue. Alternatively, and more likely, it could be due to radical exit, which would then likely lead to broad particle size distributions with lower sizes.

Table 4.2.2.1: Rate of VAc conversion (mol s^{-1}) vs feed rate of VAc (mol s^{-1}) in the semi-batch soap free emulsion copolymerisation of VAc and Na-AMPS (0.5 mol% wrt VAc), with varying concentrations of DBDS in the feed. The total combined volume of VAc and DBDS was kept constant, hence slight reductions in the moles of VAc fed.

[DBDS]/[VAc] in feed	Conversion rate (mol s^{-1})	Feed rate of VAc (mol s^{-1})
0	6.97×10^{-5}	6.45×10^{-5}
1.22×10^{-3}	7.03×10^{-5}	6.44×10^{-5}
2.38×10^{-3}	6.67×10^{-5}	6.42×10^{-5}
4.76×10^{-3}	6.78×10^{-5}	6.39×10^{-5}
9.40×10^{-3}	6.50×10^{-5}	6.33×10^{-5}

As can be seen from the size evolution in Figure 4.2.2.2 the particle size is seen to decrease as [DBDS] increases up to $[DBDS]/[VAc] = 2.38 \times 10^{-3}$. This is similar behaviour to that observed

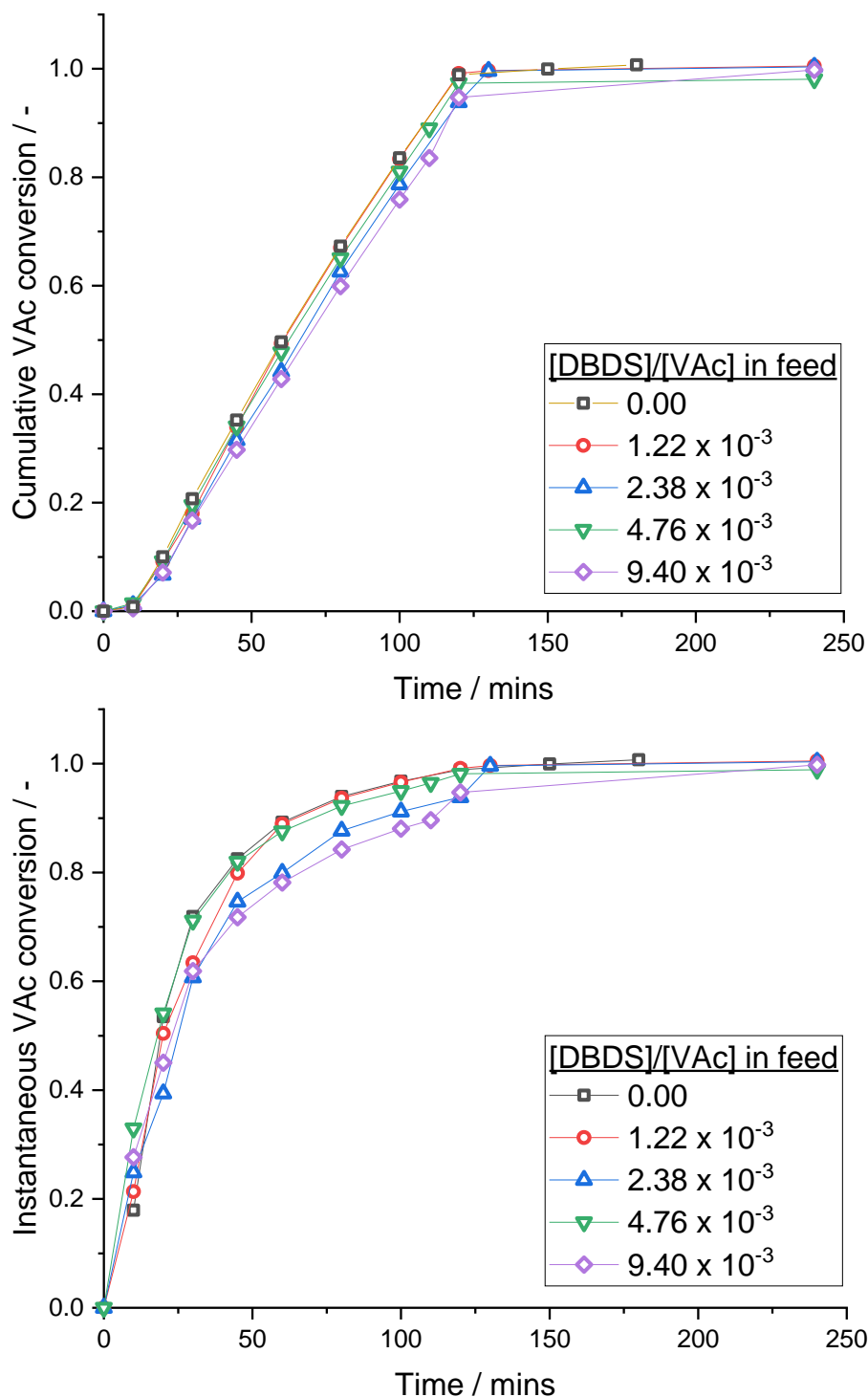


Figure 4.2.2.1: Cumulative (top) and instantaneous (bottom) VAc conversion for the semi-batch soap free emulsion copolymerisation of VAc and Na-AMPS (0.5 mol% wrt VAc), in the presence of DBDS (quantities detailed in the figure legend), determined gravimetrically.

by Fujita *et al.* (1982) for styrene with DDT, as discussed previously.⁵¹ PDI remains relatively low in these experiments suggesting narrow particle size distributions. Interestingly, when $[\text{DBDS}]/[\text{VAc}] = 4.76 \times 10^{-3}$ and 9.40×10^{-3} the size data recorded via DLS became erratic. The PDI values were extremely large, and particularly early into the reaction, the sizes appear

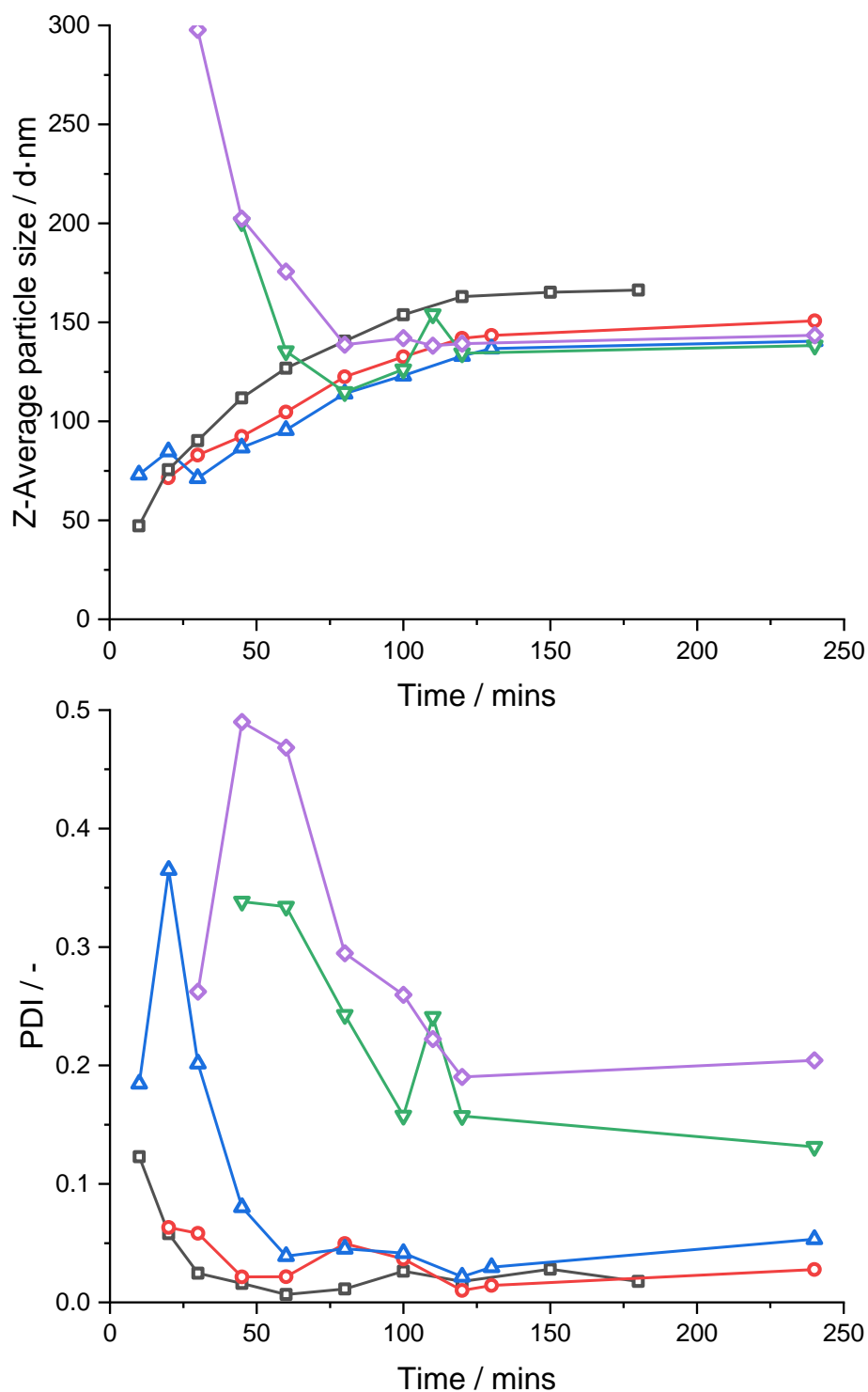


Figure 4.2.2.2: Z-average particle size (top) and PDI (bottom) for the semi-batch soap free emulsion copolymerisation of VAc and Na-AMPS (0.5 mol% wrt VAc), in the presence of DBDS. [DBDS]/[VAc] in feed = 0 (\square), 1.22×10^{-3} (\circ), 2.38×10^{-3} (\triangle), 4.76×10^{-3} (∇) and 9.40×10^{-3} (\diamond).

significantly larger than may be expected. However, it becomes evident when looking at the raw intensity distribution that there is some material present with a significant size, which dramatically effects the data. Given that the scattering intensity (I) scales with $I \propto r^6$, where

r is the radius of the particle (Rayleigh scattering for small particles), a dramatic contribution to the signal is observed from this large contaminant. Indeed, converting to the number distribution (RI PVAc = 1.467) shows that very little material is present at these higher sizes, however, dramatically influences the reported Z-average particle size.

As an example, both the intensity and number distributions are shown of some of the samples for the experiments where $[DBDS]/[VAc] = 4.76 \times 10^{-3}$ and 9.40×10^{-3} in Figures 4.2.2.3. One primary distribution and one distribution at particularly large sizes is observed in the intensity distributions at lower conversion.

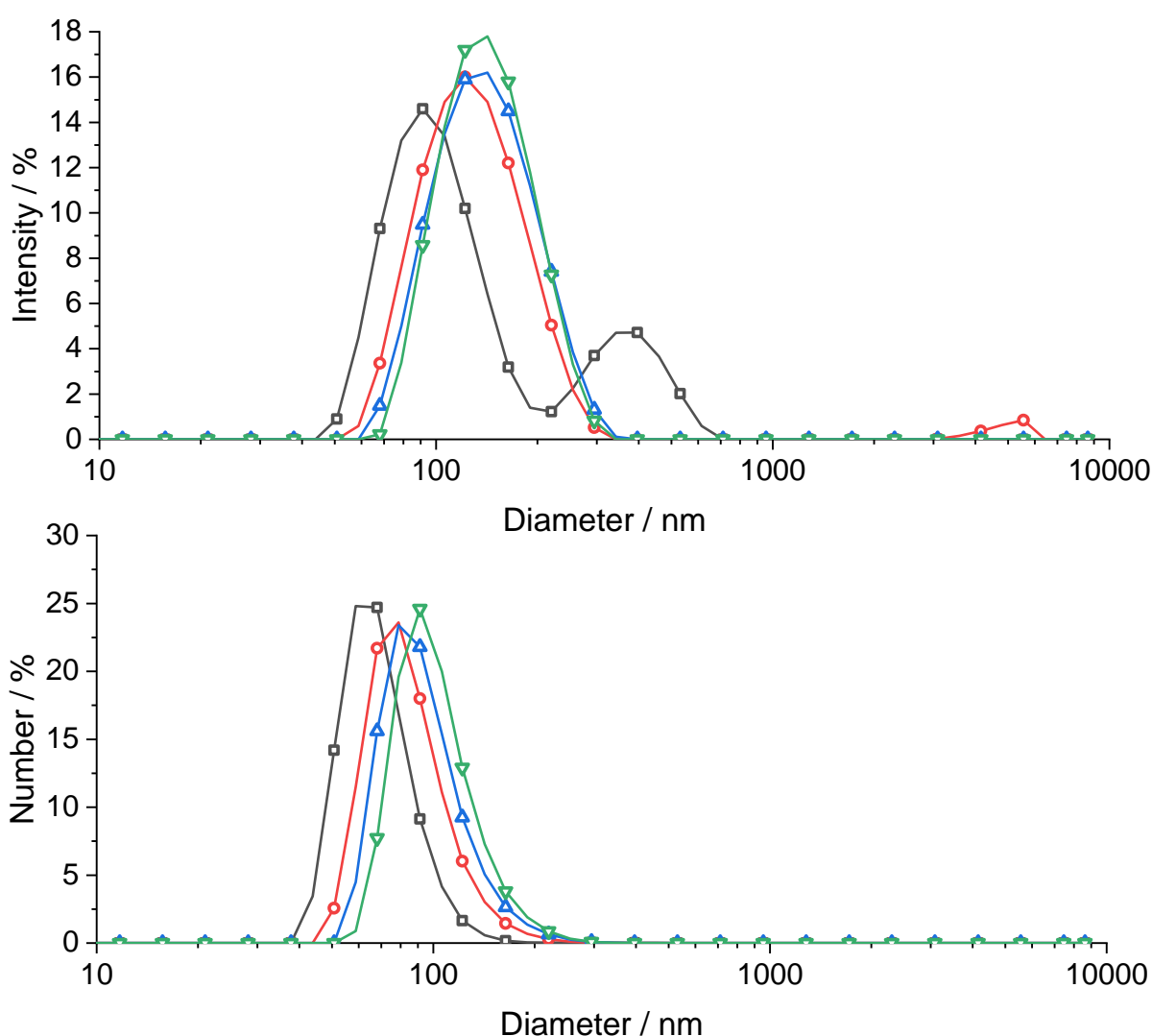


Figure 4.2.2.3: Particle size distributions by scattering intensity (top) and number (bottom) for the semi-batch soap free emulsion copolymerisation of VAc and Na-AMPS (0.5 mol% wrt VAc), in the presence of $[DBDS]/[VAc] = 4.76 \times 10^{-3}$. The distributions correlate to the samples withdrawn after 60 mins (\square), 100 (\circ), 120 (\triangle) and 240 (∇) mins.

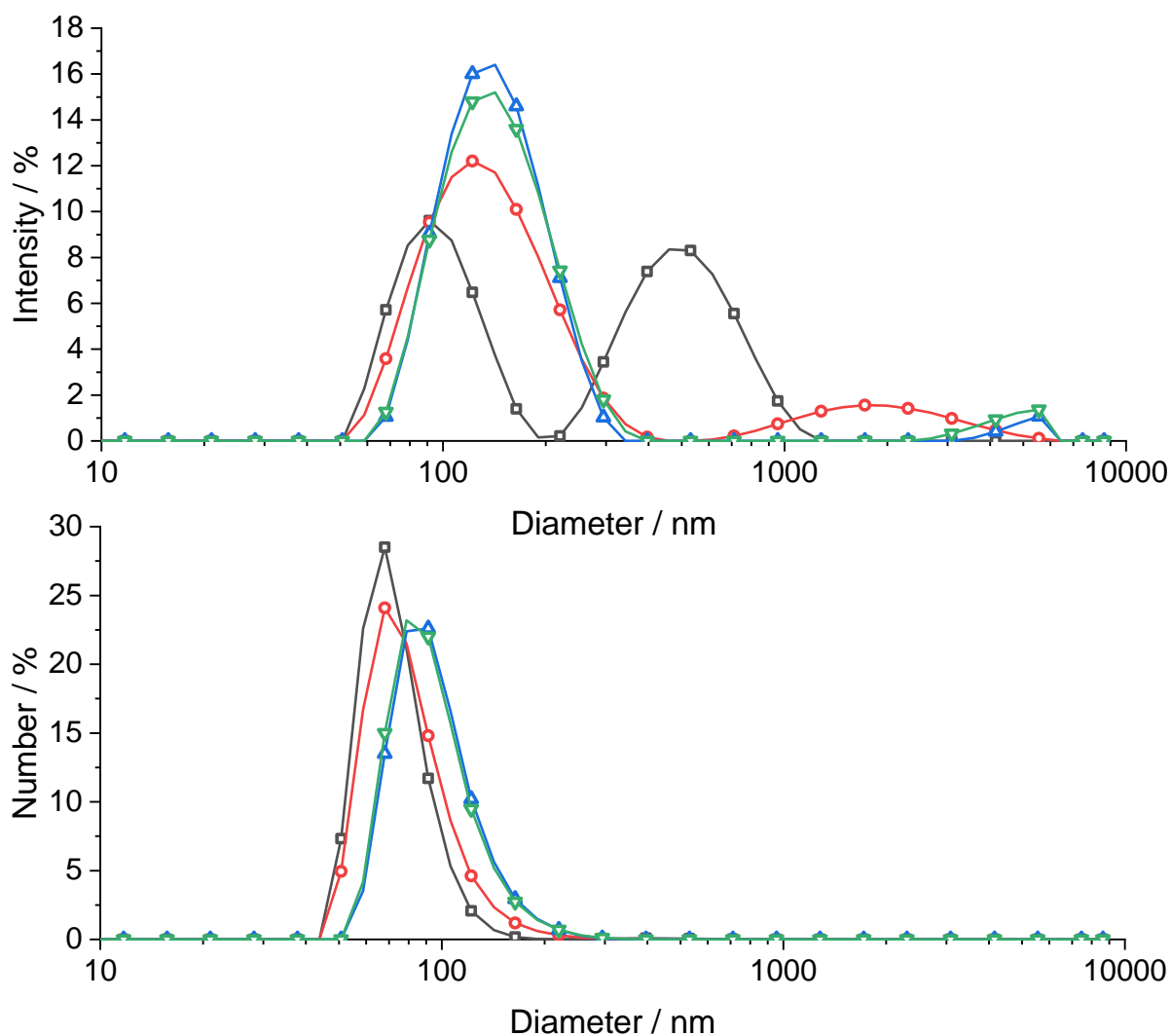


Figure 4.2.2.4: Particle size distributions by scattering intensity (top) and number (bottom) for the semi-batch soap free emulsion copolymerisation of VAc and Na-AMPS (0.5 mol% wrt VAc), in the presence of $[\text{DBDS}]/[\text{VAc}] = 9.4 \times 10^{-3}$. The distributions correlate to the samples withdrawn after 60 mins (\square), 100 (\circ), 120 (\triangle) and 240 (∇) mins.

This could be attributed to small amounts of flocculation/coagulation in the latex, resulting in a number of particles sticking together, due to the aforementioned increase in radical exit and aqueous transfer. It is noted that the distribution at higher size becomes decreasingly significant as the reaction proceeded. No distribution at high sizes is observed in the number distribution for any of the samples, indicating just how small this population is. According to the number distributions, the final particle sizes were 134.9, 116.3, 103.8 and 95.6 $\text{d} \cdot \text{nm}$ for $[\text{DBDS}]/[\text{VAc}]$ in the feed of 1.22×10^{-3} , 2.38×10^{-3} , 4.76×10^{-3} and 9.40×10^{-3} M respectively.

The SEM micrographs of the final latexes can be seen in Figure 4.2.2.5. It becomes evident that up to $[\text{DBDS}]/[\text{VAc}] = 4.76 \times 10^{-3}$ M, monomodal latexes are produced, albeit with relatively broad particle sizes, although these sizes correlate well to those measured in the number

distributions via DLS. However, the latex formed at 9.40×10^{-3} is distinctly bimodal. The larger distribution is around 400-450 nm, with the smaller particles being around 90-110 nm.

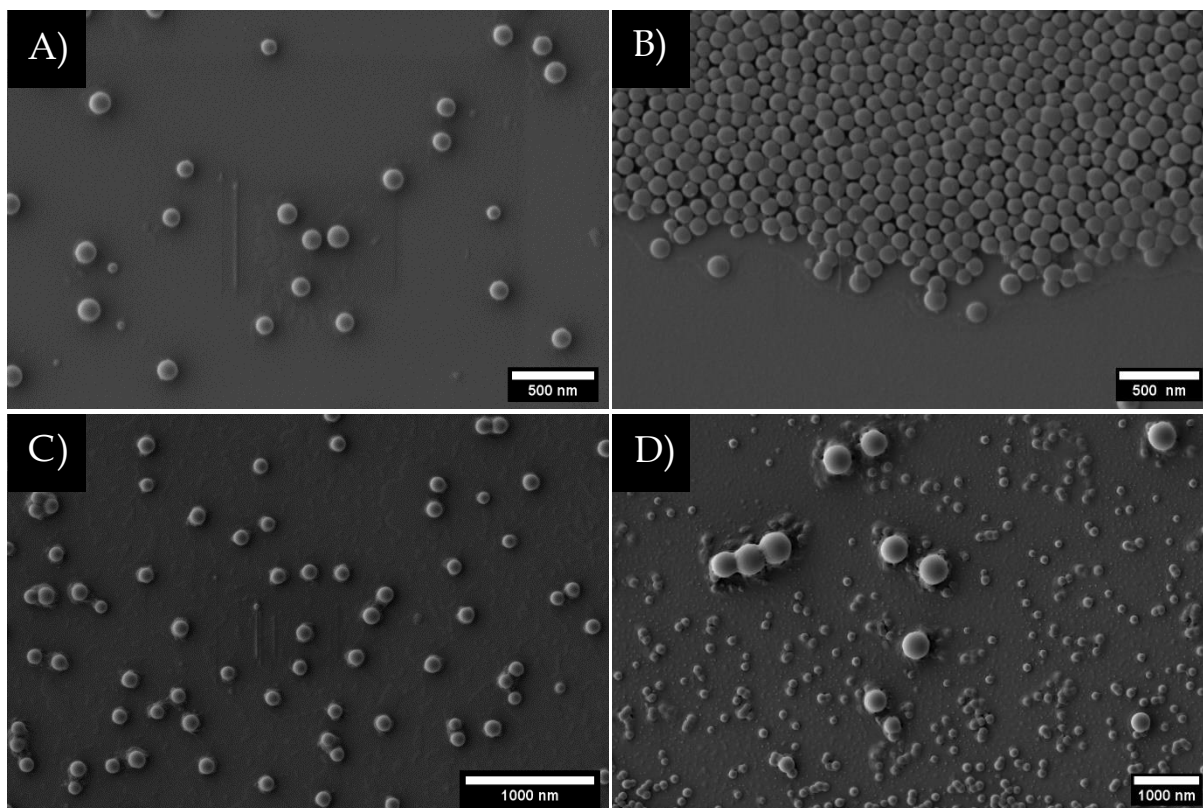


Figure 4.2.2.5: SEM images taken of the final latexes, formed at $[\text{DBDS}]/[\text{VAc}]$ in the feed of 1.22×10^{-3} (A), 2.38×10^{-3} (B), 4.76×10^{-3} (C) and 9.40×10^{-3} (D).

As discussed previously, the increase in radical exit associated with the increase in chain transfer in the particles will result in a higher concentration of radicals in the water phase, and as such will result in more aqueous termination. This, coupled with an increase in aqueous transfer may result in a build-up of water-soluble polymer, which may trigger additional nucleation events. Given the large size of the larger particles observed for $[\text{DBDS}]/[\text{VAc}] = 9.40 \times 10^{-3}$ in the feed, these could also be formed through depletion flocculation, encouraged by the presence of water-soluble polymer. The low T_g of VAc, 31.4°C (which drops even lower below $\text{DP} = 150$),¹¹⁰ could facilitate the interdiffusion of polymer chains in flocculated particles, resulting in the particles merging at the polymerisation temperature (60°C). Alternatively, the larger crop of particles is the primary particle crop, which, as polymerisation progresses grows, with the smaller crop of particles being formed in a secondary nucleation event, again triggered through the presence of significant water-soluble polymer. Unfortunately, due to the ambiguity in the size data this cannot be explored further. The ultimate proof here would be to use SEM as a function of monomer conversion, and

analyse the particle size distributions. The appearance of new particles could then be used to justify the observed behaviours. Comparing the dependence of the particle size distribution on the CTA with DDT, it is clear that DBDS has a larger effect. After transfer to DBDS, the resultant radical is analogous to that of *n*-butanethiol, which is expected to have a significantly higher water solubility than DDT and as such, radical exit will be significantly more prevalent.

In the presence of DBDS, the molecular weight distributions of the final latexes could now be measured, and the collated distributions can be seen in Figure 4.2.2.6. The molecular weight distribution observed when $[DBDS]/[VAc] = 1.22 \times 10^{-3}$ shows a significant high molecular weight shoulder, which as the $[DBDS]$ increases is seen to diminish, along with the whole distribution shifting to lower MW. This is reflected by a decrease in M_n and M_w , along with a general reduction in the ratio M_w/M_n (being the dispersity), as seen in Table 4.2.2.2. The high molecular weight shoulder can be attributed to transfer to polymer. This led the reactions in the absence of DBDS to gel to the point that molecular weight information could not be obtained. The increasing concentration of CTA results in a lower proportion of chains terminated through transfer to polymer. Interestingly, looking at the distributions, even when $[DBDS]/[VAc] = 9.40 \times 10^{-3}$, there is still evidence of transfer to polymer with a high MW tail observed.

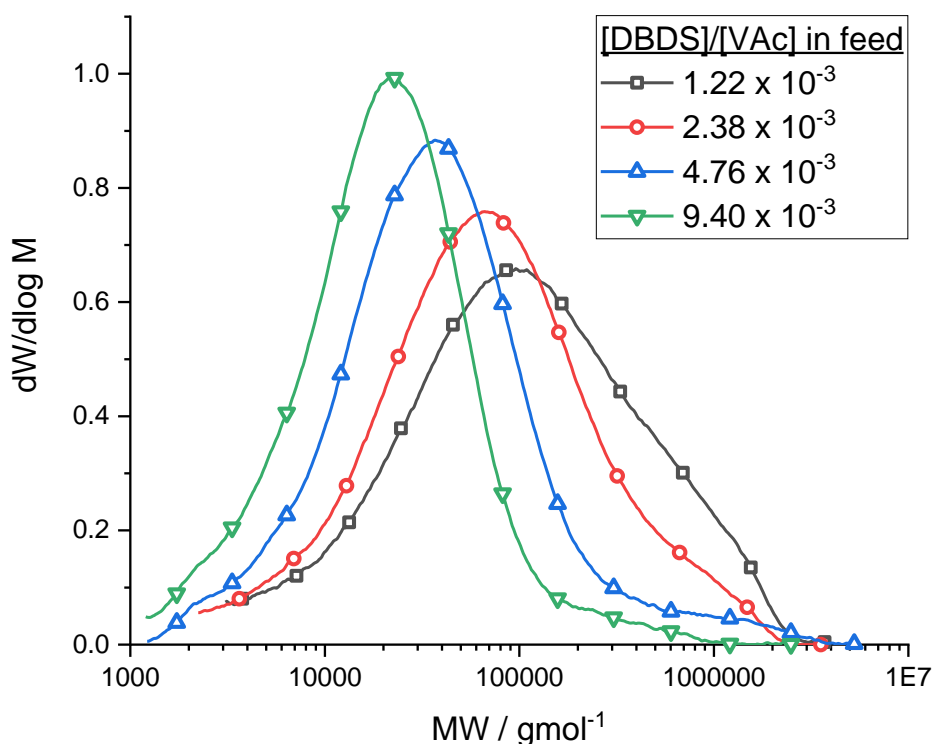


Figure 4.2.2.6: $dw/d\log M$ vs MW distribution for the semi-batch soap free emulsion copolymerisation of VAc and Na-AMPS (0.5 mol% wrt VAc), in the presence of varying $[DBDS]/[VAc]$.

Looking at the molecular weight evolution as a function of time for DBDS = 2.38×10^{-3} , seen in Figure 4.2.2.7, a very marginal drift to lower MW and a slight reduction in the intensity of the high MW shoulder, albeit very slight, is observed. It was noted however that a molecular weight distribution could not be obtained for the sample withdrawn after 30 mins reaction time due to issues filtering the polymer solution, implying gelation. This suggested that perhaps transport of the CTA into the particles was slow. If immediately after nucleation of a new particle there is a delay before CTA diffuses into it, then high molecular weight polymer may be formed. Once the CTA diffuses into these particles however, chain transfer to DBDS should effectively reduce MW, reducing the number of branches per chain. The fact that molecular weight information could not be obtained after 30 mins may imply nucleation was still occurring up to this point. Once enough particles are present to capture radicals effectively, and therefore new particles are not created and all particles contain an appreciable [DBDS], subsequent polymer will be of sufficiently low MW to measure a distribution. This would imply that nucleation finishes between 30 and 60 minutes, which corresponds to a cumulative conversion of $0.17 < p < 0.44$, and a solids content of 4 % to 9%, which seems realistic.¹¹¹ In fact, nucleation must stop significantly before $p = 0.44$ for enough polymer to be formed in the presence of DBDS to obtain molecular weight data. This behaviour may also

Table 4.2.2.2: Number average (M_n) and weight average (M_w) molecular weights for the final latexes produced during the semi-batch soap free emulsion copolymerisation of VAc and Na-AMPS (0.5 mol% wrt VAc), in the presence of varying [DBDS]/[VAc].

[DBDS]/[VAc] in feed	M_n / gmol^{-1}	M_w / gmol^{-1}	M_w/M_n
0	gel	gel	gel
1.22×10^{-3}	40,200	240,300	5.978
2.38×10^{-3}	29,700	150,200	5.057
4.76×10^{-3}	18,500	95,400	5.157
9.40×10^{-3}	11,700	37,700	3.222

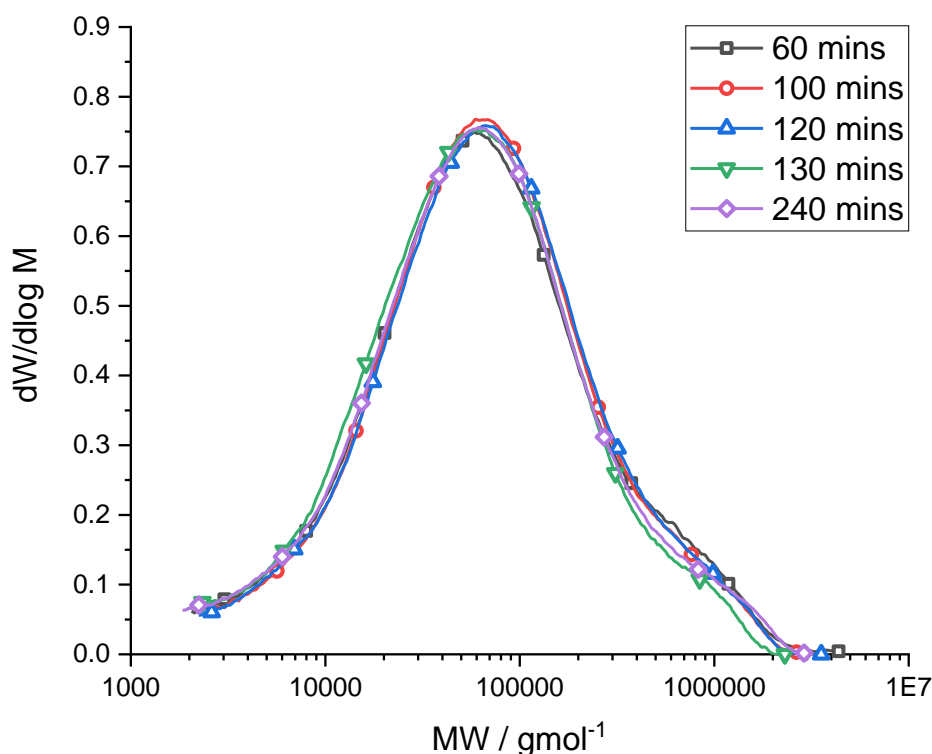


Figure 4.2.2.7: $dW/d\log M$ vs MW distributions as a function of time for the semi-batch soap free emulsion copolymerisation of VAc and Na-AMPS (0.5 mol% wrt VAc), in the presence of $[DBDS]/[VAc] = 2.38 \times 10^{-3}$.

explain the observed increase in slope in the plot of $p^{1/3}$ vs average size discussed earlier in Figure 4.2.1.3, as the efficient capture of radicals in pre-existing particles will cause them to grow faster, instead of new particles nucleating.

This proposal, alongside the relatively small reduction in the intensity of the high MW shoulder with increasing conversion implies the shoulder is due to transfer to polymer, which still occurs to a small extent at the highest $[DBDS]$, encouraged by the high instantaneous monomer conversion. The slight reduction in MW, and the corresponding intensity of the high molecular weight shoulder may be due to $C_{tr,S} < 1$, resulting in an accumulation of DBDS with increasing conversion.

The final molecular weight distributions were used to determine an apparent chain transfer constant, $C_{tr,S}^{app}$, of DBDS in the emulsion polymerisation of VAc, utilising the Mayo method,¹¹² covered extensively in Chapter 1 and 2. The plots of $[DBDS]/[M]$ vs \bar{X}_n^{-1} and vs $2\bar{X}_w^{-1}$ can be seen in Figure 4.2.2.8, from which values for $C_{tr,S}^{app}$ of 0.639 and 0.472 were extracted from the slopes. Evidently, the use of $2\bar{X}_w^{-1}$ introduces significant error, and curvature can be seen in the plot, which can be explained by an increase in branching in the lower $[DBDS]$ concentrations (significantly influencing the weight average molecular weight, M_w). The

obtained values are significantly higher than that observed in solution, where $C_{tr,S}$ was found to be 0.221. This result implies that DBDS partitions more into the particle phase than VAc, which is expected given the difference in water solubility.

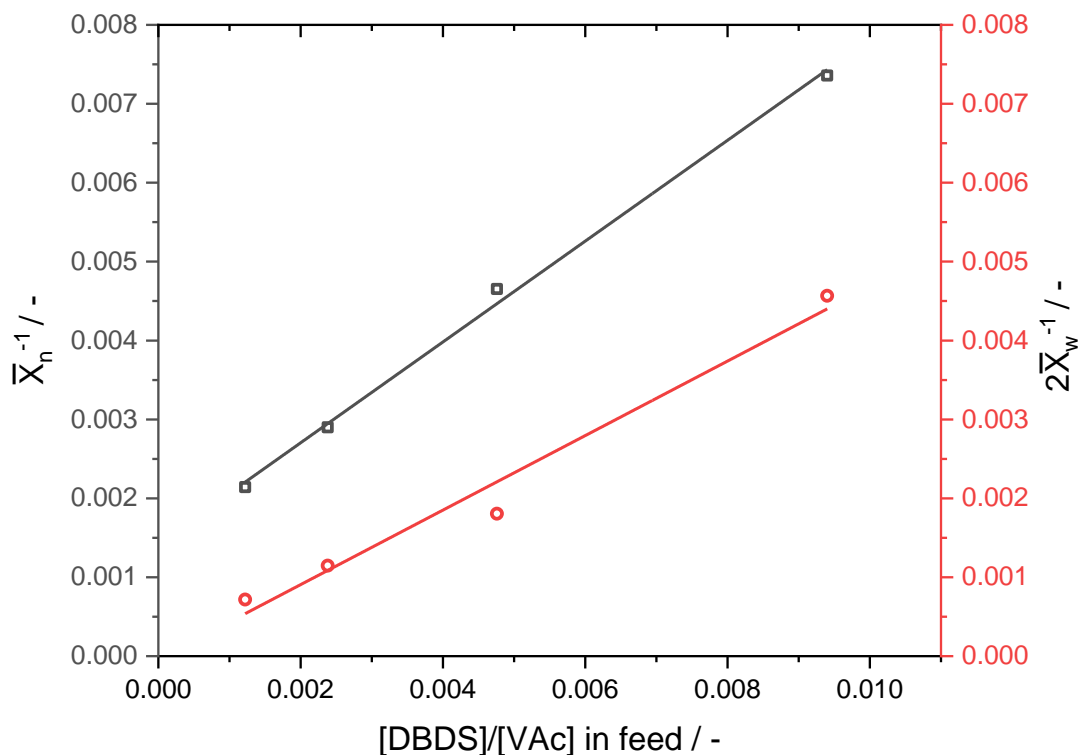


Figure 4.2.2.8: Plots of [DBDS]/[VAc] in the feed vs \bar{X}_n^{-1} and vs $2\bar{X}_w^{-1}$ for the final latexes obtained in the semi-batch soap free emulsion copolymerisation of VAc and Na-AMPS (0.5 mol% wrt VAc), in the presence of varying [DBDS]/[VAc].

This is not without uncertainty however, and many questions are drawn to the validity of these numbers. Firstly, it is worth noting that chain transfer to polymer invalidates Mayo's expression, and significantly influences the molecular weight distributions. Additionally, \bar{X}_n is particularly sensitive to baseline selection. Due to the amount of material seen at very low molecular weight (down to 2000 g mol⁻¹), the elution of some material overlapped with the elution of other low molecular weight species (potentially residual unreacted monomer/CTA etc), and as such the distribution does not tend to 0 on this side, likely dramatically influencing M_n . Also, as mentioned previously, \bar{X}_w is more sensitive to transfer to polymer, which is seen here, further invalidating the use of Mayo's equation.

An alternate and potentially more accurate approach would be to utilise Gilberts CLD method, the details of which were discussed in Chapter 1, wherein the slope of the CLD plot ($\ln n(i)$ vs i) is related to the chain transfer constant through Equation 4.2.2.1.

$$\frac{d \ln n(i)}{d(i)} = - \left(C_{tr,S} \frac{[S]}{[M]} + C_M \right) \quad (4.2.2.1)$$

Careful selection of the region of the distribution used for analysis must be performed to minimise the inaccuracies introduced through transfer to polymer. As discussed by Moad *et al.* (1996), the use of the high molecular weight portion of the CLD plot is typically only used to avoid the potential complication of other termination mechanisms such as combination, or the influence of chain length dependant termination.¹¹³ Authors often use data close to the peak in the $dW/d\log M$ distribution, as the increase in the signal intensity often leads to more accurate $C_{tr,S}$ determination, which has been validated experimentally for chain transfer dominated systems.¹¹³⁻¹¹⁷ Also the marginal drift observed with increasing conversion leads to the assumption that the instantaneous number distribution and the cumulative distributions are essentially equal ($\ln n(i) = \ln N(i)$). Applying this treatment to the data observed here could minimise the error introduced by transfer to polymer. As all parameters besides the [DBDS] are expected to be equivalent between reactions (i.e. radical flux and monomer concentration), any change in the extracted value of $C_{tr,S}^{app}$ between experiments can be assigned to the changing [DBDS].

The plots of $\ln N(i)$ vs i for the final latexes can be seen in Figure 4.2.2.9, and it is clear that curvature is observed at the higher molecular weight side of the distribution, which is explained by transfer to polymer. This correlates well with the high molecular weight fractions seen in the $dw/d\log M$ distributions. However, around the peak of the $dw/d\log M$ distribution, where the signal is most intense, a linear region was observed and the slope was extracted, with the coefficient of determination $R^2 > 0.99$ in all cases. This slope was then used to determine $C_{tr,S}^{app}$ for each sample, (assuming $C_M = 2.7 \times 10^{-4}$, and $[S]/[M]$ is that of the feed). The results for each data set are given in Table 4.2.2.3, with the molecular weight limits utilised for slope extraction.

Table 4.2.2.3: Molecular weight range of each distribution seen in Figure 4.2.2.8 from which $C_{tr,S}^{app}$ was determined using Gilberts CLD method. $[DBDS]/[M]$ (theoretical) is calculated from the slope assuming the real value of $C_{tr,S}$ determined in Chapter 2 in bulk (0.221 at 60 °C).

[DBDS]/[VAc] in feed	Data range used	$C_{tr,S}^{app}$	[DBDS]/[M] (theoretical)
1.22×10^{-3}	$610 < i < 1331$ (52,500 - 114,600 g mol ⁻¹)	1.44	7.96×10^{-3}
2.38×10^{-3}	$334 < i < 1289$ (28,800 - 111,000 g mol ⁻¹)	1.01	1.09×10^{-2}
4.76×10^{-3}	$234 < i < 714$ (20,100 - 61,500 g mol ⁻¹)	0.92	1.97×10^{-2}
9.40×10^{-3}	$152 < i < 495$ (13,100 - 42,500 g mol ⁻¹)	0.74	3.16×10^{-2}

Firstly, it is noted that, like the Mayo method, $C_{tr,S}^{app}$ is higher than the value measured in solution ($C_{tr,S} = 0.221$), which can again be explained by a difference in partitioning between VAc and DBDS between the water/particle phases. Interestingly, $C_{tr,S}^{app}$ decreases with increasing concentration of [DBDS] in the feed. It is hypothesised that this may be due to the lower particle size (therefore higher number of particles) observed with increasing [DBDS],

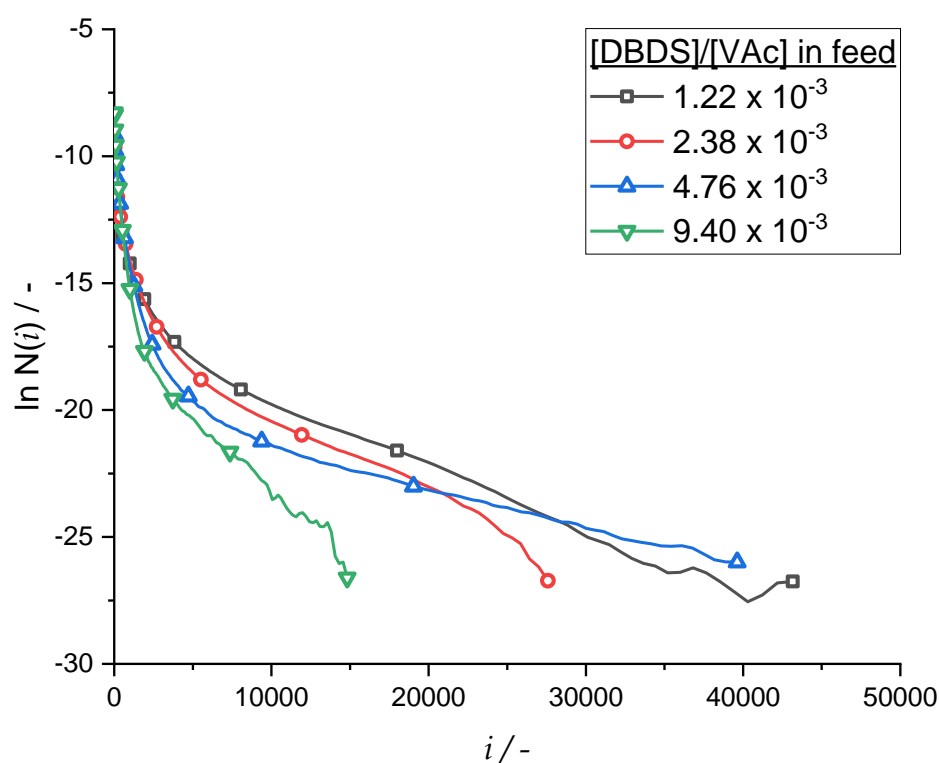


Figure 4.2.2.9: Plots of $[DBDS]/[VAc]$ in the feed vs \bar{X}_n^{-1} and vs $2\bar{X}_w^{-1}$ for the final latexes obtained in the semi-batch soap free emulsion copolymerisation of VAc and Na-AMPS (0.5 mol% wrt VAc), in the presence of varying $[DBDS]/[VAc]$.

which was proposed to be due to more exit and therefore more homogenous nucleation. In the event that transport of DBDS to the particles is slow, an increase in the number of particles would result in a lower concentration of DBDS per particle.

The contribution of the comonomer to the formulation was also assessed, firstly by reducing the concentration of Na-AMPS used. The size (Figure 4.2.2.10) and conversion (Figure 4.2.2.11) evolution of the experiment performed with $[\text{DBDS}]/[\text{VAc}] = 4.76 \times 10^{-3}$ was compared when using 0.5 mol% and 0.25 mol% Na-AMPS wrt VAc in the comonomer feed. This reaction was selected as the evolution of particle size was shown to be particularly erratic during DLS measurements when using 0.50 mol% Na-AMPS, with the previous explanation being aqueous transfer or radical exit leading aqueous termination, both of which contributing to depletion flocculation. Given the copolymerisation behaviour would tend to produce blocky copolymers, and Na-AMPS would primarily reside in the water phase, it was thought that some water-soluble Na-AMPS homopolymer may also be present, which may further contribute to depletion flocculation. As seen in Figure 4.2.2.9, a decrease in $[\text{Na-AMPS}]$ results in much less erratic particle size data, which may support this hypothesis. An additional consequence is an increase in the final particle size achieved, which can be explained through the more logical explanation of less stabilising moieties. The increase in particle size could be used to explain the slight reduction in the rate of polymerisation extracted from the conversion time data given in Figure 4.2.2.10, given the dependence of the rate of polymerisation on the number of particles after nucleation.

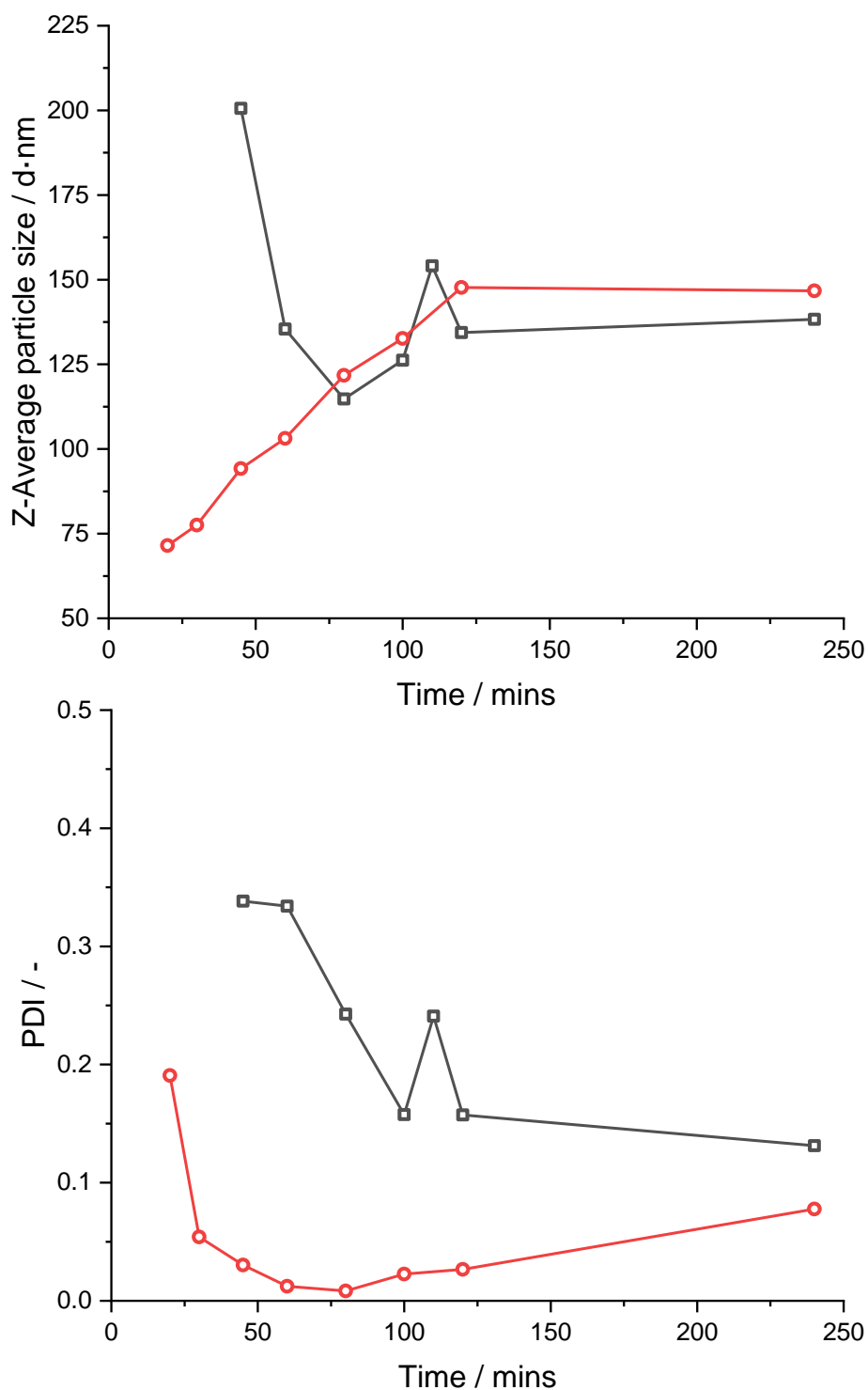


Figure 4.2.2.10: Plots of Z-Average particle size (top) and PDI (bottom) vs time for the semi-batch soap free emulsion copolymerisation of VAc and Na-AMPS. Na-AMPS = 0.5 mol% (□) and 0.25 mol% (○) wrt VAc respectively.

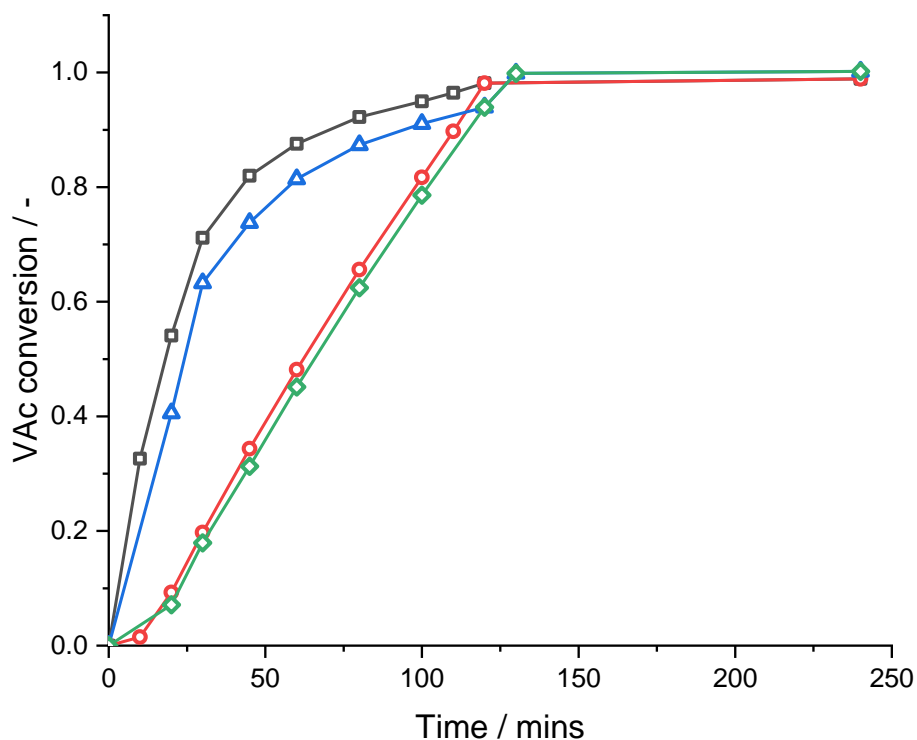


Figure 4.2.2.11: Cumulative VAc conversion vs time where Na-AMPS = 0.50 mol% (○) and 0.25 mol% (◇) wrt VAc, as well as instantaneous VAc conversion vs time where Na-AMPS = 0.50 mol% (□) and 0.25 mol% (△) wrt VAc.

The low PDI's recorded through DLS are supported by the SEM image of the final latex shown in Figure 4.2.2.12, which appears to show a monomodal latex with a relatively narrow particle size distribution.

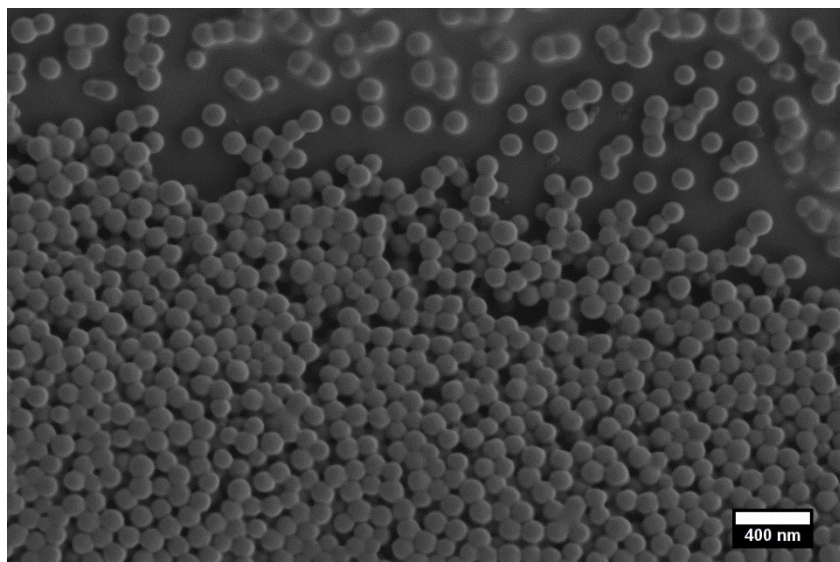


Figure 4.2.2.12: SEM image of the final latex formed in the presence of Na-AMPS fed at 0.25 mol% wrt VAc.

Given the observed influence of the comonomer on the particle size distribution, it was suggested that changing the comonomer to a structure which may copolymerise in a less blocky fashion may contribute to increased stability. The sodium salt of 3-allyloxy-2-hydroxy-1-propanesulfonic acid (Na-AHPSA) was chosen for this purpose (structure given in Figure 4.2.2.13). Although copolymerisation behaviour with VAc could not be found for this monomer, Shigetomi *et al.* (1992) reported kinetics for the copolymerisation of VAc with allyl ethyl ether (AEE), which possessed the same vinylic functionality, reporting $r_{\text{VAc}} = 1.56$ and $r_{\text{AEE}} = 0.041$.¹¹⁸ These values indicate a preference for cross propagation from terminal AEE radicals, with terminal VAc radicals being less selective and more statistical. This is the opposite behaviour of that observed for Na-AMPS ($r_{\text{VAc}} = 0.05$, $r_{\text{Na-AMPS}} = 11.6$).¹⁰⁹

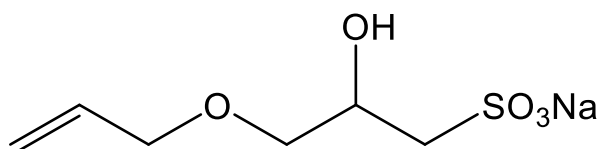


Figure 4.2.2.13: Structure of the sodium salt of 3-allyloxy-2-hydroxy-1-propanesulfonic acid (Na-AHPSA).

$[\text{DBDS}]/[\text{VAc}] = 4.76 \times 10^{-3}$ was used in all experiments utilising Na-AHPSA, so any changes in the kinetics could be attributed to the comonomer alone. Experiments were performed feeding in the comonomer at 0.5 mol% and 0.25 mol% wrt VAc, as was performed with Na-AMPS. Given that blocky regions of comonomer were not expected in copolymerisation with Na-AHPSA, an additional experiment was performed where all of the comonomer was batch added at the start of polymerisation. The overall and instantaneous conversion evolution of these experiments, as well as that for the feed of 0.5 mol% Na-AMPS (for reference) can be seen in Figure 4.2.2.14. The differences between the experiments are slight, with the experiments feeding 0.25 mol% Na-AHPSA and batch addition of 0.5 mol% Na-AHPSA appearing to polymerise slightly slower than the analogous 0.5 mol% Na-AHPSA and Na-AMPS feed experiments. It was noted that after standing overnight, the latexes formed through Na-AHPSA feeds at both concentrations underwent significant sedimentation, although the batch addition was very stable.

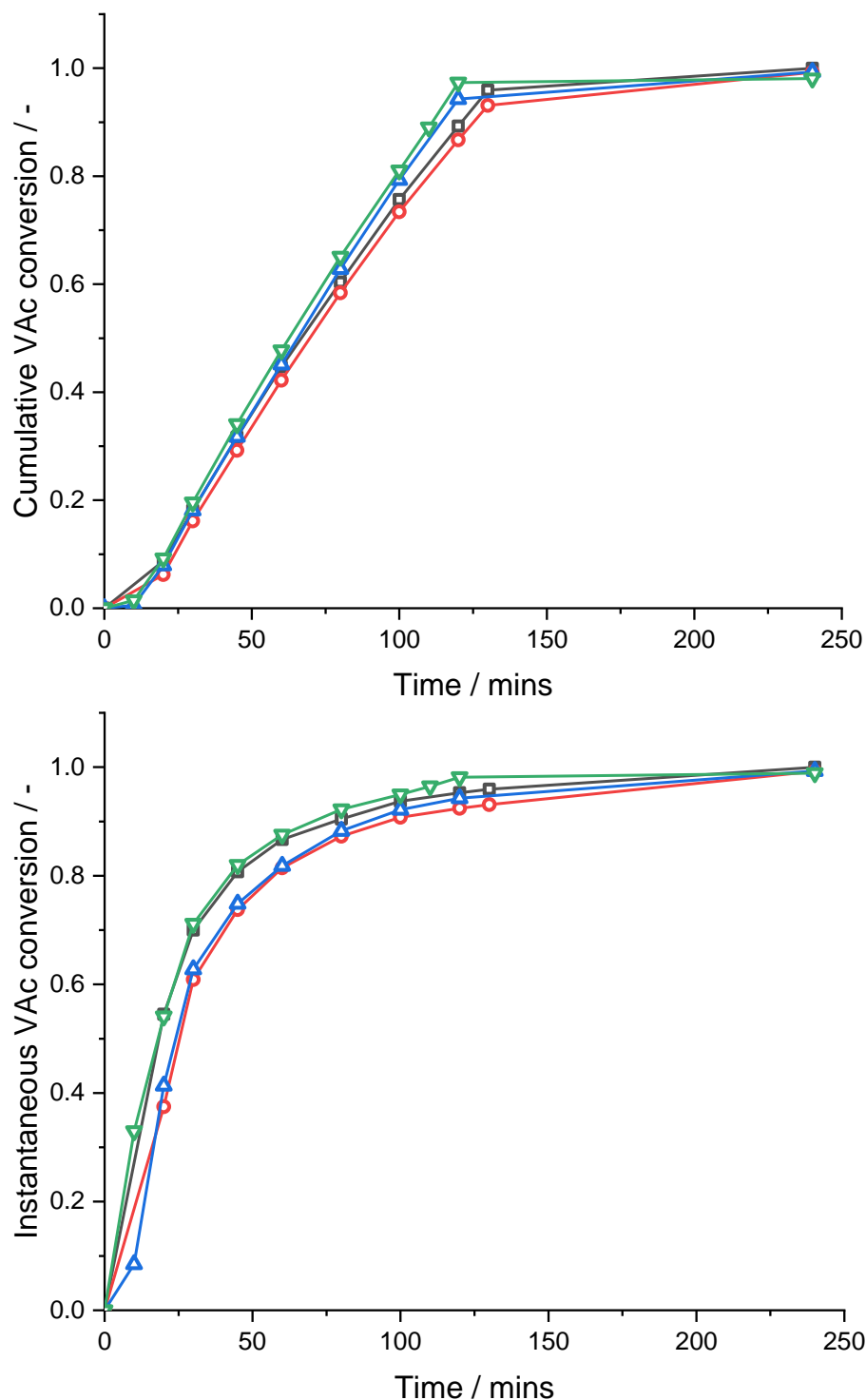


Figure 4.2.2.14: Cumulative VAc conversion (top) and instantaneous VAc conversion (bottom) for the soap free emulsion copolymerisation of VAc and Na-AHPSA/Na-AMPS, in the presence of DBDS ($[DBDS]/[VAc] = 4.76 \times 10^{-3}$). Displayed are experiments performed with linear monomer feeds of Na-AHPSA at 0.5 (\square) and 0.25 (\circ) mol% wrt VAc. Additionally, data for the batch loaded Na-AHPSA (\triangle), where 0.5 mol% is added wrt total VAc fed, and the previously discussed 0.5 mol% Na-AMPS fed linearly (∇) as reference.

The size evolution seen in Figure 4.2.2.15 suggests that the semi-batch experiments with Na-AHPSA yield significantly larger particle sizes than those observed with Na-AMPS, explaining the observed sedimentation. However, they are rather erratic in their growth, and

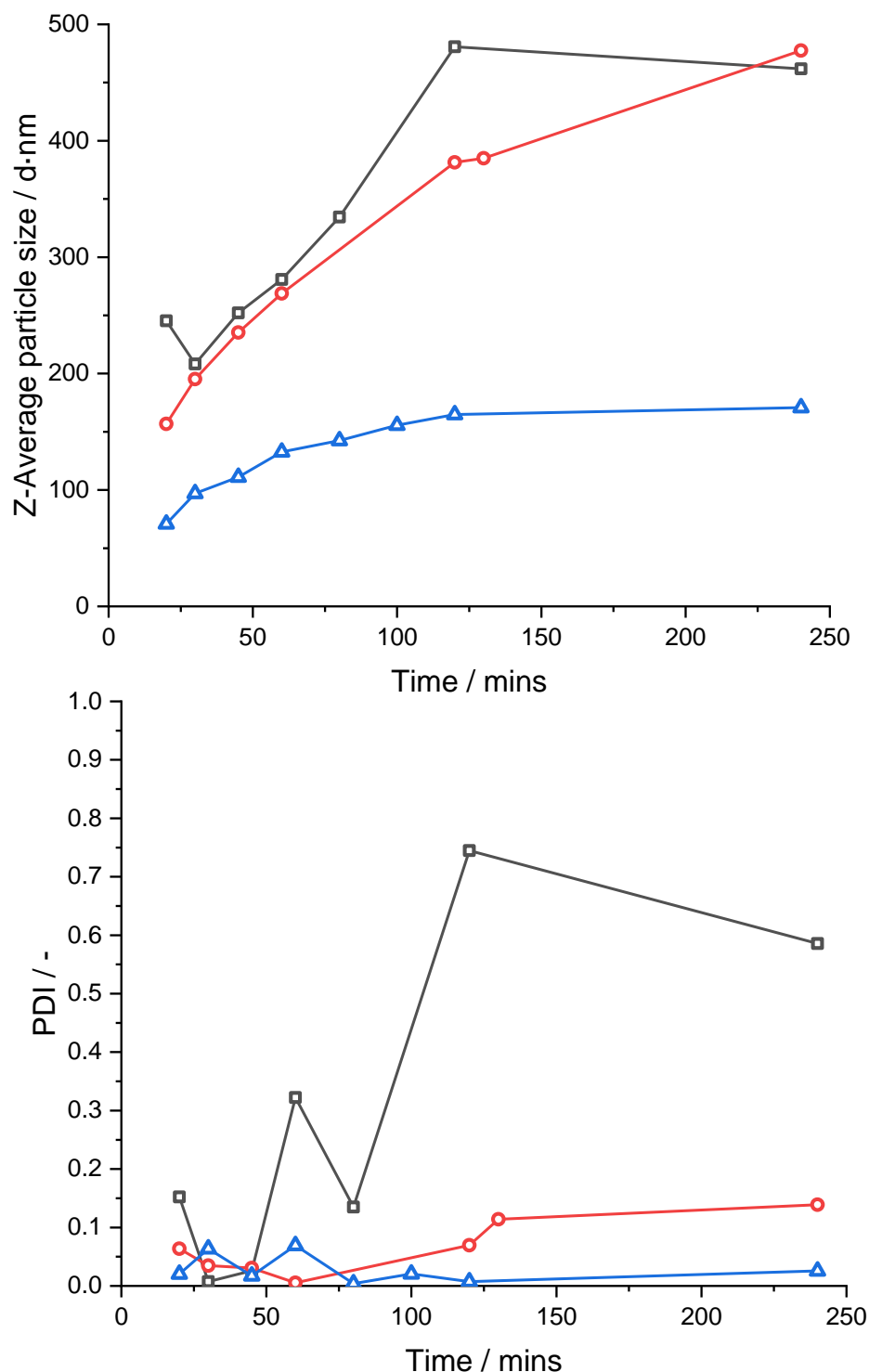


Figure 4.2.2.15: Plots of Z-Average particle size (top) and PDI (bottom) vs time for the semi-batch soap free emulsion copolymerisation of VAc and Na-AHPSA. Na-AHPSA = 0.5 mol% (\square) and 0.25 mol% (\circ) wrt VAc respectively. Also included is the data wherein Na-AHPSA was added batchwise (\triangle).

particularly where Na-AHPSA = 0.5 mol%, the PDI values are extremely high. In fact, the PDI is so high that the reported Z-average particle size cannot be trusted at all. On the other hand, the experiment with batch added Na-AHPSA was extremely stable and shows a gradual increase in particle size with time, and the corresponding low PDI values suggest a very narrow size distribution.

The latexes were imaged by SEM (Figure 4.2.2.16) and some interesting observations can be made. In the case of 0.5 mol % and 0.25 mol% semi batch addition of Na-AHPSA, very little difference in the particle size is observed, with diameters ranging between 330-370 nm in both cases. The particle size distributions appear remarkably monodisperse given the irregularities in the particle size data. However, given the observed sedimentation of the latex after leaving to stand overnight, and the significantly larger particles seen here compared to those formed with AMPS, it is suggested that the copolymerisation results in less effective stabilisation. This may be due to the blocky nature of the AMPS copolymerisation forming poly(Na-AMPS) hairs which extend from the particles offering both electrostatic and steric stabilisation, preventing coagulation of small particles formed through homogenous nucleation.

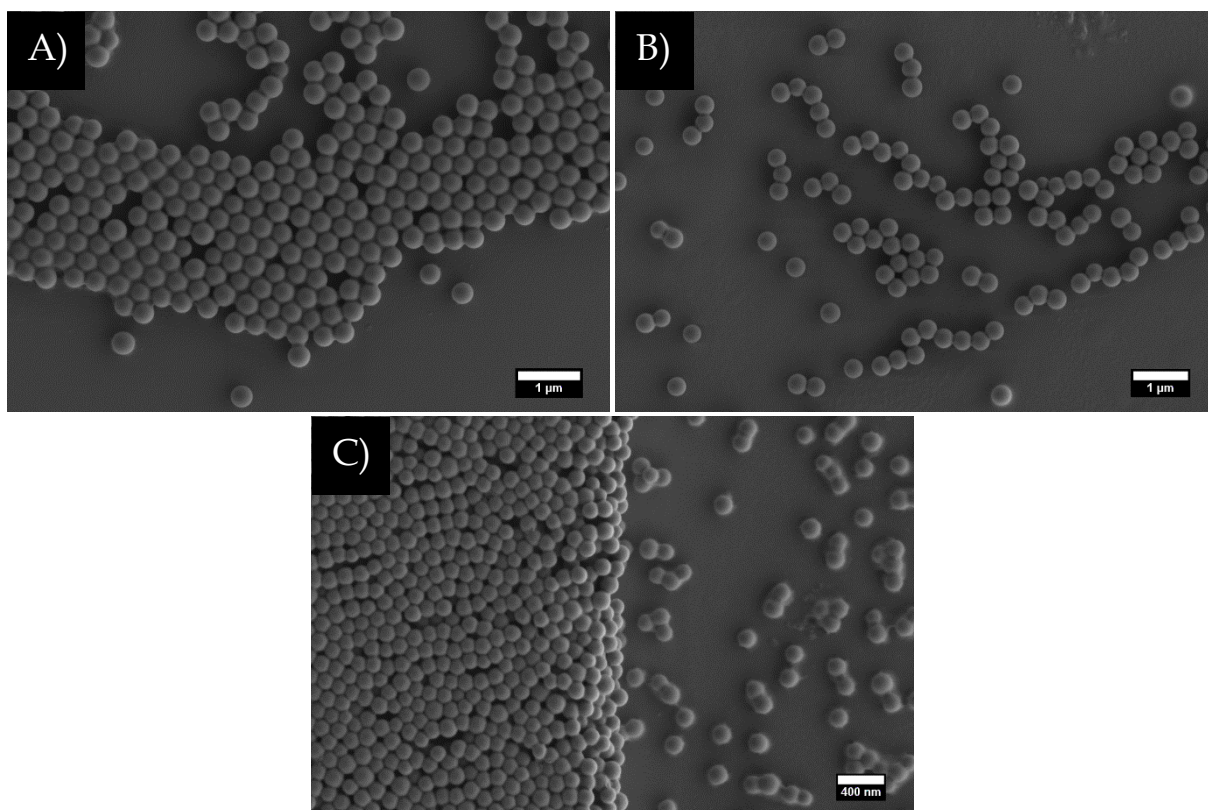


Figure 4.2.2.16: SEM images taken of the final latexes, formed in the presence of 0.5 mol% (A) and 0.25 mol% (B) Na-AHPSA fed alongside VAc, as well as 0.5 mol% Na-AHPSA added batchwise (C). Scale bars = 1 µm, 1 µm and 400 nm for A, B and C respectively.

An alternate conjecture would be an increase in aqueous termination, as after a VAc radical undergoes cross propagation, the relatively unreactive allyl radical does not polymerise well, leading to an increase chance of termination before entry/nucleation.

Batch addition of Na-AHPSA may result in similar behaviour, as at low conversion significant proportions of comonomer will be in the polymers, owing simply to the higher instantaneous concentration ratio of $[Na-AHPSA]/[VAc]$. In this case it is worth noting that the concentration of Na-AHPSA in the polymer at higher degrees of conversion will be significantly lower. As the particles grow, and more interface is created, this may result in insufficient stability afforded to the particles, which may hinder this method of comonomer addition if the solids content of the formulation was increased. Additionally, when the difference in behaviour when acting as a stabiliser in the suspension polymerisation of VCM, two notable distributions of polymer may be expected, one distribution rich in Na-AHPSA, and one distribution rich in VAc.

4.2.3 S-PVC synthesis.

4.2.3.1 Synthesis and analysis

Now that a series of latexes with good stability had been produced in the presence of disulfide chain transfer agents, some of these were trialled as stabilisers in the suspension polymerisation of VCM. This series of experiments was performed at Synthomer plc, due to the safety concerns surround the handling of VCM under high pressure (as discussed in the general introduction, VII). These latexes were applied at the same concentration of polymer in all cases (375 ppm), in addition to a commercial primary stabiliser to aid colloidal stability, at a fixed concentration of 1125 ppm, denoted SYN 1 (DH = 73 mol%). The properties of the produced granules were compared to a commercial secondary stabiliser, denoted SYN 2 (DH = 55 mol%). Although specifics regarding the molecular weight of SYN 2 were not obtainable, this offered a good point of reference to compare the activity. SYN 2 is produced industrially through solution polymerisation of VAc followed by hydrolysis to give the desired DH, a process which is expensive. The one step process used to produce the latexes should reduce this. Additionally, the latexes possess the benefits of being water based rather than synthesised in solvents which are more expensive to acquire and dispose of.

The behaviour of these PVAc latexes in the suspension polymerisation process was hypothesised to proceed through two potential mechanisms, outlined in Figure 4.2.3.1.1. Initially, collision of a latex particle with a VCM monomer droplet would need to occur. The

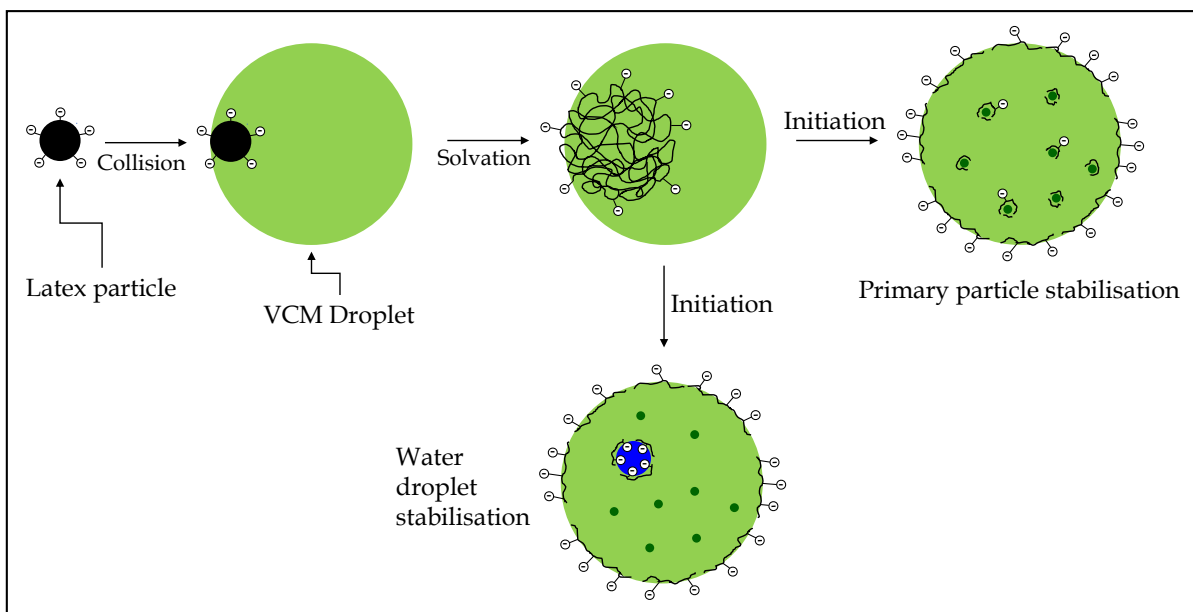


Figure 4.2.3.1.1: Proposed involvement of surfactant free latex particles in the suspension polymerisation of VCM.

compatibility between VCM and VAc would then result in solvation of the VAc particle. However, the surface charge, originating from the charged comonomer or initiator residues, may prevent full entry of the latex particle into the droplet as depicted, meaning this swelling process may well occur at the interface of the droplet. The interesting portion of the process occurs after full solvation, where two behaviours may be observed.

The first proposal is that chains with significant charge would occupy the interface of the droplet, offering colloidal stability and interfacial tension reduction. Additionally, as these chains are at the interface, they may contribute to the pericellular membrane as with conventional PVAc/PVOH copolymers. This is particularly expected for chains with blocky regions of Na-AMPS. However, it is also likely that some chains will remain in the droplet, given that some chains will be PVAc homopolymer with no Na-AMPS residues and no terminal initiator residues (due to initiation by CTA derived radicals). These solvated chains could provide both electrostatic and steric stabilisation to the growing PVC primary particles after introduction of initiator.

Another consideration is the assembly of charged residues within the droplet, which may promote water ingress, forming water droplets within the polymerising droplet. The presence of water droplets within the polymerising droplet may be extremely advantageous, as this may leave a void in the particle, increasing the overall porosity.

The latexes formed with Na-AHPSA as comonomer may behave differently to Na-AMPS latexes, with a different comonomer distribution expected. Full descriptions of the latexes

Table 4.2.3.1.1: Description of the samples test in S-PVC synthesis.

Stabiliser	[DBDS]/[M] in feed	Comonomer
PVAc-1	1.22×10^{-3}	0.50 mol% Na-AMPS
PVAc-2	2.38×10^{-3}	0.50 mol% Na-AMPS
PVAc-3	4.76×10^{-3}	0.50 mol% Na-AMPS
PVAc-4	4.76×10^{-3}	0.25 mol% Na-AMPS
PVAc-5	4.76×10^{-3}	0.50 mol% Na-AHPSA (Batch)
PVAc-6	4.76×10^{-3}	0.50 mol% Na-AHPSA

analysed can be found in Table 4.2.3.1.1. PVAc-6 was included in the study in spite of stability issues, with the latex being filtered through 100 μm gauze to remove any large chunks of coagulum prior to use (with the TSC of the filtered latex being used to determine the loading).

The produced granules were analysed for a number of properties to determine the effectiveness of the stabilisers. The average size of the granules, the so called D50 value, and the grain size distribution (GSD), are mainly influenced if the stabilisers reside at the water/VCM interface. A VCM droplet with increased stabiliser about the interface may occupy a smaller size at a given shear rate due to lower interfacial tension, and would be more colloiddally stable, reducing coagulative events between neighbouring polymerising droplets. The cold plasticiser absorption (CPA) is a measure of porosity, with a more porous grain absorbing more plasticiser. An increase in CPA may imply the internal grain morphology is influenced, however could also reflect a strengthening of the pericellular membrane discussed previously. The bulk density is another commonly measured quantity, and is a function of the porosity, grain size and GSD. Given the parameter measures weight per volume, the presence of significant porosity acts to reduce this number. Additionally, the size and size distribution will contribute to how the granules pack. This parameter is often useful to manufacturers when predicting the outputs rates during extrusion.¹¹⁹

The properties of the resultant PVC granules can be seen in Table 4.2.3.1.2. Generally, the latexes formed in the presence of Na-AMPS appear to reduce the average grain size (D50) compared to SYN 2. When increasing [DBDS]/[VAc] in the feed from 1.22×10^{-3} to 2.38×10^{-3} , the D50 value decreases from 114 μm to 101 μm , which implies that the lower molecular

Table 4.2.3.1.2: Summary of the properties of the PVC granules produced in the presence of SYN 2 and the PVAc latexes described in Table 4.2.3.1.1.

Stabiliser	D50 / μm	GSD	CPA / %	BD Dry / g L^{-1}
SYN 2	120	0.26	28.2	478
SYN 2	114	0.30	29.6	451
SYN 2	129	0.32	32.6	435
PVAc-1	114	0.29	26.6	488
PVAc-2	101	0.33	26.0	487
PVAc-3	109	0.31	26.6	473
PVAc-4	106	0.32	24.0	473
PVAc-5	115	0.29	24.0	489
PVAc-6	124	0.25	24.0	487

weight polymer has more interfacial activity, acting more as a primary stabiliser. However, this is coupled with a marginal increase in GSD. Additionally, a minor decrease in CPA from 26.6 % to 26 % is observed when increasing $[\text{DBDS}]/[\text{VAc}]$. Further increasing $[\text{DBDS}]/[\text{VAc}]$ in the feed to 4.76×10^{-3} , results in an increase in D50 to 109 μm , an increase in CPA back to 26.6, and a reduction of GSD to 0.31. Given the marginal difference between the parameters in this series, attempting to justify these behaviours is likely over analysis of the data, with the likely explanation being variability between batches. In fact, the variability in the data is noted through the 3 entries for SYN 2, which were all performed under identical conditions. The properties of the granules between the 3 runs show notable variability, similar to that in the series of PVAc 1-3. The only observation which appears consistent throughout the runs is that D50 is lower for the latex formulations than for SYN 2, and CPA is higher, implying more activity at the VCM droplet interface than with the primary PVC particles. Another key observation is found when comparing PVAc-3 and PVAc-4, wherein a reduction in CPA from 26.6 to 24.0 is observed when decreasing the feed of Na-AMPS from 0.5 to 0.25 mol% wrt VAc during the emulsion polymerisation process. The implication here is that Na-AMPS affords a difference in the secondary role of the stabiliser, with D50 and GSD remaining virtually unchanged.

The latexes formed with Na-AHPSA appear to have a larger grain size than those formed with Na-AMPS. Comparison between PVAc-3 and PVAc-6, wherein the molar feed rate of comonomer is identical, D50 is 109 and 124 μm for Na-AMPS and Na-AHPSA, respectively.

Additionally, CPA decreases from 26.6 to 24.0 %. Restrictions in time meant further analysis of the produced granules was not possible, however the next steps in this analysis will be outlined in the future work section.

4.2.3.2 Future work

Of particular interest for these experiments would be analysis of the fine structure of the particles through SEM analysis. During this work, a method was optimised to visualise PVC granules internal morphology, through swelling with water, freezing and milling. This was demonstrated for some PVC granules provided by Synthomer plc., formed in the presence of commercial stabilisers, with some example images given in Figure 4.2.3.2.1, which are of significantly higher quality than other examples in the literature. Using this method, the internal morphology could be visualised, and the size of the primary particles could be measured. Additionally, the presence and thickness of the pericellular membrane was observed, which may be a vital parameter in comparing the behaviours of the stabilisers.

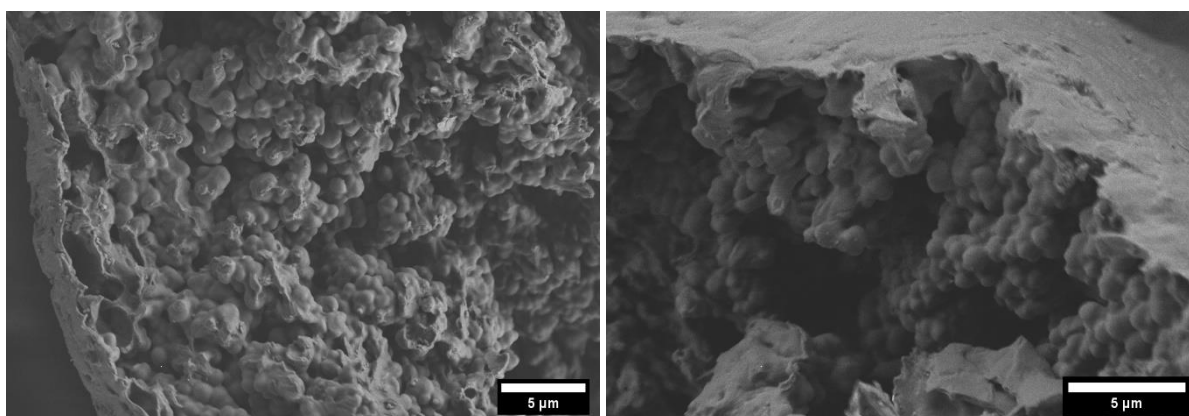


Figure 4.2.3.2.1: Example SEM images of freeze fractured PVC particles.

One experiment which may support the hypothesis of water ingress would be to simply prepare an emulsion of VCM in water in the presence of latex, and to observe the droplet under a light microscope. However, given the high pressure required to maintain VCM in a liquid state, a model compound, such as 1-chlorobutane, may be used.^{120,121} In the event that water droplets are formed in the polymerising droplets, the actual mechanism is likely a blend between the two proposed behaviours, with some solvated polymer also contributing to PVC primary particle stability.

Additional areas of interest for furthering this chapter would be the control of branch density in the emulsion polymerisation of VAc, utilising the knowledge gained in copolymerisation with multi-functional vinyl monomer in chapter 3. It is thought that the polymer architecture

may play a role in the stabiliser's activity in S-PVC synthesis, therefore would be a beneficial avenue for exploration. The industrial applicability of these formulations could be pushed even further, through increasing the solids contents of the latexes, an advancement which was outside of the scope of this work.

4.2.4 Conclusions.

The soap free emulsion polymerisation of vinyl acetate has been demonstrated in the presence of two comonomers, Na-AMPS and Na-AHPSA, exploiting disulfide chain transfer agents. The evolution of the polymerisation was shown to be highly dependent on both the selection of the comonomer, and the concentration of CTA used. The dependence of the comonomer was attributed to the copolymerisation behaviour, dramatically influencing the particle size evolution. The influence of the CTA on the course of the polymerisation was justified through desorption of CTA derived radicals from the particles. The molecular weight distribution of the produced polymers was effectively reduced with an increase in [CTA], despite starved monomer feed addition. These latexes were tested for effectiveness as stabilisers in S-PVC synthesis and appeared to act as primary stabilisers, influencing the granule size more than the porosity of the final granules.

Given the ability to reduce molecular weight through introduction of CTA, the introduction of complex branched architectures, discussed in chapter 3, could be extended to work in emulsion polymerisation. These branched polymers may show interesting behaviours as S-PVC stabilisers. Additionally, the limits of stability of these latexes was not pushed to high solids contents, which may pose another challenge. Although the latexes tested here did not increase porosity to the same extent as the commercial secondary stabilisers, this work provides a good foundation for further exploration, particularly through the aforementioned polymer architecture, as well as through modification of the comonomer system in both composition and loading.

4.3 Experimental

Materials

Vinyl acetate (VAc, Aldrich, $\geq 99\%$), sodium bicarbonate (Aldrich, $\geq 99.7\%$), sodium citrate monobasic (Aldrich, $\geq 99.0\%$), sodium persulfate (NaPS, Aldrich, $\geq 99\%$), 2-acrylamido-2-methyl-1-propanesulfonic acid (sodium salt solution) (Na-AMPS, Aldrich, 50 wt% in H₂O), 3-Allyloxy-2-hydroxy-1-propane sulfonic acid (sodium salt solution) (Na-AHPSA, Aldrich, 40

wt% in H₂O), were all used without further purification. S-PVC samples were made and characterised by Synthomer plc, although the SEM images given in Figure 4.2.3.2.1 were obtained by the author.

Characterization

Size exclusion chromatography (SEC).

Molecular weight distributions were determined on an Agilent Infinity II MDS instrument equipped with differential refractive index (DRI), viscometry (VS), dual angle light scatter (LS) and multiple wavelength UV detectors. The system was equipped with 2× PLgel Mixed C columns (300 × 7.5 mm) and a PLgel 5 μm guard column. The eluent was THF with 0.01 % BHT (butylated hydroxytoluene). Samples were run at 1 mL min⁻¹ at 30 °C. Polystyrene standards (Agilent EasyVials) were used for calibration. Analyte samples were filtered through a PTFE filter with a 0.2 μm pore size before injection. Polymer molecular weight information was estimated using universal calibration, utilizing the Mark-Houwink-Sakurada parameters, $K = 5.01 \times 10^{-5} \text{ dL mol}^{-1}$ and $\alpha = 0.78$ for poly(vinyl acetate), and $K = 14.1 \times 10^{-5} \text{ dL mol}^{-1}$ and $\alpha = 0.70$ for polystyrene.¹²²

Dynamic Light Scattering (DLS).

Particle size measurements were performed on a Malvern Zetasizer Ultra at 25 °C in deionized water, at a scattering angle of 173° at 25 °C in filtered deionized water. Three replicate runs were conducted for each sample, and the reported values of Z-average particle size and PDI are averages of these three runs.

Scanning electron microscopy (SEM).

Images of latex particles were recorded on a ZEISS Gemini scanning electron microscope. Samples were imaged at an accelerating voltage of 0.25 kV, at a working distance of 1.6-2 mm using an in lens detector. Before imaging, samples were sputtered with a thin layer of carbon to reduce charging. For PVC samples, imaging was achieved using a secondary electron detector, at an accelerating voltage of 2 kV and a working distance of 4.5-5 mm. The PVC samples were first swollen with water overnight, before being added to a pestle and mortar and quickly frozen with the addition of liquid N₂. Whilst frozen the granules were extensively milled in a pestle and mortar.

Cold Plasticiser Absorption (CPA).

PVC resin (2.5 g) and dioctyl phthalate (4.0 g) were added into a vessel containing a membrane. The sample was then centrifuged at 10,000 rpm for 60 minutes. The vessel was then reweighed and the mass of absorbed dioctyl phthalate determined. This value was then divided by the mass of PVC resin to give the final CPA value in %.

Final bulk density (FBD) - In accordance with ASTM 1895B.

PVC resin was thoroughly dried in a fluid bed dryer at 50 °C for 60 minutes. The PVC was then allowed to cool before being poured into a stainless-steel container with a precise volume of 100 cm³. The mound of PVC was levelled with a sharp blade and the container weighed. The recorded mass of PVC was then used to determine the bulk density in g L⁻¹.

Grain size (D50) and Grain size distribution (GSD).

PVC resin (12.5 g) was placed in the top of a stack of sieves consisting of 315, 250, 200, 160, 100 and 75 µm sieves and a collecting pan for anything smaller than 75 µm. The stack was secured to a vibrating device and shaken for 15 minutes. The mass of PVC in each individual sieve was recorded and each value divided by 12.5 to give a percentage of the total mass made up by that sieve size. These values were plotted on a logarithmic scale and the value at which 50 % of the mass is reached (D50) determined. The values for 16 % (D16) and 84 % (D84) are also determined for calculation of the GSD. The reported GSD is the ratio of $\sigma/D50$, where $\sigma = (D84-D16)/2$.

Synthesis

Semi-batch soap free emulsion copolymerization of vinyl acetate with sulfonated comonomer (example quantities for [DBDS]/[VAc] = 4.76×10^{-3} , [sodium bicarbonate]_{aq} = 8.5×10^{-3} M, with 0.5 mol% Na-AMPS wrt VAc). Note: Buffer type, buffer amount, CTA amount, comonomer and comonomer amount and comonomer addition methods were all varied as detailed in the text).

Water (157 g) and sodium bicarbonate (0.1125 g, 5.3×10^{-4} mol) were added to a 4 necked jacketed 250 mL glass reactor, fitted with a PTFE anchor overhead stirrer, and a PTFE temperature probe. The other necks were sealed with rubber septa. The reactor contents were purged with N₂ for 1 h, with stirring at 250 rpm. Vinyl acetate (60 g, 0.7 mol) and dibutyl disulfide (0.6 g, 3.3×10^{-3} mol) were added to a 100 mL RBF, fitted with a magnetic stirrer and

sealed with a suba seal. A 50 wt% aqueous Na-AMPS solution (3.60 g, 7.9×10^{-3} mol) was diluted with further water (12.00 g) and added to a 20 mL crimp vial, fitted with a magnetic stirrer and sealed with a PTFE crimp lid. Alongside this, a solution of NaPS (1.17 g, 4.9×10^{-3} mol) in water (12.00 g) was prepared in a 20 mL crimp vial fitted with a magnetic stirrer and sealed with a PTFE crimp lid. All solutions were purged with N_2 for 1 h. The reactor temperature was raised to 60 °C, at which point 4 mL of the NaPS solution was injected under N_2 . Simultaneously, the two monomer feeds were started at 21.41 and 2.5 mL/h for the VAc/DBDS and AMPS feeds respectively. Both feeds were allowed to proceed for 2 h, after which time polymerisation was allowed to proceed for a further 2 h. (Note in the case of the batch addition of Na-AHPSA, all of the comonomer feed was added before initiator injection, and the VAc/DBDS was fed as before over 2 h). $p = 0.99$. SEC: $M_n = 18,500 \text{ g mol}^{-1}$, $M_w = 95,400 \text{ g mol}^{-1}$. DLS: Z-average particle size = 138.3 d · nm, PDI = 0.131.

Suspension polymerisation of PVC. (Example quantities & characterisation for secondary stabiliser formed at $[DBDS]/[VAc] = 4.76 \times 10^{-3}$, $[\text{sodium bicarbonate}]_{\text{aq}} = 8.5 \times 10^{-3} \text{ M}$, with 0.5 mol% Na-AMPS wrt VAc).

Water (350 g), sodium bicarbonate (800 ppm wrt VCM), Perkadox 16 (0.19 g, 4.8×10^{-4} mol) SYN 1 (1125 ppm wrt VCM) and secondary stabiliser (375 ppm wrt VCM) were added to a stainless steel 1 L reactor, which was then sealed. Nitrogen was added to a pressure of 10 bar to confirm a good seal. The pressure was then released and VCM (189 g, 3.02 mol) was added. The temperature of the reactor was raised to 57 °C and stirring was started at 750 rpm. After 15 minutes the pressure was recorded. Once the pressure inside the reactor had dropped by 2 bar, the reactor was vented, and the removal of unreacted VCM was achieved under vacuum for 1 h. The resultant PVC was filtered and dried in air to constant mass. $D_{50} = 109 \text{ }\mu\text{m}$, $GSD = 0.31$, $CPA = 26.6 \%$, $FBD = 473 \text{ g L}^{-1}$.

4.4 References

- 1 R. Darvishi, M. N. Esfahany and R. Bagheri, *Ind. Eng. Chem. Res.*, 2015, **54**, 10953–10963.
- 2 Y. Saeki and T. Emura, *Prog. Polym. Sci.*, 2002, **27**, 2055–2131.
- 3 *PVC Autoclave model [study group report]*, ICI Engineering, 1995.
- 4 Y. Bao and B. Brooke, *J. Appl. Polym. Sci.*, 2002, **85**, 1544–1552.
- 5 C. Kiparissides, I. Moustakis and A. Hamielec, *J. Appl. Polym. Sci.*, 1993, **49**, 445–459.
- 6 D. G. Rance and E. L. Zichy, *Polymer (Guildf.)*, 1979, **20**, 266–268.
- 7 D. E. Witenhafer and J. A. Davidson, *J. Polym. Sci. Phys. Ed.*, 1980, **18**, 51–69.
- 8 S. Ormondryod, *Br. Polym. J.*, 1988, **20**, 353–359.
- 9 A. H. Alexopoulos and C. Kiparissides, *Chem. Eng. Sci.*, 2007, **62**, 3970–3983.
- 10 M. K. Naqvi, *JMS-REV. Macromol. Chem. Phys.*, 1985, **C25**, 119–155.
- 11 W. H. Starnes, *J. Polym. Sci. A-1 Polym. Chem.*, 2005, **43**, 2451–2467.
- 12 D. Braun, *Pure Appl. Chem*, 1971, **26**, 173–192.
- 13 M. Asahina and M. Onozuka, *J. Polym. Sci. A-1 Polym. Chem.*, 1964, **2**, 3505–3513.
- 14 M. Zerfa, *PhD Thesis, Univ. Loughbrgh.*, 1994, 292.
- 15 H. Nilsson, T. Norviit, C. Silvegren and B. Tornell, *J. Vinyl Technol.*, 1985, **7**, 119–122.
- 16 W. D. Harkins, *J. Am. Chem. Soc.*, 1947, **69**, 1428–1444.
- 17 W. D. Harkins, *J. Polym. Sci.*, 1950, **5**, 217–251.
- 18 P. A. Lovell and F. J. Schork, *Biomacromolecules*, 2020, **21**, 4396–4441.
- 19 I. A. Maxwell, B. R. Morrison, D. H. Napper and R. G. Gilbert, *Macromolecules*, 1991, **24**, 1629–1640.
- 20 H. De Bruyn, *PhD Thesis, University of Sydney, 'The Emulsion Polymerization of Vinyl Acetate'*, 1999.

- 21 W. V. Smith, *J. Am. Chem. Soc.*, 1948, **70**, 3695–3702.
- 22 W. V. Smith and R. H. Ewart, *J. Chem. Phys.*, 1948, **16**, 592.
- 23 B. R. Patsiga, M. Litt and V. Stannett, 1960, **171**, 1958–1961.
- 24 S. Okamura and T. Motoyama, *J. Polym. Sci.*, 1962, **58**, 221–227.
- 25 J. W. Breitenbaeh, H. Edelhauser and R. Hochrainer, *Monatshefte für Chemie*, 1968, **99**, 625–634.
- 26 M. Litt, R. Patsiga and V. Stannett, *J. Polym. Sci. A-1 Polym. Chem.*, 1970, **8**, 3607–3649.
- 27 D. M. French, *J. Polym. Sci.*, 1958, **32**, 395–411.
- 28 J. T. O'Donnell, R. B. Mesrobian and A. E. Woodward, *J. Polym. Sci.*, 1958, **28**, 171–177.
- 29 S. Werner and H. Freudenberger, *US Patent 2227163*, 1940.
- 30 J. W. Bristol, W. A. Harrington and T. Norris, *US Patent 2662863*, 1953.
- 31 W. R. Conthwaite and H. W. Bryant, *US Patent 2485141*, 1946.
- 32 W. H. Starnes, H. Chung and G. M. Benedikt, *Polym. Prepr. (Am. Chem. Soc., Div. Polym. Chem.)*, 1993, **34**, 604.
- 33 H. Bruyn and R. G. Gilbert, *Macromolecules*, 1996, **29**, 8666–8669.
- 34 C. M. Gilmore, G. W. Poehlein and F. J. Schork, *J. Appl. Polym. Sci.*, 1993, **48**, 1449–1460.
- 35 G. S. Whitby, M. D. Gross, J. R. Miller and A. J. Costanza, *J. Polym. Sci.*, 1955, **16**, 549–576.
- 36 W. P. Hohenstein and H. Mark, *J. Polym. Sci.*, 1946, **1**, 549–580.
- 37 R. M. Fitch, M. B. Prenosil and K. J. Sprick, *J. Polym. Sci. Part C*, 1969, **27**, 95–118.
- 38 R. M. Fitch and C. H. Tsai, in *Polymer Colloids*, 1971, pp. 73–102.
- 39 F. K. Hansen and J. Ugelstad, *J. Polym. Sci. A-1 Polym. Chem.*, 1978, **16**, 1953–1979.
- 40 F. K. Hansen and J. Ugelstad, *J. Polym. Sci. A-1 Polym. Chem.*, 1979, **17**, 3033–3045.

- 41 J. Ugelstad and F. K. Hansen, *Rubber Chem. Technol*, 1976, **49**, 536–609.
- 42 R. G. Gilbert, *Emulsion polymerisation: a mechanistic approach*, 1995.
- 43 C. S. Chern and G. W. Poehlein, *J. Appl. Polym. Sci.*, 1987, **33**, 2117–2136.
- 44 N. Friis and L. Nyhagen, *J. Appl. Polym. Sci.*, 1973, **17**, 2311–2327.
- 45 W. J. Priest, *J. Phys. Chem.*, 1952, **56**, 1077–1082.
- 46 M. Harada, W. Eguchi, M. Nomura, K. Nakagawara and S. Nagata, *Chem. Eng. Jpn.*, 1971, **4**, 160–166.
- 47 V. Stannett, A. Klein and M. Litt, *Br. Polym. J.*, 1975, **7**, 139–154.
- 48 R. L. Zollars, in *Emulsion polymerisation of vinyl acetate*, eds. M. S. El-Aasser and J. W. Vanderhoff, Applied Science Publishers Ltd.: London, 1981.
- 49 D. Britton, F. Heatley and P. A. Lovell, *Macromolecules*, 1998, **75**, 2828–2837.
- 50 M. S. El-Aasser, T. Makgawinata, J. W. Vanderhoff and C. Pichot, *J. Polym. Sci. A-1 Polym. Chem.*, 1983, **21**, 2363–2382.
- 51 M. Nomura, Y. Minamino, K. Fujita and M. Harada, *J. Polym. Sci. A-1 Polym. Chem.*, 1982, **20**, 1261–1270.
- 52 C. J. Ferguson, G. T. Russell and R. G. Gilbert, *Polymer (Guildf)*., 2003, **44**, 2607–2619.
- 53 N. Nomura, K. Shinoda, A. Takasu, K. Nagata and K. Inomata, *J. Polym. Sci. A-1 Polym. Chem.*, 2013, **51**, 534–545.
- 54 F. Zhao, A. R. Mahdavian, M. B. Teimouri, E. S. Daniels, A. Klein and M. S. El-Aasser, *Colloid. Polym. Sci*, 2012, **290**, 1247–1255.
- 55 O. W. Smith, M. J. Collins, P. S. Martin and D. R. Bassett, *prog. org. coat.*, 1993, **22**, 19–25.
- 56 V. Šipailaitė-Ramoškienė, E. Fataraitė, K. V Mickus and R. Mažeika, *Mater. Sci.*, 2003, **9**, 271.
- 57 X. Z. Kong, C. Pichot, J. Guillot and J. Y. Cavailté, in *Polymer Latexes, Chapter 11, ACS Symposium Series, Vol .492;*, 1992, pp. 163–187.

- 58 D. Donescu and L. Fusulan, *J. Disp. Sci. Tech.*, 1994, **15**, 543–560.
- 59 A. L. Back, *Ind. Eng. Chem.*, 1947, **39**, 1339–1343.
- 60 J. R. Martin, J. F. Johnson and A. R. Cooper, *J. Macromol. Sci. Part C*, 1972, **8**, 57–199.
- 61 R. W. Nunes, J. R. Martin and J. F. Johnson, *Polym. Eng. Sci*, 1982, **22**, 205–228.
- 62 H. Mitsui, H. A. Spikes and Y. Suita, *Elastohydrodynamics*, 1997, **32**, 487–500.
- 63 E. Arda and O. Pekcan, *J. Colloid. Interface. Sci.*, 2001, **234**, 72–78.
- 64 E. Arda, V. Bulmuş, E. Pişkin and Ö. Pekcan, *J. Colloid. Interface. Sci.*, 1999, **213**, 160–168.
- 65 A. Tzitzinou, J. L. Keddie, J. L. Geurts, M. Mulder, R. Satguru and K. E. Treacher, *Film Form. coatings; ACS Symp. Ser.*, 2001, **790**, 58–87.
- 66 J. K. Oh, P. Tomba, X. Ye, R. Eley, J. Rademacher, R. Farwaha and M. A. Winnik, *Macromolecules*, 2003, **36**, 5804–5814.
- 67 H. Zecha, R. Weissgerber and F. P. Petrocelli, *European Patent 1304339B2*, 2008.
- 68 S. Suzuki, K. Kikuchi, A. Suzuki, T. Okaya and M. Nomura, *Colloid. Polym. Sci*, 2007, **285**, 523–534.
- 69 J. I. Amalvy, M. J. Unzué, H. A. S. Schoonbrood and J. M. Asua, *J. Polym. Sci. A-1 Polym. Chem.*, 2002, **40**, 2994–3000.
- 70 E. Aramendia, J. Mallégo, C. Jeynes, M. J. Barandiaran, J. L. Keddie and J. M. Asua, *Langmuir*, 2003, **19**, 3212–3221.
- 71 M. E. Dobrowolska, J. H. Van Esch and G. J. M. Koper, *Langmuir*, 2013, **29**, 11724–11729.
- 72 P. J. Feeney, D. H. Napper and R. G. Gilbert, *Macromolecules*, 1984, **17**, 2520–2529.
- 73 D. Munro, A. R. Goodall, M. C. Wilkinson, K. Randle and J. Hearn, *J. Colloid. Interface. Sci.*, 1979, **68**, 1–13.
- 74 R. M. Fitch and R. C. Watson, *J. Colloid. Interface. Sci.*, 1979, **68**, 14–20.
- 75 S. S. Ivanchev, V. N. Pavljuchenko and N. A. Byrdina, *J. Polym. Sci. A-1 Polym. Chem.*,

- 1987, **25**, 47–62.
- 76 J. M. . Kusters, 1994.
- 77 J. M. H. Kusters, D. H. Napper, R. G. Gilbert and A. L. German, *Macromolecules*, 1992, **25**, 7043–7050.
- 78 K. Tauer and S. Kosmella, *Polym. Int.*, 1993, **30**, 253–258.
- 79 T. Hamaide, A. Revillon and A. Guyot, *Eur. Polym. J.*, 1987, **23**, 787–794.
- 80 F. Vidal and T. Hamaide, *Polym. Bull.*, 1995, **35**, 1–7.
- 81 A. Guyot and F. Vidal, *Polym. Bull.*, 1995, **34**, 569–576.
- 82 J. M. Asua and H. A. S. Schoonbrood, *Acta. Polym.*, 1998, **49**, 671–686.
- 83 H. H. Freedman, J. P. Mason and M. A. I, *J. Org. Chem.*, 1958, **23**, 76–82.
- 84 Z. Mingyue, Q. Weihong, L. Hongzhu and S. Yingli, *J. Appl. Polym. Sci.*, 2008, **107**, 624–628.
- 85 H. Wu, S. Kawaguchi and K. Ito, *Colloid. Polym. Sci*, 2004, **282**, 1365–1373.
- 86 A. Guyot, C. Graillat and C. Favero, *C. R. Chim.*, 2003, **6**, 1319–1327.
- 87 S. Abele, C. Gauthier, C. Graillat and A. Guyot, *Polymer (Guildf.)*, 2000, **41**, 1147–1155.
- 88 I. Uzulina, A. Zicmanis, C. Graillat, J. Claverie and A. Guyot, *J. Dispers. Sci. Technol.*, 2002, **23**, 799–808.
- 89 J. F. Morizur, D. J. Irvine, J. J. Rawlins and L. J. Mathias, *Macromolecules*, 2007, **40**, 8938–8946.
- 90 M. B. Urquiola, V. L. Dimonie, E. D. Sudol and M. S. El-Aasser, *J. Polym. Sci. A-1 Polym. Chem.*, 1992, **30**, 2619–2629.
- 91 M. B. Urquiola, V. L. Dimonie, E. D. Sudol and M. S. El-Aasser, *J. Polym. Sci. A-1 Polym. Chem.*, 1992, **30**, 2631–2644.
- 92 M. B. Urquiola, V. L. Dimonie, E. D. Sudol and M. S. El-Aasser, *J. Polym. Sci. A-1 Polym. Chem.*, 1993, **31**, 1403–1415.

- 93 K. A. Shaffei, A. B. Moustafa and A. I. Hamed, *Int. J. Polym. Sci.*, , DOI:10.1155/2009/731971.
- 94 V. Chabrol, J. Batty, P. Shaw, C. Davis and M. Farrell, *WO2015145174A1*, 2015.
- 95 Y. Sun, W. Qiao and H. Liu, *Polym. Adv. Technol.*, 2008, **19**, 1164–1167.
- 96 H. Y. Erbil, *Vinyl acetate emulsion polymerisation and copolymerisation with acrylic monomers*. CRC Press;, 2000.
- 97 B. Derjaguin and L. Landau, *Acta Physicochim. U.R.S.S*, 1941, **14**, 633.
- 98 E. J. W. Verwey, *J. Phys. Chem.*, 1947, **51**, 631–636.
- 99 J. T. G. Overbeek, *J. Colloid. Interface. Sci.*, 1977, **58**, 408.
- 100 H. C. Hamaker, *Physica*, 1937, **4**, 1058–1072.
- 101 D. H. Napper, *J. Colloid. Interface. Sci.*, 1969, **29**, 168–170.
- 102 D. H. Napper, *J. Colloid. Interface. Sci.*, 1970, **32**, 106–114.
- 103 D. H. Napper and A. Netschey, *J. Colloid. Interface. Sci.*, 1971, **37**, 528–535.
- 104 D. H. Napper, *Trans. Faraday. Soc.*, 1968, **64**, 1701–1711.
- 105 D. H. Napper, *J. Colloid. Interface. Sci.*, 1970, **33**, 384–392.
- 106 S. Asakura and F. Oosawa, *J. Chem. Phys.*, 1954, **22**, 1255–1256.
- 107 S. Asakura and F. Oosawa, *J. Polym. Sci.*, 1958, **33**, 183–192.
- 108 H. N. W. Lekkerkerker and R. Tuinier, *Colloids and the Depletion Interaction*, Springer, 2011.
- 109 K. Arap and Y. Ogiwara, *Makromol. Chem., Rapid Commun.*, 1981, **367**, 363–367.
- 110 T. Sato and T. Okaya, *Polym. J.*, 1992, **24**, 849–856.
- 111 J. I. Amalvy, M. J. Unzué, H. A. S. Schoonbrood and J. M. Asua, *Macromolecules*, 1998, **31**, 5631–5638.
- 112 R. A. Gregg, D. M. Alderman and F. R. Mayo, *J. Am. Chem. Soc.*, 1948, **70**, 3740–3743.

- 113 G. Moad and C. L. Moad, *Macromolecules*, 1996, **29**, 7727–7733.
- 114 K. G. Suddaby, D. R. Maloney and D. M. Haddleton, *Macromolecules*, 1997, **30**, 702–713.
- 115 J. P. A. Heuts, T. P. Davis and G. T. Russell, *Macromolecules*, 1999, **32**, 6019–6030.
- 116 D. Kukulj, J. P. A. Heuts and T. P. Davis, *Macromolecules*, 1998, **31**, 2894–2905.
- 117 J. L. De La Fuente and E. L. Madruga, *J. Polym. Sci. A-1 Polym. Chem.*, 1998, **36**, 2913–2925.
- 118 N. Ono, Y. Shigetomi, H. Kato and M. Oki, *Polym. J.*, 1992, **24**, 247–255.
- 119 M. A. Kauffman and R. S. Guise, *J. Vinyl Technol.*, 1994, **16**, 39–45.
- 120 L. I. Atanase, S. Bistac and G. Riess, *Soft Matter*, 2015, **11**, 2665–2672.
- 121 S. Hong, R. Albu, C. Labbe, T. Lasuye and B. Stasik, 2006, **1434**, 1426–1434.
- 122 H. L. Wagner, *J. Phys. Chem. Ref. Data*, 1985, **14**, 1101–1106.
- 123 B. Hawket, University of Sydney, 1974.
- 124 M. J. Ballard, D. H. Napper and R. G. Gilbert, *J. Polym. Sci. A-1 Polym. Chem.*, 1984, **22**, 3225–3253.
- 125 I. Capek, J. Bartoň and E. Orolínová, *Chem. Zvesti*, 1984, **38**, 803–822.
- 126 W. Lane, *Ind. Eng. Chem.*, 1946, **18**, 295.
- 127 L. F. Halnan, D. H. Napper and R. G. Gilbert, *J. Chem. Soc., Faraday Trans. 1.*, 1984, **80**, 2851–2865.

VIII Conclusions and Outlook

Throughout this thesis we have explored the free radical polymerisation (FRP) of vinyl acetate (VAc), with the main goal of producing soap free VAc latexes for use as stabilisers in the suspension polymerisation of vinyl chloride monomer (VCM). This was a challenging goal, as the tendency for the propagating radical to undergo transfer, particularly to another polymer chain, is especially high, and the use of a chain transfer agent (CTA) was deemed essential to produce particles with low gel contents.

In Chapter 1, the use of thiols as CTAs was explored, and it was determined that the value of the chain transfer constant ($C_{tr,S}$) is so high (≈ 223 for transfer to *n*-dodecanethiol at 60 °C), that an unavoidable composition drift occurs. This can lead to a broad molecular weight distribution, and the number of cross links per chain as a result of transfer to polymer will increase as the chain length increases, which may not be desirable. This is a particular issue during emulsion polymerisation where the polymer concentration is particularly high. The magnitude of $C_{tr,S}$ could not be determined through the use of conventional instantaneous approaches, which led to the conception of a new cumulative approach, divulged in Chapter 1. This new approach makes use of cumulative molecular weight distribution data and monomer conversion data, exploiting an analytical solution to the cumulative weight molecular weight distribution. It has been demonstrated that this method is powerful for determining $C_{tr,S}$ for systems where substantial drift in the ratio $[S]/[M]$ occurs (being the concentration ratio of CTA and monomer).

In future work, it would be very interesting to see this new cumulative method applied to other reactive CTA/monomer systems, and to compare the magnitude of $C_{tr,S}$ determined with that determined using the conventional means. Systems such as styrene/dodecanethiol (DDT) ($C_{tr,S} = 15.26$ at 50 °C)¹ would be an excellent benchmark for these purposes. Additionally, as this method has been designed with VAc/thiols in mind, it may be interesting to see how different thiols behave in VAc FRP. For example, how does the proximity of heteroatoms to the thiol, or the length of the aliphatic chain, influence the reactivity of the S-H bond, and therefore the value of $C_{tr,S}$. 2-Mercaptoethanol is a good example of a thiol with additional functionality (being a

hydroxyl group) relatively close to the S-H bond which may be interesting to explore using the new method.

Although this method was devised through necessity for systems where $C_{tr,S}$ is substantially greater than 1, in theory, it can be applied universally, therefore, application to systems for which substantial data exists, where $C_{tr,S}$ is closer to unity, would also be very interesting to acquire. One common example might be methyl methacrylate/DDT ($C_{tr,S} = 0.711$ at 50 °C)¹. This may then prove that this method is a universal method to determine the value of $C_{tr,S}$ regardless of the degree of conversion and system of study (as long as the starting concentrations and monomer conversion are known), and in theory only requires data from one experiment, thereby being more applicable than the conventional methods. This would justify the methods use for determining unknown values of $C_{tr,S}$ regardless of the predicted reactivity.

After learning of the difficulties of using a thiol as CTA in VAc FRP, Chapter 2 demonstrated the use of disulfides as CTAs. These compounds were particularly interesting to study, as they have values of $C_{tr,S}$ closer to unity. di-*n*-butyl disulfide (DBDS) was shown to be the most promising candidate for VAc FRP (for DBDS, $C_{tr,S} = 0.221$ at 60 °C), with the other species tested, 2-hydroxyethyl disulfide (2-HEDS) ($C_{tr,S} = 2.043$ at 60 °C), significantly retarding the polymerisation. The molecular weight was shown to be effectively reduced, with only a minimal and very manageable reduction in the rate of polymerisation when DBDS was used. Key to the findings of Chapter 2 was the suggestion that the chain transfer proceeded through 2 sequential steps: addition to the disulfide, and subsequent fragmentation. This was argued on the premise of the rate data, although direct proof of the existence of the intermediate addition product was not found. This proof may be provided through analysis by electron paramagnetic resonance (EPR), wherein the intermediate radical species may be identified, and potentially its concentration measured, which may give some indication as to its lifetime. Further to this, comparison of this lifetime between DBDS and 2-HEDS may provide direct proof for the proposal that the proximity of heteroatoms to the disulfide bonds changes the rate of fragmentation from the addition product.

The involvement of the disulfide bond in the transfer reaction was demonstrated through direct measurement of the mass of the polymer chains through electrospray ionisation mass spectrometry (ESI-MS). The result of this mechanism is that the propagating radical is terminated

with a thioether group, with the CTA derived radical (a thiyl radical) then going on to reinitiate, resulting in telechelic poly(vinyl acetate) (PVAc) (due to the use of symmetrical disulfides). Therefore, the functionality of the end groups could be controlled simply through the selection of the disulfide used. The author does suggest that the proximity of any heteroatoms to the disulfide bond be limited, i.e. potentially using a disulfide with an aliphatic linker between the disulfide bond and any functional group to limit any potential retardation. An alternate method would be to use an aliphatic disulfide and to subject the resultant polymer to post polymerisation modification. As was alluded to in the conclusions to Chapter 2, a number of organic synthesis pathways are available to convert thioethers into more functional species, such as oxidation to the corresponding sulfoxide or sulfone.² This transformation would greatly increase the hydrophilicity of the end groups, and potentially give interesting properties to the polymers. The sulfone may even be susceptible to nucleophilic attack, thereby providing a simple means for a host of further modifications by nucleophilic species.³

The use of cyclic disulfides was also very briefly discussed as part of Chapter 2, and the consequences of having the produced thiyl radical tethered to the polymer chain results in a copolymerisation of sorts. This process would produce polymers with thioether linkages in the polymer backbone, which could open doors for some very interesting applications in future studies. As an example, applying the same modifications discussed previously, i.e. oxidation, could facilitate highly tuneable hydrophilicity of polymer chains. Additionally, assuming the proposed electrophilicity of sulfones, the polymer chains could be snapped at these linkages when exposed to a nucleophile. This could be interesting for applications such as controlled release, or decomposable polymers in future works. One additional observation was made when attempting to saponify polymers with thioether linkages as part of the end groups. The reaction introduced colouration, which was accompanied by the creation of proton environments analogous to unsaturated groups in the nuclear magnetic resonance spectra. These were assigned to unsaturation introduced through elimination of acetate, which appeared to be promoted by the presence of the thioether end groups.

In Chapter 3, DBDS was used to reduce the molecular weight in copolymerisations between VAc and multivinyl monomers (MVMs). The goal of this chapter was to produce branched copolymers, and was inspired by the knowledge of the ability of DBDS to reduce molecular weight without exhibiting a significant drift in the polymer composition. It was demonstrated

that the degree of branching could be controlled with the amount and nature of the comonomer used, and that the molecular weight could be reduced effectively with DBDS. Kinetic data for the copolymerisation of VAc with 3 MVMs was provided, with divinyl adipate (DVA) appearing to copolymerise well with VAc, providing a measurable increase in molecular weight and the degree of branching, with relatively small influences on the rate of polymerisation. 1,4-butanediol divinyl ether (BDDVE) also increased molecular weight and molecular density, albeit to a lesser extent, and the rate of polymerisation was affected more through increasing concentrations of BDDVE. 1,3,5-triallyl-1,3,5-triazine-2,4,6(1H,3H,5H)-trione (TTT) was also studied, and appeared to increase the molecular density the most, which was justified by the number of vinyl functionalities (three for TTT, two for DVA and BDDVE). TTT appeared to have the most significant influence on the rate of polymerisation, attributed to the lack of reactivity of the allylic radical formed after addition.

One key oversight of the work was the lack of high monomer conversion data obtained, therefore, it is as of yet unclear if gelation could be totally prevented under the conditions tested. The next logical step in this work would therefore be to assess the actual gel point in these series, and compare to experiments in the absence of CTA and to the theoretical gel point calculations. Through tweaking of the relative concentrations of the species involved (VAc/DBDS/MVM), a particularly efficient route to hyper branched PVAc may well be possible.

It should again be stressed that the results of using disulfides as CTA is the introduction of end groups, and in the copolymerisation with an MVM this could be a means to introduce significant functionality. Given that the end of every branch will contain a residue from the CTA (assuming the chain is terminated by transfer and the produced thiyl radical reinitiates), all of the considerations regarding different functionalities of disulfides, or post modification, are again valid, and may have an even stronger influence over the polymer's properties.

The branched polymers prepared with different comonomers were also saponified in Chapter 3, with the hope that the saponification could yield the corresponding branched polyvinyl alcohol (PVOH). It was proposed that DVA would be susceptible to saponification, and as a result would likely not retain the branched architecture after saponification. However, perhaps divinyl ether would resist the saponification, and the architecture could be retained. The molecular weight distributions of the branched copolymers were compared before and after saponification and

reacetylation, and some unpredicted observations were made. In the case of DVA copolymers, a slight decrease in the number average molecular weight was observed, alongside a large decrease in the weight average molecular weight, implying the saponification did indeed cleave some of the branches present in the polymer. However, the molecular density, expressed through the increase in intrinsic viscosity as a function of molecular weight (so called α value), remained essentially unchanged. With BDDVE, increases in both M_n and M_w were observed, alongside a dramatic increase in molecular density, which actually implied an increase in the degree of branching. Although direct proof for this was not provided, it was hypothesised that in both cases unreacted vinylic functionalities, be that from the MVMs or formed through elimination of acetate during the saponification, went on to react due to the high temperatures employed during the reacetylation protocol (115 °C). Therefore, in the case of DVA, although some branches may have undergone saponification, some chains also underwent addition to each other, resulting in the comparable molecular density. With BDDVE, the branches were more resistant, therefore did not snap, and the same addition occurred, accounting for the increases in molecular weight. This was indeed speculative, however, in future work one may conceive of a protocol with milder conditions to prevent this happening, or indeed use polymers formed at high conversion of vinyl groups.

Armed with the knowledge acquired in Chapters 1-3, Chapter 4 then details the journey towards the production of soap free latexes of VAc. Charged comonomers were used to provide colloidal stability to the latex, but are also inbuilt to allow the chains to stabilise interfaces in the subsequent application to the suspension polymerisation of VCM. The molecular weight distribution of the PVAc is highly influenced by the introduction of DBDS, and prevention of gelation was demonstrated. It is, however, still evident in the molecular weight distributions that a high molecular weight fraction is present, attributed to transfer to polymer. The introduction of chain transfer agent does appear to have a large effect on the course of the emulsion polymerisation process, firstly through a reduction in particle size. As the concentration is increased significantly, the particle size distribution broadens significantly, and in the extreme case, additional nucleation events are clearly visible due to multiple size distributions. This behaviour is attributed to an increase in radical exit as a result of chain transfer to the disulfide, with the CTA transfer adduct radical suspected to be water soluble enough to leave the polymer particles. This results in an

increase in the amount of aqueous polymerisation/termination, and the build-up of polymeric material in the water phase can trigger additional nucleation events.

The comonomer used also appeared to influence the course of the polymerisation, which was suggested to be due to the difference in the copolymerisation behaviour. The two comonomers demonstrated as part of this study were 2-acrylamido-2-methyl-1-propane sulfonic acid (Na-AMPS) and 3-allyloxy-2-hydroxypropane sulfonate (Na-AHPSA). At the same loading of each comonomer, the final particle size was dramatically larger for Na-AHPSA compared to Na-AMPS. This was justified as the Na-AMPS copolymers were likely to contain more blocky regions of comonomer, which may act like hairs extruding from the surface of the particle, invoking further stability.

The latexes formed in the presence of Na-AMPS also appeared to influence the properties of PVC granules more than those latexes formed with Na-AHPSA. When used as stabilisers at the same concentrations, Na-AMPS bearing latexes produced granules with measurably smaller size distributions and higher porosity. This draws into question two key considerations. Firstly, how does the particle size of the latex used as a stabiliser influence the particle size distribution of the resultant granules. Secondly, how does the distribution of comonomer units through the polymer chains influence their ability to act as stabiliser in the suspension polymerisation process. In future work, these avenues could be explored through use of different comonomers, with different copolymerisation behaviour, but also potentially different stabilising moieties, such as different anionic or indeed a cationic species.

Another interesting area of exploration is whether the molecular architecture would influence the stabilising action of the polymer chains. For example: do highly branched polymers have the potential to act differently as stabilisers in this process? Perhaps the simplest way to test this would be produce the branched polymers in solution as per the procedures outlined in Chapter 3. Alternatively, some MVM could be introduced into the emulsion polymerisation formulation, producing branched PVAc in emulsion polymerisation, controlling the degree of gelation through the relative ratios of VAc/DBDS/MVM. It is suspected that this would require a significant amount of optimisation, due to the differences in partitioning between all of the species. The branched species could contain significant amounts of functionality introduced through both the comonomer, and the end groups provided by the CTA, which may

consequentially influence the interfacial activity and consequently the ability to act as a stabiliser in the suspension polymerisation process.

The use of different disulfides could also be hugely beneficial to this process. For example, the use of a more hydrophobic disulfide could reduce the significance of radical exit on the course of polymerisation. Also, increasing the functionality of the disulfides may influence the aforementioned interfacial activity of the polymer chains due to the nature of the end groups.

The key take homes from this thesis are that molecular control in VAc FRP is certainly possible with conventional chain transfer, and that it is imperative that this is achieved in emulsion polymerisation if gelation is to be avoided.

References

- 1 J. L. De La Fuente and E. L. Madruga, *J. Polym. Sci. A-1 Polym. Chem.*, 2000, **38**, 170–178.
- 2 A. Napoli, M. Valentini, N. Tirelli, M. Müller and J. A. Hubbell, *Nature. Mater.*, 2004, **3**, 183–189.
- 3 B. M. Trost and C. A. Kalnmals, *Chem. Eur. J.*, 2019, **25**, 11193–11213.

IX Supporting Information

S1: McPolymer input model file "Example-VAc.tcl".

```
# include Interface
source mcPolymerInterface.tcl
# activate Hamielec model
source userPlugin.tcl

# define low molecular species
Initiator AIBN 0.70
Monomer VA 86.09
Species CTA
Species S
Species I#
Species R#
Species CTA#
Species VA#
Species S#

TransferSpecies VA
TransferSpecies CTA
TransferSpecies S

# define macromolecules
SpeciesMacro P#
SpeciesMacro D

# set initial concentrations
Concentration VA 8.634
Concentration CTA 8.59e-03
Concentration S 2.080
Concentration AIBN 7.80e-04

# debug function
ListAllSpecies

# define reaction rate constants

# reaction coefficients
RateConstant kd 9.67e-06
RateConstant kp 8548.00

RateConstant kpi 8548.00
RateConstant kps 8548.00
RateConstant kpcta 8548.00
```

```

RateConstant ktrm 2.317
RateConstant ktrs 2.317
RateConstant ktrcta 1.54e+05

RateConstant ktll 2.4e+08
RateConstant ktls 2.4e+08
RateConstant ktss 2.4e+08

# debug function
ListAllRateConstants

# define reactions

# VA polymerization
InitiatorDecomposition AIBN --> I# + I# kd

Initiation I# + VA --> P# kpi
Initiation S# + VA --> P# kps
Initiation CTA# + VA --> P# kpcta

Propagation P# + VA --> P# kp

Transfer2monomer P# + VA --> D + P# ktrm
Transfer_PL-PL P# + S --> D + S# ktrs
Transfer_PL-PL P# + CTA --> D + CTA# ktrcta

Termination P# + P# --> D ktll
Termination P# + S# --> D ktls
Termination P# + VA# --> D ktls
Termination P# + CTA# --> D ktls
Termination VA# + VA# --> D ktss
Termination S# + S# --> D ktss
Termination CTA# + CTA# --> D ktss
Termination VA# + S# --> D ktss
Termination VA# + CTA# --> D ktss
Termination S# + CTA# --> D ktss

# debug function
ListAllReactions

# set reaction temperature
Temperature 60.0

# set frequency for writing intermediate results

Setdt 60

```

```
set addDataProcessing(PolymerAnalysis) "PolymerAnalysis.cfg"
```

```
# define number of molecules for simulation 1e8..1e11  
InitSimulation 1e8
```

```
# start simulation to overall reaction time in s  
puts [clock seconds]  
Simulation 600  
puts [clock seconds]
```

S2: Loop extension, "append.py".

```
"""
append.py
this script is used to run an external simulation program (mcpolymer.exe)
multiple times
it combines the output of each simulation to all previous runs of the
simulation, at each time interval
this enables the simulation to be repeated and increase the size of the
dataset
"""

import sys
import os
import glob
import shutil
import subprocess
from collections import Counter

firstRun = True
# the value range() specifies the desired number of loops of the
simulation, in this example 12500 loops will be performed.
for i in range(12500):
    # this runs the mcpolymer program with the input model (eg "Example-
    VAc.tcl")
    process = subprocess.Popen('mcpolymer.exe Example-VAc.tcl')
    process.wait()

    # dataFiles is a set of files containing the output files from the
    above run of mcpolymer.exe - there is an output file for each time
    interval
    dataFiles = glob.glob('D*.cld')
    # on the first loop of simulation only, create a results file for each
    time interval (ie each output file) by copying the output files to a new
    file
    # these results files will contain the output from the first run of
    the loop only at this time, but will go on to hold the combined results
    from all simulation loops
    if firstRun:
        for f in dataFiles:
            shutil.copyfile(f, f'results.' + f)
        firstRun = False
        # this then completes this simulation loop, and skips the
        remainder of the code
        continue

    # for all runs EXCEPT the first, the following code runs for each time
    interval (or output file)
    for f in dataFiles:
        # open the corresponding results file which contains all
        previously combined results for this time interval
        # the first 3 lines in the results_file are headers, below that is
        all previously combined data for this time interval
```

```

with open(f'results.' + f, 'r') as results_file:
    results = results_file.readlines()
headers = results[:3]
old_data = results[3:]
old_chains = {}

# each data line in the file (old_data) is a data point,
containing the chain length (data[0]) and number of chains (data[1])
# the number of chains for each chain length is the summation of
the number of chains from all previous simulation loops
# store each of these data points into old_chains, with array
index of the chain length, and value of the number of chains
for data_point in old_data:
    data = data_point.split()
    old_chains[data[0]] = int(data[1])

# open the latest output file for the current time interval, and
store these data points in new_chains, similarly to above
# in this instance, the number of chains for the chain length is
from the current simulation loop only
with open(f, 'r') as new_file:
    new_data = new_file.readlines()

new_data = new_data[3:]

new_chains = {}

for data_point in new_data:
    data = data_point.split()
    new_chains[data[0]] = int(data[1])

# for each chain length, add the number of chains from the current
simulation loop to the combined value from all previous loops
combined_dict = Counter(old_chains) + Counter(new_chains)

# rewrite the results file for the current time interval to
include the newly combined data from the current simulation loop
with open(f'results.' + f, 'w') as results_file:
    for h in headers:
        results_file.write(f'{h}')
    for key, value in sorted(combined_dict.items(), key=lambda
item: int(item[0])):
        results_file.write(f'{key}\t{value}\n')

```

S3 - Approach 1

```
import matplotlib.pyplot as plt
import numpy as np
import scipy.special as sc
import lmfit
import pandas as pd

np.random.seed(0)

#Import datafile with two columns, i and lnpi
df2 = pd.read_csv('mc120data.csv')
x = df2['i']
y = df2['lnpi']

p = lmfit.Parameters()
p.add_many(('c', 180.),('lift', 5.))

def residual(p):
#v is monomer conversion, r is [S]/[M] ratio, b is transfer to other
species term (monomer + solvent).
    v = 0.006530402
    r = 9.95523E-05
    b = 0.00025
    return np.log(((1/x)*(((v - 1)*np.exp(-b*x)*(b*b*p['c']*p['c']**x*x +
p['c']*(-2*b*b*x*x + 2*b*x + 1) + b*x*(b*x - 2))*((p['c']*r*x*((1 -
v)**(p['c'] - 1))))*(1/(1 - p['c']))) *sc.gamma((1/(p['c'] - 1)))*(1-
sc.gammainc((1/(p['c'] - 1)), (p['c']*r*(1 - v)**(p['c'] - 1))*x)) -
(p['c'] - 1)*np.exp(-x*((b + p['c']*r*(1 - v)**(p['c'] - 1))))*(-
1*p['c']*(2*b*v*x - 2*b*x + r*x*(1 - v)**p['c'] + v - 1) + 2*b*(v - 1)*x +
p['c']*p['c']*r*x*(1 - v)**p['c']))/(((1 - p['c'])**3)*x)-((0 -
1)*np.exp(-b*x)*(b*b*p['c']*p['c']**x*x + p['c']*(-2*b*b*x*x + 2*b*x + 1) +
b*x*(b*x - 2))*((p['c']*r*x*((1 - 0)**(p['c'] - 1))))*(1/(1 -
p['c']))) *sc.gamma((1/(p['c'] - 1)))*(1-sc.gammainc((1/(p['c'] - 1)),
(p['c']*r*(1 - 0)**(p['c'] - 1))*x)) - (p['c'] - 1)*np.exp(-x*((b +
p['c']*r*(1 - 0)**(p['c'] - 1))))*(-1*p['c']*(2*b*0*x - 2*b*x + r*x*(1 -
0)**p['c'] + 0 - 1) + 2*b*(0 - 1)*x + p['c']*p['c']*r*x*(1 -
0)**p['c']))/(((1 - p['c'])**3)*x))+p['lift']-y

# create Minimizer
mini = lmfit.Minimizer(residual, p, nan_policy='propagate')

# first solve with Nelder-Mead algorithm
out1 = mini.minimize(method='Nelder')
```

```

# then solve with Levenberg-Marquardt using the
# Nelder-Mead solution as a starting point
out2 = mini.minimize(method='leastsq', params=out1.params)

lmfit.report_fit(out2.params, min_correl=0.5)

ci, trace = lmfit.conf_interval(mini, out2, sigmas=[1, 2], trace=True)
lmfit.printfuncs.report_ci(ci)

# plot data and best fit
plt.figure()
plt.plot(x, y, 'b')
plt.plot(x, residual(out2.params) + y, 'r-')

# plot confidence intervals (c vs cm and c vs lift)
fig, axes = plt.subplots(1, 2, figsize=(12.8, 4.8))
cx, cy, grid = lmfit.conf_interval2d(mini, out2, 'c', 'lift', 30, 30)
ctp = axes[0].contourf(cx, cy, grid, np.linspace(0, 1, 11))
fig.colorbar(ctp, ax=axes[0])
axes[0].set_xlabel('c')
axes[0].set_ylabel('lift')

# plot dependence between two parameters
fig, axes = plt.subplots(1, 2, figsize=(12.8, 4.8))
cx1, cy1, prob = trace['c']['c'], trace['c']['lift'], trace['c']['prob']
cx2, cy2, prob2 = trace['lift']['lift'], trace['lift']['c'],
trace['lift']['prob']

axes[0].scatter(cx1, cy1, c=prob, s=30)
axes[0].set_xlabel('c')
axes[0].set_ylabel('lift')

axes[1].scatter(cx2, cy2, c=prob2, s=30)
axes[1].set_xlabel('lift')

axes[1].set_ylabel('c')
axes[0].set_ylabel('lift')

plt.show()

```

S4: Local first derivative of $\ln N(i)$ vs i

```
import matplotlib.pyplot as plt
import scipy.special as sc
from scipy.misc import derivative
from pycse import deriv
import numpy as np
import csv
import pandas as pd

#This will import a csv file, with the input being the degree of
polymerisation,  $i$  and the corresponding value of  $\ln N(i)$  (denoted  $\ln p_i$ 
here), for 6 data points above and below the target value of  $i$  (here  $i =$ 
450, with values of  $i$  between 400 and 500 being used). The first
derivative is then fit using a 3rd order polynomial, and the value of the
fit at the value of  $i$  (here being 450) is then output and taken as the
local first derivative.

df2 = pd.read_csv('450.csv')
x = df2['i']
y = df2['lnpi']
poly = np.polyfit(x, y, 3)
plt.figure()
plt.plot(x, y)
plt.plot(x, np.polyval(poly, x), 'g-')

# compute derivatives
dpoly = np.polyder(poly)
dCdt_fit = np.polyval(dpoly, x)
dCdt_numeric = deriv(x, y) # 2-point deriv
plt.figure()
plt.plot(x, dCdt_numeric, label='numeric derivative')
plt.plot(x, dCdt_fit, label='fitted derivative')
xplot = np.linspace(min(x), max(x))
plt.plot(xplot, np.polyval(dpoly, xplot), label='resampled derivative')
plt.legend(loc='best')
print ('x = 450,', np.polyval(poly, 450),',', np.polyval(dpoly, 450))
```


S5: Solving for $C_{tr,S}$ using approach 2 for $[DDT]_{p=0}/[VAc]_{p=0} = 8.00 \times 10^{-5}$, $i = 450$. Input file includes monomer conversion, the first derivative of $\text{LnN}(i)$ and $\text{LnN}(i)$.

```

import numpy as np
import matplotlib.pyplot as plt
import sympy as sym
from lmfit import Model
from ipywidgets.widgets import interact
sym.init_printing(use_latex="mathjax")
from sympy.abc import c,x,v,b, r
import pandas as pd

logpiv = sym.log((1/x)*((((v - 1)*sym.exp(-b*x)*(b*b*c*c*x*x + c*(-
2*b*b*x*x + 2*b*x + 1) + b*x*(b*x - 2))*((c*r*x*((1 - v)**(c - 1)))**(1/(1
- c)))*(sym.uppergamma((1/(c - 1)), (c*r*(1 - v)**(c - 1))*x)) - (c -
1)*sym.exp(-x*((b + c*r*(1 - v)**(c - 1))))*(-1*c*(2*b*v*x - 2*b*x +
r*x*(1 - v)**c + v - 1) + 2*b*(v - 1)*x + c*c*r*x*(1 - v)**c)/(((1 -
c)**3)*x))-(((theta - 1)*sym.exp(-b*x)*(b*b*c*c*x*x + c*(-2*b*b*x*x + 2*b*x +
1) + b*x*(b*x - 2))*((c*r*x*((1 - theta)**(c - 1)))**(1/(1 -
c)))*(sym.uppergamma((1/(c - 1)), (c*r*(1 - theta)**(c - 1))*x)) - (c -
1)*sym.exp(-x*((b + c*r*(1 - theta)**(c - 1))))*(-1*c*(2*b*theta*x - 2*b*x +
r*x*(1 - theta)**c + theta - 1) + 2*b*(theta - 1)*x + c*c*r*x*(1 - theta)**c)/(((1 -
c)**3)*x))))))
dlogpiv = logpiv.diff(x)

lam=sym.lambdify((v,x,c,b,r), logpiv)
dlam=sym.lambdify((v,x,c,b,r), dlogpiv)

x = [450]
v = np.arange(0.001,0.05,0.00001)

for xs in x:
    c = 180
    b = 0.00025
    r = 8.00E-05

    q = dlam(v, xs, c, b, r )

    plt.figure()
    plt.plot(v, lam(v, xs, c, b, r))

```

```

    plt.plot(v, fun(v))
    plt.figure()
    plt.plot(v, q)
plt.show()

def cldcs(v,c, lift):
    xs = 450
    r = 8.00E-05
    b = 0.00034
    return dlam(v, xs, c, b, r )+lift

df2 = pd.read_csv('450.csv')
v = df2['v']
y = df2['dlnpi']
yint = df2['lnpi']
vdash = (1-v)**(c-1)
gmodel = Model(cldcs)

print('parameter names: {}'.format(gmodel.param_names))
print('independent variables: {}'.format(gmodel.independent_vars))

result = gmodel.fit(y, v=v,c=180, lift=0)

print(result.fit_report())

plt.plot(v, y, 'bo')
plt.plot(v, result.init_fit, 'k--', label='initial fit')
plt.plot(v, result.best_fit, 'r-', label='best fit')
plt.legend(loc='best')
plt.show()

```